UNIVERSITAT DE BARCELONA

New mechanisms involved in the DNA replication stress response of non-transformed human cells

Amaia Ercilla Eguiarte

PROGRAMA DE DOCTORADO EN BIOMEDICINA
FACULTAD DE MEDICINA, UNIVERSIDAD DE BARCELONA

New mechanisms involved in the DNA replication stress response of non-transformed human cells

Thesis presented by

Amaia Ercilla Eguiarte

to qualify for the degree of Doctor in Biomedicine
by University of Barcelona

This thesis has been performed in

Departamento de Biología Celular, Inmunología y Neurociencias,
Facultad de Medicina,
Universidad de Barcelona

Under the supervision of Prof. Neus Agell i Jané, Ph.D.

Barcelona, April 2016

Nire familiari,

dauden eta jada ez daudenei

A Iñigo

“Badira bide batzuk derrigorrez ibili behar ditugunak,

inora ez doazela jakiteko”

Lagun izoztua, Joseba Sarrionandia

Agradecimientos

Recuerdo como si fuese ayer el primer día que entré en el laboratorio de *BioCel*, que me unía al *grup* Neus, y como no, al *checkpoint team*! Pero no fue ayer, no. Un largo camino me separa de aquel día. Un camino lleno de emociones, nervios, alegrías y alguna que otra tristeza que por supuesto volvería a recorrer mil y una veces. Pero dicen que todo llega a su fin algún día y parece que ese día ya ha llegado.

Quiero dar las gracias a todas las personas que han formado parte de ese camino, que me han ayudado tanto científica como personalmente, por todos los momentos que hemos vivido tanto en el *lab* como fuera de él, ya que sin todos ellos hoy no estaría donde estoy.

En primer lugar, quiero darle las gracias a mi directora de tesis, a Neus. Por haberme dado la oportunidad de formar parte de esta familia; por haberme introducido al maravilloso mundo de la ciencia y por enseñarme crecer en él; por enseñarme a ser crítica, a discutir y a buscar siempre nuevos caminos hasta encontrar las respuestas; por la confianza y por la oportunidad de mejorar como científica asistiendo a congresos, yendo de estancia; por cuidarnos; por no perder la paciencia; por el apoyo y por pensar tanto en mi presente como en mi futuro, *moltes gràcies*!

Por supuesto, quiero darle millones de gracias a mi *checkpoint* mayor, a mi *mini jefa*, Alba Llopis. Por acogerme, por enseñarme, por no desesperarse, por transmitirme su ilusión y su energía, por darme su confianza y enseñarme a confiar, por ser mi consejera, por todo lo que hemos compartido y que ahora ya podemos celebrar (es *super* guay!!), por enseñarme a revelar WB en blanco (siempre va bien saberlo! ;)), por compartir buenos momentos en la sala del nitrógeno (*t'enrecordes*?), por los miles de *timecourse,* cervezas y risas en general, por todos los momentos vividos tanto en el *lab* como fuera de él, *moltisimes gràcies*!!

Como no, darle las gracias también a nuestra *mini checkpoint*, a Sonia Feu. Por enseñarme a pensar, a enseñar y a ser mejor científica, por su calma y su alegría, por el interés y el entusiasmo, por todo el trabajo, por apoyarme y acompañarme en mi último tramo del camino, *moltes gràcies*! *I molta sort*! Estoy segura de que te irá genial! *No ho dubto!*

Quiero dar las gracias también a todo el resto del *grup* Neus, del pasado y del presente: A Carles Barceló por los miles de consejos; a Noe Paco por enseñarme cual es la capital mundial y a que a falta de agua siempre queda el pacharán, ¡mucha suerte en la última etapa!; a Edu por ponerle banda sonora a nuestra vida, por ser nuestro *Dexter* particular y por enseñarnos a leer *papers* sin WB!!; a Noe Salvador, a Debora, a Triana, a Sonia Brun y a Montse; por el apoyo, por la ayuda, por los miles de *buffers* compartidos, por los desayunos, por las mudanzas, por todos los momentos que hemos vivido y por hacer que seamos una pequeña gran familia. *Moltisimes gràcies a tots i totes!*

Dar las gracias también a todo el resto de compañeros del *lab* de *BioCel* del pasado y del presente: a Euge, a David, a Tula, a Anna P, a Edurne, a Judit, a Serena, a Miriam, a

Martina, a Ignasi, a Neus S, a Sara, a Eulalia, a todos en general por todo lo que me habéis enseñado, por toda la ayuda, por las risas, por los cafés, por hacer que el día a día fuese tan ameno…Y en especial quiero dar las gracias a Marta Sánchez, a Alba Gómez y a Atilla por ser más que mis compañeros de *poyata*, por apoyarme, por aconsejarme, por enseñarme cosas tan útiles como la canción del *Ponceou* (es la hora, es la hora..), por los miles de *petits* (hoy en día *royals)*, por los viajes, por las risas, por las *etxerakolanak,* por los *trikipoteos,* por las fiestas en *Roselló* y por todos los momentos compartidos dentro y fuera del *lab*! *Moltes gràcies! Eskerrik asko!! Teşekkürler!!*

Quiero dar las gracias también a todos los integrantes del *Cellex* del presente y del pasado en general: a las Anna-s, a Albert H, a Meri, a Iona, a Maite, a David, a Andrea, a Elsa, a Albert *petit*, a Alba F, a Maria M, a Marta B, a Siscu, a Albert P, a Carles E…nuestros compañeros de seminarios, de cenas, de celebraciones, de *calçodatas*, de paelladas… gracias por las ideas aportadas, por compartir/discutir vuestros y nuestros resultados, por los millones de reactivos prestados y por todos los buenos momentos compartidos!! Y en especial agradecer a Carles Rentero sus consejos y su ayuda siempre que la he necesitado, te debo un *Acuarius*! :). *Moltisimes gràcies*!!

Dar las gracias también a las *chicas del confo*: a Maria, a Anna B y a Elisenda por toda la ayuda prestada; a todos nuestros colaboradores por la confianza y por enseñarme la importancia de compartir y debatir los resultados con otros, gracias a todos! Agradecer también a todos los miembros del *Centre de Recerca Biomèdica del Hospital Universitari Sant Joan de Reus* el haber compartido mis primeros pasos en ciencia! *Of course, I would like to thank everybody at the Ernfors lab and also at the proteomic service of the Karolinska Institutet! I am especially grateful to Patrik for giving me the opportunity to go there and to Sergi for sharing his work with me, for teaching me and for making me feel at home while I was there. Tack så mycket!*

Por último, quiero dar las gracias a todos aquellos que no están directamente relacionados con la tesis pero sin los cuales llegar hasta aquí no hubiese sido posible.

Nire lagun guztiei, urrunetik emandako laguntzagatik, bisita eta bidai guztiengatik, noan bakoitzean han jarraitzeagatik, eskerrik asko danori! A Clara, a Maria, a Joan y a Jordi, compañeros de *uni* y de la vida, gracias por acogerme, por enseñarme a "hablar" (solo os costó dos meses, ;)), por todo el apoyo, por toda la ayuda, por las discusiones, por los consejos, por las risas, por las cervezas, por dejarme ser una princesita, por enseñarme que una *trikitixa* no es una *trikitixa*, por los viajes, por todas las *Santa teclas* y por todos los momentos que hemos vivido y que espero sigamos viviendo! *Moltisimes gràcies!!!* Muchas gracias también a mis otros compañeros y amigos de la *uni*, de Tarragona y de Barcelona, a Esther, a Ingrid, a Jessi… gracias por vuestra ayuda, vuestros consejos y por todos los momentos que hemos compartido!

A Ana y Carlos, y por supuesto a Iñigo por entenderme, por apoyarme, por aconsejarme, por su paciencia, por todo lo que hemos sufrido, por lo que hemos compartido, por cuidarme, por ser mi *sukaldari* favorito y por todo lo que nos queda por compartir y vivir! *Eskerrik asko laztantxu! Ez ahaztu inoiz!*

Eta nola ez, nire familiari. Lehenik, nire gurasoei, nahiz eta urrun egon beti nirekin egon direlako, behar izan dudan guztietan lagundu nautelako, sarritan ulertu gabe ere beti euren babesa eta konfiantza euki dudalako, eta laguntzarekin baina trabarik jarri gabe beti nire bidea zein den erabakitzen utzi didatelako. Eskerrik asko nire aizpa Itziarri ere Bartzelonako urte hauek nirekin partekatzeagatik eta bere laguntza guztiagatik. Eskerrak baita izeko, Mikel eta familia guztiari ere beraien babesagatik. Eskerrik asko denoi bihotz bihotzez!

Moltisimes gràcies!! Eskerrik asko!!

INDEX

ABBREVIATIONS

BER: base excision repair
BIR: break-induced replication
bp: base pairs
CFS: common fragile sites
CIN: chromosomal instability
DDR: DNA damage response
DDT: DNA damage tolerance
D-loop: displacement loop
dNTP: Deoxyribonucleotide triphosphate
DSB: double-strand break
dsDNA: double-stranded DNA
DUB: deubiquitinating enzyme
ERFS: early-replicating fragile sites
HR: homologous recombination
HS: horse serum
HU: hydroxyurea
ICL: inter-strand crosslink
iPOND: isolation of proteins on nascent DNA
Kb: kilobase
Mb: megabase
MMEJ: microhomology-mediated end-joining
MS: mass spectrometry
NER: nucleotide excision repair
NHEJ: non-homologous end-joining
OIS: oncogene-induced senescence
PFGE: pulse-field gel electrophoresis
PIC: protease inhibitor cocktail
pre-IC: pre-initiation complex
pre-LC: pre-loading complex
pre-RC: pre-replication complex
PTM: post-translational modification
RFB: replication fork barrier
RPC: replication pausing complex
RS: replication stress
RT: room temperature
SA-beta-Gal: senescence-associated β-galactosidase
SAC: spindle assembly checkpoint
SSB: single-strand break
ssDNA: single-stranded DNA
TLS: translesion synthesis

UPS: ubiquitin proteasome system
WB: Western blot

INTRODUCTION

1. The cell cycle

Life cannot exist without a previous cell division, since every cell comes from the division of a previous cell (*Omnis cellula e cellula*). This idea, first proposed by Robert Remark and Rudolf Virchow on the 19th century, has been essential for the study of the cell cycle and division, the bases of life.

The **cell cycle**, the group of processes involved in the duplication and division of a cell in two daughter cells, is essential for all organism existence. In the case of unicellular organisms, this process results in the generation of a new organism; while in pluricellular organisms, the generation, development and maintenance of all tissue and organs is dependent on thousands of consecutive cell divisions[1].

The main objective of the cell cycle is the duplication and division of the genetic material or DNA (Deoxyribonucleic acid), in a process occurring in four consecutive cell cycle phases (Figure 1). The duplication of the genetic material takes place in **S phase** or synthesis phase, in a process known as **DNA replication**[1]. This process has to be done accurately, completely and only once per cell cycle to avoid the loss of information and the acquisition of genomic instability, hallmarks of cancer[2]. Once duplicated, the genetic material has to be equally divided in two daughter cells. This division occurs on **M phase** or mitosis, which is subdivided in four different phases. The division of the genetic material starts with the condensation of DNA and the nuclear envelope breakdown during **prophase**. After that, the mitotic spindle is formed, which allows condensed chromosomes to be aligned in the center of the cell (**metaphase**). During this phase, the kinetochores of each sister chromatid are connected with the centrosomes present on each one of the poles of the cell through their attachment to the microtubules. Once all the kinetochores are properly attached to the microtubules, each sister chromatid is forced to migrate to one of the poles of the cell during **anaphase**. Finally, DNA is decondensed and the new nuclear envelopes are synthesize (**telophase**), while cell starts to divide (**cytokinesis**), thus forming two daughter cells containing the same genetic material[1].

For proper duplication and division, two additional phases are required, **G1** (gap 1) and **G2** (gap 2) phases, previous to S and M phases respectively. Cells duplicate and synthesize other necessary components for cell growth and division during those phases. Additionally, several extracellular and intracellular signals are integrated during those phases that will determine the progression or arrest of the cell cycle. During G1 phase for example, cells receive extracellular signals that determine the cell cycle entry. Once the restriction point has been bypassed, cells are forced to arrive to S phase, and to continue through all the cell cycle until next G1, independently of these extracellular signals. By contrast, the absence of growth factor or other extracellular signals during G1, before cells pass through the restriction point, can promote a reversible cell cycle exit into a **quiescent** state or **G0 phase**[1].

The ordered and correct progression thought the different cell cycle phases is accomplished by the correct regulation of cyclin-CDK (cyclin-dependent kinase) complexes[1]. Additionally, there are several mechanisms or **checkpoints** to ensure the proper completion of each cell cycle phase (Figure 1), preventing the progression

through a subsequent phase if the previous one has not properly been concluded[3]. The correct regulation of all these mechanisms is essential to guarantee a correct cell division and to avoid the transmition of errors to daughter cells.

The functions and regulation of those mechanisms are further explained in the following sections.

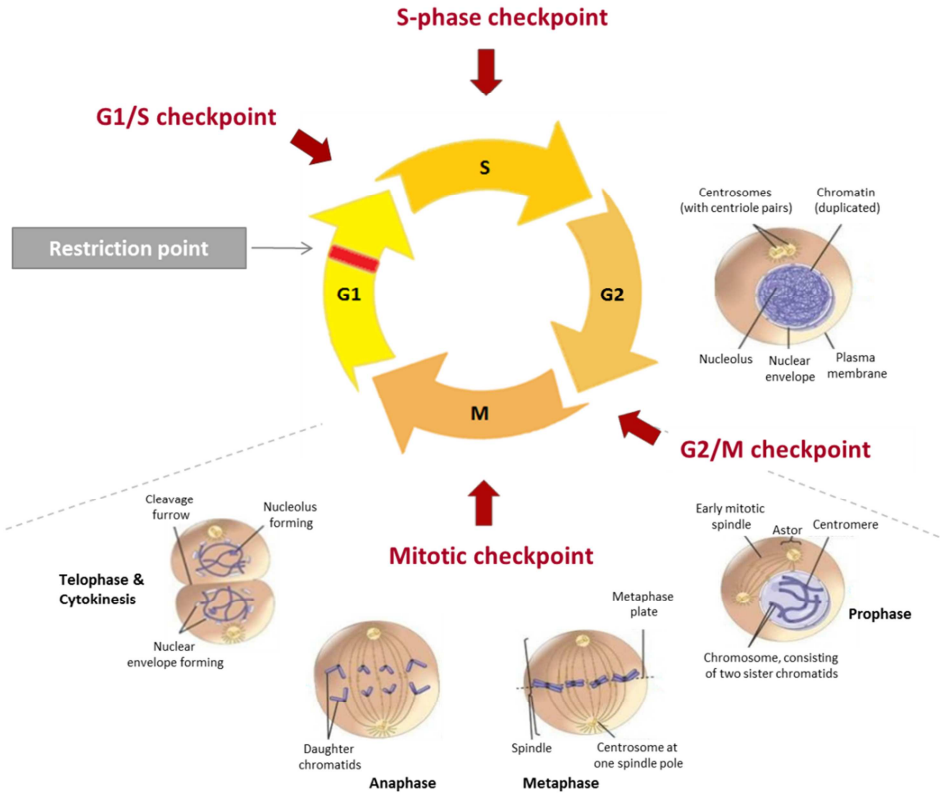

Figure 1. Cell cycle and checkpoints.
The cell cycle and mitotic phases, and the checkpoints acting on each of them are shown. Adapted from "The cell cycle, principles of control"[1].

1.1. Cell cycle regulation by cyclin-CDKs

1.1.1. Cyclin-CDK complexes

Cyclin-CDK complexes are essential factors for the progression and regulation of the cell cycle, in which **cyclin**s correspond to the regulatory subunits while CDKs represent the catalytic one. **CDK**s are Serine/Threonine protein kinases that cannot be activated without their association with cyclins. The interaction with cyclins promotes a conformational change essential for their kinase activity. Additionally, cyclins regulate the subcellular localization of CDKs, necessary for their association with substrates[1].

In mammals, CDK family contains 20 proteins although only some of them are essential for cell cycle regulation. Likewise, although 29 proteins have been shown to contain cyclin domains, not all of them are required for cell division[4,5]. From works done in mammal cells, it was described that the ordered progression through the cell cycle was accomplished by the progressive activation and inhibition of four different CDKs (CDK1, CDK2, CDK4 and CDK6) associated with four different cyclins (Cyclin A, Cyclin B, Cyclin D and Cyclin E)[6].

According to this model, CDK4 and CDK6 associated with Cyclin D are the first ones acting during G1 to promote the passage through the restriction point in response to extracellular signals. After that, Cyclin E-CDK2 is activated during G1/S transition to allow the cells to enter into S phase. Once in S phase, Cyclin E-CDK2 activity is gradually replaced by Cyclin A-CDK2, which has important roles for S-phase and G2 progression. At the end of the interphase, when cells are about to enter into mitosis, Cyclin A-CDK1 is activated to facilitate the onset of mitosis. Finally, Cyclin B-CDK1 is activated to progress through mitosis and allow the division of the cell (Figure 2)[6].

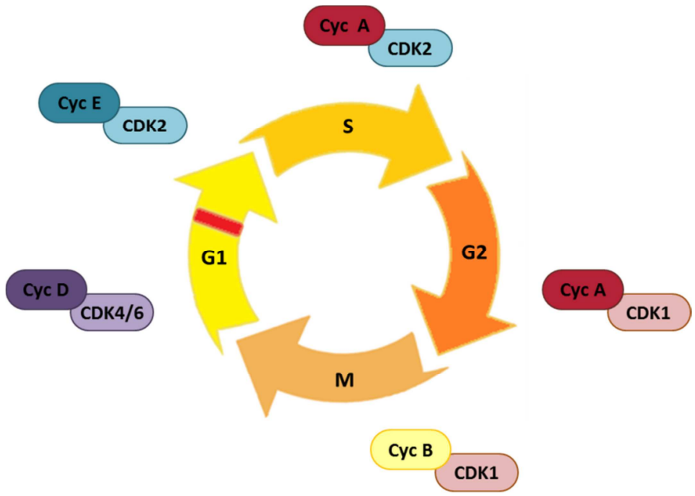

Figure 2. Cell cycle regulation by cyclin-CDKs.
The cyclin-CDK complexes acting on each cell cycle phase (or phases) are shown. Adapted from "The cell cycle: a review of regulation, deregulation and therapeutic targets in cancer"[7].

Remarkably, this classic model has recently been challenged, since studies using knockout mice have shown that there is a huge redundancy between CDKs. Those studies have shown that the deletion of CDK1 is the only one that cannot be compensated by other CDKs, and consequently, mice lacking CDK1 fail to develop morula and blastocyst stages[8]. By contrast, the deletion of the other CDKs alone or in combination does not abrogate the development at those stages[8–10]. Nevertheless, although their deletion may not be lethal for initial embryonic stages, it is thought that they are all essential for a correct development and survival of the complete organism and its germ line[6].

Similar to CDKs, cyclins do also present a huge redundancy. In mammals, there are different isoforms of each cyclin, which present specific expression patterns during embryonic development and adult tissues in some cases. These isoforms include: two Cyclin A isoforms (A1 and A2), three Cyclin B isoforms (B1, B2 and B3), three Cyclin D isoforms (D1, D2 and D3) and two Cyclin E isoforms (E1 and E2)[6]. Interestingly, although they all seem to be necessary for the development of certain tissues, Cyclin A2, Cyclin B1, Cyclin E1 and Cyclin E2 seem to be the only essential ones in most cases[11–14].

1.1.2. Regulation of cyclin-CDKs

Due to the importance of cyclin-CDK complexes for a correct cell cycle progression, these complexes are tightly regulated by several mechanisms that are explained below.

- *Synthesis and degradation of cyclins*

  As previously mentioned, it is generally accepted that each particular cyclin-CDK complex acts in a certain moment during the cell cycle, participating in different processes specifically on that phase (or phases). Therefore, cells have evolved to promote the ordered activation and inhibition of the different cyclin-CDK complexes during the cell cycle[6]. As a general rule, CDKs are constitutively expressed and are relatively stable, whereas cyclin levels oscillate[15]. Moreover, as each CDK presents affinity for a specific cyclin (or cyclins in some cases) the regulation of cyclin levels allows the ordered activation of cyclin-CDK complexes during the cell cycle. Thus, the first level of regulation of these cyclin-CDK complexes is based on the synthesis and degradation of cyclins, which allows the accumulation of a specific cyclin at each time (Figure 3)[16].

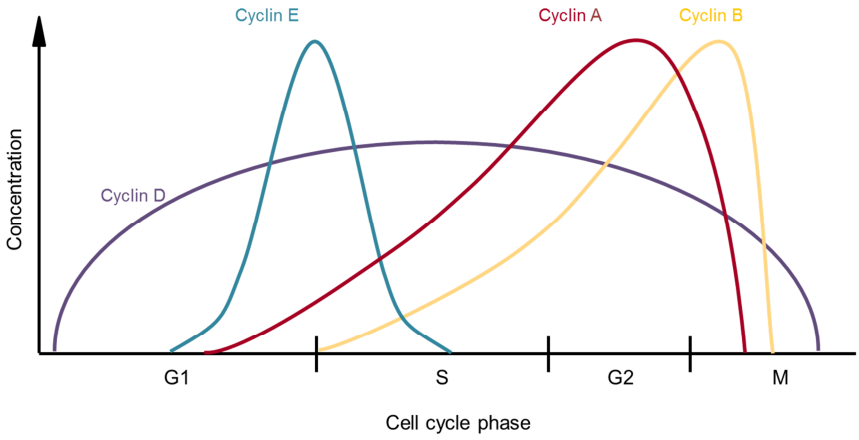

Figure 3. Cyclin levels oscillations throughout the cell cycle.
The levels of each cyclin through the cell cycle are represented on the graph.

The expression of a particular cyclin is usually promoted by the cyclin-CDK complex that acts just before during the cell cycle, thus allowing the ordered accumulation of the different cyclins. In this sense, in response to mitogenic signals, Cyclin D

expression is promoted by the activation of the Ras-Raf-MAPK (mitogen-activated protein kinase) pathway during G1. This accumulation of Cyclin D allows the activation of Cyclin D-CDK4/6, which in turn activates the E2F transcription factors, involved in the expression of Cyclin E, Cyclin A and other substrates[1,6,16].

E2F family (E2F1-8) contains 8 different transcription factors, which are classified as cell cycle activators (E2F1-3) or repressors (E2F4-8) based on their transcriptional roles[17]. However, several data suggest that in fact they can function as both depending on the cellular context. For instance, E2F1 and E2F2 depletion has been reported to result on accelerated DNA replication in bone marrow cells[18]. These transcription factors are important cell cycle regulators that control G1/S and G2/M transition, but also, processes such as apoptosis, DNA replication or repair.

E2F transcription factors are regulated by their association with ***pocket* family proteins** (pRb (Retinoblastoma protein), p107 and p130), which inhibit E2F proteins in the absence of appropriate extracellular signals[17,19–21]. In this sense, the activation of Cyclin D-CDK4/6 phosphorylates those *pocket* family proteins, promoting their dissociation from E2F1-3 transcription factors, thus allowing the expression of some of the E2F1-3 substrates such as Cyclin E in late G1. This results in the activation of Cyclin E-CDK2, which promotes G1/S transition. At this time, Cyclin E-CDK2 further phosphorylates *pocket* family proteins, resulting in an increased activation of E2F1-3 that allows the expression of Cyclin A from S phase on[1,6,16,19]. Finally, Cyclin A-CDK2/1 contributes to the expression of Cyclin B1 during S and G2 phases, as it phosphorylates and activates other transcription factors, such as NF-Y, b-Myb and FoxM1, essential for the expression of this last cyclin[22].

Apart from their synthesis, cyclins are also regulated by degradation through the ubiquitin-mediated proteasome system[16]. Two different E3 ubiquitin ligase complexes are responsible for the degradation of cyclins and other cell cycle regulators, **SCF** (Skp/Cullin/F-Box containing complex) and **APC/C** (anaphase-promoting complex/cyclosome)[23]. Cyclin D and Cyclin E are degraded by the SCF complex, either when they are free[24,25] or associated with CDKs[26–28], while Cyclin A and Cyclin B are degraded by the APC/C complex[29,30]. These complexes-mediated cyclins and other cell cycle components degradation, and their implication on cell cycle regulation, is further explained in section *(1.2)*.

- <u>*Regulation of cyclin-CDKs by phosphorylation and dephosphorylation*</u>

As previously explained, the association of cyclins with CDKs is essential for the activation of cyclin-CDK complexes. However, this interaction is not sufficient for their activation. Several phosphorylation and dephosphorylation events participate in the regulation of these complexes[16].

First, once associated with cyclins, CDK1 and CDK2 have to be phosphorylated, on Threonine 161 and 160 respectively, in order to become activate. These phosphorylations are mediated by another cyclin-CDK complex, the CAK (CDK-activating kinase)[31–34]. Notably, phosphorylation on Threonine 160 can be reverted

by Kap1 phosphatases, although it seems that this residue is only dephosphorylated once the partner cyclin has been degraded[35].

Additionally, cyclin-CDKs are phosphorylated on Threonine 14 and Tyrosine 15 in an inhibitory manner once the complex is established[36,37]. In higher eukaryotes, these phosphorylations are mediated by Myt1 and **Wee1** kinases respectively[38–40]. In order to become activate, Threonine 14 and Tyrosine 15 have to be dephosphorylated by **Cdc25** phosphatases. In mammals, three isoforms (A, B and C) of Cdc25 phosphatases have been described, which differ on their affinities for each cyclin-CDK complex, their expression pattern, subcellular localization and mechanism of action[41].

Due to the importance of the dephosphorylation of Threonine 14 and Tyrosine 15 for the activation of cyclin-CDK complexes, Wee1 and Cdc25 are tightly regulated by cell cycle checkpoints[42]. The mechanisms involved in this regulation are further explained in the following sections.

- *CKIs: cyclin-dependent kinase inhibitors*

Apart from the previously explained mechanisms, cyclin-CDK complexes are also regulated by CKI proteins, which in turn are controlled, at least in part, by the ubiquitin-mediated proteasome system[16,23]. **CKI**s are cyclin-CDK inhibitors that can be grouped in two main families that differ on their specificity to substrates and mechanism of action. **INK4** (inhibitor of Kinase 4/alternative Reading Frame) family proteins (**p16^{INK4a}**, p15^{INK4b}, p18^{INK4c} and p19^{INK4d}) can only interact with CDK4 and CDK6 kinases, disrupting their association with cyclins. On the other hand, **CIP/KIP** (CDK-interacting protein/kinase inhibitory protein) family proteins (p21^{CIP1}, p27^{KIP1} and p57^{KIP2}) can interact with all the cyclin-CDK complexes, promoting a conformational change that inhibits their kinase activity[43].

CIP/KIP proteins are important for cell cycle regulation during development and in response to stress[44]. In particular, **p21^{CIP1}** (from now on refer to as p21) for example has been shown to be implicated in differentiation, apoptosis and senescence[45–47]. Additionally, p21 is an important transcriptional target of **p53** transcription factor that mediates the DNA damage-induced G1 and G2 arrests[48,49]. Moreover, p21 has also CDK inhibitor-independent roles that regulate the cell cycle. For instance, p21 inhibits E2F1[50] and other transcription factors[45] by its direct binding to promoters. These and other p21 functions are further explained in sections *(3.2)* and *(3.4)*.

All the previously described regulatory mechanisms (summarized on Figure 4) are essential to ensure the proper coordination of cyclin-CDKs in order to guarantee the correct completion of the cell cycle[16].

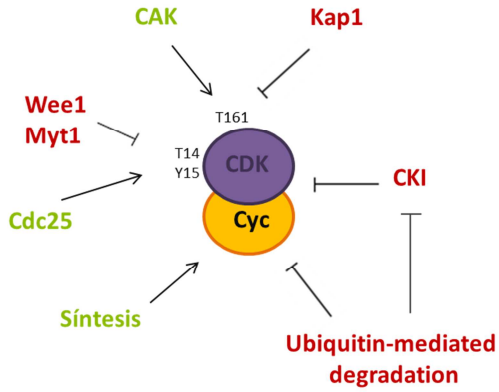

Figure 4. Regulation of cyclin-CDKs.
Summary of the mechanisms involved in the regulation of cyclin-CDK complexes. Adapted from "The role of Cdk7 in CAK function, a retro-retrospective"[51].

1.2. Cell cycle regulation by the ubiquitin proteasome system

The **UPS** (ubiquitin proteasome system) consist in the association of several **ubiquitin** (a small highly conserved protein) molecules to target substrates in a process known as **ubiquitylation**, to finally induce their degradation through the 26S proteasome complex. This ubiquitylation occurs in three consecutive enzymatic steps: 1) First, the ubiquitin molecule is linked to an ubiquitin-activating enzyme (**E1**) and activated in an ATP-dependent manner; 2) After that, the activated ubiquitin is transferred to an ubiquitin-conjugating enzyme (**E2**); 3) Finally, an (**E3**) ubiquitin ligase binds the ubiquitin molecule to a specific Lysine residue on the target protein. Once marked with several ubiquitin molecules on a specific Lysine residue (**polyubiquitylation**), target proteins are recognized and degraded by the 26S proteasome complex[52,53].

Apart from the formation of polyubiquitin chains, UPS also mediates the addition of individual ubiquitin molecules to a particular Lysine (**monoubiquitylation**) or several molecules to different Lysine residues of the same substrate (**multimonoubiquitylation**). While Lysine 11- and Lysine 48-linked polyubiquitin chains-containing substrates are committed to 26S proteasome complex-mediated degradation, mono- and polyubiquitilations in other Lysine residues induce and regulate other non-proteolytic functions[52,53].

Additionally, cells contain **DUB**s (deubiquitinating enzymes) that are able to hydrolyze ubiquitin-protein peptide bonds to reverse the ubiquitylation of substrates, leading to a model in which ubiquitylation is controlled by the balance between an E3 ligase and a DUB[52,53].

E3 ubiquitin ligases are the responsible for substrate recognition and thus, cells present multiple E3 ubiquitin ligases to provide specificity and versatility to the UPS[52,53]. These enzymes can be subdivided in two major classes: 1) **HECT** (homologous to E6-AP C-terminus) family E3 ligases, which form transient covalent linkages with ubiquitin during the ubiquitylation process; and, 2) **RING** (really interesting new gene) family E3

ligases that only mediate the transfer of ubiquitin from the E2 directly to the substrate. This last class includes proteins that contain RING and the substrate adaptor domain, and multisubunit complexes, in which these domains are part of distinct proteins within the complex[53]. From those multisubunit RING ligases, **CRL** (cullin RING ligase) superfamily is the most important for the regulation of the cell cycle as it contains the SCF and APC/C complexes, which are responsible for the degradation of several cell cycle regulators[23,52,53].

1.2.1. SCF: Skp1/Cullin1/F-box containing complex

Three invariable components (**Rbx1** RING-finger protein, **Cul1** scaffold protein and **Skp1** adaptor protein) and an additional variable component known as F-box protein form the SCF complex (Figure 5)[23,52,53].

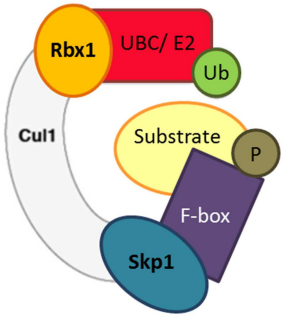

Figure 5. Structure of the SCF ubiquitin ligase.
On one side, the SCF binds to an E2 ubiquitin conjugating enzyme through its Rbx1 domain. On the other side, the SCF is connected to the substrate through its association with the F-box protein. Adapted from "The ubiquitin proteasome system"[53].

F-box proteins, which are the substrate binding subunits, are formed by a 40-amino-acid motif and an additional substrate binding domain. According to this last substrate binding domain, F-box proteins can be classified in three different groups: 1) Fbxws proteins, which contain WD-40 domains; 2) Fbxls proteins that present Leucine-rich repeats; and, 3) Fbxos proteins, which include diverse motifs such as Proline-rich motifs among others. The phosphorylation of target substrates is generally required for F-box-mediated substrate recognition, as most of them recognize specific **phosphodegron**s (phosphorylated destruction motifs)[23,52–54].

Since F-box proteins are the responsible for substrate recognition, around 70 of them have been described until now in human cells. However, from those, only three are involved in cell cycle regulation: **Skp2** (FBXL1), **Fbw7** (FBXW7) and **β-TrCP** (FBXW1/11). These F-box proteins, together with the SCF complex, regulate the S-phase entry and the mitotic onset by targeting several proteins. Some of their substrates include cyclin-CDK regulators[23,52,53]. Skp2 for example targets various cell cycle inhibitors such as CIP/KIP family proteins ($p21^{CIP1}$ and $p27^{KIP1}$ for instance)[28,55–58], and also *pocket* family proteins[59]. By contrast, Fbw7 promotes the degradation of Cyclin E[60–62] and other proliferation agents[63]. β-TRCP in turn controls the levels of cyclin-CDK regulators such

as Wee1[64] and Cdc25A[65], and it also induces the degradation of **Emi1** (an APC/C inhibitor) at the onset of mitosis[66,67].

These SCF functions and their regulation during the cell cycle are summarized on section *(1.2.3)*.

1.2.2. APC/C: anaphase-promoting complex/cyclosome

APC/C is a multisubunit cullin-RING E3 ubiquitin ligase structurally similar to the SCF complex (Figure 6), which is composed of at least 13 different proteins. This includes the **Apc11** RING-finger protein, which interacts with the ubiquitin conjugating enzyme, and the **Apc2** cullin-like subunit, that serves as scaffold protein. In somatic cells, APC/C is activated through its association with **Cdc20** or **Cdh1** (also known as Fzr1) coactivators. Additional APC/C coactivators function during meiosis and in non-dividing cells[23,52,68].

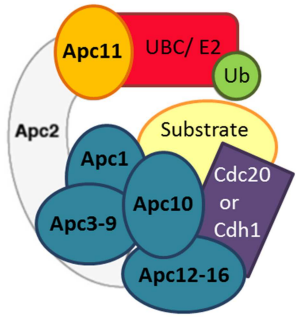

Figure 6. Structure of the APC/C ubiquitin ligase.
As in the case of SCF, one side of APC/C ubiquitin ligase is associated with the ubiquitin conjugating enzyme, in this case through its RING-finger protein Apc11. The other side of the complex is associated with the substrate through Cdc20 or Cdh1 adaptor proteins with the help of Apc10. Adapted from "The ubiquitin proteasome system"[53].

Cdc20 and Cdh1 adaptor proteins confer substrate specificity to APC/C in the same way that F-box proteins do to the SCF complex. They recognize short **degron**s (destruction motifs) on target substrates through C-terminal domains composed of WD40 repeats. The canonical destruction motifs recognized by APC/C are the **D-box** (consensus sequence RXXLXXXXN) and the **KEN-box** (consensus sequence KENXXXN). Efficient ubiquitylation of substrates depends on both degrons. However, some substrates only present one of them, in one or more copies, which gives certain specificity, since Cdc20 preferentially recognizes D-box motifs while Cdh1 recognizes both of them[52,68]. Apart from the interaction with these coactivators, the association of APC/C with its substrates is thought to require an additional interaction with Apc10 subunit of the core complex[52,68]. Additionally, a class of non-canonical APC/C recognition motif is thought to contribute to the degradation of some substrates, as some of them lack both, D-box and KEN-box, destruction motifs[68].

- *Regulation of APC/C*

APC/C^{Cdc20} is important to ensure correct chromosome segregation and to coordinate mitosis with cytokinesis. As a consequence, this complex is active from prometaphase until at least telophase[69–72]. APC/C^{Cdh1} in turn is important for mitotic exit and G1 maintenance, and thus, it is active from late mitosis until G1/S transition, when it has to be inactivated for proper S-phase completion[71–74].

The inactivation of APC/C^{Cdh1} at G1/S transition is accomplished by several mechanisms[53,68,75–77]. First, UbcH10, an APC/C specific E2 ubiquitin conjugating enzyme is ubiquitylated by APC/C^{Cdh1}, providing a negative feedback loop that starts to reduce the activity of APC/C^{Cdh1} [78]. Likewise, APC/C itself is autoubiquitylated by APC/C^{Cdh1}, further contributing to the inhibition of this E3 ubiquitin ligase[79]. Furthermore, an unidentified SCF complex participates in the degradation of Cdh1 during S phase[80]. Moreover, CDKs phosphorylate Cdh1 compromising its association with APC/C during S, G2 and early mitosis[81–89]. Nevertheless, despite all the previous mechanisms, APC/C^{Cdh1} is not completely inhibited until Emi1 is expressed[75].

Emi1 is an APC/C inhibitor that acts as a pseudosubstrate[90–92]. This protein synthesis is induced by E2F1 and E2F3 transcription factors at the end of G1, when pRb is phosphorylated and thus, E2F transcription factors are released[93]. While cells progress through the cell cycle and arrive to prophase, Emi1 levels start to decrease due to $SCF^{\beta TrCP}$-mediated proteolysis, as a result of consecutive Cyclin B-CDK1- and Plk1-mediated phosphorylations[66,67,94,95]. To avoid premature degradation of Emi1, this protein is stabilized by its association with **Evi5** during G2[96]. In mitosis, Evi5 is phosphorylated and degraded, allowing the degradation of Emi1[96]. Additionally, Emi1 has been shown to be phosphorylated in mitosis to inhibit its association with APC/C[97]. Apart from Emi1 downregulation, Cdc20 accumulation during S, G2 and mitosis, as well as Cyclin B-CDK1-mediated APC/C phosphorylation, are required for the activation of APC/C^{Cdc20} [77,98].

Until a few years ago, Emi1 downregulation was thought to be essential for the activation of APC/C^{Cdc20} in prometaphase[67,92]. However, a more recent study challenged this idea since cells expressing a non-degradable Emi1 were shown to be able to degrade Cyclin A and other APC/C^{Cdc20} substrates at the same time as control cells[99]. In any case, low Emi1 levels together with increased Cyclin B-CDK activity results in favorable conditions for the activation of APC/C^{Cdc20} in prometaphase[98], while APC/C^{Cdh1} would remain inactive due to CDK-mediated Cdh1 phosphorylations[81–89]. However, APC/C^{Cdc20} is kept inactive until anaphase by the **SAC** (spindle assembly checkpoint, also known as mitotic checkpoint), although there are proteins that can be degraded independently of it[69,72–74,77,100–103].

After anaphase, APC/C^{Cdc20} is progressively replaced by APC/C^{Cdh1} [77]. Cdh1 and UbcH10[78] re-accumulation during G2 and the decrease in cyclin-CDK activity contribute to the activation of this complex[53,77]. In yeast, Cdc14 phosphatase-mediated Cdh1 dephosphorylation participates in the activation of APC/C^{Cdh1} [104,105]. Nevertheless, the contribution of this phosphatase to the activation of

APC/C^{Cdh1} during a normal cell cycle in higher eukaryotes has not been elucidated yet.

Once activated, APC/C^{Cdh1} mediates the degradation of Cdc20[106,107], thus inducing a complete switch from APC/C^{Cdc20} to APC/C^{Cdh1} [77], which would remain active until G1/S transition when, as explained, several mechanisms will induce its inhibition[53,68,75–77].

- *Functions of APC/C during mitosis*

Cells have two major challenges during mitosis: to ensure that each daughter cell receives an equal and identical genomic material; and to prevent cell separation before chromosome segregation. These problems are solved by the controlled degradation of Securin and Cyclin B by APC/C^{Cdc20} [69,72,98,103,108,109].

At the initial stages of mitosis, cohesins maintain sister chromatids together before their segregation. For chromosome segregation, Separase-mediated Scc1 cohesin subunit cleavage is required. However, this protease is inactive through its association with a small protein known as **Securin**, which acts as a chaperone and an inhibitor of Separase. Additionally, Cyclin B-CDK1 inhibits Separase by direct binding and phosphorylation. In this sense, the activation of APC/C^{Cdc20} during mitosis initiates the ubiquitylation of Securin and Cyclin B, resulting in the activation of Separase and the inactivation of CDK1. This in turn allows Separase to cleave cohesins to liberate sister chromatids at the anaphase onset, allowing chromosome segregation. Notably, cytokinesis is inhibited by Cyclin B until its degradation, to avoid cell separation before chromosome segregation[69,72–74,77].

To prevent premature separation of sister chromatids and mitotic exit, APC/C^{Cdc20} is inhibited by the SAC, which is activated by unattached kinetochores. Only when the sister chromatids are aligned at the metaphase plate and have established bivalent spindle attachments can the APC/C^{Cdc20} be activated[69,72–74,77].

In addition to Securin and Cyclin B, APC/C^{Cdc20} targets several other proteins for degradation such as Cyclin A, Nek2 (a kinase that regulates centrosomes separation) and $p21^{CIP1}$. These proteins are degraded after nuclear envelope breakdown, before metaphase-anaphase transition, and their degradation is not inhibited by the SAC[69,72,73,100–103].

The decrease of cyclin-CDK activity as a consequence of Cyclin B degradation at the end of mitosis, results in Cdh1 dephosphorylation and the activation of APC/C^{Cdh1}. Once activated, this E3 ubiquitin ligase allows mitotic exit by targeting for destruction other kinases such as **Plk1**[110], **Aurora A**[111,112] and **Aurora B**[113]; and by completing the elimination of Securin[108] and mitotic cyclins[114]. Furthermore, as previously explained, Cdh1 also degrades Cdc20[106,107], leading to a complete switch from APC/C^{Cdc20} to APC/C^{Cdh1} during the exit from mitosis[72,73].

- *G1 maintenance and regulation of DNA replication by APC/C^{Cdh1}*

After its activation during late mitosis, APC/C^{Cdh1} is preserved in an active state during G1 to maintain cells in this phase until the extracellular signals that determine the cell cycle entry are receive and the necessary factors for a new cell cycle round are synthesize. Additionally, the activation of this ubiquitin ligase in G1 is essential for the correct regulation of DNA replication[71–74].

Due to the large size of the eukaryotic genome, DNA replication is accomplished by the coordinated activation of hundreds of thousands of replication forks, which allows timely completion of genome duplication and the establishment of a **replication timing program** (different regions of the genome are replicated at different times). However, the use of multiple origins makes it more difficult to ensure the complete replication of the genome without re-replicating certain areas. To solve it, cells have developed a system in which replication is divided in two non-overlapping steps: **origin licensing** or the formation of **pre-RC**s (pre-replication complexes) that occurs during late mitosis and G1; and **origin firing** or the activation of origins, which takes place during S phase[115–118].

During mitotic exit, replication origins are recognized by **ORC** (origin recognition complex). After that, in G1 phase, **Cdc6** and **Cdt1** allow the loading of two **MCM2–7** (minichromosome maintenance protein complex) hexamers around DNA in an antiparallel conformation, forming the pre-RC. Finally during S phase, hundreds of those pre-loaded origins are fired by the sequential action of **DDK** (Dbf4-dependent kinase) and CDK kinases, which phosphorylate key components and facilitate the recruitment of **Cdc45** and **GINS**, thus forming and stabilizing the **CMG** (Cdc45-MCM-GINS) helicase complex[117,119–124]. The factors involved in DNA replication and their regulation are further explained in section *(2)*.

Each origin can only fire once and origin licensing is limited to G1 phase. Therefore, pre-RCs are loaded in excess on the genome to allow replication to be completed in case fired origins stall[125].The limitation of origin licensing to G1 phase and the prevention of origin firing during this phase, both essential to prevent **rereplication** (the same DNA fragment is replicated more than ones), is accomplished by the activation of APC/C^{Cdh1} [72,73,116,118].

During G1, APC/C^{Cdh1} degrades several of its substrates such as Cyclin A[114], Cyclin B[114], Cdc25A[126] and Tome-1 (involved in the proteolysis of Wee1)[127] which maintains low levels of CDK activity and thus, allows the maintenance of cells in G1[71–73]. Moreover, APC/C^{Cdh1} also degrades components of the SCF complex, such as Skp2[128,129] and Cks1[129], which as previously explained are involved in p27^{Kip1} and p21^{Cip1} CKIs and other proteins degradation[28,55–58]. Consequently, APC/C^{Cdh1}-mediated Skp2 and Cks1 proteolysis, also participates in the maintenance of cells in G1 by inhibiting for example Cyclin E-CDK2 complexes[71–73].

Additionally, APC/C^{Cdh1} also targets **Geminin**[130,131], a Cdt1 inhibitor[132,133], for degradation. This, together with low CDK activity, allows Cdt1 to be in a dephosphorylated and free state necessary for origin licensing[71–73]. Furthermore, low CDK activity also prevents Cdc6 phosphorylation and its consequent

degradation[134–137] or export from nuclei[138,139], thus allowing the formation of pre-RCs[71–73]. Surprisingly, Cdc6 has been shown to be an APC/C^{Cdh1} substrate[140]. However, it is thought that APC/C reduces its affinity for Cdc6 during G1[141].

Apart from promoting origin licensing, APC/C^{Cdh1} is also important to prevent origin firing during G1. The low CDK activity levels, together with the degradation of other proteins, such as Tk1[142,143] and Tmpk[143] enzymes involved in dNTP (Deoxyribonucleotide triphosphates) synthesis, avoids origin firing during G1[71–73].

Due to the importance of APC/C^{Cdh1} in G1 maintenance and correct replication, its ablation induces genomic instability[72,73,144]. For instance, cells in which Cdh1 has been depleted, prematurely enter S phase resulting in aberrant DNA replication[145–147]. Likewise, Cdh1-depleted cells obtained from Cdh1 lacking embryos proliferate inefficiently and accumulate numeric and structural chromosomal aberrations[148]. Moreover, Cdh1 heterozygous animals show increased susceptibility to spontaneous tumors[148]. Furthermore, Cdh1-depleted cells have been shown to be able to enter into mitosis despite incomplete replication, which results in the accumulation of **DSB**s (double-strand breaks) and anaphase bridges, as well as in cytokinesis defects and tetraploidization[149]. Collectively, all the previous results seem to indicate that APC/C^{Cdh1} acts as a tumor suppressor. In fact, APC/C^{Cdh1} has been described to be activated in response to DNA damage to degrade several of its substrates and to induce a G2 arrest[150–152]. Interestingly, APC/C has been shown to be mutated in several tumor cells[153]. DNA damage-induced APC/C^{Cdh1} activation and its consequences are further explained in sections *(3.2.2)* and *(3.4.2)*.

As previously explained, the inhibition of APC/C^{Cdh1} is essential to prevent origin licensing in S phase, and thus, its aberrant activation might also cause genomic defects. In this sense, Emi1 depletion-promoted APC/C^{Cdh1} activation results in Geminin and Cyclin A degradation, causing rereplication in several non-transformed and tumor cell lines[99,154].

Apart from the previously described cell cycle regulator roles, APC/C is also involved in many other cell cycle-independent cellular functions[70,72,74].

1.2.3. Interplay between SCF and APC/C during the cell cycle

The previously explained functions of the SCF and APC/C ubiquitin ligases in cell cycle regulation are summarized on Figure 7.

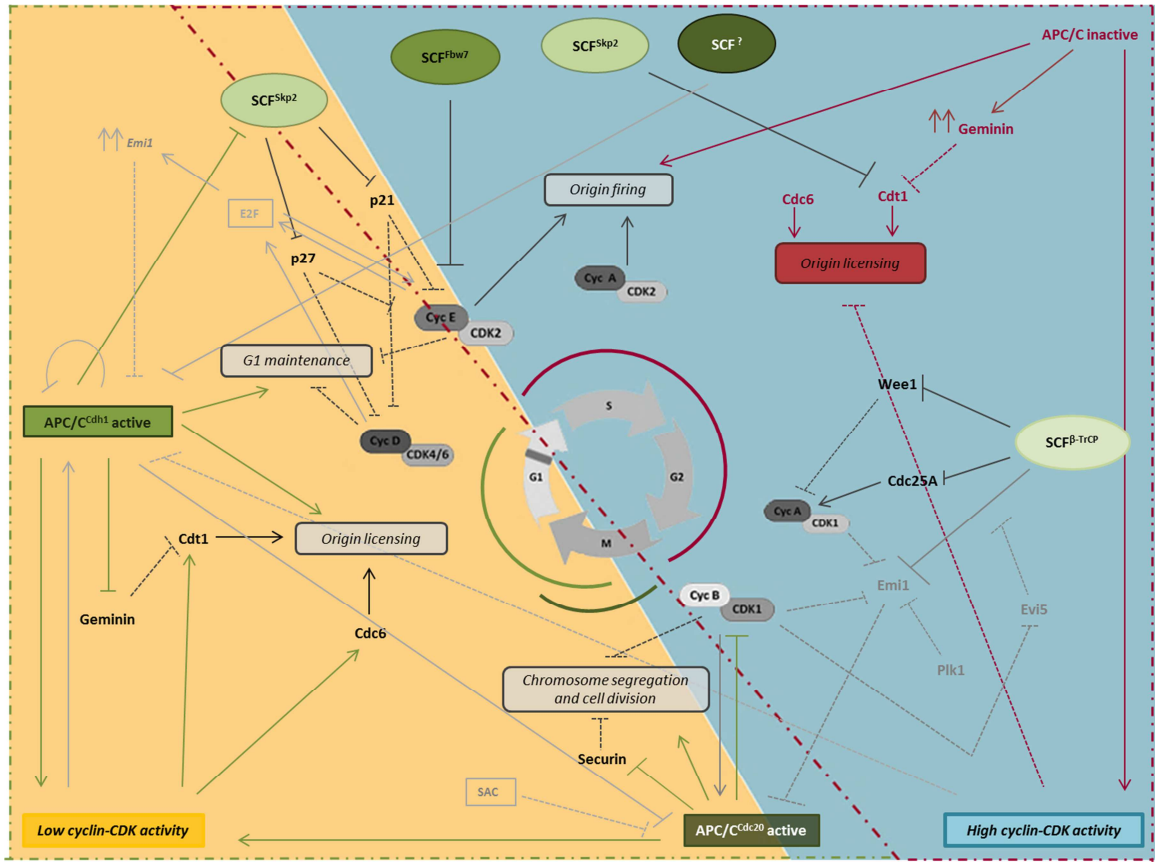

Figure 7. Interplay between SCF and APC/C during the cell cycle.
Summary of SCF and APC/C ubiquitin ligases functions during the cell cycle. The positive and negative regulations of the different proteins, is represented with arrow and bar-head lines respectively. Continuous bar-head lines correspond to degradation-mediated inhibition, while dotted ones represent other ways of inhibition. Cyclin-CDK activity levels are represented in orange (low) and blue (high). The main functions regulated by the APC/C ubiquitin ligase during cell cycle are represented as grey boxes. Green (active) and red (inactive) color correspond to APC/C and SCF activation state. Green and red lines around cell cycle phase's diagram correspond to APC/C activation state. The dotted red line defines inactive APC/C region whereas the dotted-green line represents the active one. The functions regulated by APC/C ubiquitin ligase when is active or inactive are represented with green and red colors respectively. The inactive state of one of the functions regulated by APC/C is represented as a red box. The mechanisms involved in the regulation of APC/C are represented in light grey.

2. DNA replication

DNA replication consists in the duplication of the genetic material in order to obtain two copies of the same information, to finally transmit it to daughter cells. As previously explained, this process occurs in two non-overlapping consecutive steps, each of them working on a specific cell cycle phase. During G1, pre-RCs are formed in a process known as origin licensing; whereas in S phase, thousands of those pre-loaded origins are fired, in order to duplicate the genetic material. The uncoupling of these steps in two different cell cycle phases is essential to guarantee a correct duplication of the genome[1,115–118].

Apart from DNA itself, the epigenetic information must also correctly be propagated into daughter cells to preserve epigenome integrity. Therefore, the duplication of the genetic material and the transmition of the epigenetic information to new DNA strands are tightly coordinated during S phase. Additionally, increasing evidences suggest that chromatin architecture/organization and nuclear structure are also involved in the activation of origins and correct regulation of DNA replication[155–159].

The main mechanisms involved in all this processes and their regulation are summarized on this section.

2.1. DNA replication: initiation, elongation and termination

Once origins have been licensed, DNA replication in S phase occurs in three consecutive phases that result in whole-genome duplication. In eukaryotic cells, this process requires the action of around 40–50 distinct proteins that comprise the replication apparatus or replisome[160]. This section summarizes how are origins fired during S phase (initiation), and how replication forks progress (elongation) until they converge with adjacent replication forks (termination)[161].

2.1.1. Initiation

DNA replication in S phase starts with the asynchronous activation of several pre-RCs in a process that depends on CDK2 and DDK kinases[162,163]. The phosphorylation of pre-RCs and other proteins allows a stable CMG complex formation onto chromatin, thus forming the **pre-IC** (pre-initiation complex). The following unwinding of DNA by CMG helicase results in the formation of bidirectional replication forks, and the consequent initiation of nascent DNA synthesis[164,165].

The formation of a stable CMG complex to induce the initiation of DNA replication is a process conserved from yeast to human, despite the mechanism of recruitment of Cdc45 and GINS proteins slightly differ between the different species[164,165]. These mechanisms have been mainly studied in budding yeast, where a model for CMG complex formation has been proposed (Figure 8). In this model, DDK-mediated MCM2-7 complex phosphorylation[162,166] promotes the formation of CMG complex and the initiation of DNA replication. Additionally, CDK2 phosphorylates several factors that are not part of the replisome but are essential for a stable CMG complex formation[164,167]. Some of these factors include **Sld2** and **Sld3** proteins, the phosphorylation of which

promotes their interaction with **Dpb11**, a protein required for the formation of CMG complex[168–171]. In particular, Sld3 was shown to be recruited to chromatin in a mutually dependent manner with Cdc45[172], although Sld3 is required only for initiation while Cdc45 is also necessary for elongation[172,173]. On the other hand, CDK2-mediated Sld2 phosphorylation was shown to promote the formation of a **pre-LC** (pre-loading complex). This complex is composed by GINS, Polymerase ξ (epsilon), Dpb11 and Sld2 proteins[174], and acts as a carrier of GINS to the pre-RC, where Dpb11 is thought to be the responsible for the association of this complex with the already recruited Sld3 and Cdc45 proteins, to finally form an active CMG helicase[167].

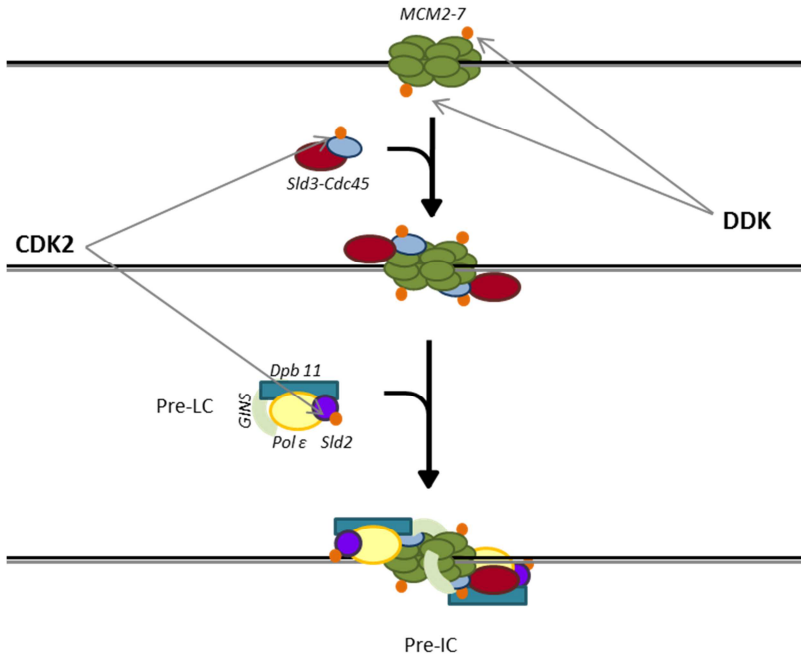

Figure 8. A model for DNA replication initiation in budding yeast.
Schematic of the mechanism involved in the formation of CMG helicase complex in budding yeast. Orange spots correspond to phosphorylations. Adapted from "Initiation of chromosomal DNA replication in eukaryotic cells; contribution of yeast genetics to the elucidation"[165].

Further studies have shown that the mechanism for the formation of pre-ICs is quite similar also in fission yeast, with a few differences such as the requirement of DDK for the phosphorylation of Sld3 and its recruitment to origins[164].

Interestingly, the process of CMG complex formation seems to be quite similar also in higher eukaryotes[164,165]. In this sense, DDK-mediated MCM2-7 phosphorylation is required for CMG complex formation also in human cells[175]. Additionally, **TopBP1**, **Treslin** and **RecQ4** (orthologs of yeast Dpb11, Sld3 and Sld2 respectively), have also been shown to be required for stable CMG complex formation[164,165]. In this sense, TopBP1 for example has been shown to interact with Cdc45[176]. Moreover, the phosphorylation of Treslin by CDK2 is essential for its interaction with TopBP1 and the

consequent CMG helicase complex formation in *Xenopus laevis* and human cells[177,178]. Furthermore, *Xenopus laevis* RecQ4 can be phosphorylated by CDK at least *in vitro*, and it can directly bind TopBP1[179]. However, in contrast to yeast, CMG complex can be assembled independently of RecQ4 in higher eukaryotes, despite it is required for the initiation of DNA replication[179,180]. In addition, other proteins such as GEMC1 (Geminin coiled-coil domain-containing protein 1) and DUE-B (DUE binding protein) have also been shown to be required for stable CMG complex formation in *Xenopus laevis* egg extracts[181,182]. Likewise, MCM10 is also thought to be important for CMG complex formation and the initiation of DNA replication[183].

2.1.2. Elongation

Once pre-IC complex has been formed, DNA starts to be unwinded by the CMG helicase, resulting in the formation of two bidirectional replication forks, each of them containing two antiparallel ssDNA (single-stranded DNA) templates together with replisome components (Figure 9). In eukaryotes, these ssDNA templates, which are used by the replicative DNA polymerases to synthesize nascent DNA strands, are stabilized by the heterotrimeric complex **RPA** (replication protein A). The heterotrimeric complex RPA is formed by RPA70 (RPA1), RPA32 (RPA2) and RPA14 (RPA3) subunits, and interacts with ssDNA to protect it from nucleases degradation[160,184,185].

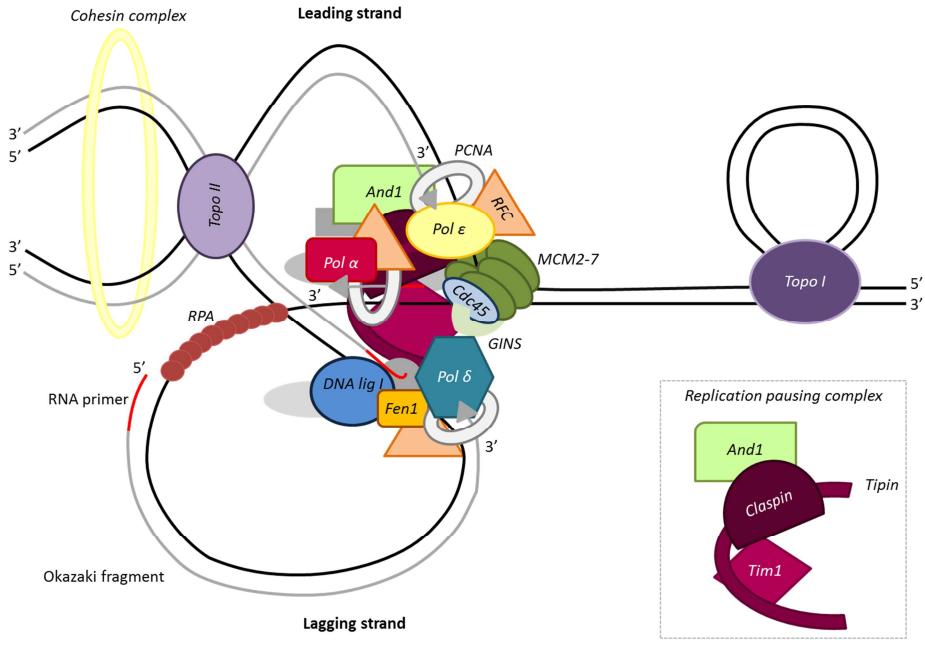

Figure 9. Ongoing replication fork.
Parental strands (in black) and nascent DNA strands (in grey) are represented together with their directionality. The proteins that compose the replication pausing complex and the main replisome components are represented.

During DNA unwinding, positive supercoils ahead of the fork and catenates behind it are formed, and thus, topoisomerases are required to relax the DNA. DNA topoisomerases are enzymes that act as swivels to relax the DNA by inducing transient DNA breaks through which strand passage can occur. There are two types of DNA topoisomerases: **type I topoisomerases**, which carry out strand passage through a reversible SSB (single-strand break), important during elongation; and **type II topoisomerases**, which mediate strand passage through a DSB, essential for termination[186].

Three replicative **DNA polymerases** have been described to be required for chromosomal DNA replication in eukaryotes: **α** (alfa), **δ** (delta) and **ξ** (epsilon). These enzymes catalyze the addition of dNTPs to 3'-OH ends of nucleotides, and as a consequence, DNA is synthesized in 5' → 3' direction. Moreover, due to the antiparallel nature of the duplex DNA, replication occurs in opposite direction on both DNA strands. In this sense, the **leading strand** is synthesized by Polymerase ξ in a continuous fashion as it progresses in the same direction as DNA unwinding. By contrast, the **lagging strand** is synthesized by Polymerase δ in the opposite direction to DNA unwinding and consequently, its synthesis is discontinuous, producing small DNA fragments of around 100-200 bases known as **Okazaki fragments** [187–192].

As DNA polymerases are not able to synthesize DNA *de novo*, pre-existing nucleotide **primers** are required for strand elongation. In this sense, Polymerase α associated with an RNA primase acts as a replicative primase generating a 10 nucleotide RNA fragment followed by 10-20 DNA bases. The presence of these primers is required at the beginning of each leading strand and at the 5' end of each Okazaki fragment. Once primers are synthesized, Polymerase α is replaced, with the help of clamp loaders, by Polymerase ξ and δ to continue the elongation of DNA strands[160,193–195].

Due to the semiclosed hand structure of polymerases, additional proteins are required to stabilize their association with DNA and increase their processivity. In eukaryotes, ring-shape trimer DNA sliding clamp known as **PCNA** (proliferating cell nuclear antigen) is the responsible for the stabilization of polymerases onto chromatin. Additionally, this protein acts as a platform for a large number of replication and repair factors[160,196]. To be loaded onto chromatin, PCNA must be opened and then closed around DNA, which in eukaryotes is accomplished by the pentameric clamp loader **RFC** (replication factor C; RFC1-5; RFCA–E; p140, p40, p36, p37 and p38)[197].

Finally, to complete lagging strand synthesis, Okazaki fragments must be processed to remove 5' RNA primers. Several proteins, such as **Fen1**, RNAseHII and Dna2 have been shown to be implicated in this process. However, the exact contribution of each of them to the maturation of Okazaki fragments is still unknown. Once primers have been removed, DNA fragments are sealed together by **DNA ligase I** to form a continuous DNA strand. Interestingly, PCNA is important for the maturation of Okazaki fragments as it acts as a platform for, among others, Fen1 and DNA ligase I recruitment[160,198].

Apart from all these factors, correct DNA replication requires additional proteins involved for instance in coupling helicases with polymerases, to avoid the accumulation of large ssDNA tracts that can induce aberrant DNA repair processes. This coupling is

mainly accomplished by the **RPC** (replication pausing complex) that travels with the replisome[199], although ATR itself is also thought to participate in this process through the regulation of MCM-mediated unwinding[200–203]. In metazoan, the RPC is composed by **Tim1**, **Tipin**, **Claspin** and **And1** proteins that can interact with several replisome components. Interestingly, these proteins are part of the **replisome progression complex** which links MCM helicase with other replisome components such as Polymerase α for proper DNA replication[199,204,205]. Additionally, while replication forks progress, the resulting sister chromatids must be maintained together for their correct segregation in mitosis. This is accomplished by the ring-shape **cohesin complex**, which in somatic vertebrate cells is composed by: **SMC1** (structural maintenance of chromosomes protein 1), **SMC3** (structural maintenance of chromosomes protein 3), Rad21 and SA1/2. The sister chromatid cohesion mediated by this complex is important not only for proper segregation but also, for **HR**- (homologous recombination) mediated DNA repair[206].

2.1.3. Termination

The termination of DNA replication occurs at random sites when two adjacent forks converge. When this happens, replisome must be disassembled from DNA and catenates must be resolved by type II topoisomerases to avoid the accumulation of aberrant structures that may induce genomic instability. In contrast to initiation and elongation steps, termination is still poorly understood, as it occurs asynchronously during replication and thus, it is difficult to study[207].

Overall, the termination of DNA replication is thought to involve four different steps: 1) Last stretch of parental DNA between the forks must be unwound by dissolution; 2) Remaining gaps on nascent-DNA strand must be filled; 3) Aberrant DNA structures such as catenates must be resolved; and, 4) Replisome must be disassembled[208].

This process has been mainly studied in SV40 system, were its been described that dissolution of parental strands during termination requires the rotation of the entire fork, which results in the formation of catenations behind the fork that must be resolved by a type II topoisomerase[209,210].

Additionally, recent works in *Xenopus laevis* and *Saccharomyces cerevisiae* have described that the disassembly of the replisome during termination is mediated by MCM7 polyubiquitylation, which promotes the disassembly of MCM2-7 from CMG complex and its further degradation, with the help of Cdc48/p97 segregase[211,212]. This MCM7 polyubiquitylation occurs only on active CMG complexes, and not in all MCM2-7 molecules present on chromatin, thus suggesting, that the mechanisms by which active and inactive helicases are disassembled are different[207]. Interestingly, this MCM7 polyubiquitylation in budding yeast have been described to be mediated by SCF^{Dia2}, which can interact with components of the replisome progression complex. However, this interaction is thought to increase the association of SCF^{Dia2} with the replisome in order to favor MCM7 polyubiquitylation, rather than inducing the ubiquitylation of this protein itself[212,213].

Based on the current knowledge, three different models have been proposed to explain the termination of DNA replication. The first one, known as "**simultaneous removal of**

converging replisomes", consist in direct collision between adjacent forks, after which both helicases are disassembled at the same time, and additional factors resolve the final sections of DNA. The second one proposes that one of the helicases is disassembled while the other one finishes replication without the requirement of additional factors. This model is known as the "**sequential removal of converging replisomes**". Finally, the third model, known as "**passing replisomes**", is based on the fact that helicases can slide onto dsDNA (double-strand DNA) and cross each other at the termination site before being disassembled[207].

Interestingly, a recent work using *Xenopus laevis* egg extracts has described that DNA synthesis is not slowed down as forks approach each other. Moreover, the authors show that helicases can pass each other while leading strand is elongated and that CMG complexes are not disassembled until the leading strand of one of the forks is ligated to the lagging strand of the adjacent fork, suggesting that termination occurs according to the "passing replisomes" model (Figure 10)[208].

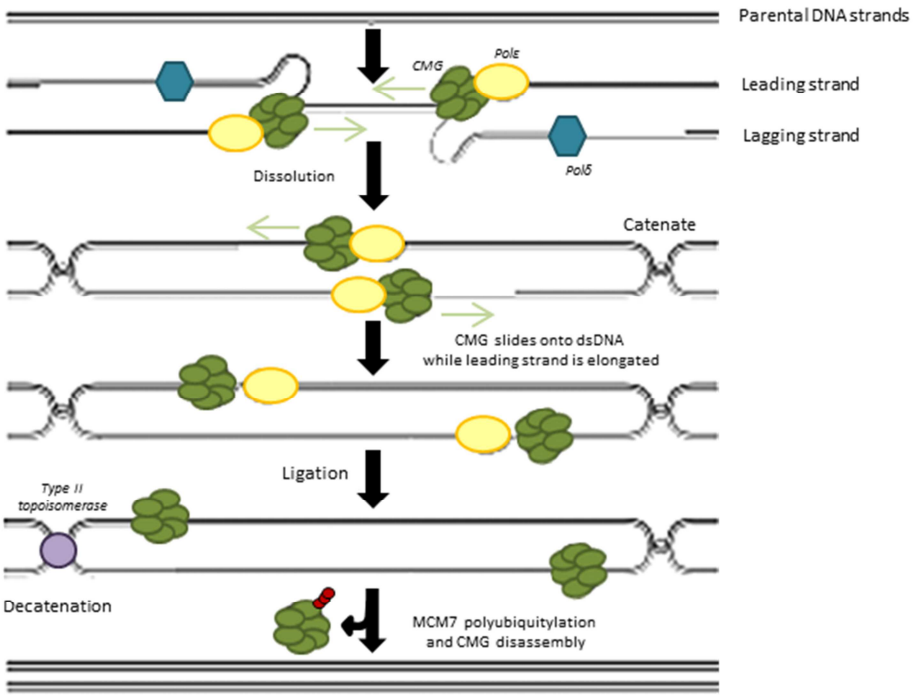

Figure 10. DNA replication termination according to "passing replisomes" model.
The different steps by which replication is terminated according to "passing replisomes" model is represented. Adapted from "The mechanism of DNA replication termination in vertebrates"[208].

2.2. The implication of epigenetic inheritance, chromatin architecture/organization and nuclear structure in DNA replication

The genomic DNA of all eukaryotes is packaged with the help of histones and other proteins into a structure known as **chromatin**, being the nucleosome its basic unit.

Nucleosomes are formed by the wrapping of about 150bp of DNA around a histone octamer core composed by two copies of each **H2A**, **H2B**, **H3** and **H4 canonical histones**. The different nucleosomes that form the chromatin are linked between them by short DNA fragments known as linker DNA, thus forming the chromatin fibers. The wrapping of DNA around histones and the short-range interactions between nucleosomes gives certain level of compaction. Under certain conditions, such as for example during mitosis, when DNA has to be condensed for its proper segregation, this packaging can be increased even more with the help of other proteins and fiber-fiber interactions, to finally form higher-order chromatin structures[214].

Nucleosomal histones suffer several PTMs (post-translational modifications), especially on their flexible tails, which are rich on Lysine residues and extended away from nucleosomal DNA. Additionally, under certain conditions, there are several histone variants that can be incorporated into the nucleosomes in a replication-independent manner. Together with DNA methylation, these histone modifications and histone variant replacements are part of epigenetic inheritance. The combination of these marks results in numerous specific and different outcomes by recruiting diverse effector proteins and modulating genome accessibility. Consequently, alterations in these epigenetic marks may induce the loss of cellular memory and disable tumor suppressor functions. Therefore, the proper segregation of those marks into daughter cells is essential to guarantee genome stability[155–157].

During DNA replication, there is a high demand of histones in order to package nascent DNA strands. However, accumulation of free histones may be potentially toxic for the cell. Thus, the synthesis of canonical histones is closely coordinated with DNA replication[215]. Additionally, since DNA must be unwinded during this process, chromatin is disrupted ahead of replication forks, and then must be restored behind the fork on new DNA strands. Furthermore, as previously mentioned, the propagation of epigenetic inheritance to newly synthesized DNA is essential for the maintenance of epigenome stability. For all that, DNA replication is tightly coordinated with nucleosome assembly and chromatin maturation[155–157].

Several factors are involved in nucleosome assembly, as well as in coupling it with DNA replication (Figure 11)[155,156]. One of this factors is **CAF-1** (chromatin-assembly factor 1), a histone chaperone involved in H3 and H4 histone deposition onto replicating DNA. In order to coordinate histone deposition with DNA replication, CAF-1 interacts with PCNA in a DDK-dependent manner[216–218]. Another histone chaperone involved in coupling chromatin assembly with DNA replication is **Asf-1**, which interacts with MCM2-6 helicase[219–221]. This protein is thought to act as a histone acceptor and donor at replication forks, finally transferring histones to CAF-1[221,222]. To complete nucleosome formation, H2A and H2B histones must also be incorporated in order to form the whole histone octamer core. In contrast to H3 and H4, the deposition of these proteins onto nascent DNA is not necessarily linked to DNA replication, and is thought to be mediated by **NAP-1** (nucleosome-assembly protein 1) chaperone and **FACT** (facilitates chromatin transcription) complex, in which FACT is thought to act as a histone acceptor and donor for NAP-1[155,156,223–225].

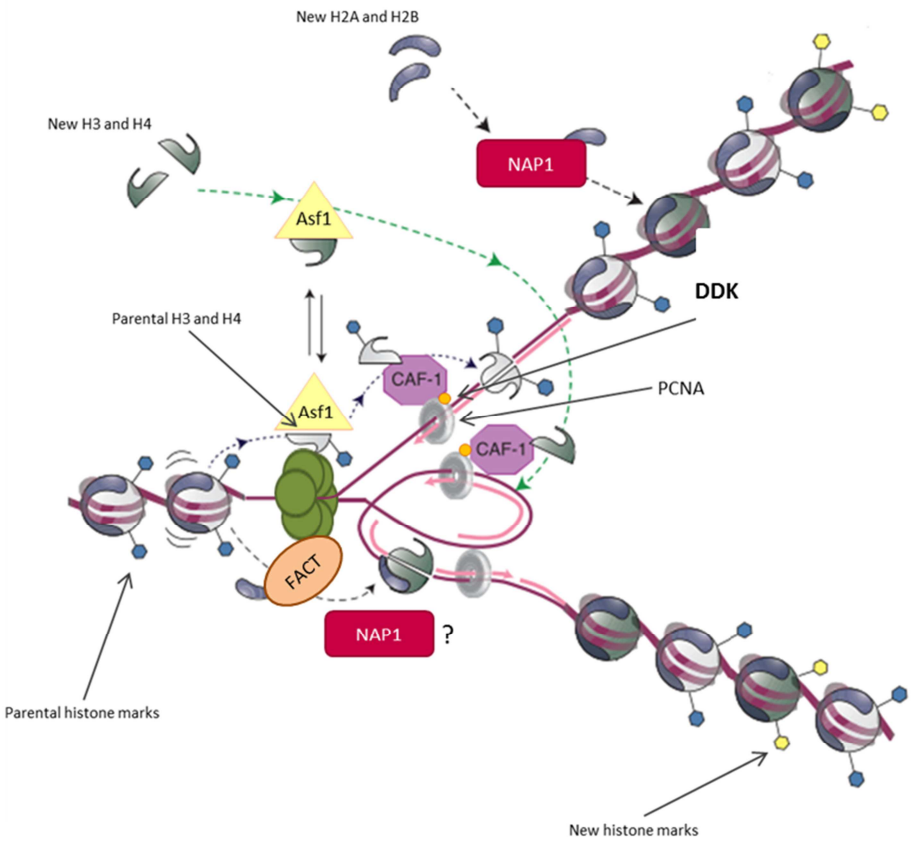

Figure 11. Nucleosome assembly and epigenetic inheritance.
The main factors involved in nucleosome assembly and in coupling this process with DNA replication are represented. Adapted from "Chromatin and DNA replication"[156].

While the process involved in nucleosome assembly is relatively well-known, the mechanisms that allow the reproduction of a similar chromatin environment on nascent DNA are still to be elucidated. According to recent data, this process is thought to be accomplished by transferring modified histones, and maybe other chromatin bound factors, from parental to daughter DNA strands, together with the newly synthesized ones. After that, new histones are thought to somehow assimilate the PTM signature present on parental histones to maintain the epigenetic state of chromatin[155,156,226]. In this sense, a recent work have shown that PTM signature is mirrored on nascent DNA strands by both, parental histone acquisition, and by copying the parental signature on the newly synthesized ones within one cell cycle[227].

In addition to their importance in maintaining a correct chromatin environment that prevents genomic instability, and consistent with their ability to modulate genome accessibility, epigenetic marks are also thought to be implicated in origin licensing and selection[155–158].

As previously explained, DNA replication is initiated at specific positions on the genome, known as origins. In prokaryotes and lower eukaryotes, these origins are usually identified by specific DNA sequences. By contrast, a universal signature that could predict the location of origins in metazoans has not been established yet[118,155,158,159]. In this sense, during the last years it has been postulated that certain DNA structures rather than specific DNA sequences may be the predictors of the metazoans origins. Accordingly, a few years ago **G-quadruplexes** (G4s; four-stranded DNA structures that can be formed in Guanine-rich regions) were postulated as possible origin predictors, as human replication origins were found to be widely associated with this structures[228]. Other studies have also determined that metazoans origins are usually localized in CG-rich regions, such as CpG islands. Additionally, the presence or absence of nucleosomes, histone modifications or even transcription, are also thought to be implicated in origin recognition by ORCs[155,158,159].

Due to the large size of their genomes, replication in higher eukaryotes is accomplished by the activation of hundreds or thousands of origins which can only fire once. Interestingly, only around the 10% of licensed origins are fired during a normal S phase in adult somatic cells, while most of them remain dormant[229]. Consistently, MCM levels can be reduced approximately 3 to 10-fold without affecting S-phase kinetics under normal situation. However, under certain circumstances that may cause replication fork stalling, these **dormant origins** might be required to complete DNA replication[118,230–232].

The choice of origins to be activated is flexible. Even in the same population, the origins that are activated vary from cell to cell[233]. Nevertheless, genome can be classified into two different megabase-scale DNA domains (**early-** and **late-replicating domains**) that replicate more or less synchronously at defined points during S phase, indicating that despite its flexibility, origin selection is not totally random. The chronological activation of origins determines a replication timing program that is established during G1. This program is thought to be regulated by the accessibility to limiting replication factors, which in turn, might be regulated by chromatin modifications, spatial organization of the genome and nuclear structure[155,156,159].

In this sense, early-replicating domains are usually enriched on replication origins and generally contain active gene-rich domains with active epigenetic marks, while late-replicating domains are associated with origin-poor regions enriched on repressive epigenetic marks, a heterochromatin hallmark[158,159]. Moreover, other proteins such as **Rif1** for example are also involved in the activation of origins through the regulation of chromatin architecture[234–237].

Additionally, the different levels of spatial organization of the thousands of origins present on metazoans genomes also regulate origin firing (Figure 12). In this sense, pre-RCs are formed around all the potential origins that are grouped into replication units or **replicon**s of around 50 – 120Kb (in metazoans), in which only one of them will be activated under normal circumstances. In turn, these replicons are grouped into **replication cluster**s or **foci** of around 400Kb - 1Mb (in mammals), in which origins of each replicon are fired synchronously[159].

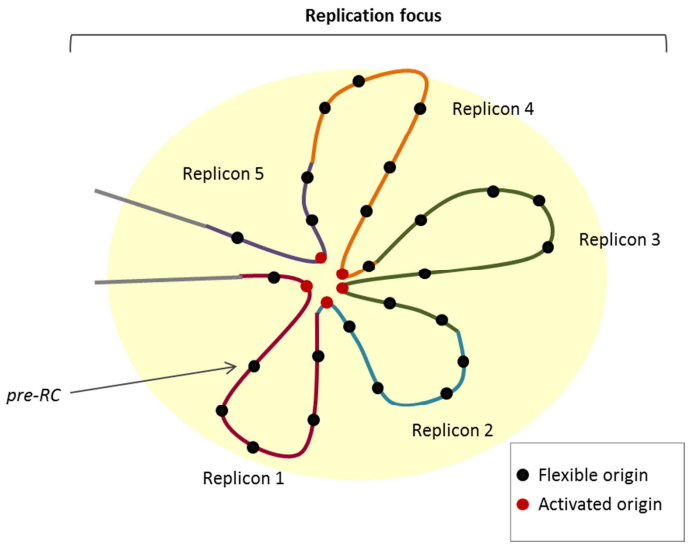

Figure 12. Organization of replication origins in higher eukaryotes.
Five different replicons (represented with different colors) from a same replication cluster, and the active or flexible origins present on each of them are shown. Adapted from "DNA replication origin activation in space and time"[159].

Apart from epigenome and chromatin organization, nuclear structure is also thought to involved in origin accessibility and firing. In this sense, the formation of the nuclear envelope at the end of mitosis is thought to introduce structural organization to DNA, essential for the regulation of origin firing[158,159]. As a consequence, the formation of the nuclear envelope is a prerequisite for origin firing[238]. Additionally, nuclear lamins are thought to regulate the replication timing through the regulation of nuclear structure. In this regard, the disruption of lamins for example has been shown to alter the elongation of origins[239], and late-replicating regions have been shown to be located at lamin-associated domains[240,241].

Notably, all this nuclear organization allows defining different replication patterns associated with different replication moments. In this regard, the S-phase state of a certain cell can be predicted through its replication foci distribution. Early S phase for instance is characterized by a homogenous distribution of small replication foci throughout the entire nuclei. By contrast, these replication foci are mainly associated with perinuclear and perinucleolar heterochromatin regions at mid S phase. Finally, a few large replication foci, associated with constitutive heterochromatin chromosomal regions, characterize the late S phase[242,243] (Figure 13).

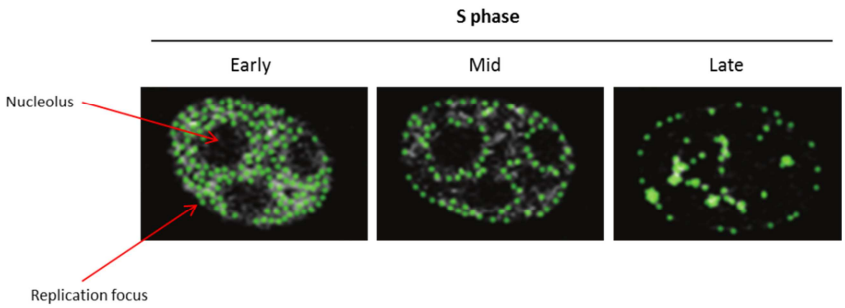

Figure 13. Distribution of replication foci during S phase.
Replication foci patterns at different S-phase stages of HeLa cells stably expressing GFP-PCNA is shown. Adapted from "Organization of DNA replication"[243].

3. The DNA replication stress response

Alterations in DNA replication dynamics result in the accumulation of **RS** (replication stress), one of the major sources of genomic instability. Cells respond to RS by activating several mechanisms to ensure stabilization and repair of forks, to coordinate these functions with cell cycle, and thus, to prevent cell division in the presence of unreplicated or damage DNA. By doing so, these mechanisms will try to overcome the damage and if so, DNA replication stress response will promote replication resumption and cell cycle progression. By contrast, in the cases of persistent damage, cells will be driven to apoptosis or senescence[244–248].

This section summarizes the main DNA replication alterations that may cause RS and how cells respond to this stress.

3.1. DNA replication-associated problems

Several endogenous and exogenous factors can compromise replication dynamics resulting in the accumulation of RS. This stress is generally characterized by the presence of stalled replication forks that can lead to fork collapse and the accumulation of DNA damage[2,244,248].

The main alterations in DNA replication dynamics that can lead to genomic instability are summarized on this section.

3.1.1. Fork stalling

Replication forks can encounter several obstacles that may lead to fork **stalling**. The accumulation of these local alterations can result in global DNA replication inhibition and in the abrogation of mitotic entry. In addition, persistent fork stalling can result in fork collapse and in the accumulation of DSBs, which can lead to the acquisition of genomic instability[2,159,244,248,249].

- *Low nucleotide or histone levels*

  Similarly to all other cellular processes, appropriate metabolic conditions are required for correct DNA replication. During S phase, there is a high demand of dNTPs and histones, the decrease of which can result in fork stalling[248]. Notably, a decrease in the pool of dNTPs can be artificially induced by the addition of ribonucleotide reductase inhibitor **HU** (hydroxyurea)[250,251]. Furthermore, overexpression of some oncogenes can also induce RS due to a nucleotide deficiency[252–254].

  Additionally, as previously explained, chromatin assembly must be coupled to DNA replication to ensure the correct transmition of epigenetic inheritance to daughter cells[155,156]. In this sense, defects on chromatin assembly have been shown to result in fork stalling and collapse[255,256]. A decrease in histone levels may cause a deregulation in the coupling of these processes, which may result in the accumulation of stalled forks[248]. Accordingly, the inhibition of canonical histones biosynthesis has been described to result on impaired replication fork

progression[257], although a sustained defect on histone supply seems to be required for the activation of the DNA replication stress response[248].

- *RFBs: replication fork barriers*

RFBs are obstacles present on DNA that result on replication fork slowdown and stalling. These barriers can arise after the addition of external agents, but they can also appear at natural pausing sites during unperturbed S phase. These **natural pausing sites** are intrinsic DNA regions where replication machinery tends to stall. This can occur for instance due to the presence of secondary DNA structures such as **hairpin loops** (folds in a single strand of DNA) and G-quadruplexes, which collide with the replication machinery promoting its stalling[157,244,248]. In this sense, the stabilization of G-quadruplexes results in slower replication speed and increased accumulation of DSBs[258].

Additionally, DNA-protein complexes or unrepaired DNA lesions that result from either exogenous or endogenous agents may also disrupt the progression of replication forks. For example, the addition of cisplatinum or mitomycin C, as well as the metabolic aldehydes that arise from alcohol metabolism, induce ICLs (inter-strand crosslinks) and probably also protein-DNA crosslinks[244,248].

Interestingly, although it is not exactly a barrier, chromatin compaction status has also been postulated as another source of impediment for fork progression[244,248].

- *Interferences between transcription and replication machineries*

Transcription has been described to be a source of genomic instability in a replication-dependent manner[259]. Consistently, the inhibition of transcription has been shown to reduce Cyclin E-induced RS in human cells, reinforcing the idea that the transcription machinery acts as an impediment for replication fork progression[260]. This is thought to be due to the fact that transcription and replication machineries share the same DNA templates, and thus, they are prone to collide.

However, a clash between replication and transcription machineries does not seem to be the sole explanation by which transcription may hinder fork progression[246,248,261]. From works showing that topoisomerases can reduce transcription-dependent RS[262,263], it has been proposed that topological perturbations, such as positive supercoilings generated when replication and transcription machineries converge, may also contribute to transcription-mediated fork stalling[248,261].

Additionally, the R-loops generated during transcription are also thought to be another cause of transcription-mediated fork stalling[246,248,262,264]. **R-loops** are RNA/DNA hybrids that are formed during transcription when the nascent RNA is annealed to the template DNA, leaving the non-template DNA strand unpaired[265]. These structures are removed by RNAseH and specialized helicases, and in fact, depletion of these factors involved in R-loop removal or prevention have been shown to induce RS[266–268].

- *Low origin density or excessive origin firing*

As previously explained, replication in higher eukaryotes is accomplished by the activation of hundreds of origins that represent around the 10% of the total licensed origins[229]. Additionally, in contrast to prokaryotes and lower eukaryotes, specific sequences that predict origin positioning in higher eukaryotes have not been established yet. In fact, although certain structures are thought to somehow define the location of metazoan origins, they are unequally distributed along the genome[118,155,158,159,228]. This, together with the fact that origin activation is flexible[233], raises the probability of having large inter-origin gaps, which in turn, increases the risk of spontaneous fork stalling[118]. In this sense, a decrease in origin density will rise the inter-origin distance, which may result in an increased risk of fork stalling[118]. Consistently, it has been shown that cells derived from MCM2-7 hypomorphic mice present an increase in fork stalling and DNA breaks[269]. Furthermore, Cyclin E overexpression has been shown to reduce the number of licensed origins, which contributes to replication impairement[270]. Collectively, these data indicate that a reduced origin density may raise the possibility of stalling, or at least, increase the risk of accumulating stalled forks due to the shortage of back-up origins to cope with those forks[118,245,246,248].

Alternatively, an excessive origin firing is also thought to promote fork stalling. In this case, a deficiency in limiting factors, such as for example insufficient dNTP levels, might be the reason for stalling[248].

3.1.2. Unscheduled replication

Another alteration in DNA replication dynamics that can result in the accumulation of RS and the acquisition of genomic instability, is the altered timing of origin firing[246]. As previously explained, replication in higher eukaryotes occurs through the activation of several origins[229]. Moreover, even if the choice of origins to be activated is flexible, there is a replication timing program that is established in G1, which defines early- and late-replicating domains that are going to be chronologically activated in S phase[155,156,159]. In this sense, the deregulation of the factors involved in controlling this replication timing program will induce unscheduled origin firing, leading to alterations in replication timing. Remarkably, this alterations may promote epigenetic changes that result in the acquisition of non-structural genomic instabilities[155–157,271,272].

In addition, as previously explained, the altered regulation of origin firing might result on a deficiency in limiting factors, which may lead to fork stalling[248]. Additionally, the deregulation of origin activation can result in the rereplication of certain DNA regions[116,118,246]. For example, alterations in origin licensing factors and their regulators, such as the upregulation of Cdt1[273]/Cdc6[274] or the downregulation of Geminin[275]/Emi1[154], causes rereplication. Moreover, the overexpression of some oncogenes, such as Cyclin E, also induces this effect[276]. Furthermore, the deregulation of histoneH4K20 methyl-transferase SETD8[277] or the overexpression of other chromatin modifiers[278] can also promote rereplication. Apart from the obvious impact that rereplication may have on genomic instability, this alteration also results in the accumulation of ssDNA, which favors the acquisition of DNA breaks[279].

3.1.3. Modified bases and alterations due to DNA damage tolerance mechanisms

UV light and other agents can cause bulky DNA adducts, such as pyrimidine dimers, that are usually repaired by **NER** (nucleotide excision repair). These alterations do not represent real barriers for replication machinery, but can stall the polymerases resulting in uncoupled unwinding and synthesis. Due to the discontinuous nature of the lagging strand, it tolerates much better than the leading strand this type of alterations. In this sense, the DNA adducts present on leading strand represent a major obstacle for the processivity of DNA replication. Therefore, to avoid fork stalling and to ensure replication fork progression in the presence of this kind of alterations, cells have developed **DDT** (DNA damage tolerance) mechanisms[280,281].

In some cases, bulky DNA adducts are bypassed by specialized DNA polymerases in a process known as **TLS** (translesion synthesis). In this case, the replicative polymerases are replaced by specific TLS polymerases in a process known as **polymerase switching**. These TLS polymerases have low fidelity and low processivity. However, they are able to accommodate bulky DNA lesions and maintain fork processivity, although they can compromise genome integrity due to reduced fidelity[282].

Another DDT mechanism that prevents fork stalling in the presence of bulky DNA adducts is **fork repriming**[280,281]. In this case, the replisome bypasses the damaged area and continues DNA synthesis downstream the damage site, by *de novo* priming of replicative polymerases (either by recycling or exchanging the polymerases that were working before bypassing the damage site)[283–285]. In human cells, the **PrimPol** primase-polymerase, which has also TLS polymerase activity, is the responsible for restarting DNA synthesis downstream the DNA adduct[286–288]. After replication, the ssDNA gap generated during adduct bypass must be repaired. This is usually mediated by HR-mediated repair mechanisms or by filling the gaps using TLS polymerases. In addition, if ssDNA gaps are not repaired they might be converted to DSBs. Thus, once again this mechanism may also compromise genome integrity[280,281].

3.1.4. Fork collapse and reversal

As previously explained, in response to fork stalling, the DNA replication stress response will promote the stabilization of replication forks, to allow replication to be restarted from the same forks when the stress is overcome. However, persistent fork stalling can result in replication fork collapse[2,244,289].

Fork **collapse** has been used to describe several potentially different processes including the dissociation of the replisome and the formation of DSBs at stalled forks[290]. Thus, it has usually been understood as a process that implies the inactivation of replication forks[289,290].

Based on chromatin immunoprecipitation studies on yeast, it was proposed that in the absence of Mec1 and Rad53 (orthologs of human ATR and Chk2 respectively), replisome components such as the replicative polymerases and the helicase are disassembled from chromatin after exposure to genotoxic agents[200,291–296]. However, this idea was later challenged by another study showing that the replisome remains associated with DNA in HU-treated checkpoint mutants[297]. An explanation that agrees

with both results would be that the replisome is not dissociated but instead, replication forks are remodeled, promoting a displacement of replisome components away from replication forks[280]. An example that might explain this displacement of replisome components without necessarily implying their dissociation would be fork reversal[281,298–300].

Fork **reversal** was first described in 1976 as a process that induces the remodeling of replication forks into four-way junctions, by the coordinated reannealing of parental strands, and the annealing of nascent DNA strands. This results in the formation of a fourth regressed arm at the fork elongation point which is also known as **chicken foot**[301]. Several DNA translocases and helicases, such as **SMARCAL1** (SWI/SNF-related matrix-associated actin-dependent regulator of chromatin subfamily A-like protein 1) and **WRN** (Werner syndrome ATP-dependent) respectively, have been described to promote fork reversal *in vitro*[281]. However, only the FBH1 helicase has been described to be able to induce fork reversal *in vivo*[302]. Additionally, Rad51, a protein that mediates strand invasion during HR (explained in section *(3.3.2)*), has been reported to be required for replication fork reversal[303].

Due to the lack of technical approaches to properly study fork reversal, until very recently, it has mainly been studied only in prokaryotes. The first direct observation of reversed (also known as regressed) forks in eukaryotes by two-dimensional (2D) gel electrophoresis[304] and later by electron microscopy[201], linked these structures with the inability to restart stalled replication forks. Since then, fork reversal has been interpreted as a pathological mechanism linked to fork collapse[261,289]. Consistently, it has been described that reversed forks are processed by nucleases and/or break repair mechanism to result in illegitimate ligation or toxic intermediates[280,292,305–308]. Consistent with this, several studies have shown that the DNA replication stress response tries to prevent this remodeling of the fork[305,307]. Moreover, cohesin complex have also been implicated in preventing this process[309], indicating that several mechanism have evolved to act against it.

However, during the last years several works have shown that fork reversal is a common and general feature in response to several genotoxic stress-inducing agents[303,310–312]. Furthermore, fork reversal has been proposed to occur even in the absence of those agents[303,310,313–315] and in the absence of DSBs[302,303]. In fact, mechanisms of restart from reversed forks have been described[311,312]. Therefore, it is started to consider that fork reversal may have a dual role, being harmful under certain conditions, but also, being a protective evolutionary conserved response that contributes to the safeguarding of genome integrity[298].

The mechanisms described to promote replication restart from reversed forks are explained in section *(3.3.1)*.

3.2. Cell cycle checkpoints

Cell cycle checkpoints are the mechanisms responsible for damage or abnormalities detection, and for coordination of cell cycle progression with DNA repair pathways, avoiding cell division in the presence of damage or unreplicated DNA. These mechanisms act as signal transduction cascades that are divided in three major levels:

1) First, **sensor proteins** are the responsible for damage or abnormalities detection and for the initial cascade activation; 2) Secondly, **transducer proteins**, usually protein kinases, mediate signal amplification by phosphorylating other kinases or target proteins; 3) Finally, **effector proteins** are the ones that act on several downstream target proteins in order to activate all the checkpoint responses, such as the inhibition of cell cycle progression[3,316,317].

Cells are constantly being challenged by endogenous and exogenous forms of damage, which can appear in all the cell cycle phases. As a consequence, checkpoints can be activated in every cell cycle phase. In this sense, cell cycle checkpoints can be classified according to the cell cycle phase in which they are activated as the: G1/S checkpoint, S-phase checkpoint, G2/M checkpoint and mitotic or spindle checkpoint (Figure 1)[3,316,317].

From the different cell cycle phases, the S phase is the most vulnerable to the acquisition of DNA damage. As previously explained, several mechanisms can induce fork stalling during this phase, which leads to the accumulation of ssDNA. This results on the activation of the **DNA replication checkpoint** in order to monitor the fidelity of copying the DNA. Additionally, if this stalling is persistent, cells are prone to collapse and accumulate DSBs. When this happens, the **DDR** (DNA damage response), including the **DNA damage checkpoint**, is activated. All together, these mechanisms will promote replication fork stabilization and repair, while inhibiting cell cycle progression, to avoid mitotic entry with damaged or unreplicated DNA[245–248,316].

Two **PIKK** (Phosphoinositide 3-kinase related protein kinase) family members, **ATR** (ATM and Rad3 related) and **ATM** (Ataxia-telangiectasia mutated), are the major regulators of the DNA replication stress and damage responses[318,319]. In addition, several works have described that **p38** and **JNK** (c-Jun N-terminal kinase) **SAPK**s (stress-activated protein kinases) also contribute to the prevention of aberrant mitotic entry in response to several genotoxic stresses, including RS, and even during unperturbed cell cycle[320–324]. Specifically, ATR sensor protein is the main upstream kinase of the DNA replication checkpoint, while ATM is the one of the DNA damage checkpoint[316]. Both kinases target an overlapping set of substrates that promote cell cycle arrest and DNA repair, and thus, the DNA replication and DNA damage checkpoints are tightly connected during S phase[318,319]. Although both mechanisms are essential to preserve genome integrity, ATR (or its downstream kinase Chk1) deletion results in embryonic lethality[325–327], whereas ATM-depleted embryos are viable despite they present several problems such as growth retardation, infertility and cancer predisposition[328–330]. Interestingly, a recent work has described that in stark contrast to ATM null mice, point mutations on ATM that cause the loss of its kinase activity also result in embryonic lethality[331].

Additionally, a third PIKK family member known as **DNA-PK** (DNA-dependent protein kinase) is also activated in response to DSBs. Nevertheless, the function of this last one seems to be limited to **NHEJ-** (non-homologous end-joining) mediated repair rather than in coordinating a global response, although there are evidences indicating that it may be important for checkpoint signaling in the absence of ATM[318,319].

All three PIKK family members phosphorylate preferentially Serine/Threonine residues that are adjacent to a Glutamine residue (S/TQ)[332]. Remarkably, they share some common substrates, such as for example **H2AX** histone variant[333,334]. The phosphorylation of H2AX on S139 (**γ-H2AX**) has been commonly used as a DSB marker[335]. However, latest evidences suggest that this phosphorylation is a common event in response to several genotoxic stresses, which does not always colocalize with other DSB markers[336]. Another common substrate for all three PIKKs is RPA32[337]. During unperturbed cell cycle, RPA32 is phosphorylated at G1/S transition and it remains phosphorylated until mitotic exit[338]. These cell cycle-regulated phosphorylation events are mediated by CDK1[339,340] and CDK2[340,341]. In addition, in response to DNA damage, RPA32 is further phosphorylated by ATR, ATM and DNA-PK in several of its residues, although the exact implication of each of those phosphorylations is still unknown[337].

The DNA replication and DNA damage checkpoint activation cascades, their functions, and the crosstalk between both pathways are summarized below.

3.2.1. The DNA replication checkpoint

As previously explained, several mechanisms can induce the stalling of replication forks[2,244,248]. When this happens, ssDNA is accumulated as a result of the uncoupling of the replicative polymerases and the helicase. Likewise, in the presence of damage templates, the uncoupling of the leading and lagging strands may also generate ssDNA. Additionally, the replication forks that are stalled due to the presence of barriers can be processed by nucleases and helicases resulting in the accumulation of ssDNA[281]. In all cases, the accumulation of ssDNA will result on the activation of the DNA replication checkpoint[319,342,343] (Figure 14).

The activation of this checkpoint starts with the loading of RPA protein onto ssDNA. This RPA-coated ssDNA acts as a platform for the recruitment of other proteins, essential for the activation of the DNA replication checkpoint. One of these proteins is ATR, which is recruited to this platform with the help of **ATRIP** (ATR-interacting protein)[344], a protein that directly binds RPA. ATR-mediated ATRIP phosphorylation at S68 and S72 is thought to be important for the activation of the DNA replication checkpoint[345]. Additionally, Sirtuine-2-mediated ATRIP deacetylation has been reported to be required for its interaction with RPA[346]. ATRIP-mediated recognition of RPA-coated ssDNA is essential for the recruitment of ATR onto chromatin. Nevertheless, this is not sufficient to the activation of ATR[319,342]. In this sense, a second group of proteins are also recruited to RPA-coated ssDNA independently of ATR-ATRIP. This group includes the heterotrimeric ring-shape protein **9-1-1** (Rad9-Rad1-Hus1), which is phosphorylated on S387[347] and S341 by CKII (Casein kinase 2)[348], allowing the recruitment of TopBP1, an essential protein for the activation of ATR[349–351]. 9-1-1 protein recognizes RPA-coated ssDNA regions that are adjacent to DNA ends. This protein complex is related, in structure and sequence, to PCNA, and accordingly, it requires the action of clamp loaders to bind the chromatin[352]. In this case, **Rad17**-RFC complex, a RFC-like complex in which RFC1 has been substituted by Rad17[353] is the responsible for the recruitment of 9-1-1[319,342,354].

The main role of this second group of proteins is to bring TopBP1 in close vicinity to ATR-ATRIP[349,350]. TopBP1 directly interacts with ATR-ATRIP[355,356] and stimulates the kinase activity of ATR *in vitro*[355]. However, the exact mechanism by which TopBP1 favors or mediates the activation of ATR *in vivo* still remains to be elucidated[319,342,357]. In this sense, it has been reported that ATR can be autophosphorylated in *trans* on T1989 and that this phosphorylation assists its binding to TopBP1[358]. Nevertheless, although this phosphorylation is a mark of ATR activation, mutations on this phosphorylation site do not have an strong impact on ATR function[359]. Remarkably, ATM-mediated TopBP1 phosphorylation on S1131 has been reported to be important for TopBP1-mediated stimulation of ATR activity in *Xenopus laevis*[360]. Moreover, other proteins such as MRN (Mre11-Rad50-Nbs1) and RHINO (Rad9, Rad1, Hus1 interacting nuclear orphan) are also thought to be important for the recruitment of TopBP1, and thus, for the activation of ATR[357]. In this case, **RHINO** for instance has been described to interact with 9-1-1 and TopBP1, stabilizing the interaction between them, to retain TopBP1 on damage sites or to promote conformational changes on TopBP1 that may contribute to the activation of ATR[361]. In any case, sustained interaction between ATR-ATRIP and 9-1-1-TopBP1 is thought to favor the activation of ATR[319,357], although additional proteins, such as FANCM (Fanconi anemia group M protein)[362] or Dna2[363], may also be required for full ATR activation.

The fact that the DNA replication checkpoint activation requires two independent initial recruitments is thought to be important to activate it only when is really needed. During an unperturbed S phase, ssDNA is generated, which will recruit RPA onto chromatin. Additionally, the 5'-junction and the ssDNA generated on the lagging strand could also act as a platform for the recruitment of 9-1-1. Thus, the requirement of two individual signals may force a situation in which the amount of the initial signal is critical for the activation of this checkpoint[319]. Consistent with this hypothesis, larger gaps of ssDNA have been shown to be more efficient on the activation of the DNA replication checkpoint[364].

Once activated, ATR phosphorylates several substrates to mediate the different DNA replication checkpoint responses[319,342]. **Chk1** kinase is the main downstream substrate of ATR, which acts as a transducer protein to mediate the variety of functions of the DNA replication checkpoint response[316,327]. This kinase is transiently localized to damage sites to be activated by ATR, and then, it is released from chromatin and spread over the nucleus to interact with its different substrates[365]. ATR phosphorylates Chk1 on S345 and S317[366], which induces conformational changes on Chk1 that allow its own autophosphorylation on S296[367] and its further activation. Additionally, other mediator proteins also contribute to ATR-mediated Chk1 activation. One of such proteins is Claspin[368], which is phosphorylated on T916 and S945[369,370] by CS1γ1 (Casein kinase 1 gamma 1) in an ATR-dependent manner[371], to interact with Chk1 favoring its activation. Apart from Claspin, Tim and Tipin have also been described to contribute to ATR-mediated Chk1 activation[372,373].

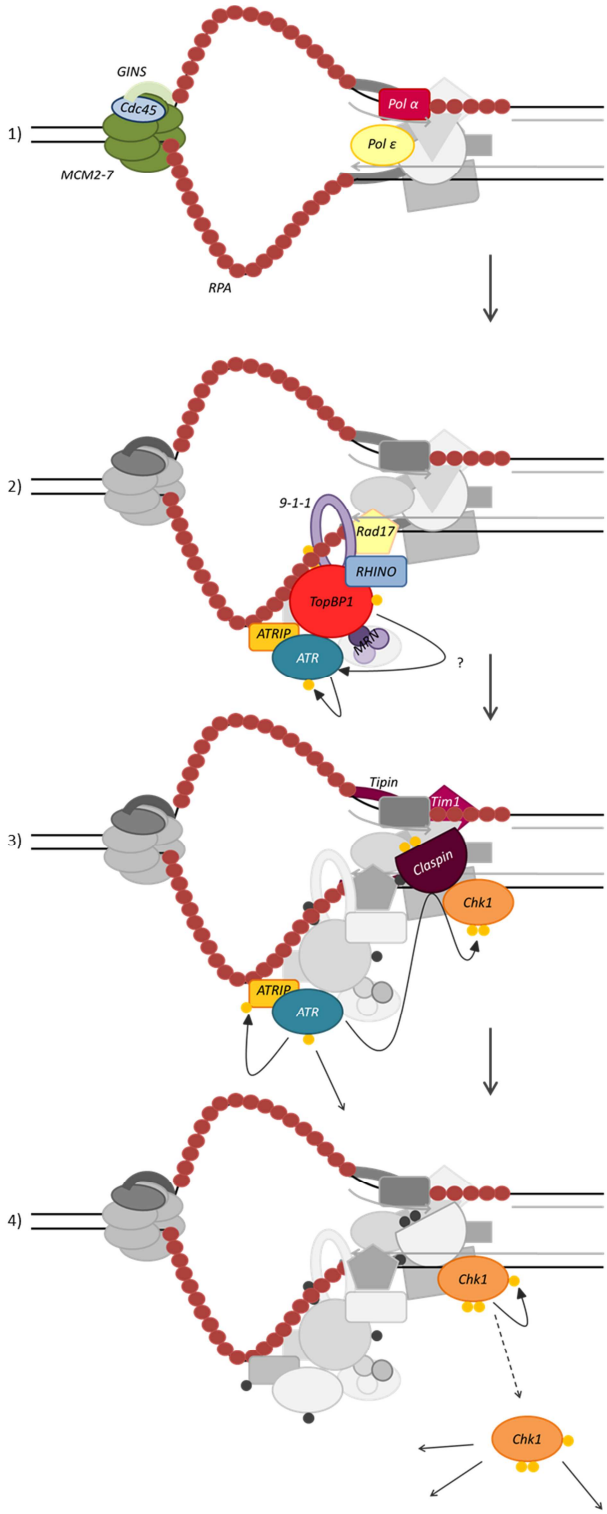

Figure 14. A model for DNA replication checkpoint activation in metazoans.
1) The uncoupling of CMG helicase and replicative polymerases results in the accumulation of high amounts of ssDNA that are wrapped by RPA. 2) This RPA-coated ssDNA is recognized by ATRIP which brings ATR close to the ssDNA. Additionally, 9-1-1 protein recognizes the RPA-coated ssDNA that is adjacent to a DNA end, and is recruited to the damage site with the help of Rad17-RFC, bringing with it TopBP1 protein. Other proteins such as MRN and RHINO also contribute to this recruitment of TopBP1. The vicinity of TopBP1 favors ATR activation, which is autophosphorylated in *trans* on T1989. Other proteins also contribute to the activation of ATR. 3) Once activated, ATR phosphorylates several substrates. Chk1, the main transducer protein of the DNA replication checkpoint, is one of those ATR substrates. ATR phosphorylates Chk1 on S345 and S137, with the help of mediator proteins such as Claspin, Tim1 and Tipin. 4) Chk1 phosphorylation by ATR induces a conformational change on Chk1 that allows its own autophosphorylation on S296. Once activated, Chk1 is released from chromatin and spread over the nucleus to interact with its several substrates.

- *Functions of the DNA replication checkpoint*

As previously mentioned, the DNA replication checkpoint is activated in response to ssDNA accumulation. When this happens, this checkpoint promotes a reversible cell cycle arrest (through mitotic entry and origin firing inhibition), as well as the stabilization of replication forks, to avoid mitotic entry with unreplicated or damage DNA, and to maintain the competence to recover when the stress is overcome. Additionally, this checkpoint also regulates other functions, such as DNA repair and transcription, altogether contributing to safeguarding the genome integrity[247,318,319,342,343].

The molecular mechanisms involved in the most important DNA replication checkpoint functions are summarized below:

- *Inhibition of mitotic entry:* ATR/Chk1 prevents mitotic entry by inducing the inhibition of cyclin-CDK complexes, which is accomplished by Chk1-mediated Wee1 and Cdc25 phosphorylation. These phosphorylations result on Wee1 activation while promoting Cdc25 degradation, mislocalization or export from nuclei, altogether contributing to the inhibition of CDKs[41,42]. Additionally, Nek11 kinase has also been shown to be activated by Chk1, which contributes to the degradation of Cdc25A[374]. The inhibition of these cyclin-CDK complexes is the main mechanism to avoid mitotic entry with unreplicated or damage DNA[319].

- *Origin firing inhibition:* Inhibition of replication initiation is the other mechanism used by the DNA replication checkpoint to prevent cell cycle progression. In this case, ATR and Chk1 are involved in global origin firing inhibition, while allowing local dormant origin firing[118].
  ATR/Chk1 inhibits origin firing through several mechanisms. For example, ATR-mediated FANCI (Fanconi anemia group I protein) phosphorylation inhibits origin firing to promote fork restart[375]. In addition, Chk1 inhibits Treslin[376], which is required for a stable CMG complex formation[164,165]. Additionally, since CDK2 and DDK are essential kinases for the initiation of DNA replication[162,163], the previously explained Chk1-mediated CDK inhibition will contribute to origin firing prevention. Moreover, Dbf4, the regulatory subunit of DDK kinase, is also an ATR substrate[377]. However, whether DDK is inactivated in response to RS in human cells is still controversial[378]. In this sense, the phosphorylation of Dbf4 by ATR does not affect the DDK kinase activity[377]. Moreover, through Claspin phosphorylation, DDK has been described to be required for Chk1 activation[379,380]. Furthermore, ATR/Chk1-promoted APC/C^{Cdh1} inhibition, prevents the degradation of Dbf4 and results on the accumulation of DDK onto chromatin in response to RS[381]. As DDK is a crucial player for TLS, it seems conceivable that it may be required, at least under certain circumstances, for the DNA replication stress response[378].
  However, if DDK is activated in response to RS, how is origin firing inhibited under these conditions? And most importantly, how does ATR/Chk1 promote dormant origin firing while inhibiting the activation of late origins? Interestingly, it has been described that ATR-/ATM-mediated PP1 phosphatase recruitment to chromatin counteracts DDK-mediated MCM phosphorylation[382]. The selective

inhibition of certain origins by this machinery has been postulated as a mechanism for late origin firing inhibition[378]. In this sense, Rif1, one of the major regulators of the replication timing program[234–237], has been shown to recruit PP1 to late origins on yeast, in order to counteract DDK-mediated MCM phosphorylation[383,384]. In addition, ATR/Chk1 has also been described to specifically inhibit late origin firing by preventing the activation of new replication factories[385]. The specific inhibition of only the new replication factories will allow dormant origin firing, since they are located in the already activated ones. Interestingly, the DNA replication checkpoint not only allows but also promotes the activation of dormant origins. In this sense, ATR has been shown to phosphorylate MCM in Xenopus laevis, which induces PLx1 (ortholog of human PLK1) recruitment to stalled forks. This PLx1 attenuates the inhibitory activity of the checkpoint towards unfired origins that are close to the stalled ones[386].

Importantly, ATR/Chk1 have been shown to regulate origin firing, and consequently fork progression, not only in response to RS, but also in unperturbed S phase[387,388]. Consistent with this, Claspin has also been described to regulate normal fork progression[389].

- *Stabilization of replication forks:* Fork stabilization has been described to be another important function of the DNA replication checkpoint, to avoid fork collapse and to allow replication to be resumed from the same forks when the stress is overcome[247,318,319,342].

  As previously explained, based on data from yeast, it was described that replisome components are disassembled from replication forks in response to RS when checkpoint kinases are abscent[200,291–296]. However, this hypothesis was later challenged[297]. A possible explanation that agrees with both results is that replication forks are remodeled into chicken foot structures, which do not necessarily imply the dissociation of the replisome[280,281,298–300]. In this sense, ATR for instance has been described to phosphorylate the DNA translocase SMARCAL1 to restrain fork reversal and to avoid fork collapse[305].

  Nonetheless, recent data indicate that replication can be restarted from reversed forks[298]. Thus, the accumulation of DNA damage rather than fork remodeling, seem to be the mechanism that hinders the stability of replication forks, resulting in fork inactivation. Consistently, a recent work has shown that fork collapse in the absence of ATR is due to other mechanisms rather than the deregulation of replisome mainteinance[390]. Accordingly, replication checkpoint kinases have been shown to protect replication forks from the accumulation of DSBs through several mechanisms. For instance, ATR-mediated origin firing inhibition prevents RPA exhaustion-promoted DSBs[391]. Moreover, ATR promotes the association of FANCD2 (Fanconi anemia group 2 protein) with MCM helicase to prevent massive ssDNA accumulation, which can result in the formation of DSBs[391,392]. Furthermore, Chk1 protects replication forks from **Mus81** endonuclease-mediated breakages[393].

  Interestingly, proteins involved in HR-mediated repair (explained in section (3.3.2)), such as **Rad51**, **BRCA2** (breast cancer type 2 susceptibility protein) and

FANCD2 have been reported to play a repair-independent role in protecting stalled replication forks from nucleases degradation[394–396]. Specifically, the association of Rad51 with ssDNA protects replication forks from **Mre11** nuclease-mediated degradation[396]. Likewise, FANCD2 and BRCA2 also prevent Mre11-mediated degradation in a Rad51-dependent manner[394,395]. Additionally, WRN helicase presents a nonenzymatic role in protecting nascent DNA strands from Mre11-dependent degradation after camptothecin treatment[397]. If these functions are regulated or not by the DNA replication checkpoint is still unknown[398], but in any case, fork protection seems to be necessary to allow fork restart once the stress is overcome[244,247,289]. Consistently, cohesins, which are involved in the maintenance of fork integrity, are also thought to be important to allow replication restart from stalled forks[206,399]. In this sense, Rad50-mediated cohesin recruitment at replication sites has been shown to be required for the recovery of stalled replication forks[400].

- *Regulation of DNA repair mechanisms:* ATR is predominantly activated in response to RS. Nevertheless, DSB-inducing agents can also lead to its activation. Moreover, the RS generated during S phase can lead to the accumulation of DNA damage. Furthermore, DNA repair mechanisms have to be coordinated with cell cycle progression to guarantee genome integrity. Thus, the regulation of DNA repair mechanisms is another function of the DNA replication checkpoint. Since DSBs are also sensed by the DNA damage checkpoint, there is a high crosstalk between both pathways at this point (further explained in section (3.2.3))[247,318,319,342].

  DNA replication checkpoint mediators, such as the 9-1-1 protein complex, have been reported to be implicated in the regulation of several DNA repair mechanisms including for instance BER (base excision repair)[247,342].

  In addition, ATR has been described to be implicated in HR-mediated repair rather than in NHEJ-mediated one[401]. For instance, ATR regulates **BRCA1** (breast cancer type 1 susceptibility protein), a tumor suppressor involved in HR-mediated repair[402] (explained in section (3.3.2)). Moreover, ATR-mediated FANCD2 phosphorylation promotes its monoubiquitylation, required for its recruitment onto damage sites[403]. In addition, Chk1-mediated Rad51 or BRCA2 phosphorylations have been shown to stimulate HR[404–406]. However, as previously explained, the DNA replication checkpoint promotes the stabilization of forks to avoid fork collapse. Thus, ATR/Chk1-induced HR might be restricted only to certain cellular conditions. Consistently, it has been reported that the DNA processing and initiation events required for HR-mediated repair, are actively suppressed by the DNA replication checkpoint[407–410].

- *Regulation of transcription:* Several data from yeast have connected the DNA replication checkpoint with the regulation of cellular transcription. In response to fork stalling, hundreds of genes are up- or down-regulated[247,342].

  In addition, as explained in section (1.1.2), the synthesis of each cyclin is usually regulated by the cyclin-CDK complex that acts just before during the cell cycle. In this regard, the inhibition of cyclin-CDK complexes by the DNA replication checkpoint may compromise the synthesis of cyclins. For example, the synthesis

of Cyclin B1 requires the activation of NF-Y, b-Myb and FoxM1 transcription factors, which are activated by Cyclin A-CDK2/1. Thus, the inhibition of CDK2/1 by the DNA replication checkpoint will prevent the activation of those transcription factors, resulting in a reduced Cyclin B1 expression that will contribute to mitotic entry abrogation[1,6,16,22,319].

Additionally, E2F transcription factors, which are involved in the regulation of DNA replication and repair[19,20], are also controlled by cyclin-CDK complexes[19]. Thus, the inhibition of these cyclin-CDK complexes may disturb E2F-dependent functions.

Notably, the checkpoint-induced regulation of transcription is thought to have little impact on fork stabilization or cell viability[247,343], since inhibiting protein synthesis (by cycloheximide treatment) has little impact on cell survival after RS[411].

3.2.2. The DNA damage checkpoint

As previously mentioned, the RS generated during S phase can result in the accumulation of DSBs[244–248]. In addition, during S phase, as in the other cell cycle phases, certain agents can also induce DSBs on DNA. When this happens, the DDR is activated (Figure 15) to detect DNA lesions, signal their presence and promote their repair, all this coordinated with the inhibition of cell cycle progression, to prevent mitotic entry with damaged DNA. All these functions are mediated by the DDR, through the coordinated action of the DNA damage checkpoint and the DNA repair mechanisms[412].

DSBs are sensed by the **MRN** complex[413], which as previously mentioned is composed by Mre11, Rad50 and Nbs1 proteins. Mre11 presents endonuclease and 3' → 5' exonuclease activities, while **Rad50** exhibits ATPase and adenylate kinase activities. By contrast, **Nbs1** contains FHA (forkhead-associated domain) and BRCT (tandem BRCA1 C-terminal domains) domains to interact with other proteins and to regulate their activities by modulating their protein-protein interactions and structure[414].

In the presence of DSBs, MRN is rapidly recruited to damage sites[415]. Once there, it promotes ATM recruitment[416–418] and monomerization, necessary for the activation of ATM[418]. This kinase is predominantly found as an inactive noncovalent homodimer in the nucleus. In response to DNA damage, its monomerization and autophosphorylation in *trans* on S1981 allow its activation[419]. Further autophosphorylation sites on ATM have also been described. However, studies in other species have reported that phosphorylation of ATM on S1981 is not essential for its function, despite being a sensitive marker of ATM activation state[415]. In any case, ATM autophosphorylation has been shown to depend on **Tip60** histone acetyltransferase-mediated K3016 acetylation on ATM[420,421]. Interestingly, mutations on this acetylation site have been shown to disrupt not only ATM autophosphorylation, but also, the phosphorylation of ATM downstream targets[421].

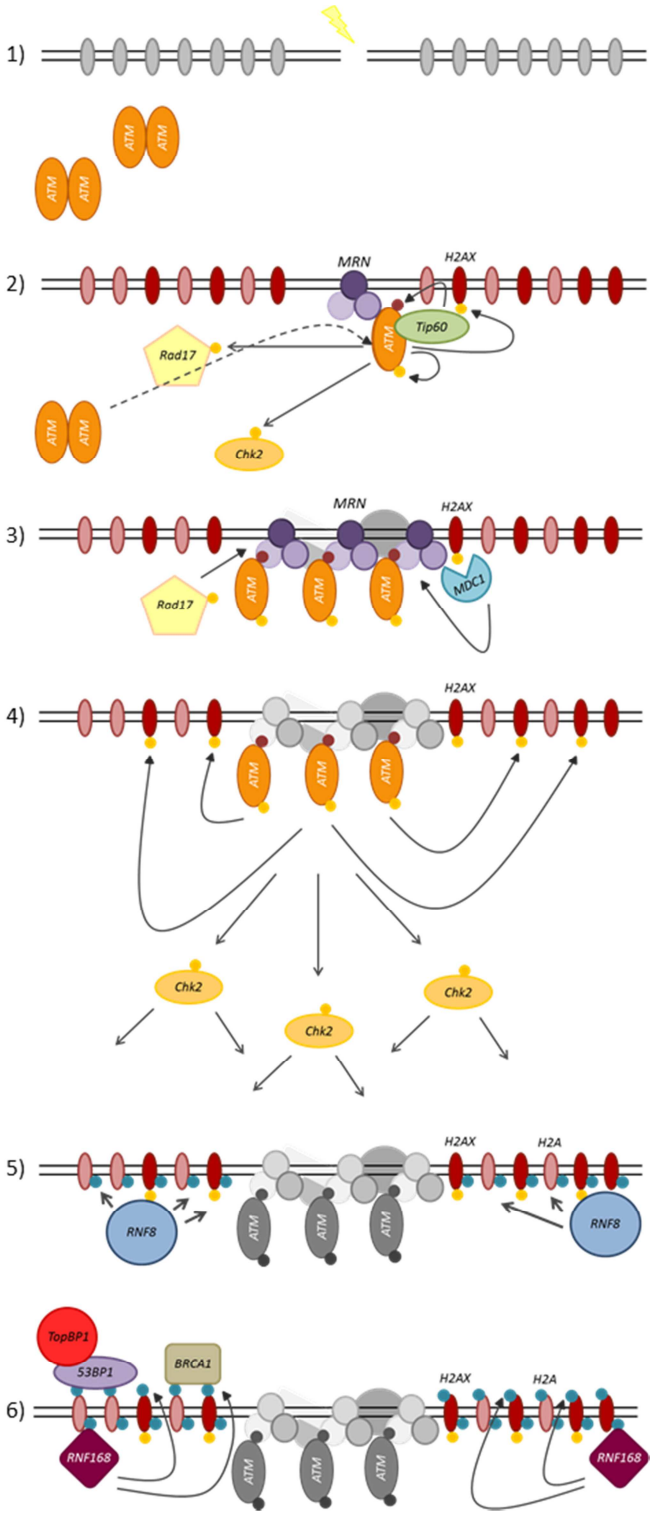

Figure 15. A model for DDR activation and signal amplification.
1) ATM is commonly found as noncovalent homodimers in the nuclei. 2) In response to DSBs, MRN is rapidly recruited to damage sites. Once there, MRN contributes to ATM recruitment, monomerization and autophosphorylation, being Tip60-mediated acetylation necessary for this last one. Once activated, ATM phosphorylates several substrates such as Chk2, Rad17 or H2AX. 3) H2AX phosphorylation on S139 promotes the recruitment of MDC1 to damage sites. From there, MDC1 favors the association and recruitment of MRN. Rad17 also contributes to this function. This MRN stabilization contributes to further ATM recruitment. 4) Increased ATM recruitment and activation favors further substrate phosphorylation. 5) The phosphorylations of H2AX are recognized by the RNF8 ubiquitin ligase, which ubiquitylates H2AX and H2A histones. 6) RNF8-mediated ubiquitylations are in turn recognized by RNF168, which further ubiquitylates H2AX and H2A histones, contributing to signal amplification. Finally, all these modifications promote a proper DNA damage checkpoint activation and favor the recruitment of repair proteins to damage sites.

Once activated, ATM phosphorylates Chk2, the main transducer protein of the DNA damage checkpoint[316], on T68[422]. Additionally, together with the other PIKKs, ATM phosphorylates H2AX histone variant on S139[333–335]. This γ-H2AX is detected by the **MDC1** (mediator of DNA damage checkpoint 1) protein, which is recruited to damage sites. Once there, MDC1 protein retains and allows the propagation of MRN to adjacent chromatin[423]. Moreover, the interaction of MRN with phosphorylated Rad17 (by ATM) contributes to its maintenance onto damage sites[424]. This MRN retention and spread to adjacent chromatin may further increase the recruitment and the activation of ATM. Accordingly, MDC1 protein has been described to enhance the association of ATM with chromatin, which allows γ-H2AX signal amplification[425]. Moreover, it has been reported that the association of ATM with undamaged chromatin might be important to correctly activate the ATM pathway[426]. Collectively, these suggest that chromatin context is important for correct signal amplification, and thus, for a correct DNA damage checkpoint activation and response[415]. In this sense, several acetylations, SUMOylations, ubiquitylations and other PTMs have been described to be required for the correct activation of the DNA damage checkpoint[427]. For example, MDC1 triggers the recruitment of the **RNF8** E3 ubiquitin ligase, which ubiquitylates γ-H2AX[428,429] and H2A[429]. This ubiquitylations are recognized by another E3 ubiquitin ligase, the **RNF168**, which further ubiquitylates γ-H2AX[430] and H2A[430,431] to amplify the signal. This signal amplification may be important for a correct DNA damage checkpoint activation, but also, it is required for the recruitment of repair proteins such as BRCA1 or **53BP1**, being this last one involved in the recruitment of, among others, TopBP1[427,432].

- *Functions of the DNA damage checkpoint*

The main function of the DNA damage checkpoint is to prevent cell cycle progression, to avoid mitotic entry in the presence of damaged DNA[3,316]. In this sense, by phosphorylating Cdc25 phosphatases, Chk2 inhibits CDKs as an early response to DNA damage[3,41].

Additionally, in response to persistent damage, ATM/Chk2 promotes the stabilization of p53 transcription factor[3,316], which regulates several mechanisms involved in the maintenance of the cell cycle arrest[433,434]. ATM/Chk2 promotes the stabilization of p53 in several ways. First, ATM phosphorylates p53 on S15, inducing its transcriptional activation[435,436]. Moreover, Chk2 phosphorylates p53 on S20 reducing its ability to interact with the **MDM2** ubiquitin ligase[437–440]. Furthermore, ATM phosphorylates MDM2, preventing the export of p53 to the cytoplasm where it is degraded[441].

Once active and stabilized, p53 tumor suppressor regulates the expression of several proteins involved in processes such as cell cycle arrest, apoptosis or senescence[433,434]. Most of this p53-regulated functions, are mediated by its downstream target p21[48,49]. The contribution of p53/p21 to apoptosis and senescence are further explained in section (3.4).

As previously explained, p21 is a CKI, and thus, it abrogates cell cycle progression by inhibiting the cyclin-CDK complexes[43]. In addition, p21 has also CDK inhibitor-independent roles that regulate cell cycle progression[45,50,442]. One of those

functions is the inhibition of E2F1 transcription factor by direct binding to its promoter[45]. In this sense, since, as previously mentioned, the APC/C inhibitor Emi1 is an E2F1 target[93], the inhibition of E2F by p21, either by direct binding or through the regulation of CDKs, may induce APC/C activation. Accordingly, premature APC/C^{Cdh1} activation in response to DNA damage[443] has been described to be mediated, at least in part, by p21-dependent Emi1 downregulation[152]. This APC/C^{Cdh1} activation in response to DNA damage induces a permanent arrest in G2 by degrading several substrates such as Cyclin A, Cyclin B, Aurora A and Plk1[150–152].

In addition, p21 is also involved in the regulation of several DNA repair mechanisms[45]. For instance, p21 competes with other repair proteins for PCNA binding to regulate replication and repair processes[444]. In this sense, p21 binding to PCNA induces a DNA replication blockade[442]. Moreover, p21 inhibits TLS by preventing PCNA monoubiquitylation, required for the recruitment of TLS polymerases[445,446].

3.2.3. Crosstalk between the DNA replication and DNA damage checkpoints

As previously explained, DNA damage promotes the activation of both ATM and ATR. In addition, since stalled replication forks can eventually collapse and accumulate DSBs, fork stalling can also result in the activation of both pathways. Moreover, ATM and ATR present several common substrates, and in turn, several proteins are involved in the activation of both pathways. These observations underline the high redundancy between the DNA replication and DNA damage checkpoints[318,319,342].

This redundancy is highlighted for instance in response to fork reversal, since it has been described that reversed forks are able to activate, not only ATR, but also ATM pathway. In this particular case, the free DNA ends exposed by reversed forks are sufficient to activate ATM in the absence of DSBs[302].

This crosstalk is also evident during the repair of DSBs. In this case, the 3' overhang of ssDNA generated by **DNA resection,** during HR-mediated repair, will also promote the activation of ATR[319]. HR-mediated repair is further explained in section *(3.3.2)*.

Additionally, upon persistent RS, not only ATM/Chk2 but also, ATR/Chk1 has been reported to induce the stabilization of p53[440,447]. Accordingly, prolonged ATR activation, even in the absence of DNA damage, has been shown to be sufficient to promote senescence in a p53-dependent manner[448].

3.3. Replication restart and repair pathways

In response to RS, cells will try to stabilize the replisome to allow replication to be resumed from the same forks once the damage or stress has been overcome[247]. Replication resumption from the same forks contributes to the safeguarding of genome integrity, since it guarantees the replication of the whole genome, maintaining the replication timing program[271,449].

Additionally, upon RS, replication can also be restored from dormant origins, which also contributes to the preservation of genome integrity. The existence of those dormant origins ensures whole genome replication and contributes to prevent rereplication.

Furthermore, since dormant origins are located in the same replicons as the stalled forks, their activation do not alter the replication timing program[118,159]. However, dormant origins allow replication to be resumed once the replication forks have been processed into DSBs[450], and thus, in this case they might contribute to the acquisition of genomic instability[290,451].

In addition, in contrast to what it was thought, recent data have shown that replication can also be restarted from broken replication forks by BIR (break-induced replication)[452–455]. Notably, this mechanism is highly error-prone and mutagenic[456–459].

This section summarizes the main mechanisms involved in replication resumption after RS.

3.3.1. Direct restart or restart from reversed forks

Once the stress is removed, replication can be restarted from unbroken stalled forks, either by direct restart or through fork remodeling processes. The maintenance of replisome components and the stabilization of replication forks by the DNA replication checkpoint, allows replication to be resume by **direct restart** from the same forks (Figure 16)[247,280,289].

Additionally, as previously explained, replication forks are commonly regressed into chicken foot structures[303,310]. Moreover, although these structures have been linked to the accumulation of illegitimate ligations and toxic intermediates[280,292,305–308], it is started to consider that fork reversal may also have a role in safeguarding genome integrity[298]. In this sense, in contrast to what it was thought, replication restart from reversed forks has been described[300,311,312], although this mechanism is still poorly understood.

The first question that still remains to be elucidated in this regard is whether fork reversal implies replisome dissociation or not[281,298]. The first direct evidences of fork reversal on eukaryotes came from studies on Rad53 (the yeast ortholog of human Chk2) mutants, in which the presence of these structures was linked to a replication recovery failure[201,304]. In this sense, it was postulated that fork reversal might entail replisome disassembly[298,299], thus compromising DNA synthesis resumption. However, the fact that replication can be restarted from reversed forks[300,311,312] have compromised this hypothesis, since MCM helicase for instance, which is part of the active CMG helicase complex, can only be loaded onto chromatin during G1[116], and thus, its disassembly would hinder replication resumption. Consistent with this, a recent study have shown that at least in the T4 bacteriophage system, fork reversal can occur without dissociation of replisome components[300]. Nevertheless, further studies are necessary to know if this is also the case in higher eukaryotes.

Regarding the replication resumption mechanisms to resume replication from reversed forks, two recent studies have described two different pathways of replication **restart from reversed forks** in human cells (Figure 16): 1) **RecQ1** helicase mediates **branch migration**, to reverse regressed forks and to restore their initial status, allowing replication to be resumed from the same place. In this case, RecQ1 helicase is inhibited by PARP1 (poly [ADP-ribose] polymerase 1) until the damage is repaired or the stress is

overcome[311]; 2) **Dna2** nuclease and WRN helicase-mediated 5' → 3' resection creates a 3' overhang, promoting fork restart. In this case, fork restart has been postulated to occur either by an unknown branch migration factor or by **strand invasion** (search and invasion of homologous sequences), for instance mediated by Rad51[281,312]. Remarkably, consistent with what has been postulated[206,399], cohesin complexes might be necessary for replication restart under this condition, since they are required for proper strand invasion. Interestingly, Mre11 nuclease does not contribute to this resection. Moreover, in this case resection is restricted by RecQ1 to prevent massive degradation of nascent DNA[312].

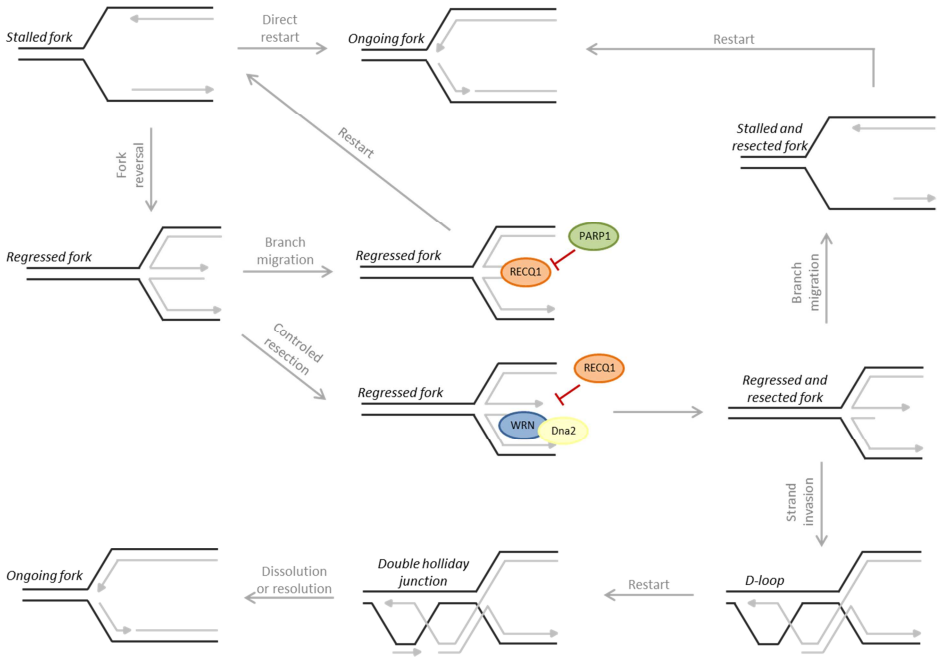

Figure 16. Models of mammalian replication fork restart in the absence of DSBs.
The mechanisms used to restart replication from unbroken forks are represented. Some of the molecules involved in certain steps are also represented. Adapted from "Pathways of mammalian replication fork restart"[289] and "Replication stress: getting back on track"[281].

3.3.2. Dormant origin firing and the repair of DSBs

Due to the bidirectional nature of replication forks, when a replication fork is stalled, a converging fork can compensate and replicate the entire intervening DNA. However, if both converging forks stall, dormant origins must be required to ensure replication of that area, unless replication is restarted from those stalled forks when the stress is overcome. In this regard, **dormant origin firing** is one of the mechanisms used to resume replication once replication forks have been processed into DSBs (Figure 17). However, even if replication is resumed by dormant origin firing, DSBs must be repaired afterwards[118,450].

DSB are repaired either by NHEJ- or HR-mediated mechanisms. It is generally accepted that NHEJ is the main repair mechanism during G1, although it is active throughout the entire cell cycle, while HR acts predominantly on S and G2 phases, when sister chromatids are present[412,432]. However, it has also been reported that NHEJ is the dominant repair pathway also in G2[460]. Several proteins have been described to be implicated in the choice of each of the pathways[432]. For instance, 53BP1 negatively regulates resection in G1 by protecting DSB ends, which is antagonized by BRCA1 in S phase to promote HR-mediated repair[461,462].

NHEJ consist in the ligation of broken DNA ends without homology, although there is a subtype of NHEJ, known as MMEJ (microhomology-mediated end-joining), that uses a little homology for this process[412,463]. On the other hand, HR uses homologous sequences, usually from the sister-chromatid, for the repair of DSBs.

HR-mediated repair starts with MRN complex and its interacting partner CtIP-induced DNA resection. The first step is the creation of nicks upstream the DSBs, which are followed by an initial 3'→ 5' resection. These resections are then further extended in 5' → 3' direction by Exo1 and Dna2 nucleases with the help of helicases such as BLM (Bloom syndrome protein). The resulting product is a 3' overhangs required for strand invasion[412,414,463]. This ssDNA is first wrapped by RPA protein, which is afterwards replaced by Rad51 with the help of several proteins such as BRCA1, BRCA2 and PALB2 (partner and localizer of BRCA2)[464]. The formed Rad51 nucleofilament mediates distant homologous sequence search and strand invasion. This invasion results in the formation of **D-loops** (displacement loops), since the invading ssDNA is paired to the homologous sequence, displacing the complementary strand. Finally, these structures lead to the formation of double-**Holliday junctions** (branched structures containing four double-stranded arms joined together) that are resolved either by dissolution or resolution mechanisms[463]. Due to the importance of maintaining sister chromatids together to allow strand invasion, cohesin complex is thought to be important also for HR-mediated repair[206,399].

3.3.3. Break-induced replication

In contrast to what it was thought, during the last years, increasing evidences agree on the possible reactivation of collapsed forks[452,453,455]. In this sense, Mus81 endonuclease-created DSBs were shown to contribute to replication restart[465], although another study showed that the terminally arrested replication forks were not efficiently restarted by Mus81[450].

The generation of breaks at replication forks results in the formation of one-end DSBs, which are thought to be repaired by a sub-type of HR-mediated mechanism known as **BIR**[452,453,455] (Figure 17). Notably, BIR-based mechanisms seem to be implicated not only in the repair of DSBs, but also, in the reactivation of broken replication forks. In fact, a couple of years ago, replication restart from broken forks by BIR was confirmed for the first time in human cells[454].

BIR consist in a Rad51-mediated strand invasion event that allows copying hundreds of kbs of DNA from a template strand. Interestingly, from works done in yeast it has been reported that the D-loop formed during strand invasion is not immediately resolved

during BIR to reestablish a functional replication fork. Instead, replication proceeds by D-loop migration while lagging strand is synthesize by using the nascent DNA as a template, being Polymerase 32 (ortholog of human PolD3) required for this process[466–468]. Notably, the CMG complex and Cdt1 are required for BIR[469].

Interestingly, since reversed forks have been shown to be processed by nucleases and/or break repair mechanisms[292,306,307], and as Mus81-induced DSBs have been shown to promote fork restart[465], it has been postulated that reversed forks that are unable to resume DNA replication might also use this mechanism to restart[281].

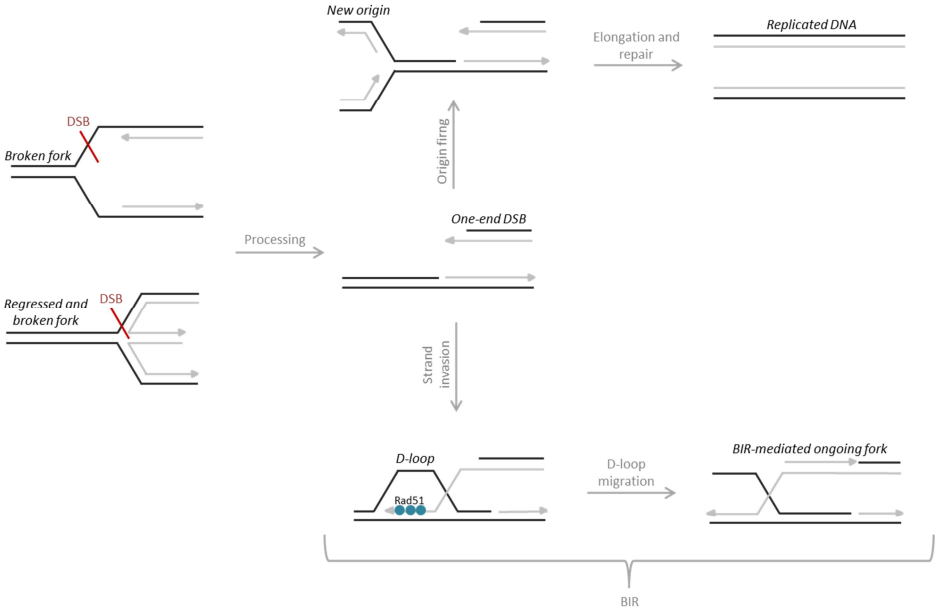

Figure 17. Models of mammalian replication resumption mechanisms from or in the presence of broken forks.
The mechanisms used to resume replication once replication forks have been processed into one-end DSBs are represented. Some of the molecules involved in certain steps are also represented. Adapted from "Pathways of mammalian replication fork restart"[289] and "Sources of DNA double-strand breaks and models of recombinational DNA repair"[463].

3.4. Cell cycle exit

As previously mentioned, in response to RS, cells will try to stabilize the forks and repair the damage in order to resume replication once the stress has been overcome. However, in response to persistent damage, cells are withdrawal from the cell cycle to avoid cell division in the presence of unreplicated or damage DNA, contributing to safeguarding the genome integrity[244–248].

The mechanisms that determine a cell going to apoptosis or senescence are not clear, but this choice seems to be cell type specific[47,433]. Consistently, extensive genotoxic stress has been shown to promote apoptosis in thymocytes[470], while fibroblasts are shown to initiate cellular senescence under this condition[471].

3.4.1. Apoptosis

One of the mechanisms that promotes cell cycle exit in response to persistent damage is **apoptosis**, a programmed cell death that serves to eliminate deregulated or damaged cells[433,472]. Proteins involved in cell cycle regulation and arrest are also regulators of apoptosis[472]. For instance, p53 regulates the expression of several proteins involved in apoptosis[433]. Additionally, apoptosis can also occur independently of the cell cycle arrest machinery[472].

As previously mentioned, p21 is one of the main downstream targets of p53, which mediates most of the tumor suppressor functions of this protein[48,49]. Paradoxically, in this case, p21 has been reported to have anti-apoptotic functions. Cytoplasmic p21 inhibits the activity of pro-apoptotic proteins such as caspases or SAPKs. Moreover, p21 induces the upregulation of anti-apoptotic genes, while it suppresses the induction of pro-apoptotic genes by Myc and E2F[45]. In this sense, p21 protects against apoptosis for instance in response to a deprivation of growth factors or to p53 overexpression. However, it is also thought to promote apoptosis either by p53-dependent or independent mechanisms under certain cellular stresses, although the mechanism is not clear[45].

3.4.2. Senescence

Senescence was first described as the finite proliferative capacity. This concept is used to describe a permanent cell cycle exit, which, as explained in section *(4.1)*, has been proposed to be a tumor suppressor mechanism. In contrast to other non-proliferative cells (arrested or quiescent cells), senescent cells express several markers and suffer morphological changes that are characteristic of them[47,473], although not all of them are universal[474].

Senescence has been described to occur either in G1, S or G2 phases depending on the cellular context. Additionally, depending on the factor promoting this phenomenon, two types of senescence have been described. The first one, known as **replicative senescence** (sometimes termed as cellular aging), is the one promoted by telomere shortening. The other one is induced by several aging- or telomere shortening-independent factors that promote stress, such as oncogenes or genotoxic agents, and is known as **premature senescence**[47].

Two different mechanisms have been reported to activate this permanent arrest, the ARF/p53 and p16/pRb pathways (Figure 18), although some evidences have suggested that there also additional pathways. These two pathways can interact between them, and proteins involved in one of them can induce senescence through the other pathway. In this sense, different stimuli are thought to activate different mechanisms to finally induce senescence[47,473].

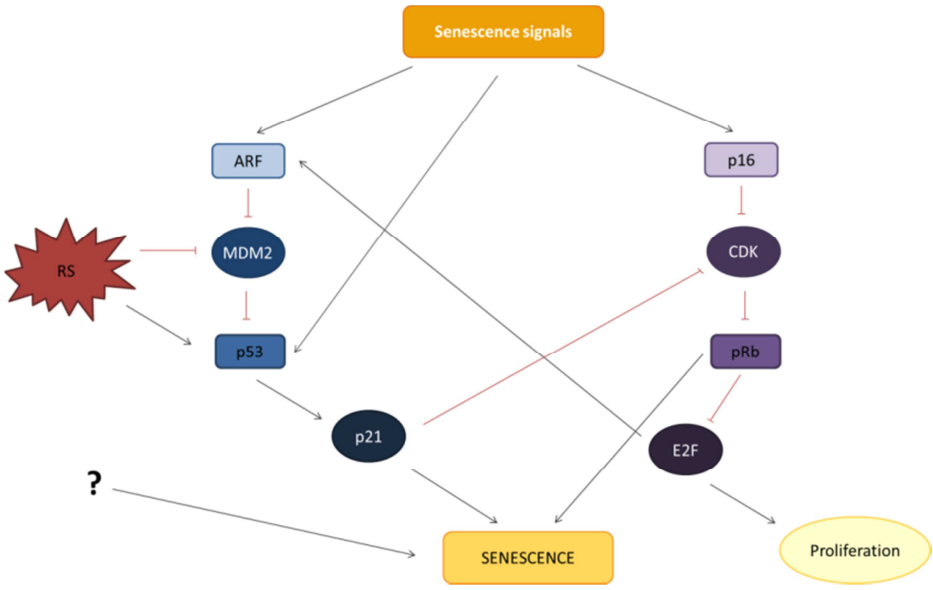

Figure 18. Senescence signaling pathways.
The signaling cascades that promote senescence are shown. In response to RS, p53 stabilization promotes p21-mediated senescence. In response to other intracellular or extracellular signals, senescence can be induced by other mechanisms. p53 and p16/pRb are the classical signaling pathways. However, there is a high crosstalk between them and proteins from one of the cascades can act on the other pathway. Moreover, the existence of additional pathways has also been postulated. Adapted from "Cellular senescence: when bad things happen to good cells"[47].

In response to persistent damage, p53 and p21 are the mediators of cellular senescence[45,433]. p21 promotes senescence by inhibiting CDKs, which indirectly will also inhibit E2F1-3-induced proliferation[45,47]. In addition, p21 may also promote senescence through CDK inhibition-independent roles, such as by direct binding to E2F1[50]. Nevertheless, since these are also the mechanisms used to induce a transient arrest, the determinants that promote senescence remain to be elucidated. In this sense, it has been postulated that rapid repair would quickly terminate p53/p21 signaling, promoting a transient arrest, whereas a permanent p53/p21 signaling due to unrepaired or persistent stress would induce senescence[47]. However, a transient p53 activation has recently been reported to be sufficient to induce senescence[475]. Remarkably, p53-/p21-mediated nuclear Cyclin B translocation has been described as the restriction point for a permanent withdrawal from the cell cycle in this case[475–477].

4. Replication stress, genomic instability and cancer

The accumulation of RS is one of the major sources of genomic instability, a hallmark of cancer. Alterations generated during replication are the major source of deletions, translocations, amplifications and other aberrations that can be carried until mitosis if the DNA replication stress response fails. This results in the accumulation of abnormalities in the genome that contribute to the development and/or progression of human malignancies such as cancer[245,246,451,478].

Tumor cells tend to accumulate mutations and increased copy number of chromosomes to silence or overexpress certain genes, in order to acquire growth, survival or metastatic advantages[451,479]. In this regard, proteins involved in the DNA replication stress response and in cell cycle regulation, such as p53, pRb or ATM, are some of the most commonly mutated genes on human cancers[478]. In addition, **CIN** (chromosomal instability), which reflects ongoing changes on chromosome structure and number, is also commonly observed in tumor cells. Likewise, **aneuploidy** (abnormal number of chromosomes) is another common feature of cancer cells, which has been reported to contribute to increase the numerical and structural chromosomal aberrations[479].

This ongoing acquisition of mutations and alterations seems to be required for cancer development. In fact, cancer development seems to be a multistep process in which each particular mutation confers a unique capability that cancer cells need to acquire to proliferate, survive and metastasize[480].

The complexity and variety of the alterations that lead to cancer development makes it almost impossible to find universal therapies to act against it. For this reason, the identification of critical characteristics for the survival of cancer cells would be crucial to develop successful therapies. Accordingly, new promising therapies based on the increased RS[252,253] and dependency that tumor cells present on ATR/Chk1 pathway[245], or on the ability to incorporate damaged dNTPs[481] have been proposed.

This section summarizes the contribution of replication-related alterations and RS to the acquisition of genomic instability.

4.1. Genomic instability due to alterations during DNA replication

4.1.1. Common fragile sites and early replicative fragile sites

CFSs (common fragile sites) are the most vulnerable regions to RS. This stress induces DNA breaks on CFSs and ERFSs (early-replicating fragile sites), which lead to chromosomal aberrations such as deletions[245,246].

CFSs are late-replicating genome regions that accumulate breaks, gaps and constrictions that can be observed in metaphase chromosomes. These regions are characterized for presenting lower density of origins, A-T rich repetitive sequences and for being at euchromatin-heterochromatin transition regions. As previously mentioned, this lower density of origins increases the risk to accumulate stalled forks[246,248,482], which may explain the genomic instability associated with CFS. Accordingly, decreased

origin firing capability as a result of reduced MCM2-7 function, has been shown to increase genomic instability and breast cancer risk[483].

However, regardless the accumulation of stalled forks, the increased number of DNA breaks in those CFS regions is thought to be due to active, rather than passive, mechanisms such as Mus81- or ERCC1-induced breaks[244], and thus, the resulting genomic instability might also be promoted by those mechanisms.

By contrast, **ERFS**s are located at open chromatin regions that are replicated early in S phase, and which present high levels of transcription. In this case, RS that might lead to the acquisition of genomic instability is thought to arise from R-loops or other transcription-replication interferences[244,245].

CFSs and ERFSs are often found rearranged in human tumors. In this sense, a high number of cancer-associated deletions, and most of the cancer-specific translocation breakpoints are found at CFSs and ERFSs[245,246,482]. Additionally, CFSs are the favorite targets of oncogene-induced RS in precancerous lesions[246].

4.1.2. Replication restart and DNA repair mechanisms-induced genomic instability

Replication restart after RS does not necessarily imply the acquisition of genomic instability. In fact, if the DNA replication checkpoint works properly, forks would be stabilized to resume replication from the same place once the stress is removed, and thus, genome integrity would not be compromised[247,280,289]. However, if forks are not properly stabilized and they acquired DSBs, replication resumption from broken forks or in the presence of them can compromise genome integrity[290,451]. In addition, even in the absence of DSBs, DDT mechanisms may also induce genomic instability after RS[280,281].

As previously explained, replication resumption after replication forks have been processed into DSBs is meditated either by origin firing or BIR[450,454], which can both compromise genome integrity. In this sense, deregulated origin firing could for instance alter the replication timing program and modify epigenetic inheritance[271,449]. Moreover, unscheduled origin firing can result in overreplication, promoting ssDNA accumulation or a deficiency in limiting factors, and lead to chromosomal breakages. Furthermore, these alterations can result in genome rereplication which has been associated with gene amplification events, which are one of the major drivers of cancer[451].

Additionally, even if replication is correctly resumed from dormant origins[118], DSBs must be repaired afterward, and this may also compromise genome integrity since repair mechanisms can be error-prone[248,450]. For example, HR in S phase can result in epigenetic alterations[272]. Moreover, HR using repetitive sequences can lead to large-scale genome rearrangements[248]. In this sense, it has been shown that small insertions or deletions at repetitive regions can lead to big genome rearrangement if this regions are used to recombine[484].

In addition, BIR has also been shown to be highly mutagenic[456–459]. Indeed, BIR-based mechanisms can explain the complexity of the chromosomal changes that occur on cancer cells[252,253,485–487]. For instance, BIR-based mechanisms can generate complex genome rearrangements if the broken replication fork is annealed with microhomology

on any ssDNA that is nearby[487]. Furthermore, since BIR can occur by several rounds of strand invasion, dissociation and reinvasion within a dispersed repeated sequence can lead to genome rearrangements[456]. In addition, the non-canonical polymerase activity of Pol32 has been described to be highly mutagenic[458].

Finally, even if the used repair mechanism is not error-prone, the increased accumulation of DSBs enhances the risk of leaving unrepaired breaks that can lead to chromosomal rearrangements or deletions that contribute to the acquisition of genomic instability[451,479].

4.1.3. OIS: Oncogene-induced senescence

Oncogenes are positive regulators of cell cycle progression, and thus, they are commonly mutated in cancer. Indeed, oncogenes are considered as one of the drivers of cancer development[478].

However, some years ago it was shown *in vivo* that oncogene overexpression results in the accumulation of senescent cells in precancerous lesions[488,489]. At the same time, it was reported that precancerous lesions present an increased DDR, and it was postulated that this response was an important tumorogenic barrier[276,490]. In fact, shortly after, it was shown that the establishment of a correct DDR after oncogene overexpression was essential for the induction of senescence in precancerous lesions, which was as an important tumorogenic barrier[252,253,491]. Since then, the inactivation of the DDR is thought to be required to abrogate **OIS** and to promote tumorogenesis, after oncogene overexpression or their constitutive activation[252,253,491]. Indeed, this might explain why precancerous lesions present much higher DDR than tumors at later and more aggressive stages[276,490]. Interestingly, DNA hypereplication and the accumulation of RS as a result of oncogene overexpression were shown to be essential for the establishment of the DDR under these conditions[252,253]. In this sense, the inhibition of DNA replication was shown to abrogate the DDR activation and senesce after oncogene overexpression, confirming that the accumulation of RS is important for OIS establishment[252]. Accordingly, and consistent with the idea that ATR/Chk1 pathway limits RS[318,319], the incorporation of an extra allele of Chk1 results on increased transformation due to reduced RS after H-Ras^{G12V} expression[492].

Oncogene overexpression or constitutive activation is known to promote fork stalling, which can ultimately lead to the accumulation of DSBs, resulting in the activation of the DDR. However, how these oncogenes promote RS is still controversial. In this sense, several hypotheses have been postulated. On the one hand, it has been shown that the overexpression of Cyclin E results in premature S-phase entry with reduced number of licensed origins[270], which results in shortage of back-up origins to cope with stalled forks[118,245,246,248]. In addition, Cyclin E overexpression has been reported to increase origin firing, resulting on replication-transcription interferences and increasing the topological stress, which results in fork reversal and reduced replication fork progression[260,313]. Additionally, it has also been described that Cyclin E overexpression can promote rereplication[276], which as previously explained, increases the risk of fork stalling due to ssDNA accumulation or to insufficient limiting factors among other[248,279]. In relation with this, it has also been reported that oncogene overexpression-induced

RS is due to a nucleotide deficiency[254,493–495]. In this case, H-Ras^{G12V} expression, as well as Ras or c-Myc overexpression, resulted in reduced expression of RR (Ribonucleotide reductase) and TS (Thymidylate synthase), promoting a decrease in dNTP levels that can explain the RS[493–495]. Nevertheless, this is somehow controversial with the fact that RR is generally overexpressed in human cancers[496].

Notably, the decrease in dNTP levels induced by Ras and c-Myc was shown to be important for OIS establishment and maintenance[493–495]. By contrast, a decrease in RS, induced by an extra supply of nucleotides, was shown to decrease transformation in HPV-16 E6/E7 expressing cells[254], indicating that the response to different oncogenes may be diverse.

4.1.4. CIN: chromosomal instability

CIN is a hallmark of cancer. However, whether CIN can initiate cancer, of if by contrast it is a consequence is still under debate. Several evidences indicate that although CIN might favor cancer initiation, further mutations may also be required[479].

Until very recently, altered mitotic checkpoint, supernumerary centrosomes and other aberrations that cause chromosome segregation errors during mitosis were thought to be the drivers of CIN[479]. Accordingly, tetraploidy has also been reported to promote CIN[497]. However, a few years ago it was described that RS was the major driver of CIN. In this sense, it was reported that CIN positive tumor cells present several structural and numerical chromosomal alterations associated with RS-mediated DNA damage. This alterations were reverted by preventing RS-induced DNA damage by nucleoside addition, supporting a direct role of RS in driving CIN[485].

Nevertheless, this affirmation is still somehow controversial. It has been generally accepted that alterations during DNA replication would contribute to structural rearrangements of chromosomes. However, if these pre-mitotic alterations, such as unresolved or unreplicated regions that result in acentric fragments or anaphase bridges among others, are sufficient to cause numerical instability is still under debate[479]. In this sense, it has been postulated that errors arising from mitosis, such as lagging chromosomes, rather than pre-mitotic defects, may be the main drivers of numerical instability-associated CIN[498].

PREVIOUS DATA

1. Non-transformed human cells are able to resume replication and enter into mitosis after short but not long RS

As explained in the introduction, DNA replication is highly vulnerable to the acquisition of DNA damage. Defects in this process are known to promote genomic instability, a hallmark of cancer. Therefore, several mechanisms have evolved to ensure accurate duplication of the genomes[2,480]. While the DDR has been extensively studied in tumor cells, the pathways involved in the DNA replication stress response are less understood especially in non-transformed human cells. In this regard, the main goal of our group is to analyze and characterize the DNA replication stress response of human cells, using mainly the ribonucleotide reductase inhibitor HU as a RS agent[250,251]. Previous data from our group showed that tumor and non-transformed human cells present different responses to RS[324,499,500]. In the presence of HU, tumor cells, such as HeLa or HCT116, entered into mitosis after the inhibition of checkpoint kinases. By contrast, all the analyzed non-transformed human cells remained arrested in S phase under the same conditions (Figure 1).

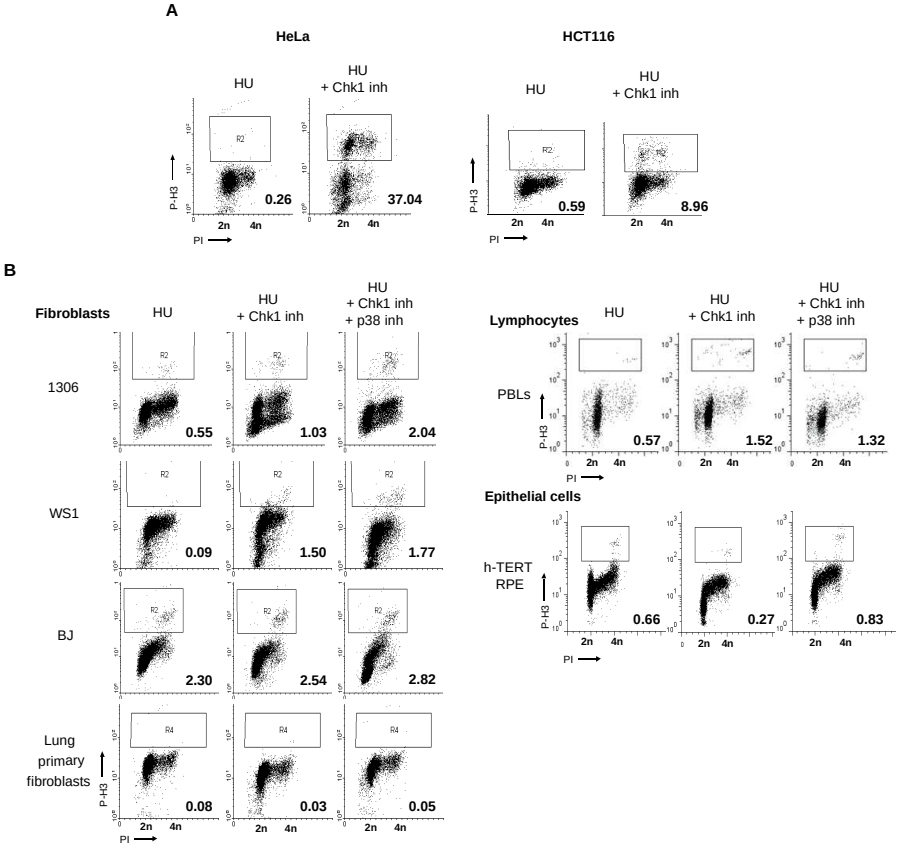

Figure 1. Non-transformed human cells remain arrested in S phase despite the inhibition of checkpoint kinases.

(A) HeLa and HCT116 cell were treated with 1.5mM HU +/- Chk1 inhibitor (inh, 300nM UCN-01) for 24h (Chk1 inhibitor was added during the last 10h of treatment). (B) Several non-transformed human cells were treated

with 1.5mM HU for 24h. Nocodazole +/- Chk1 (300nM UCN-01) and p38 (20µM SB203580) inhibitors were added during the last 6h of treatment. hTERT-RPE cells were synchronized in S phase and then treated with HU +/- Chk1 (300nM UCN-01) and p38 (20µM SB203580) inhibitors for 6h in the presence of nocodazole. DNA content (PI: propidium iodide) and the percentage of mitotic cells (P-H3: P-histone 3 positive cells) were analyzed by flow cytometry. Representative percentages of P-H3 positive cells are indicated.

These results demonstrate that non-transformed human cells have a more robust DNA replication checkpoint response, and thus, during the last years our group has focused on studying the additional mechanisms present on non-transformed human cells that contribute to preserve genome integrity in those cells.

Given the importance of a correct DNA replication in safeguarding genome integrity, the next objective of our group was to analyze the determinants of the cell cycle arrest observed in non-transformed human cells. For this purpose, hTERT-RPE cells[501] were labeled with BrdU (5-bromo-2'-deoxyuridine) and then treated during 2 or 14 hours with 10mM HU, which was shown to be the minimal dose able to induce a complete arrest in S phase (Figure 2A). Cells were finally released into nocodazole containing medium for 24 hours, after which S-phase arrest and mitotic entry from BrdU positive population was analyzed by flow cytometry. This experiment showed that hTERT-RPE cells are able to resume DNA replication and arrive to mitosis after short (2-hour) but not long (14-hour) HU treatment (Figure 2B).

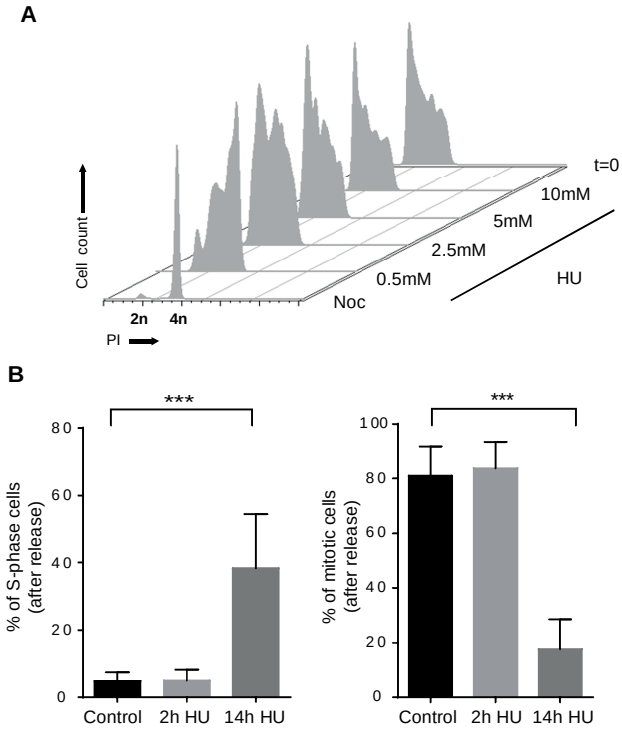

Figure 2. hTERT-RPE cells are able to resume cell cycle after a short but not long HU treatment.
(A) hTERT-RPE cells were labeled with BrdU for 30min and then treated with the indicated HU concentration for 14h. DNA content (PI: propidium iodide) from BrdU positive population was analyzed by flow cytometry. Noc: cells were treated with nocodazole for 14h. t=0h: cells were harvested just after the BrdU labeling. (B)

hTERT-RPE cells were labeled with BrdU as in *(A)*, treated during the indicated time with HU (or left untreated, control), and finally released into nocodazole containing medium for 24h. DNA content and mitotic entry, from BrdU positive population, was analyzed by flow cytometry. The average percentages of BrdU positive cells that remain in S phase (left panel) or that enter into mitosis (right panel) after release are shown in the graphs. Error bars represent standard deviation, (paired *t test*, n=6).

Similar results were also obtained in two additional non-transformed human cells (BJ-5ta and MCF10A), and in response to DNA damage-inducing agents (camptothecin or etoposide) (Figure 3).

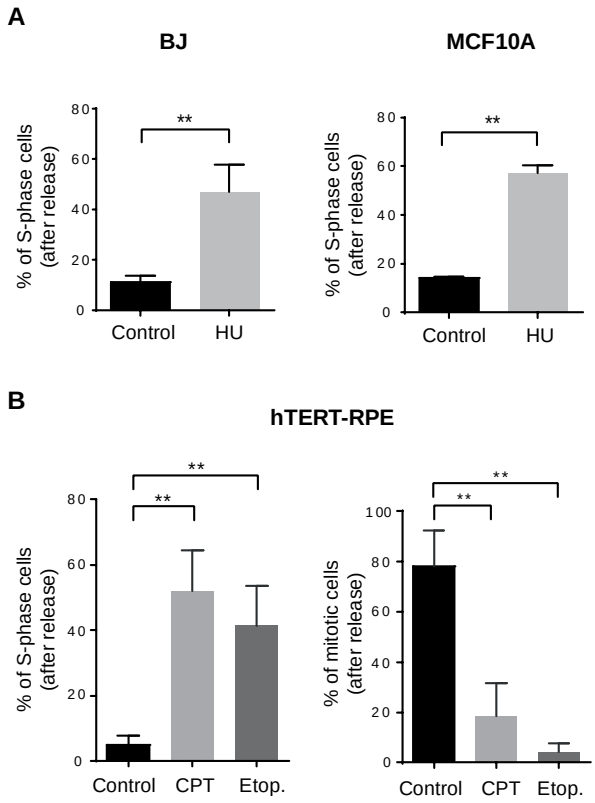

Figure 3. Non-transformed human cells lose the ability to recover upon severe replication stress.
(A) Asynchronously growing MCF10A and BJ-5ta cells were labeled with BrdU for 30min, treated during 14h with HU (or left untreated, control) and then released into fresh medium with nocodazole for 24h. The average percentages of BrdU positive cells that remain in S phase after release are shown in the graphs. (B) hTERT-RPE cells were labeled with BrdU as in *(A)*, treated with the indicated drug for 14h, and finally released into nocodazole containing fresh medium. The average percentage of cells that remain in S phase (left panel) or mitosis (right panel) from BrdU positive population are shown in the graphs. CPT: camptothecin. Etop.: etoposide. Error bars represent standard deviation, (paired *t test*, n=3).

2. Cyclin A2 and Cyclin B1 are degraded in S phase after prolonged DNA replication inhibition

Due to the importance of cyclins for cell cycle progression[1], it was though that low cyclin levels could be the responsible for the observed arrest. Consistently, Cyclin B1 expression had been shown to be repressed in several cell lines in response to HU[499,500].

Interestingly, Cyclin A2 and Cyclin B1 levels decreased in response to HU, despite cells were arrested in S phase (Figure 4A and 2A). Moreover, this decrease was due to degradation since the addition of MG132 proteasome inhibitor recovered their levels (Figure 4B).

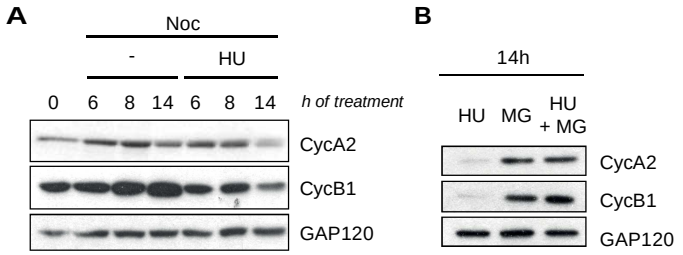

Figure 4. Cyclin A2 and Cyclin B1 are degraded in hTERT-RPE cells after prolonged DNA replication inhibition.
(A, B) hTERT-RPE cells were synchronized in S phase and then treated during the indicated time with HU or left untreated (-). Proteasome inhibitor MG132 (MG) and nocodazole (Noc) were added where indicated. Whole cell lysates were analyzed by WB with the indicated antibodies. GAP120 was used as loading control. Cyc: cyclin.

3. The degradation of Cyclin A2 and Cyclin B1 correlates with the loss of replication recovery competence

To determine if the degradation of Cyclin A2 and Cyclin B1 was responsible for the observed loss of replication recovery competence, hTERT-RPE cells were synchronized in S phase, treated with HU and then harvested at different time points simultaneously for WB (Western blot) or flow cytometry (cell were released into nocodazole containing medium for 24 hours before harvest them in the second case). This experiment showed that there is a correlation between the time in which these proteins start to degrade and the replication recovery competence is lost (Figure 5).

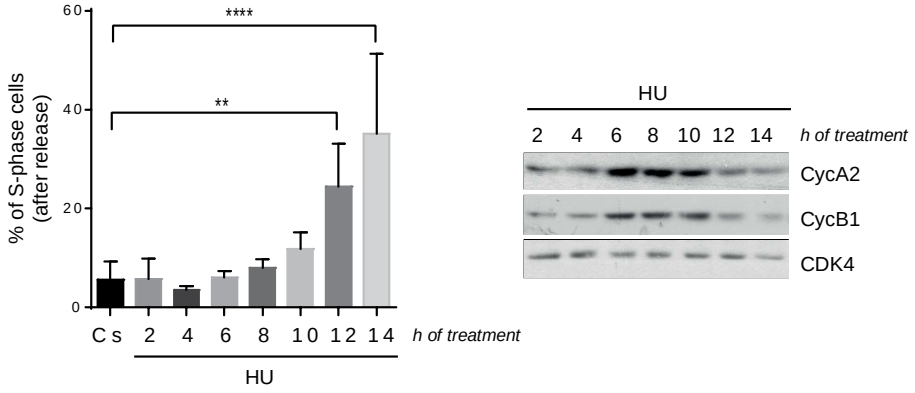

Figure 5. Cyclin A2 and Cyclin B1 degradation timing correlates with the loss of replication recovery competence in hTERT-RPE cells.
S-phase synchronized hTERT-RPE cells were treated during the indicated time with HU (or left untreated, Cs) and then harvested (for WB) or released into nocodazole containing fresh medium for 24h (for flow cytometry). DNA content was used to determine the number of cells that remain in S phase after release (left panel). The average percentages of cells that remain in S phase are shown. Error bars represent standard

deviation, (paired *t test*, n=4). Whole cell lysates were analyzed with the indicated antibodies (right panel). CDK4 was used as loading control. Cyc: cyclin.

Additionally, this experiment confirmed that thymidine synchronization had no effect on cell cycle progression in hTERT-RPE cells (Figures 5 and 2).

OBJECTIVES

The general aim of this thesis was to define and characterize new DNA replication stress response pathways that contribute to preserve genome integrity of non-transformed human cells. From the data presented in the previous section, we defined three specific objectives for this thesis:

I. To study the mechanisms involved in the loss of replication recovery competence of non-transformed human cells.

II. To establish the differences, at replication fork level, between short and long HU treatments that determine the loss of replication recovery competence in hTERT-RPE cells.

III. To analyze the contribution of severe replication stress-induced S-phase arrest towards safeguarding genome integrity.

RESULTS

Chapter I

Deciphering the mechanisms involved in the loss of replication recovery competence and defining their role in preventing genomic instability

The results presented in this chapter have been obtained working in collaboration with Alba Llopis, Ph.D.

As previously explained, our group is interested in studying the DNA replication stress response of non-transformed human cells, in order to define the mechanisms involved in preventing genomic instability in this model. Previous studies from our group showed that non-transformed human cells present a more robust DNA replication stress response than tumor cells[324,499,500]. Moreover, non-transformed human cells were shown to lose the ability to recover from severe replication stress. Furthermore, a correlation between the degradation of Cyclin A2 and Cyclin B1 in S phase and the loss of replication recovery competence was described. However, the mechanism behind this degradation and its implication in the loss of replication recovery competence were still unknown. Likewise, the contribution of this loss of replication recovery competence towards safeguarding genome integrity also remained to be elucidated.

1.1. hTERT-RPE cells become senescent after prolonged DNA replication inhibition

The previous data from our group indicating that the recovery from severe replication stress was impaired in non-transformed human cells came from studies in which recovery was only analyzed during the first 24 hours of release. Thus, in order to verify that the observed S-phase arrest was maintained over time, we decided to perform a cell proliferation assay.

To this end, S-phase synchronized hTERT-RPE cells were treated during 14 hours with HU and then released into fresh medium during different times. Finally, cell proliferation was analyzed by measuring the absorbance of crystal violet (λ595) (Figure 1). This experiment showed that proliferation was impaired even after 72 hours of release, indicating that cells remain arrested after 3 days of HU treatment.

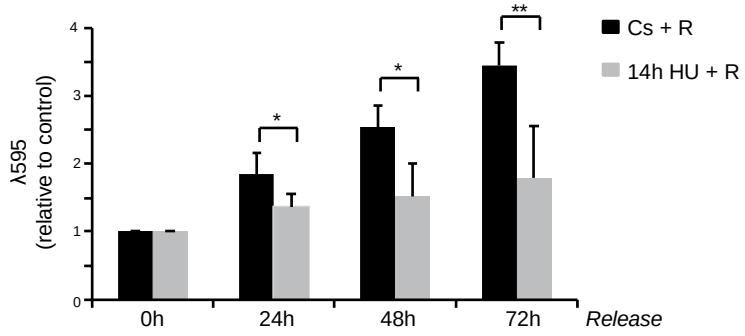

Figure 1. Cell proliferation is strongly compromised in hTERT-RPE cells after a 14-hour HU treatment.
S-phase synchronized hTERT-RPE cells were treated during 14h with HU or left untreated (Cs) and then released (R) into fresh medium during the indicated time. Finally, cells were harvested and stained with crystal violet to analyze cell proliferation by measuring its absorbance (λ595). The average fold increase, relative to t=0h, in each time point is shown in the graph. Error bars represent standard deviation, (unpaired *t test*, n=4).

In order to define the fate of those S-phase arrested cells, we decided to analyze several senescence markers[47]. Interestingly, pRb was shown to be hypophosphorylated after a 24-hour release from long HU treatment (Figure 2). Likewise, an increase in p21 levels was observed under the same conditions. Moreover, hTERT-RPE cells present SA-

β-Gal (senescence-associated β-galactosidase activity)[502] after a 48-hour release from long HU treatment.

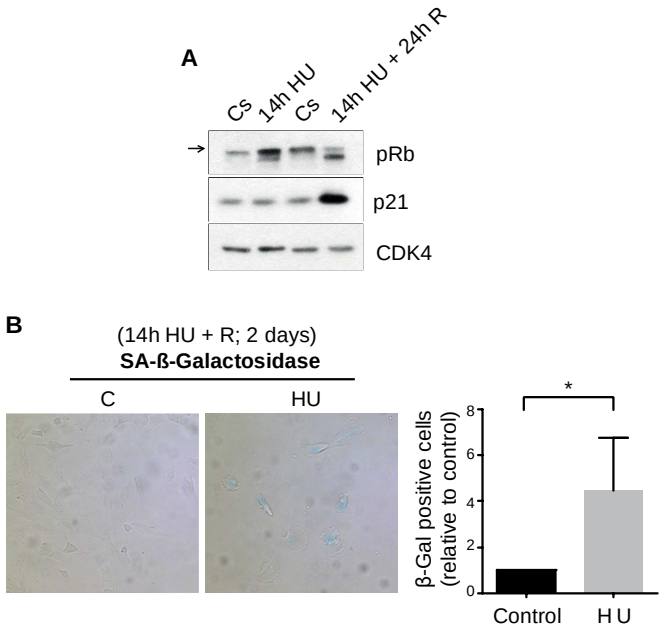

Figure 2. hTERT-RPE cells become senescent after prolonged DNA replication inhibition.
(A) S-phase synchronized hTERT-RPE cells were treated during 14h with HU or left untreated (Cs) and then harvested (for WB) or released (R) into fresh medium for 24h. Whole cell lysates were analyzed by WB with the indicated antibodies. CDK4 was used as loading control. The arrow indicates the hyperphosphorylated band of pRb. (B) hTERT-RPE cells were synchronized in S phase, treated during 14h with HU (or left untreated (C or Control)) and then released into fresh medium for 48h. Representative images of SA-β-Gal staining (left panel) and the average fold increase in SA-β-Gal positive cells relative to control are shown (right panel). Error bars represent standard deviation, (unpaired, n=4).

Altogether, the above results indicate that the previously observed S-phase arrest, correlates with an increase in senescent cells in response to prolonged DNA replication inhibition.

1.2. The degradation of Cyclin A2 and Cyclin B1 in S phase is a general feature of non-transformed human cells in response to severe replication stress

The degradation of Cyclin A2 and Cyclin B1 in S phase in response to prolonged HU treatment has been described by our group. Additionally, a correlation between the time those proteins start to degrade and the replication recovery competence is lost has been established. In this sense, while recovery studies had been validated in several non-transformed human cells and in response to different stress-inducing agents, the degradation of Cyclin A2 and Cyclin B1 in S phase had only been studied in HU-treated hTERT-RPE cells. Thus, we wondered whether, consistent with our previous data, the degradation of these proteins was also a general feature of non-transformed human cells, observed in response to several stress-inducing agents.

In this regard, the degradation of Cyclin A2 and Cyclin B1 was analyzed in hTERT-RPE cells treated with other DNA damage-inducing agents, such as camptothecin or etoposide, known to promote an S-phase arrest after a long treatment (as shown by previous data from our group). As expected, a long treatment with those DNA damage-inducing agents also promoted a decrease in CyclinA2 and Cyclin B1 levels in hTERT-RPE cells (Figure 3).

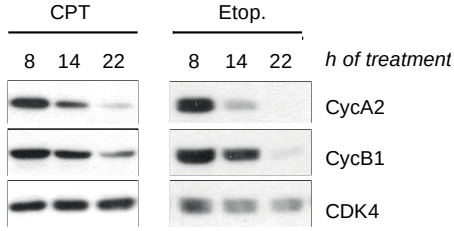

Figure 3. Cyclin A2 and Cyclin B1 levels decrease in hTERT-RPE cells after a long treatment with DNA damage-inducing agents.
hTERT-RPE cell were synchronized in S phase and then treated during the indicated time with camptothecin (CPT) or etoposide (Etop.). Whole cell lysates were analyzed by WB with the indicated antibodies. CDK4 was used as loading control. Cyc: cyclin.

Moreover, those proteins degradation was also observed in BJ-5ta and MCF10A cells (Figure 4), which had previously been shown to become arrested in S phase in response to prolonged HU treatment. Thus, consistent with our previous data, these results indicate that the degradation of Cyclin A2 and Cyclin B1 in S phase is also a general feature of non-transformed human cells upon severe replication stress.

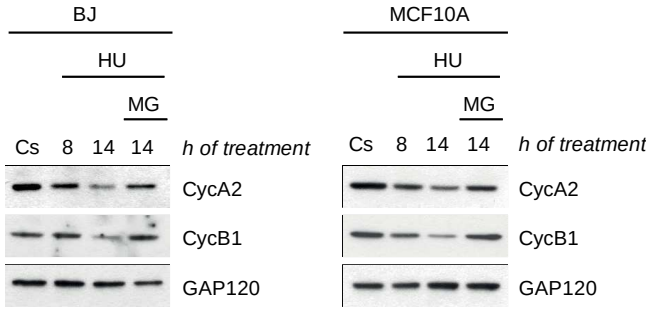

Figure 4. Cyclin A2 and Cyclin B1 are degraded in BJ-5ta and MCF10A in response to prolonged DNA replication inhibition.
BJ-5ta and MCF10A cells were synchronized in S phase and then treated during the indicated time with HU or left untreated (Cs). MG132 (MG) proteasome inhibitor was added during the last 6h of treatment where indicated. Whole cell lysates were analyzed by WB with the indicated antibodies. GAP120 was used as loading control. Cyc: cyclin.

To further confirm the previously observed correlation, we wanted to verify if, as in the case of replication resumption, thymidine synchronization had no effect either on the degradation of Cyclin A2 and Cyclin B1. To this end, hTERT-RPE cells were synchronized by serum starvation and then treated with HU during different times. As expected,

Cyclin B1 levels decreased after prolonged HU treatment also in this case, indicating that thymidine had no effect in the degradation of this protein (Figure 5).

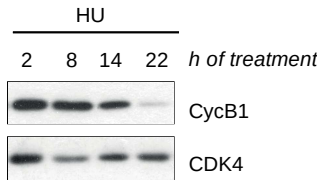

Figure 5. Cyclin B1 levels decrease in response to HU in serum starvation synchronized hTERT-RPE cells. hTERT-RPE cells were synchronized by serum starvation and then treated during the indicated time with HU. Whole cell lysates were analyzed with the indicated antibodies. CDK4 was used as loading control. Cyc: cyclin

Furthermore, as replication recovery competence had been analyzed on cells released from HU treatment, we wondered if the degradation of these proteins was also observed under this condition. To analyze it, we treated S-phase synchronized hTERT-RPE cells during 14 hours with HU, and then released them into fresh medium during different times to analyze Cyclin A2 and Cyclin B1 levels. Remarkably, the degradation of these proteins continued even after HU removal under these conditions (Figure 6).

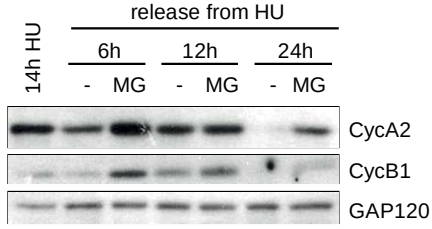

Figure 6. The degradation of Cyclin A2 and Cyclin B1 continues even after HU removal in hTERT-RPE cells. hTERT-RPE were synchronized in S phase and then treated during 14h with HU. Cells were then harvested or released into fresh medium during the indicated time. MG132 (MG) proteasome inhibitor was added during the last 6h of treatment where indicated. Whole cell lysates were analyzed by WB with the indicated antibodies. GAP120 was used as loading control. Cyc: cyclin.

Collectively, the above results showing that the degradation of Cyclin A2 and Cyclin B1 is a general feature of non-transformed human cells in response to severe replication stress, observed even after HU removal, reinforces the idea that there is a correlation between the degradation of these proteins and the loss of replication recovery competence in those cells.

1.3. APC/C^{Cdh1} is prematurely activated in S phase in response to prolonged DNA replication inhibition in hTERT-RPE cells

According to our previous data, the characterization of the mechanisms involved in the degradation of Cyclin A2 and Cyclin B1 in S phase in response to severe replication stress, may be useful to study how replication recovery competence is lost under these conditions. Therefore, we decided to analyze which was the ubiquitin ligase responsible for the degradation of those proteins, and how was it regulated.

1.3.1. The activation of APC/C^{Cdh1} in S phase is the responsible for, among others, Cyclin A2 and Cyclin B1 degradation in response to prolonged HU treatment

During a normal cell cycle, Cyclin A2 and Cyclin B1 are regulated by the APC/C[29,30]. Moreover, this ubiquitin ligase, associated with its coactivator Cdh1, has been shown to be activated in response to DNA damage in G2 in order to degrade several of its substrates[150–152,443]. Thus, we wondered whether this complex was also the responsible for the degradation of Cyclin A2 and Cyclin B1 in S phase in response to prolonged DNA replication inhibition.

In this regard, we decided to analyze the degradation of Cyclin A2 and Cyclin B1 in S-phase synchronized hTERT-RPE cells that had been treated with HU and the APC/C inhibitor proTAME[503]. Interestingly, the pharmacologic inhibition of the APC/C ubiquitin ligase recovered Cyclin A2 and Cyclin B1 levels in HU-treated hTERT-RPE cells (Figure 7).

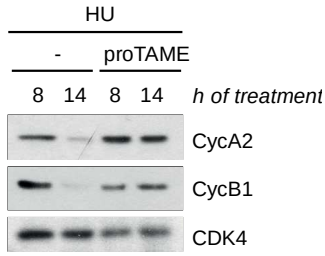

Figure 7. Cyclin A2 and Cyclin B1 are degraded by APC/C in hTERT-RPE cells in response to prolonged DNA replication inhibition.
hTERT-RPE cells were synchronized in S phase and then treated during the indicated time with HU +/- proTAME. Whole cell lysates were analyzed by WB with the indicated antibodies. CDK4 was used as loading control. Cyc: cyclin.

Additionally, since proTAME is a general inhibitor of APC/C, we decided to analyze if specifically APC/C^{Cdh1} was the responsible for the degradation of those proteins. Remarkably, Cdh1 depletion (by siRNA) recovered Cyclin A2 and Cyclin B1 levels under these conditions in hTERT-RPE cells (Figure 8). Moreover, the addition of MG132 proteasome inhibitor did not further increase the levels of those proteins, indicating that this ubiquitin ligase was the sole responsible for the observed degradation.

In addition, other APC/C^{Cdh1} substrates, such as Plk1 and Aurora A, were also degraded in S phase by this ubiquitin ligase after prolonged DNA replication inhibition, and once again, their degradation did not further increase after the addition of MG132 (Figure 8).

Collectively, the above results indicate that the activation of APC/C^{Cdh1} in S phase is the responsible for, among others, Cyclin A2 and Cyclin B1 degradation after prolonged HU treatment in hTERT-RPE cells.

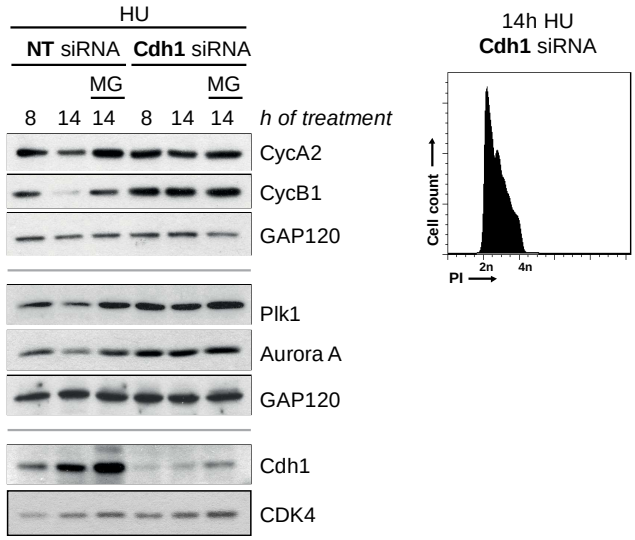

Figure 8. APC/C^{Cdh1} is activated in S phase in hTERT-RPE cells to degrade several of its substrates in response to prolonged HU treatment.
hTERT-RPE cells were transfected with the indicated siRNAs and then synchronized in S phase before HU treatment. Cells were harvested at the indicated time of HU treatment. MG132 (MG) was added during the last 6h of treatment where indicated. DNA content (PI: propidium iodide) of Cdh1-depleted 14h HU-treated cells was analyzed by flow cytometry. A representative DNA profile is shown (right panel). Whole cell lysates were analyzed by WB with the indicated antibodies (left panel). GAP120 and CDK4 were used as loading control. Cyc: cyclin. NT: non-target.

1.3.2. The activation of APC/C^{Cdh1} in S phase correlates with a decrease in Emi1 levels, is not prevented by the inhibition of ATM/ATR, but is abrogated in p53-/p21-depleted cells

Once having defined that the activation of APC/C^{Cdh1} in S phase was the responsible for the degradation of Cyclin A2 and Cyclin B1 in response to prolonged DNA replication inhibition, we wanted to know how this complex was activated under these conditions.

- *The inhibition of ATM/ATR does not prevent the activation of APC/C^{Cdh1} in response to HU*

In response to DNA damage, APC/C^{Cdh1} has been described to be activated either by ATM-dependent or -independent mechanisms[150–152]. Thus, we decided to analyze if ATM was required for the activation of this ubiquitin ligase in S phase. Moreover, since ATR is the main kinase involved in the DNA replication stress response[247], we decided to analyze also its contribution to this ubiquitin ligase activation.

To this end, S-phase synchronized hTERT-RPE cells were treated with HU in the presence of ATM or ATR inhibitors, and Cyclin A2/Cyclin B1 levels were analyzed (as markers of APC/C^{Cdh1} activation) during different time points. As shown in Figure 9, the pharmacological inhibition of ATM and ATR alone or in combination did not abrogate the activation of APC/C^{Cdh1} in S phase in response to prolonged

HU treatment. However, whereas ATR inhibition alone resulted in advanced degradation of Cyclin A2 and Cyclin B1, the sole ATM inhibition had no effect on the APC/C^{Cdh1} activation dynamics.

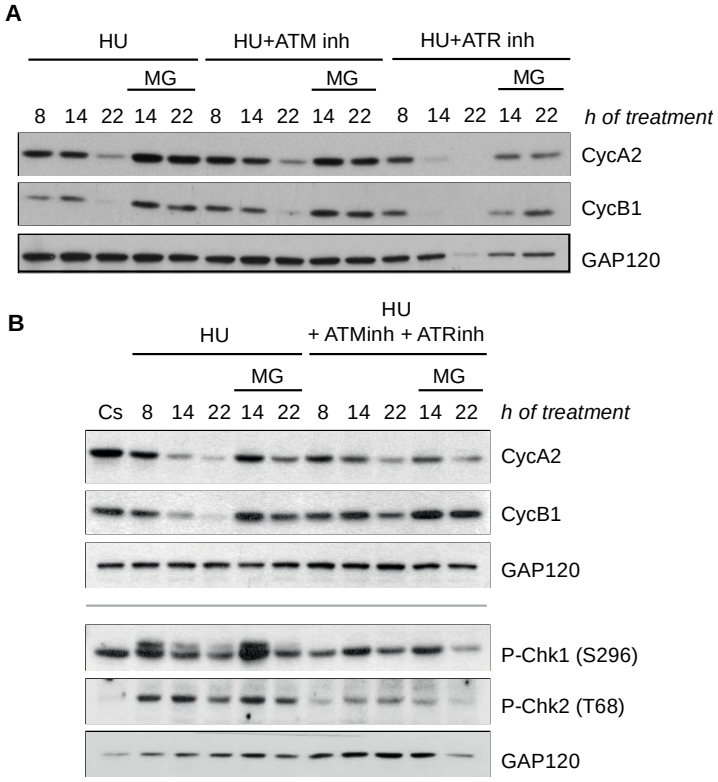

Figure 9. The inhibition of ATM and ATR does not abrogate the activation of APC/C^{Cdh1} in S phase in HU-treated hTERT-RPE cells.
(A, B) S-phase synchronized hTERT-RPE cells were treated with HU +/- ATM (KU-55933) or ATR (VE 821) inhibitor (inh) during the indicated time. MG132 (MG) was added during the last 6h of treatment where indicated. Whole cell lysates were analyzed with the indicated antibodies. GAP120 was used as loading control. Cyc: cyclin.

Additionally, consistent with the previously described correlation between the degradation of Cyclin A2 and Cyclin B1 and the loss of replication recovery competence, the inhibition of ATM and ATR did not either abrogate the S-phase arrest induced by prolonged HU treatment (Figure 10).

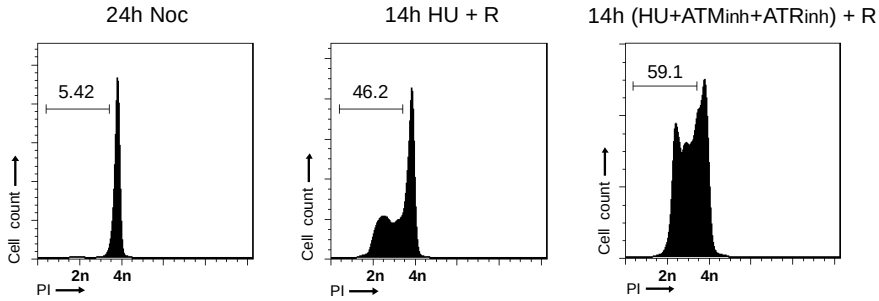

Figure 10. The inhibition of ATM and ATR does not abrogate prolonged DNA replication inhibition-induced S-phase arrest in hTERT-RPE cells.
Asynchronously growing hTERT-RPE cells were labeled with BrdU and then treated with HU +/- ATM and ATR inhibitors (inh) (KU-55933 and VE 821 respectively) for 14h or left untreated (24h Noc). Cells were then released (R) into nocodazole (Noc) containing fresh medium for 24h more. DNA content (PI: propidium iodide) of BrdU positive cells was analyzed by flow cytometry. The percentage of S-phase arrested cells from BrdU positive population is indicated. Similar results were obtained in at least three independent experiments.

- *The activation of APC/C^{Cdh1} in S phase correlates with a decrease in the levels of phosphorylated Chk1*

The above result showing that the degradation of Cyclin A2 and Cyclin B1 started earlier when ATR was inhibited, prompted us to analyze if, as it had been previously described[381], Chk1 might be implicated in the inhibition of APC/C^{Cdh1} in response to RS.

Interestingly, the analysis of Chk1 phosphorylation in response to HU treatment, allowed us to determine that there was a correlation between the activation of APC/C^{Cdh1} in S phase and the time the levels of phosphorylated Chk1 started to decrease (Figure 11).

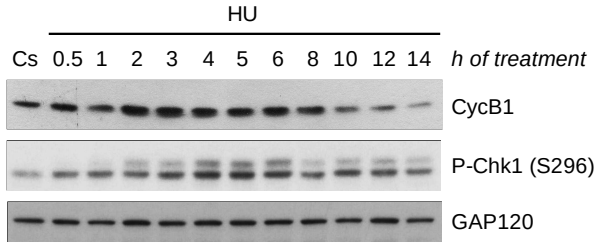

Figure 11. The activation of APC/C^{Cdh1} in response to HU correlates with a decrease in the levels of phosphorylated Chk1 in hTERT-RPE cells.
hTERT-RPE cells were synchronized in S phase and then treated during the indicated time with HU or left untreated (Cs). Whole cell lysates were analyzed by WB with the indicated antibodies. GAP120 was used as loading control. Cyc: cyclin.

- *The activation of APC/C^{Cdh1} in S phase correlates with a decrease in Emi1 levels in response to HU*

As explained in the introduction, Emi1 is an APC/C inhibitor involved in the regulation of this ubiquitin ligase during a normal cell cycle[90–92,99]. Furthermore,

p21-mediated Emi1 repression has been postulated as one of the mechanisms involved in the activation of APC/C^{Cdh1} in G2 in response to DNA damage[152]. Thus, to analyze if the activation of APC/C^{Cdh1} in S phase might be due to a decrease in Emi1 levels, we synchronized hTERT-RPE cells, treat them with HU and analyzed Emi1 levels in a timecourse experiment. Remarkably, this analysis showed that there was a correlation between the time Emi1 started to decrease and the APC/C^{Cdh1} was activated (as shown by the degradation of Cyclin B1) (Figures 12 and 11).

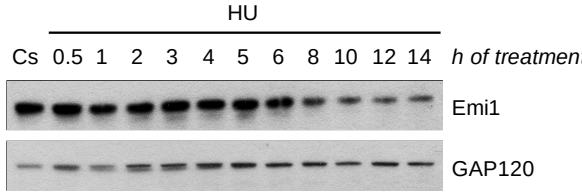

Figure 12. Emi1 levels decrease after a long HU treatment in hTERT-RPE cells.
Same samples as in *(Figure 11)* were used for WB analysis with the indicated antibodies. GAP120 was used as loading control. Cs: Untreated S-phase cells.

- *p53/p21 depletion prevents the activation of APC/C^{Cdh1} in S phase*

As a decrease in Emi1 levels seemed to be implicated in the activation of APC/C^{Cdh1} in S phase, we decided to analyze if, as it has been previously described[151,152], p21 was involved in this activation. Moreover, as p53, which is upstream p21[48,49], has also been described to be implicated in the activation of APC/C^{Cdh1} in response to DNA damage[151], we decided to analyze the implication of both, p53 and p21, in the activation of this ubiquitin ligase in S phase.

To this end, first we analyzed the stabilization of p53 and the induction of p21 in response to a 14-hour HU treatment. Surprisingly, although HU induced an increase in p53 levels, similar to the one observed after the addition of DNA damage-inducing agents, p21 was not induced under this condition (Figure 13). Moreover, even a low HU treatment was shown to be sufficient to stabilize p53, while p21 was not induced either in this case.

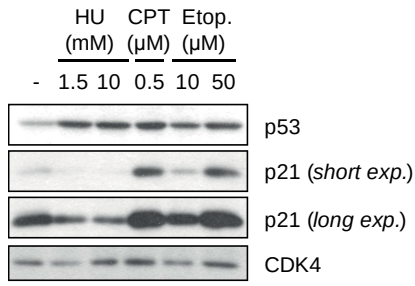

Figure 13. p53 levels increase while p21 is not induced in hTERT-RPE cells in response to prolonged HU treatment.
S-phase synchronized hTERT-RPE cells were treated with the indicated drugs for 14h or left untreated (-). Whole cell lysates were analyzed by WB with the indicated antibodies. CDK4 was used as loading control. Exp.: exposure.

However, p21 depletion by siRNA, abrogated the activation of APC/C^{Cdh1} in S phase in hTERT-RPE cells treated during 14 hours with HU, as shown by the recovery on Cyclin B1 levels under these conditions (Figure 14). Moreover, in agreement with previous works[152], Emi1 levels were higher in p21-depleted cells. Likewise, an increase in the levels of hyperphosphorylated pRb was observed under these conditions.

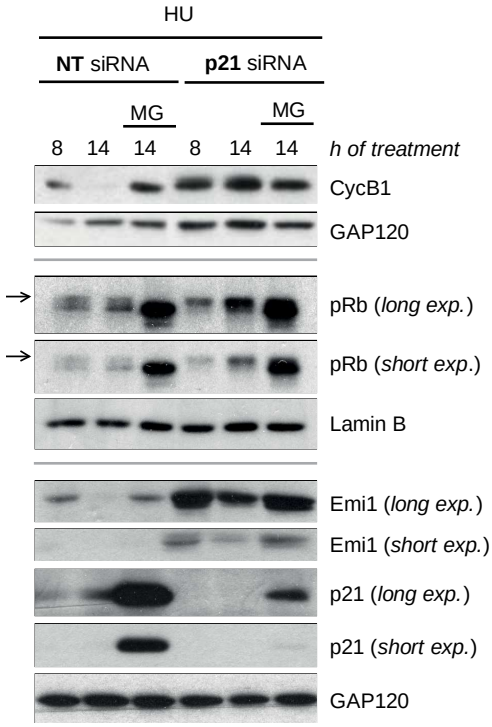

Figure 14. p21 depletion abrogates the activation of APC/C^{Cdh1} in response to prolonged DNA replication inhibition in hTERT-RPE cells.
hTERT-RPE cells were transfected with the indicated siRNAs, synchronized in S phase and then treated with HU during the indicated time. MG132 (MG) was added during the last 6h of treatment where indicated. Whole cell lysates were analyzed with the indicated antibodies. GAP120 and Lamin B were used as loading control. The arrow indicates the hyperphosphorylated band of the pRb. NT: non-target. Cyc: cyclin. Exp.: exposure.

Remarkably, knockdown analysis showed that p21 was being degraded in the presence of HU, as the addition of MG132 proteasome inhibitor highly increased its levels (Figure 14). Thus, although p21 was not induced in response to HU (Figure 13), we thought that p53 might be important to maintain its basal levels. To prove it, p53 was depleted in hTERT-RPE cells. As expected, p53 depletion promoted a decrease in p21 levels, which, according to our previous results, correlated with a recovery on Cyclin B1 levels after a 14-hour HU treatment (Figure 15). Furthermore, once again, the abrogation of APC/C^{Cdh1} activation, due to p53 depletion in this case, correlated with an increase in Emi1 levels and with an accumulation of the hyperphosphorylated band of pRb under these conditions.

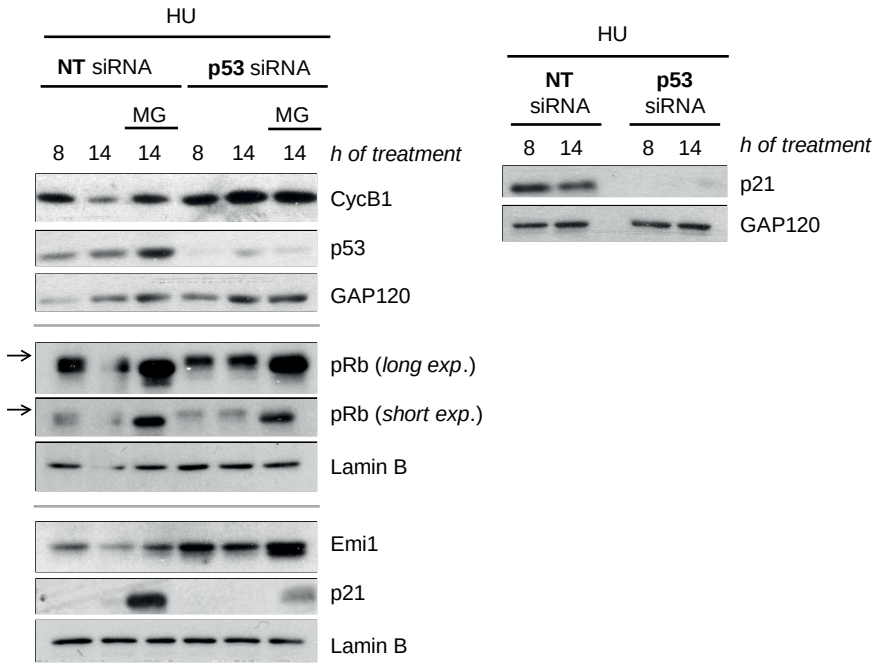

Figure 15. p53 depletion prevents the activation of APC/C^{Cdh1} in response to a long HU treatment in hTERT-RPE cells.
Non-target (NT) or p53 siRNA was transfected to hTERT-RPE cells. After that, cells were synchronized in S phase and treated with HU during the indicated time. MG132 (MG) was added during the last 6h of treatment where indicated. Whole cell lysates were analyzed by WB with the indicated antibodies. The arrow indicates the hyperphosphorylated band of pRb. GAP120 and Lamin B were used as loading control. Cyc: Cyclin. Exp.: exposure.

Collectively, these results indicate that the presence of p53 and p21, which are important to maintain low Emi1 levels, is required for the activation of APC/C^{Cdh1} in S phase in response to prolonged DNA replication inhibition.

Additionally, these last experiments showed that the previously observed decrease in Emi1 levels at the time APC/C^{Cdh1} was activated (Figures 11 and 12) was due to degradation, since the addition of MG132 recovered its levels (Figures 14 and 15). In this sense, neither p53 nor p21 depletion abrogated the degradation of Emi1 in response to HU (Figures 14 and 15). In addition, the increase in Emi1 levels shown after p53 or p21 depletion was already observed in untreated S-phase cells, indicating that it was not a response to RS (Figure 16). Likewise, the accumulation of hyperphosphorylated pRb was also observed under this condition.

Altogether, the above results indicate that the activation of APC/C^{Cdh1} in S phase in response to prolonged HU treatment is not prevented by the inhibition of ATM/ATR, but requires the presence of p53 and p21, which are necessary to maintain low Emi1 levels. However, whereas the decrease in Emi1 levels correlated with the activation of APC/C^{Cdh1}, we were unable to observe any change on p53 or p21 at this time, suggesting they were not the triggers of APC/C^{Cdh1} activation in response to HU. Moreover, the decrease in Emi1 levels was shown to

be due to its degradation, which was independent of p53 and p21. Thus, collectively, this data suggest that the degradation of Emi1, rather than p53- or p21-mediated Emi1 down-regulation, is the responsible for the activation of APC/C^{Cdh1} in S phase in response to severe replication stress.

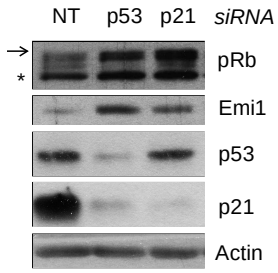

Figure 16. p53 or p21 depletion promotes an increase in Emi1 levels even in the absence of HU treatment in hTERT-RPE cells.
hTERT-RPE cells were transfected with the indicated siRNA, synchronized in S phase and harvested for WB analysis with the indicated antibodies. The asterisk indicates a non-specific band. The arrow indicates the hyperphosphorylated band of pRb. Actin was used as loading control. NT: non-target.

1.4. The activation of APC/C^{Cdh1} in S phase contributes to the loss of replication recovery competence upon prolonged DNA replication inhibition

As previously explained, one of the objectives of this thesis was to analyze the mechanisms involved in the loss of replication recovery competence. In this sense, previous data from our group indicated that there was a correlation between the degradation of Cyclin A2 and Cyclin B1 and the loss of replication recovery competence. Thus, defining the mechanisms involved in the degradation of these proteins could be helpful to figure out how the loss of replication recovery competence was promoted. In this sense, our results showed that APC/C^{Cdh1} activation in S phase was the mechanism responsible for the degradation of Cyclin A2 and Cyclin B1 upon prolonged HU treatment. Moreover, we showed that its activation was not abrogated by the inhibition of ATM/ATR, which consistent with our previous results, did not either abrogated the S-phase arrest under this condition. Collectively, the above results pointed to the activation of APC/C^{Cdh1} in S phase as the mechanism responsible for the loss of replication recovery competence.

To prove it, replication recovery was analyzed in Cdh1-depleted hTERT-RPE cells treated during 14 hours with HU. To avoid Cdh1 depletion to promote a premature entry into S phase, which can result in the accumulation of DNA damage[145–147], cells were transfected with the indicated siRNA, and once they were properly attached to the plate (~12 h), thymidine was added to block the cells into S phase. By doing so, thymidine accumulates the cells in S phase before Cdh1 depletion is noticeable, and thus, the effect of Cdh1 depletion on G1/S transition is avoided. Remarkably, this experiment showed that the cells in which Cdh1 had been depleted were able to resume replication and acquired a DNA content of 4n after a 14-hour HU treatment, indicating that as postulated, APC/C^{Cdh1} contributes to the loss of replication recovery competence in response to severe replication stress (Figure 17).

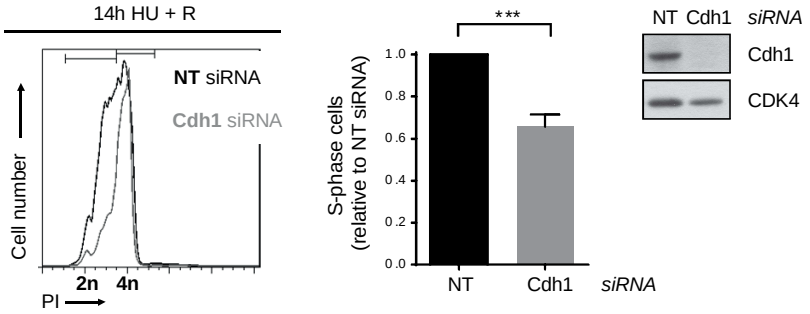

Figure 17. hTERT-RPE cells are able to resume replication after a 14-hour HU treatment when Cdh1 is depleted.

hTERT-RPE cells were transfected with the indicated siRNAs, synchronized in S phase, labeled with BrdU and then treated during 14h with HU. After that, cells were released into nocodazole containing fresh medium for 24h. DNA content (PI: propidium iodide) from BrdU positive cells was analyzed by flow cytometry. A representative DNA profile is shown (left panel). The average fold increase in the number of S-phase arrested cells in Cdh1-depleted relative to non-target (NT) siRNA transfected cells is shown in the graph (middle panel). Untreated S-phase synchronized cells were harvested and analyzed by WB with the indicated antibodies (right panel). CDK4 was used as loading control. Error bars represent standard deviation, (unpaired *t test*, n=4).

Moreover, consistent with our previous results showing that p53 or p21 depletion avoids APC/C^{Cdh1} activation in S phase, cell were shown to be able to resume replication and arrive to 4n when these proteins were depleted in hTERT-RPE cells (Figure 18).

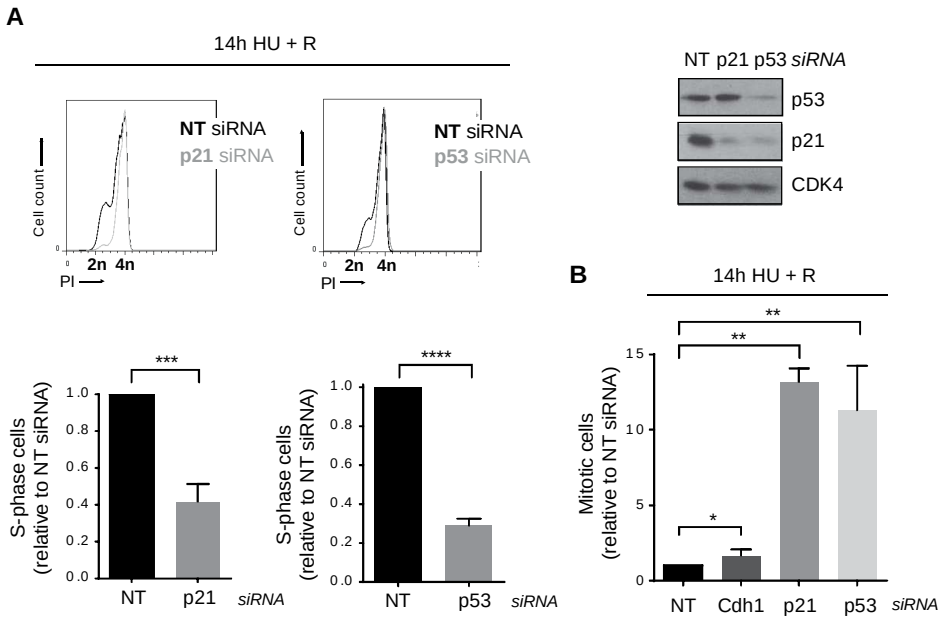

Figure 18. p53- or p21-depleted hTERT-RPE cells maintain the competence to recover from prolonged HU treatment.

(A) siRNA transfected and S-phase synchronized cells were labeled with BrdU and then treated with HU for 14h. After the treatment, cells were released into nocodazole containing fresh medium for 24h. DNA content (PI: propidium iodide) was used to analyze the number of S-phase arrested cells from BrdU positive

population. Representative DNA profiles (upper-left panel) and the average fold increase in the number of S-phase arrested cells on p53- or p21-depleted relative to non-target (NT) siRNA transfected cells are show (bottom-left panel). Untreated S-phase synchronized cells were harvested for WB analysis with the indicate antibodies (right panel). CDK4 was used as loading control. (B) Samples from *(A)* and *(Figure 17)* were used for mitotic entry (MPM2 positive) analysis. The average fold increase in the number of mitotic cells in Cdh1-/p53-/p21-depleted relative to NT siRNA transfected cells, from BrdU positive population is shown. Error bars represent standard deviation, (unpaired *t test*, n=4).

Interestingly, while the ability to enter into mitosis was also recovered in p53- or p21-depleted cells, Cdh1-depleted cells were shown to become mainly arrested in G2 (Figures 17 and 18). Likewise, whereas senescence was abrogated on p53- or p21-depleted cells, the fate of the cells in which Cdh1 had been depleted did not change (Figure 19).

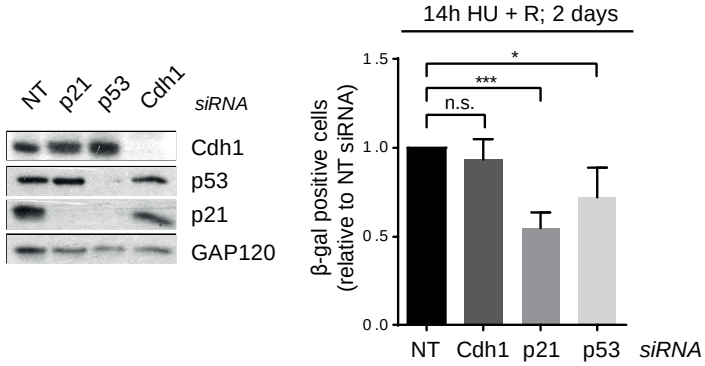

Figure 19. Senescence is abrogated by p53 or p21 depletion in hTERT-RPE cells treated during 14 hours with HU.

siRNA transfected hTERT-RPE cells were synchronized in S phase and then treated during 14h with HU or left untreated for WB analysis. Cells were then released into fresh medium for 48h before harvest them for SA-β-Gal analysis. Whole cell lysates were analyzed by WB with the indicated antibodies (left panel). GAP120 was used as loading control. The average fold decrease in the number of senescent cells in Cdh1-/p53-/p21-depleted relative to non-target (NT) siRNA transfected cells is shown (right panel). Error bars represent standard deviation, (unpaired *t test*, n=3).

Collectively, the above results indicate that, as expected, the activation of APC/C^{Cdh1} in S phase promotes the loss of replication recovery competence. However, while Cdh1-depleted cells are unable to enter into mitosis, p53 or p21 depletion recovers also the mitotic entry and senescence, indicating that these proteins have additional functions in response to prolonged DNA replication inhibition.

1.5. New origin firing inhibition by premature APC/C^{Cdh1} activation in S phase contributes to the loss of replication recovery competence in hTERT-RPE cells

The above results indicated that the activation of APC/C^{Cdh1} in S phase was, at least in part, responsible for the observed S-phase arrest in response to prolonged DNA replication inhibition. However, how was the activation of this ubiquitin ligase promoting the loss of replication recovery competence, still remained to be elucidated. In this regard, we decided to analyze which were the replication resumption pathways that failed to be activated in response to prolonged HU treatment in hTERT-RPE cells, to

finally analyze if Cdh1 depletion was able to recover any of them, to determine the function of APC/C^{Cdh1} in S phase.

1.5.1. Replication forks of hTERT-RPE cells are processed into DSBs after a long but not short HU treatment

As explained in the introduction, from works done in tumor cells, it was reported that stalled replication forks can eventually collapse and be processed into DSBs in response to prolonged HU treatment[450]. Additionally, previous data from our group indicated that non-transformed human cells loss the ability to recover from prolonged but not acute RS. Thus, these results prompted us to wonder if replication forks of hTERT-RPE cells were being processed into DSBs, promoting the loss of replication recovery competence under these conditions. In this regard, we decided to analyze the presence of both 53BP1^{504} and γ-H2AX^{335} foci, two markers of DSBs, in cells that had been treated during a short or a longer time with HU.

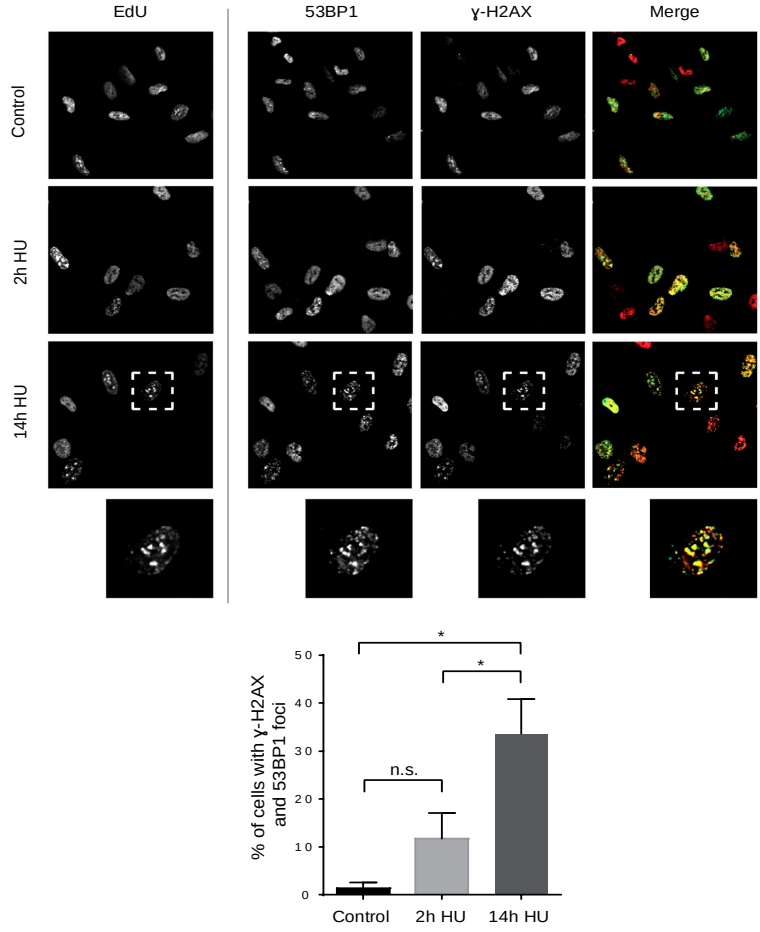

Figure 20. hTERT-RPE cells present 53BP1 and γ-H2AX foci after prolonged DNA replication inhibition. Asynchronously growing hTERT-RPE cells were labeled with EdU for 30min and then treated with HU during the indicated time or left untreated (Control). Click chemistry was performed to conjugate 488 fluorescent

dyes to EdU after cell fixation. Finally 53BP1 and γ-H2AX immunofluorescences were performed. Representative images (upper panel) and the average percentage of cells presenting 53BP1 (>6) and γ-H2AX (>10) foci from EdU positive population (bottom panel) are shown. Error bars represent standard deviation, (paired *t test*, n=3).

In agreement with published data[450], replication forks of hTERT-RPE cells were shown to accumulate DNA damage after a long HU treatment (Figure 20).

To further confirm the presence of DNA damage in hTERT-RPE cells after sustained HU treatment, we decided to validate the previous results by a more direct DSB indicator, the DNA break analysis by PFGE (pulse-field gel electrophoresis)[505]. As expected, this technique showed once again that replication forks of hTERT-RPE cells were being processed into DSBs after a long but not short HU treatment (Figure 21).

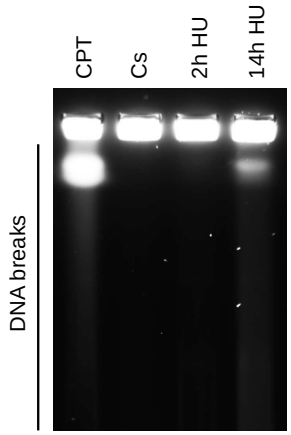

Figure 21. Replication forks of hTERT-RPE cells are processed into DSBs after a long HU treatment.
S-phase synchronized hTERT-RPE cells were treated during the indicated time with HU, during 14h with camptothecin (CPT) or left untreated (Cs). Cells were finally harvested and prepared for DNA break analysis by PFGE. A representative image of three independent experiments is shown.

1.5.2. The mechanisms able to resume replication in the presence of DSBs are inhibited in hTERT-RPE cells after a 14-hour HU treatment

As previously explained, once replication forks have been processed into DSBs, replication can be resumed either by BIR, which depends on the formation of a Rad51 coated 3' DNA end[452–455], or by new origin firing[118,450]. Thus, we wondered whether these mechanisms were inhibited in hTERT-RPE cells upon prolonged DNA replication inhibition.

In this regard, we decided to monitor replication by DNA fiber analysis[506], to analyze the possible failures on the activation of those mechanisms. To set up the experimental conditions for this analysis, we first decided to validate if, as indicated by previous works done in our laboratory (see chapter II results), HU (10mM) triggers 15 minutes to completely stall replication forks in hTERT-RPE cells. To this end, we labeled the cells with CldU (5-Chloro-2'-deoxyuridine) thymidine analog for 30 minutes, and then, we treated them with HU in the presence of IdU (5-Iodo-2'-deoxyuridine) analog to analyze its incorporation. Additionally, we included another condition in which CldU was

replaced by IdU during the first 15 minutes of HU treatment, to compare it with the previous one, and discern if there was any incorporation at this time.

As shown in Figure 22, HU addition completely abrogated the incorporation of IdU thymidine analog after the first 15 minutes of treatment. Additionally, the number of forks that were able to incorporate IdU during those first minutes of HU treatment was very low. Moreover, the length of those few IdU tracks that had incorporated the IdU analog during the first 15 minutes of treatment was very short. Altogether, with these results, we concluded that HU (10mM) completely blocks replication fork progression after 15 minutes of treatment, and that even during this first minutes of treatment, fork progression is strongly compromised.

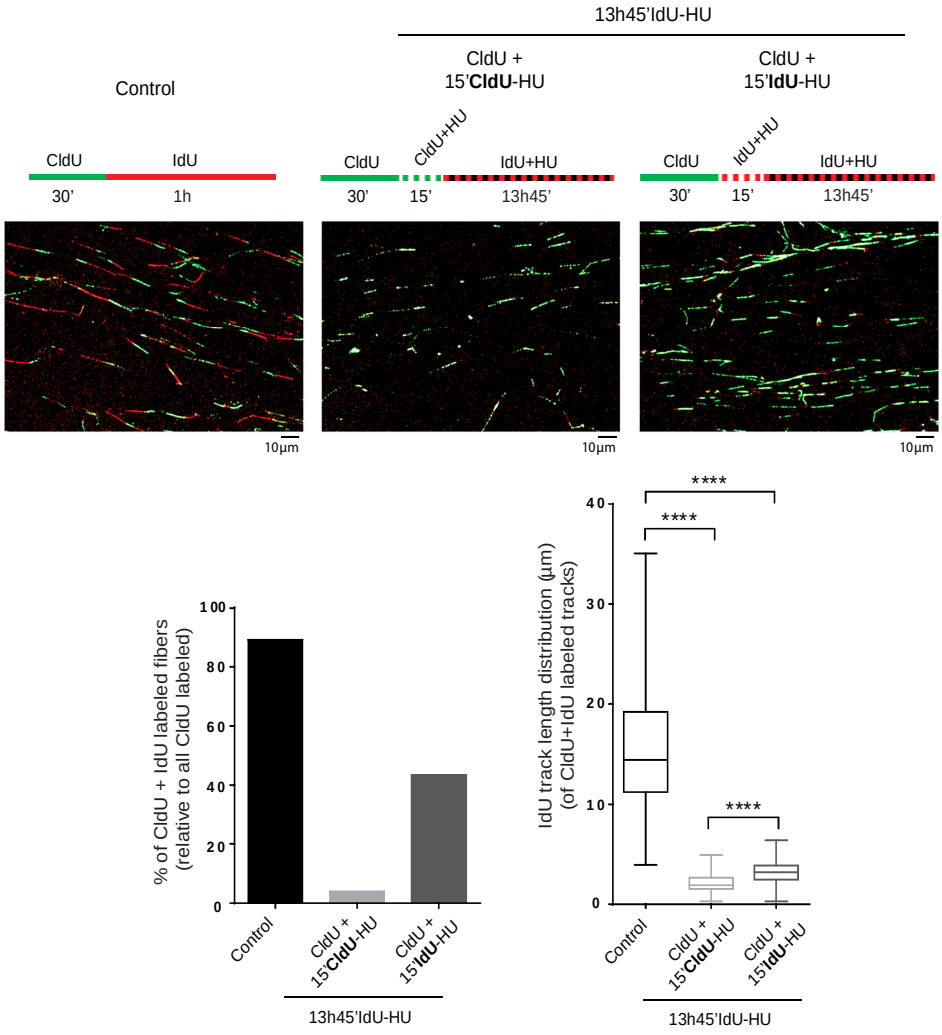

Figure 22. HU completely inhibits replication fork progression after 15 minutes of treatment.
Asynchronously growing hTERT-RPE cells were labeled and treated as indicated (upper panels). After the treatment, cells were harvested and prepared for DNA fiber analysis. Representative images are shown (middle panels). The percentage of DNA fibers labeled with both analogs, relative to total CldU labeled ones is

represented (bottom-left panel). The IdU track length distribution of those fibers labeled with both analogs is represented (bottom-right panel). More than 150 fibers were measured. Box and whiskers show: Min, Max, Median and first quartiles, (unpaired t test).

Once having validated that HU was completely stalling replication fork progression, we decided to perform the DNA fiber experiment to analyze if any of the previously explained mechanisms was being abrogated in hTERT-RPE cells in response to prolonged HU treatment. To this end, cells were labeled with CldU for 30 minutes, then treated during 2 or 14 hours with HU, and finally labeled with IdU for 1 hour more. The second labeling period was prolonged to avoid the possible delay in restarting stalled forks interfering in the analysis. Additionally, CldU was maintained in the media during the first 15 minutes of HU treatment, to avoid fork progression in the absence of CldU incorporation.

Remarkably, a decrease in the number of restarted forks and an increase in the number of stalled forks were observed after a 14-hour but not 2-hour HU (Figure 23). Moreover, in contrast to tumor cells[450], this decrease in the number of restarted forks did not correlate with an increase in new origin firing events in hTERT-RPE cells. Thus, DNA fiber analysis indicated that the pathways involved in replication restart, once DSBs are present, were inhibited in hTERT-RPE cells, explaining why those cells loss the ability to resume replication under these conditions.

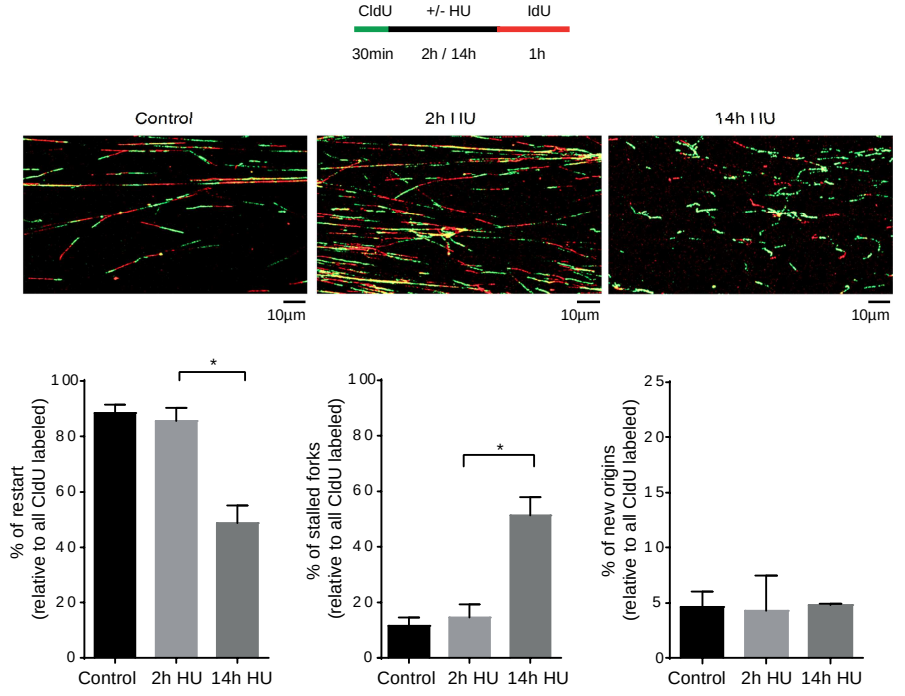

Figure 23. Replication forks of hTERT-RPE cells become inactivated after sustained DNA replication inhibition.

S-phase synchronized hTERT-RPE cells were labeled and treated as indicated (upper panel). CldU was present on the medium during additional 15min during the HU treatment. After the treatment, cells were harvested

and prepared for DNA fiber analysis. Representative images are shown (middle panels). The percentage of replication fork restart, stalled replication forks and new origin firing relative to total CldU labeled fibers is shown in the graphs (bottom panels). At least 1500 fibers were counted in each condition. Means and standard deviation (bars) are shown, (paired *t test*, n=3).

To further verify that BIR-mediated restart was impaired in hTERT-RPE cells treated during 14 hours with HU, the association of Rad51 with chromatin was analyzed. In agreement with previous data[396,450], Rad51 was shown to be associated with chromatin after a short HU treatment, and even in untreated cells. However, the association of Rad51 with chromatin was lost after a long HU treatment in hTERT-RPE cells, and this association was not reestablished either after release from this treatment (Figure 24). Moreover, consistent with its already known repair-independent role in protecting DNA from nucleases degradation[394–396], the analysis of CldU (first labeling) track length showed that nascent DNA was being degraded after a long HU treatment.

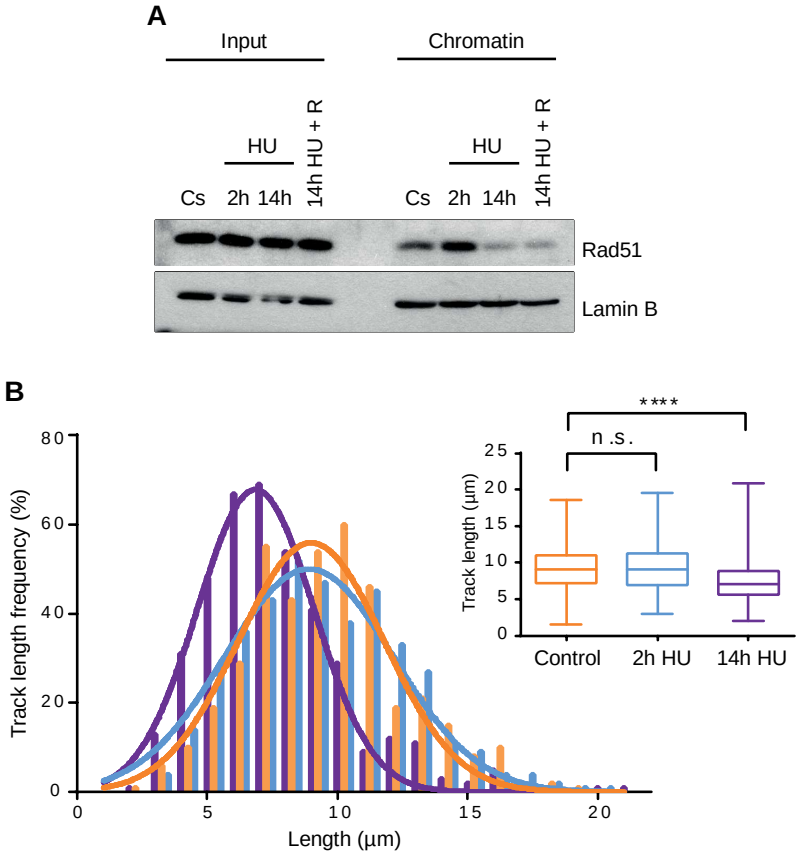

Figure 24. Rad51 is dissociated from chromatin after prolonged DNA replication inhibition in hTERT-RPE cells.

(A) S-phase synchronized hTERT-RPE cells were treated with HU during the indicated time or left untreated (Cs). After the treatment cells were harvested or released (R) into fresh medium for 30min. Chromatin extraction was performed and extracts were analyzed by WB with the indicated antibodies. Lamin B was used as loading control. Input: whole cell extracts. (B) DNA fibers from *(Figure 23)* were used to measure CldU

track length. At least 300 fibers were measured for CldU track length distribution and statistical analysis. Box and whiskers show: Min, Max, Median and first quartiles, (unpaired *t test*, n=3).

Collectively, the above results indicated that both BIR-mediated restart and new origin firing were inhibited in hTERT-RPE cells after prolonged HU treatment. Thus, together with the previously observed accumulation of DSBs, these results explained why hTERT-RPE cells remained arrested in S phase under these conditions.

1.5.3. The activation of APC/C^{Cdh1} in S phase inhibits new origin firing in response to prolonged HU treatment

As previously explained, once having established which replication resumption pathways were inhibited in hTERT-RPE cells in response to prolonged HU treatment, our next goal was to analyze if the inhibition of any of them might be reverted by Cdh1 depletion, with the idea of deciphering which was the function of APC/C^{Cdh1} in S phase.

To this end, we first analyzed the association of Rad51 with chromatin in Cdh1-depleted hTERT-RPE cells treated during 2 or 14 hours with HU. As shown in Figure 25, Cdh1 depletion did not recover the association of Rad51 with chromatin after a 14-hour HU treatment.

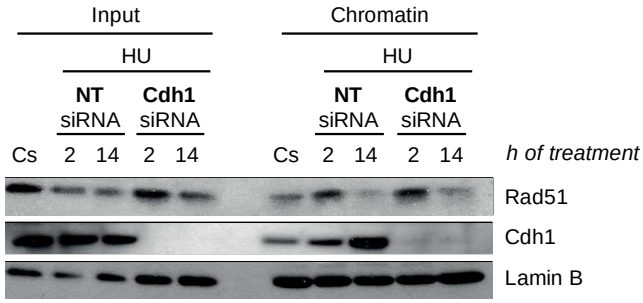

Figure 25. Cdh1 depletion does not recover the association of Rad51 with chromatin after a 14-hour HU treatment.
hTERT-RPE cells were transfected with the indicated siRNA, synchronized in S phase and then treated during the indicated time with HU or left untreated (Cs). Chromatin extracts were prepared and analyzed with the indicated antibodies. Lamin B was used as loading control. NT: non-target. Input: whole cell extracts.

Consistently, DNA fiber analysis showed that nascent DNA was degraded at stalled, but not restarted, replication forks of hTERT-RPE cells treated during 14 hours with HU, independently of Cdh1 depletion (Figure 26).

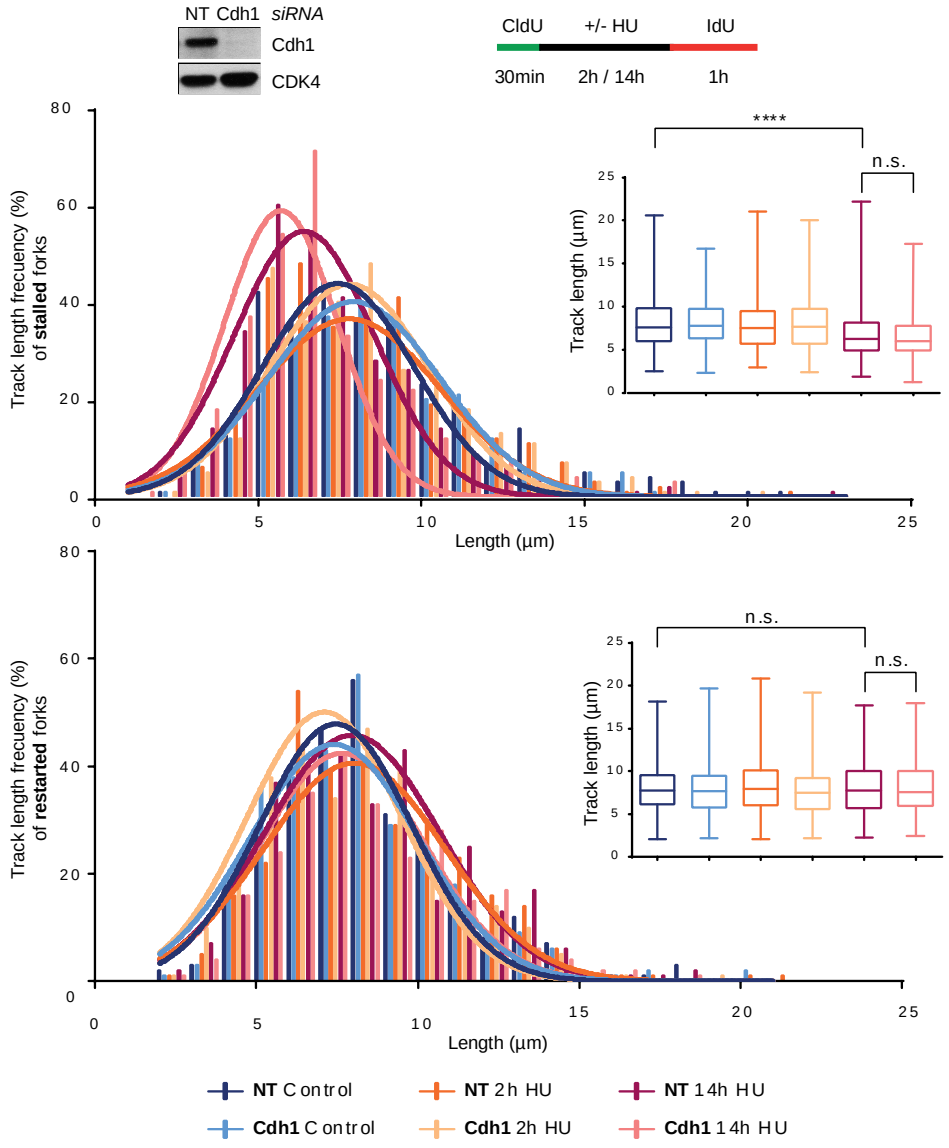

Figure 26. Nascent DNA is degraded at stalled replication forks of hTERT-RPE cells after prolonged HU treatment.

hTERT-RPE cells were transfected with the indicated siRNA, synchronized in S phase and then treated and labeled as indicated for DNA fiber analysis (upper-right panel). CldU (250µM) was present on the media for additional 15min during the HU treatment. Untreated S-phase synchronized cells were harvested in parallel for knockdown analysis by WB with the indicated antibodies (upper-left panel). CDK4 was used as loading control. At least 300 fibers were measured for CldU track length distribution and statistical analysis (middle and bottom panels). Box and whiskers show: Min, Max, Median and first quartiles, (unpaired t test, n=3). NT: non-target.

Moreover, Cdh1 depletion did not increase the number of restarted forks after prolonged HU treatment. Likewise, the number of stalled forks did not either change under these conditions (Figure 27).

Altogether, the above results indicated that Rad51-dependent BIR was not the mechanism used by Cdh1-depleted hTERT-RPE cells to resume replication after sustained DNA replication inhibition. Thus, we next wondered if the loss of replication recovery competence upon severe replication stress was promoted by APC/C^{Cdh1}-mediated origin firing inhibition.

Interestingly, Cdh1 depletion strongly increased the number of new origin firing events after prolonged HU treatment (Figure 27). Furthermore, similarly to 2 hour HU-treated or to untreated cells, the percentage of active forks (restart + new origin) in Cdh1-depleted 14 hour HU-treated cells, relative to the initial ones (all CldU labeled ones), corresponded approximately to the 80% (Figure 27). Notably, this indicated that the observed increase in new origin firing events might be potentially sufficient to restore DNA synthesis after prolonged replication inhibition in those cells.

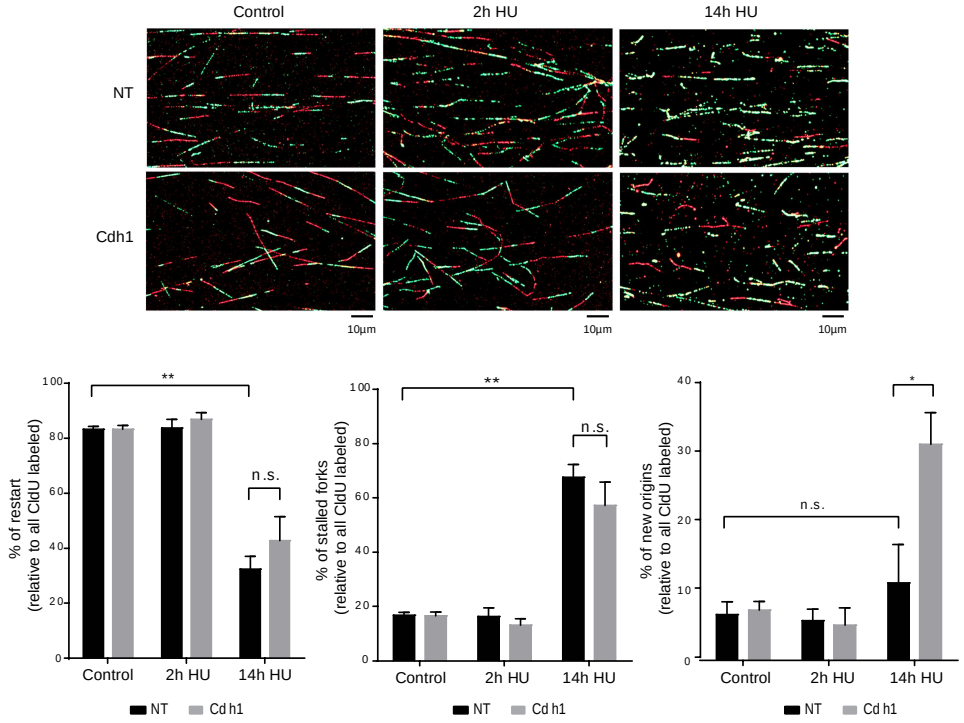

Figure 27. Cdh1 depletion increases the new origin firing events in hTERT-RPE cells treated during 14 hours with HU.

Samples from *(Figure 26)* were used to analyze the percentage of replication fork restart, stalled replication forks and new origin firing events relative to total CldU labeled fibers (bottom panels). Representative images are shown (upper panels). More than 1000 fibers were counted in each condition. Means and standard deviation (bars) are shown, (paired *t test*, n=3). NT: non-target.

Accordingly, in the absence of Cdh1, the IdU (second labeling) incorporation rate (measured by the average IdU intensity per nuclei) was similar in both short- and long-treated cells (Figure 28), which further supported the idea that the new origin firing observed in the absence of APC/C^{Cdh1} activation was sufficient to reestablish the DNA replication rate.

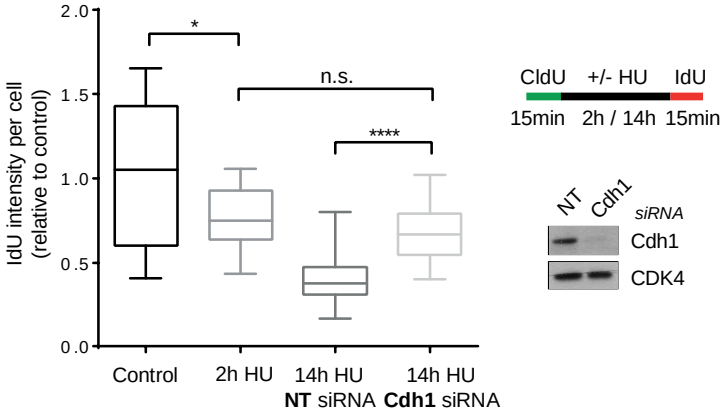

Figure 28. Cdh1-depleted and 14-hour HU-treated hTERT-RPE cells incorporate the same amount of IdU as the 2-hour HU-treated cells.
siRNA transfected (NT: non-target) hTERT-RPE cells were synchronized in S phase followed by a 15min labeling with CldU (250 μM) and then treated with HU during the indicated time or left untreated (control). After that, cells were released into fresh media for 30min before label them during 15min with IdU. Cells were finally fixed and immunostained with anti-BrdU antibodies. Schematic of the labeling protocol is shown (upper-right panel). Relative IdU intensity distribution per nuclei from CldU positive population, normalized by untreated cells, is shown in the graph (left panel). Box and whiskers show: Min, Max, Median and first quartiles, (unpaired *t test*). Whole cell extracts of untreated S-phase synchronized cells were harvested in parallel and analyzed by WB with the indicated antibodies (bottom-right panel). CDK4 was used as loading control.

In conclusion, the above results showed that the activation of APC/C^{Cdh1} in S phase inhibits new origin firing in hTERT-RPE cells, compromising replication resumption upon severe replication stress. Remarkably, it should be considered that with the used methodology the firing of nearby origins is not distinguished from real fork restart[155,159] and thus, Cdh1 depletion-induced new origin firing events may correspond mainly to the ones activated in different replicons in this case.

1.6. Replication resumption after prolonged DNA replication inhibition increases genomic instability

As previously explained, once having described the mechanisms that promote the loss of replication recovery competence after prolonged HU treatment, our next objective was to define the contribution of this S-phase arrest to the prevention of genomic instability. Remarkably, the fact that, in contrast to tumor cells, non-transformed human cells are arrested in S phase after a long but not short HU treatment, when DSBs are already present, suggests that these cells are arrested to avoid cell cycle progression in the presence of DNA damage.

To prove it, and taking advantage of our knowledge regarding the mechanisms involved in the loss of replication recovery competence, we decided to analyze the acquisition of genomic instability in Cdh1-depleted cells. According to our previous results, Cdh1 depletion may allow replication to be resumed after prolonged HU treatment (Figure 17). However, Cdh1-depleted cells will be mainly arrested in G2 due to a correct G2-checkpoint (Figures 17 and 18). Thus, this model would not allow us to elucidate the real impact of Cdh1 depletion to the acquisition of genomic instability. Therefore, we decided to evaluate also the acquisition of genomic instability in p21-depleted HU-treated hTERT-RPE cells, in which not only the activation of APC/C^{Cdh1} but also the G2 arrest would be abrogated (Figure 18).

Interestingly, consistent with our previous results showing that replication forks were being processed into DSBs after a 14-hour HU treatment, non-target-/Cdh1-/p21-depleted cells presented in all cases an increase in the number of cells containing 53BP1 foci when cells were released from a 14-hour HU treatment (Figure 29).

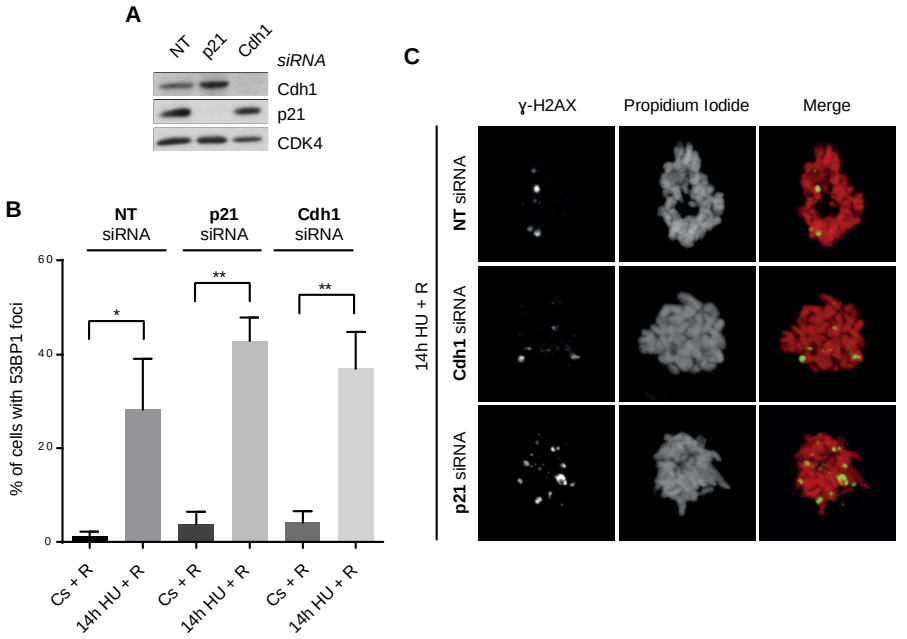

Figure 29. hTERT-RPE cells accumulate DNA damage after prolonged DNA replication inhibition.
(A) hTERT-RPE cells were transfected with the indicated siRNA, synchronized in S phase and then harvested for WB analysis with the indicated antibodies. CDK4 was used as loading control. (B) siRNA transfected and S-phase synchronized, as in *(A)*, hTERT-RPE cells were treated with HU for 14h or left untreated (Cs), and then released (R) into fresh media for 12h. Finally cells were immunostained with 53BP1 antibody. The average percentage of cells presenting 53BP1 foci (>6) from total population is shown. Error bars represent standard deviation, (paired *t test*, n=3). (C) hTERT-RPE cells were transfected and synchronized as in *(A)*. After that, cells were treated with HU for 14h and then released into nocodazole containing fresh medium for 24h. Cells were finally immunostained with γ-H2AX antibody. DNA was counterstained with propidium iodide. Representative images of γ-H2AX positive mitotic cells are shown. NT: non-target.

Moreover, the cells that eventually escaped the arrest and arrived to mitosis, also presented γ-H2AX foci in mitosis under these conditions (Figure 29). Of course, as

previously explained, the difference would be that, while p21-depleted cells might be able to arrive to G1 with DNA damage, non-target- and Cdh1-depleted cells would become mainly arrested in S and G2 phases respectively when released from prolonged HU treatment. Accordingly, cells that present 53BP1 foci in G1 (as analyzed by Cyclin D1) were found in p21-depleted hTERT-RPE cells under these conditions (Figure 30). Likewise, p21-depleted cells presenting micronuclei were also found when these cells were released from prolonged HU treatment.

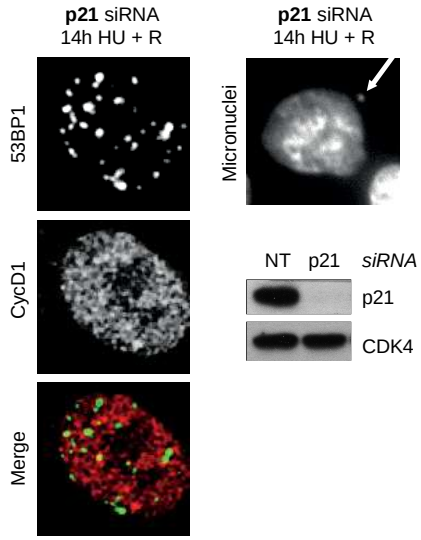

Figure 30. p21-depleted cells present 53BP1 foci in G1 and micronuclei.
p21-depleted cells were synchronized in S phase and then treated during 14h with HU. Cells were then released (R) into fresh medium for 12h after which cells were fixed and immunostained with 53BP1 and Cyclin D1 (CycD1) antibodies (left panel). Cells were counterstained with DAPI to analyze the presence of micronuclei (upper-right panel). siRNA transfected and S-phase synchronized untreated cells were harvested for WB analysis with the indicated antibodies (bottom-right panel). CDK4 was used as loading control.

All together, these results highlighted the importance of adding previous barriers to the G2 arrest, such as by the activation of APC/C^{Cdh1} in S phase, to prevent cell cycle progression in case this arrest fails, and thus, to avoid cell division in the presence of damage DNA.

To further study the contribution of the S-phase arrest to the prevention of genomic instability, we decided to analyze the acquisition of genomic instability in cells that, in contrast to hTERT-RPE cells, do not activate APC/C^{Cdh1} and thus, are not arrested in S phase.

As explained in the introduction, APC/C^{Cdh1} has been reported to be usually mutated in tumor cells[153]. Consistently, works done in our laboratory have shown that tumor cell preferentially do not activate APC/C^{Cdh1} in response to HU, which correlates with the ability to resume replication after release from prolonged HU treatment[507]. Thus, we decided to analyze the consequences of this lack of APC/C^{Cdh1} activation in one of those cell lines.

As shown in Figure 31, HCT116 colorectal cancer cells did not activate APC/C^{Cdh1} in S phase after prolonged HU treatment, and consistent with our previous results, they maintained the ability to resume replication when the stress was removed. Moreover, these cells were not only able to resume replication but also to divide and proliferate under these conditions.

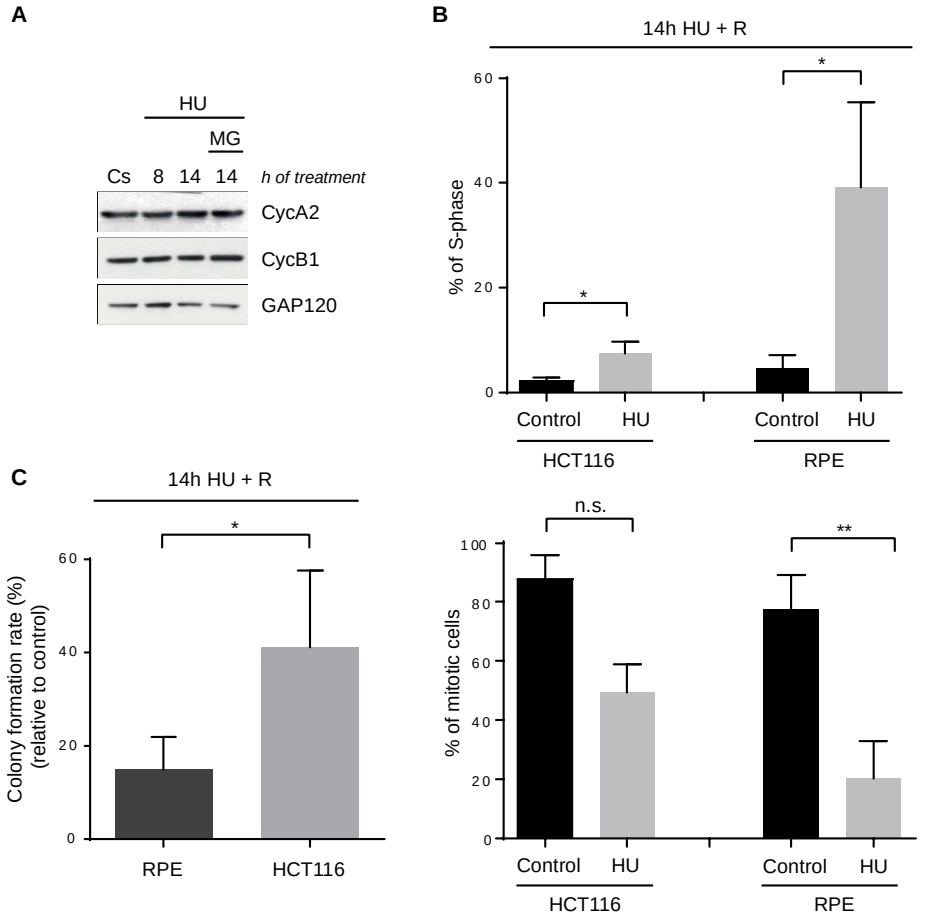

Figure 31. HCT116 cells maintain the competence to recover upon prolonged HU treatment.
(A) HCT116 cells were synchronized in S phase and then treated with HU during the indicated time or left untreated (Cs). MG132 (MG) was added during the last 6h of treatment where indicated. Whole cells lysates were analyzed by WB with the indicated antibodies. GAP120 was used as loading control. (B) HCT116 and hTERT-RPE cells were labeled with BrdU and then treated with HU for 14h or left untreated (Control). Cells were then released into nocodazole containing fresh medium for 12h (HCT116) or 24h (hTERT-RPE). The average percentage of S-phase arrested (DNA content; propidium iodide; upper panel) and mitotic (MPM2 positive; bottom panel) cells from BrdU positive population are shown. Error bars represent standard deviation, (paired *t test*, n= 3). (C) HCT116 and hTERT-RPE cells were synchronized in S phase and then treated during 14h with HU or left untreated. Cells were then released into fresh media for 12h and diluted (250 cells per well on 6-well plates) for colony formation assay. Colonies were harvested 8 days later. The average percentage of colonies in HU-treated relative to control was calculated in each case. Error bars represent standard deviation, (unpaired *t test*, n=3).

Interestingly, the analysis of the acquisition of genomic instability in response to prolonged HU treatment in this model, showed that HCT116 cells were able to arrive to G1 with DNA damage, since there was an increase in the percentage of HCT116 cells presenting 53BP1 foci in G1 (analyzed by Cyclin D1) after prolonged HU treatment (Figure 32). Moreover, the increase in G1 cells presenting 53BP1 foci correlated with an increase in the percentage of cells with micronuclei under these conditions.

These data further support the idea that an S-phase arrest, such as by the activation of APC/C^{Cdh1}, may act as an additional barrier to prevent cell cycle progression with damaged DNA, consequently contributing to safeguarding the genome integrity of non-transformed cells in response to severe replication stress.

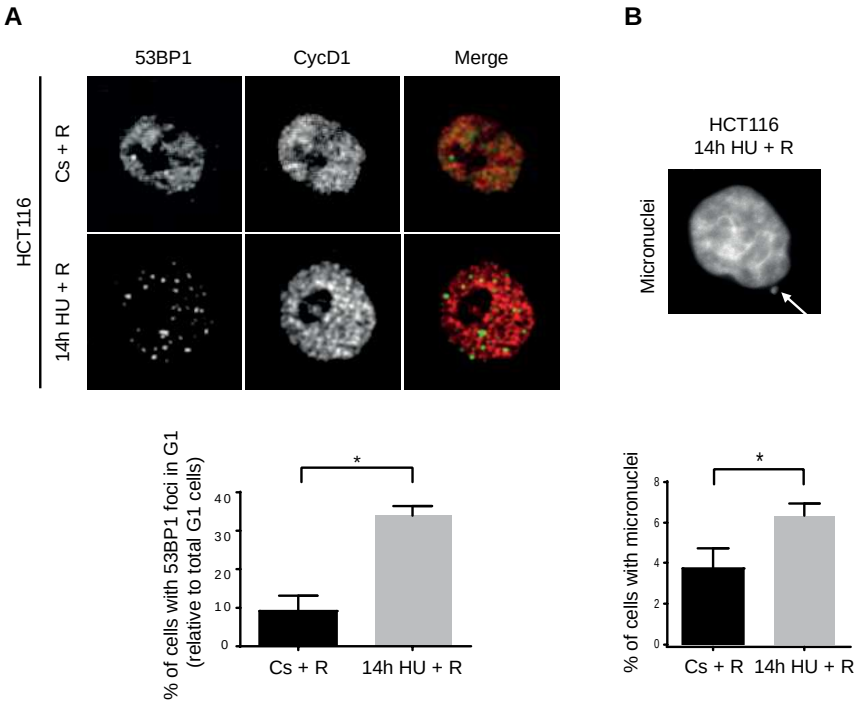

Figure 32. HCT116 cells accumulate genomic instability after prolonged DNA replication inhibition.
HCT116 cells were synchronized in S phase and then treated with HU for 14h or left untreated (Cs). Cells were then released into fresh medium for 12h, after which they were fixed and immunostained with 53BP1 and Cyclin D1 antibodies. DNA was counterstained with DAPI. The average percentage of 53BP1 foci (>6) containing cells in G1 (CycD1: Cyclin D1) relative to total G1 cells is shown (A). The average percentage of cells presenting micronuclei from total population is shown (B). Representative images are shown (upper panels). Error bars represent standard deviation, (paired *t test*, n=3).

All the previous data showing a connection between replication resumption after prolonged HU treatment and the acquisition of genomic instability was based on correlations. Therefore, to analyze the real impact of an S-phase arrest on the maintenance of genome integrity, we decided to artificially induce an S-phase arrest in HCT116 cells. To this end, taking advantage of our knowledge regarding the activation of APC/C^{Cdh1} in S phase, we decided to analyze genomic instability in Emi1-depleted

HCT116 cells. Emi1 depletion had been reported to be sufficient to promote APC/C^{Cdh1} activation[154,508]. Thus, we thought that an artificial Emi1-induced APC/C^{Cdh1} activation in S phase, could compromise replication resumption under these conditions. Remarkably, Emi1 depletion allowed the activation of APC/C^{Cdh1} in S phase (as shown by the degradation of Cyclin A2 and Cyclin B1) in HCT116 cells, even after HU addition (Figure 33). Moreover, this artificial activation of APC/C^{Cdh1} in S phase compromised the ability to resume replication after prolonged HU treatment in those cells. Interestingly, this resulted in a reduced number of 53BP1 foci containing G1 cells. Likewise, a reduction in the number of cells presenting micronuclei was also observed in under these conditions.

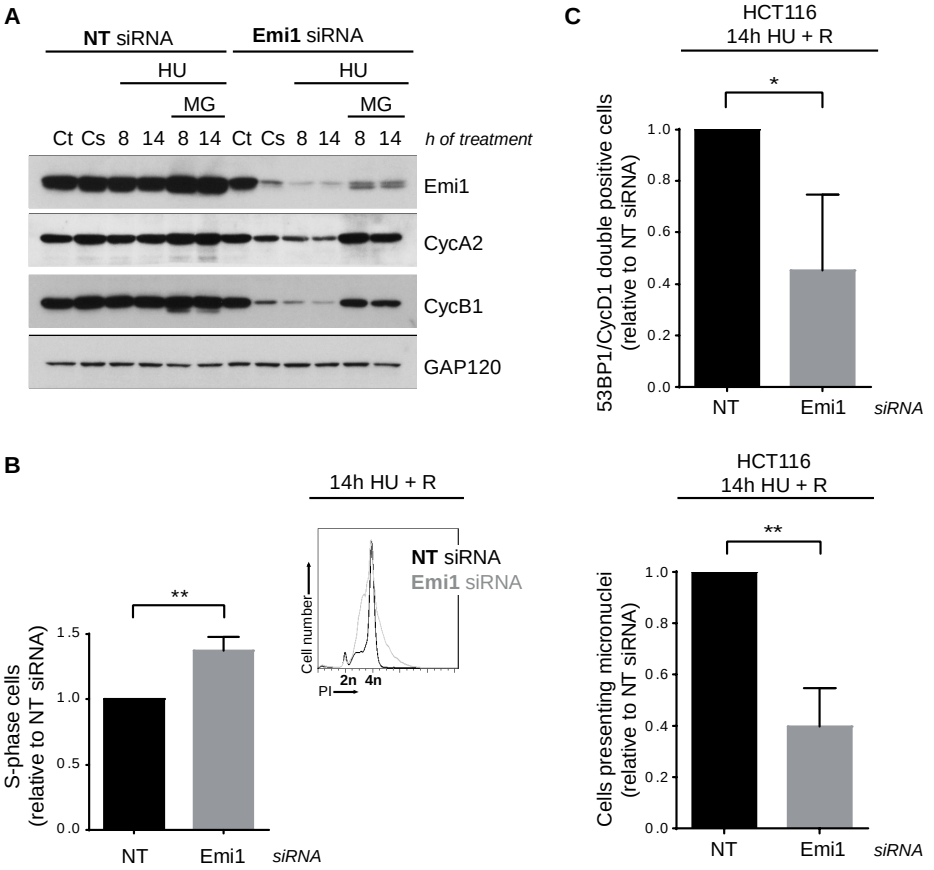

Figure 33. Abrogation of replication resumption after prolonged HU treatment contributes to the prevention of genomic instability in HCT116.

(A) HCT116 cells were transfected with the indicated siRNA (NT: non-target) and 4 h later (Ct), thymidine was added to synchronize cells in S phase. After synchronization, cells were treated with HU during the indicated time or left untreated (Cs). Whole cell extracts were prepared and analyzed by WB with the indicated antibodies. MG132 (MG) was added during the last 6h of treatment where indicated. GAP120 was used as loading control. Cyc: cyclin. (B) HCT116 cells were transfected and synchronized as in *(A)*. After synchronization, cells were treated with HU for 14h and then released into fresh medium with nocodazole for 12h. DNA content (PI: propidium iodide) was analyzed by flow cytometry. Representative DNA profiles (right panel) and the average fold increase of cells that remain in S phase after release relative to non-target siRNA

transfected cells (left panel) are shown. Error bars represent standard deviation, (unpaired *t test*, n=3). (C) HCT116 cells were transfected and synchronized as in *(A)*. After synchronization, cells were treated during 14h with HU and then released into fresh medium for 12h, before fixing and immunostaining them for 53BP1 and Cyclin D1 analysis. DNA was counter stained with DAPI. The average fold increase in the number of Emi1-depleted cells with 53BP1 foci in G1 (upper panel) and in the number of Emi1-depleted cells with micronuclei (bottom panel) relative to NT transfected cells are shown. Error bars represent standard deviation, (unpaired *t test*, n=3).

Collectively, all the previous data support the idea that the abrogation of replication resumption, such as by the activation of APC/C^{Cdh1}, contributes to the safeguarding of genome integrity upon severe replication stress.

Chapter II

Analysis of nascent DNA-bound proteins after acute or prolonged HU treatment in hTERT-RPE cells

One of the main objectives of our group is to identify new mechanisms involved in the DNA replication stress response of non-transformed human cells. Previous data from our group indicated that non-transformed human cells loss the ability to recover from a 14-hour, but not 2-hour, HU treatment. Thus, we decided to perform a comparative analysis of the proteins associated with replication forks under those conditions, in order to define the changes, at replication fork level, that promote this loss of replication recovery competence. Additionally, this approach would allow us to discover new essential proteins of the DNA replication stress response, important to maintain the competence to recover from a RS.

2.1. Proteomic analysis of the proteins associated with replication forks after acute or prolonged HU treatment

iPOND (isolation of proteins on nascent DNA)[509] in combination with MS (mass spectrometry)[510] had been described as a powerful tool to characterize the human replisome and replisome-associated proteins. Furthermore, a more efficient modified version of iPOND coupled with MS had been described by the laboratory of Prof. Patrik Ernfors Ph.D. at the *Karolinska Institutet*[511]. Therefore, in collaboration with them, we decided to perform a comparative analysis of the proteins associated with replication forks after acute or prolonged HU treatment using this approach. The study was conducted in S-phase synchronized hTERT-RPE cells.

2.1.1. Set-up and experimental design

iPOND technology is based on the isolation of protein complexes crosslinked to EdU (5-ethynyl-2'-deoxyuridine) thymidine analog-containing DNA fragments. However, in contrast to other thymidine analogue-based, DNA-mediated chromatin coimmunoprecipitation and pulldown technics[450,512], it incorporates a new idea. This idea consist in comparing EdU-containing DNA fragments that are located at active replication forks, with those fragments present on mature chromatin, in order to discern between the proteins associated specifically with replication forks or throughout the entire chromatin[509] (Figure 34).

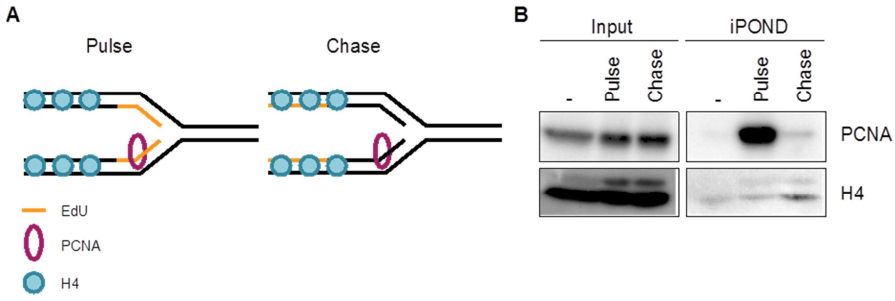

Figure 34. iPOND technology.
(A) The pulse and chase conditions used during iPOND, together with the proteins bound to EdU in each of them, are represented. Pulse: Cells are harvested just after a 15min EdU labeling. Chase: Cells are labeled with EdU for 15min and then released into fresh medium for 2h more. Thymidine (low dose, 50μM) is added during the release to displace the residual EdU present on cells. (B) Analysis of PCNA by iPOND as an example

of replisome components visualization using this technic. Histones are used as an immunoprecipitation control. Input: nuclear extract. -: negative control (no EdU). H4: Histone 4.

Three conditions are essential when performing iPOND: negative control, the pulse and the chase (Figure 34). Moreover, in order correctly analyze our particular experimental data, it was necessary to add an additional control. This new control would consist in the addition of EdU until the HU had completely blocked replication forks, to avoid the incorporated EdU to be displaced away from replication forks during the first minutes of HU treatment. This extra EdU addition would increase the number of labeled forks, as well as the length of the labeled nascent DNA. Thus, it was important to include an extra control in which cells had been treated with HU and EdU at the same time (after the pulse), until the HU had completely blocked replication fork progression, to correctly analyze the HU-treated samples. Thus, in order to set up our experiment conditions, first, we decided to analyze the time the HU required to completely block replication forks.

To this end, we decided to analyze the BrdU incorporation rate in cells that had been treated with HU during different times. BrdU was added to the medium during the last 30 minutes of HU treatment, and its incorporation was analyzed by flow cytometry (Figure 35). This experiment showed that replication forks of hTERT-RPE cells were completely stalled after 30 minutes of HU treatment.

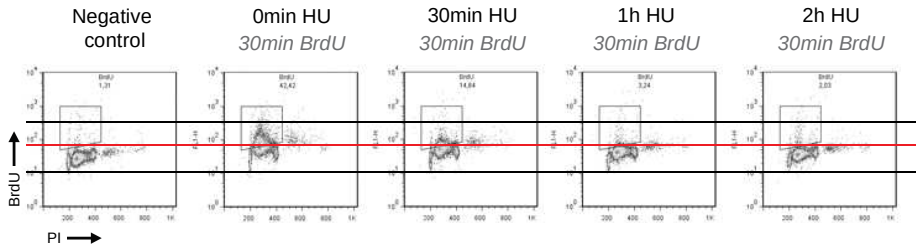

Figure 35. Replication forks of hTERT-RPE cells are completely stalled after 30 minutes of HU treatment. S-phase synchronized hTERT-RPE cells were treated during the indicated time with HU. BrdU was added during the last 30min of HU treatment. 30min BrdU: untreated cells labeled with BrdU for 30min. Negative control: untreated cells without BrdU. DNA content (PI: propidium iodide) and BrdU incorporation rate were analyzed by flow cytometry. Representative images are shown.

Once narrowed down the time necessary to completely inhibit replication fork progression after HU addition, we wanted to define more precisely this time. As iPOND is a very sensitive technic[509], we decided to perform an iPOND experiment with several EdU and HU conditions (as indicated), using equal protein levels for the immunoprecipitation in all of them (Figure 36). By doing so, immunoprecipitated histone levels would be proportional to the amount of incorporated EdU. Thus, this experiment would allow us to analyze more precisely the EdU incorporation rates.

As expected, an increase in the EdU incorporation time correlated with an increase in the levels of immunoprecipitated histones (Figure 36; lanes 2 and 3). Remarkably, this experiment showed that, although there was a slight incorporation of EdU during the

first 15 minutes of HU treatment (Figure 36; lanes 2, 3 and 4), replication forks of hTERT-RPE cells were completely stalled after this time (Figure 36; lanes 4, 5 and 6).

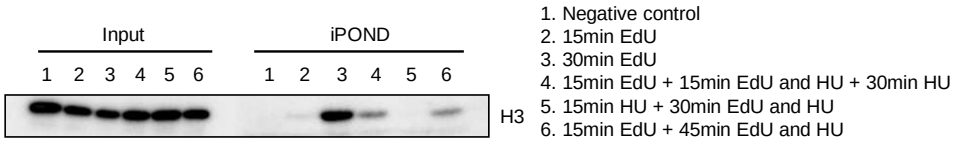

Figure 36. Replication forks of hTERT-RPE cells do not incorporate EdU after 15 minutes of HU treatment.
hTERT-RPE cells were synchronized in S phase and then treated with EdU and HU as indicated. Cells were harvested and iPOND was performed using equal protein levels in all conditions. Negative control: no EdU. Input: nuclear extract. H3: Histone 3.

With the above results, we defined the experimental conditions for the iPOND+MS experiment as follows (Figure 37):

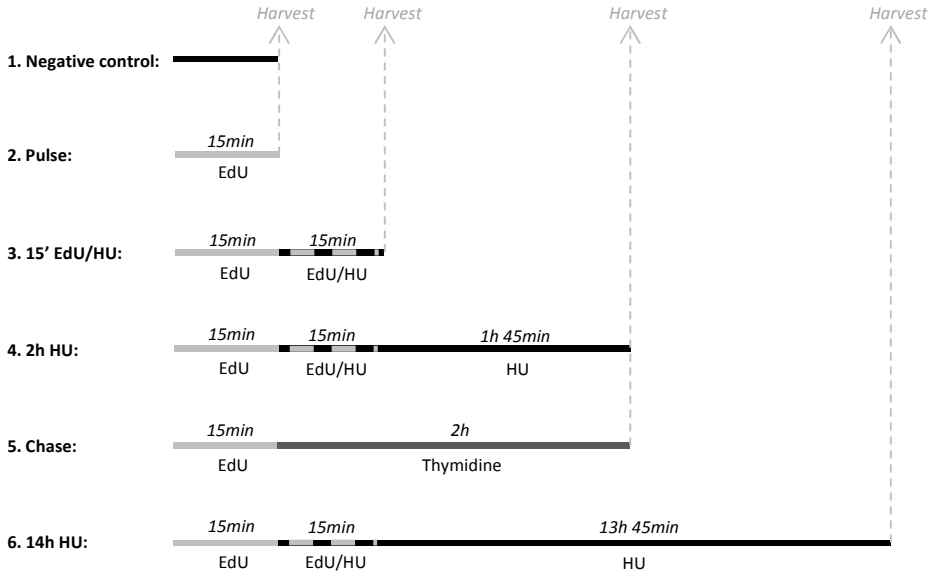

Figure 37. Experimental conditions for the iPOND+MS experiment.
Schematic of the experimental conditions used for the iPOND+MS experiment. Negative control: no EdU. Thymidine is added (low dose, 50µM) during the chase to displace the residual EdU present on cells.

2.1.2. Preparation of samples, protein isolation and identification/quantification by MS

Once established the experimental conditions, the following step was to harvest and prepare the samples to perform the modified version of iPOND. The experiment was conducted in triplicate, using three p150 plates per condition in each of them. Samples were harvested in parallel for flow cytometry, in order to analyze the percentage of S-phase arrested cells in each case (Figure 38).

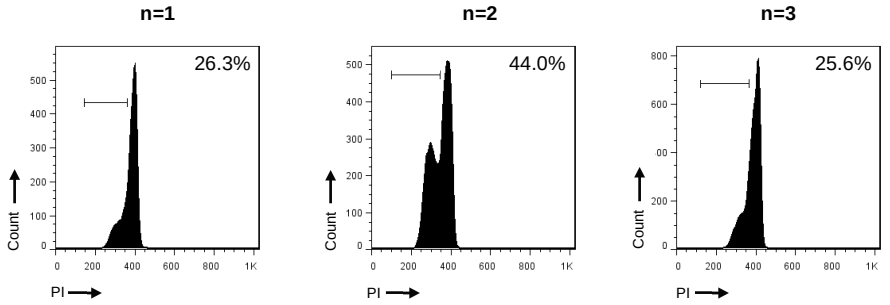

Figure 38. More than the 25% of BrdU positive hTERT-RPE cells were arrested in S phase after a 14-hour HU treatment in each experiment.
hTERT-RPE cells were synchronized in S phase, labeled with BrdU for 30min, treated with HU for 14h and the released into nocodazole containing fresh medium for 24h. DNA content (PI: propidium iodide) of BrdU positive cells was used to analyze the number of cells arrested in S phase after HU treatment. The percentage of S-phase arrested cells from BrdU positive population, in each experiment, is shown.

Before performing iPOND, cell extracts have to be processed in order to obtain properly biotinylated and sonicated samples. The biotinylation of the samples was verified by dot-blot analysis using a peroxidase conjugated anti-biotin antibody (Figure 39A). In addition, around the 5% of the processed sample was used to validate the sonication of the samples in each case. To this end, the purified DNA was run in a 1.5% agarose gel, and the size of the obtained DNA fragments was analyzed. As shown in Figure 39B, the size of the obtained fragments was between 100 and 300 bp in all cases, indicating that sonication had been correct.

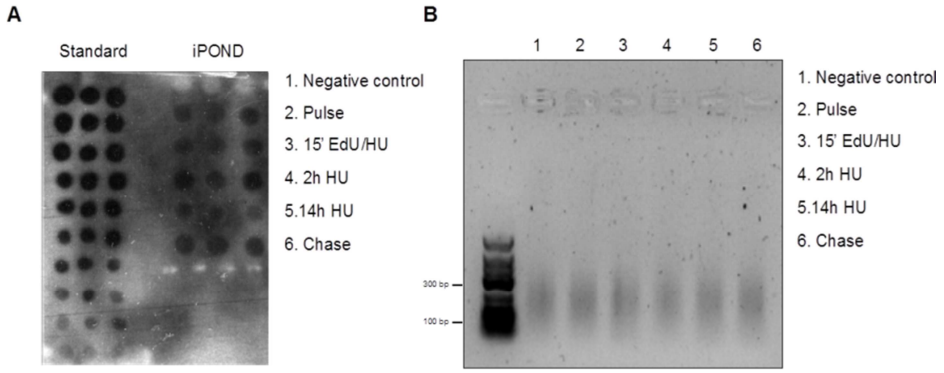

Figure 39. The samples used for the iPOND+MS experiment were properly biotinylated and sonicated.
(A) The biotinylation of the samples used for the iPOND+MS experiment was confirmed by dot-blot analysis. (B) DNA from the same processed samples was purified and run in a 1.5% agarose gel to validate the sonication. Representative images are shown. Conditions have been previously described *(Figure 37)*.

Once having validated that samples were correct, the modified version of iPOND was performed. Finally, the proteins isolated by this approach were identified/quantified by high-resolution MS.

2.1.3. Data analysis

The proteomic data are summarized on Appendix 1. This table shows the protein ID of the identified proteins, as well as their relative abundance (**RA**) value in each condition and replicate. Only the proteins from which more than one peptide was identified by MS were included on this table. Due to experimental problems, we had to perform the MS analysis in two rounds and besides, the 14h HU sample of the first biological replicate had to be analyzed by MS together with the second and third replicates in the second MS round. Consequently, the negative control, the pulse, the chase, the 15'EdU/HU and the 2h HU samples of the first biological replicate were analyzed in a first MS round, while all the other samples were analyzed in a second MS round. Unfortunately, some of the proteins were only identified in one of the MS rounds.

A total of 716 proteins were identified by MS (Appendix 1). The pulse/chase **enrichment ratios** (RA of a certain protein in the pulse/RA of the same protein in the chase) showed that the proteins most enriched at nascent DNA in the pulse condition include: DNA polymerase delta, DNA polymerase epsilon, CAF-1, DNA primase, DNA ligase, RFC1, RFC2, MCM4 and RFC5; validating the strength of the used proteomic approach for the identification of nascent DNA-bound proteins (Figure 40).

	First MS round
PROTEIN ID	*Pulse/Chase*
1433S_HUMAN	5,140E+12
RN166_HUMAN	4,089E+12
DPOD3_HUMAN	2,640E+12
DPOE1_HUMAN	2,340E+12
CAF1B_HUMAN	1,934E+12
PDLI5_HUMAN	1,671E+12
WDHD1_HUMAN	8,562E+11
SPB4_HUMAN	423,300
NTKL_HUMAN	195,852
LEG7_HUMAN	96,738
PRI2_HUMAN	43,938
DNLI1_HUMAN	39,823
RFC1_HUMAN	33,089
RFC2_HUMAN	31,065
MSH6_HUMAN	20,867
TOM70_HUMAN	16,703
EPIPL_HUMAN	14,850
S10A8_HUMAN	13,388
MSH2_HUMAN	12,849
GRWD1_HUMAN	11,848

	Second MS round
PROTEIN ID	*Pulse/Chase*
OAT_HUMAN	1,871E+12
KINH_HUMAN	1,652E+12
TBC8B_HUMAN	1,624E+12
RRBP1_HUMAN	1,145E+12
CTBP2_HUMAN	1,014E+12
FBRL_HUMAN	8,552E+11
PRI2_HUMAN	8,484E+11
RO60_HUMAN	8,343E+11
DYR_HUMAN	7,710E+11
UBP2L_HUMAN	6,086E+11
PDCD4_HUMAN	4,653E+11
ESTD_HUMAN	4,287E+11
SK2L2_HUMAN	4,103E+11
MCM4_HUMAN	3,968E+11
U5S1_HUMAN	3,475E+11
KI21B_HUMAN	2,560E+11
ACL6B_HUMAN	1,819E+11
HMGB2_HUMAN	1,762E+11
RFC5_HUMAN	1,707E+11
SF01_HUMAN	1,542E+11

Figure 40. Proteins most enriched at nascent DNA in the pulse.
The protein ID and the pulse/chase enrichment ratio values of the 20 proteins most enriched at nascent DNA in the pulse condition, in each MS round, are shown. The pulse/chase enrichment ratio values of the second

MS round correspond to the average pulse/chase enrichment ratio values between the second and third replicates. Keratins were not considered. (Related to Appendix 1)

In order to monitor the HU-induced changes, raw data from Appendix 1 were processed as follows:

1. For every protein, the RA value in each condition was divided by the maximum RA value for that protein in that replicate:

   ***nRA**= RA of a protein in a certain condition/max. RA value for that protein in that replicate*

   With this division, for each protein we obtained nRA values between 0-1 in each condition and replicate.

2. The proteins that showed very different kinetics in each biological replicate were removed from the study. Additionally, the proteins that presented a higher value than 0.6 in the negative control were not considered. In addition, Keratins and ribosomal proteins were also removed from the study (keratin contamination was similar in all the conditions of a certain replicate).

3. The average of nRA (**anRA**) values from the different triplicates was calculated for each protein and condition. A new table containing those anRA values was created. The proteins that had been identified only in the first MS round were included on this new table with the values obtained in the first step (written in grey to distinguish them), since there were no more replicates to calculate their average values.

4. In order to normalize the entire data of the new table, the anRA values were corrected again as in the first step. By doing so, we obtained a new table in which for each protein, the normalized anRA (**NRA, normalized relative abundance**) value in each condition was represented with a value between 0 and 1, being 1 the condition where a certain protein was the most abundant compared to the other conditions.

5. To facilitate the visualization, a heatmap was created by dividing the NRA values (from lowest to highest) into 5 groups and giving increasing color intensities to each of them.

6. Finally, proteins were manually classified by their best known function with the help of PANTHER database[513]. Each function was represented by a defined color.

The resulting final table (Appendix 2) shows: 1) protein ID; 2) each protein function, represented with different colors; and 3) the NRA values combined with different color intensities to represent them as a heatmap.

This final table contains 101 proteins. From those, a total of 50 proteins were considered nascent DNA-bound proteins, since they present fold enrichments higher than 2 compared to the chase. 8 of those proteins were considered as nascent DNA-

bound proteins on the pulse and 13 on the HU-treated samples, while 29 were considered as nascent DNA-bound proteins in both conditions (Figure 41).

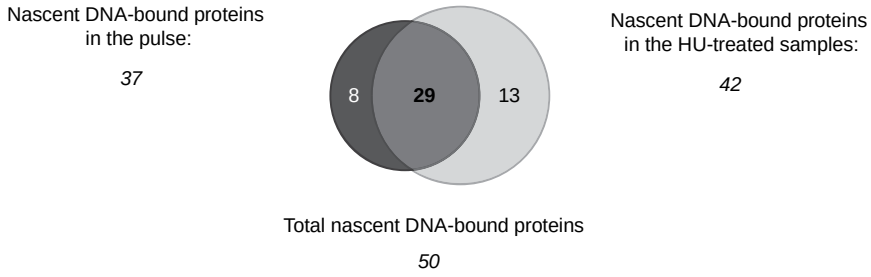

Figure 41. Classification of the nascent-DNA bound proteins of our proteomic analysis.
Venn diagram comparing the proteins classified as nascent DNA-bound proteins on different iPOND+MS experimental conditions. The total number of proteins in each group is indicated (in italic). Each circle represents a protein group. The number of proteins found in common (in bold) or individually in each group are represented inside the circles.

Additionally, 29 proteins were considered to be enriched at mature chromatin as they present a fold decrease higher than 2 compared to the pulse. Accordingly, 22 proteins were not considered either nascent DNA-bound proteins or mature chromatin-associated proteins, since they present similar NRA values in all conditions.

A comparative analysis between our data and the data available from other published works[390,392,510,511,514,515], confirmed the reliability of our approach since 30 out of 37 (81%) of the proteins classified as nascent DNA-bound proteins on the pulse in our proteomic analysis were also found as nascent DNA-bound proteins in other reports (Appendix 3). Furthermore, gene ontology (GO) analysis of the biological processes[516] confirmed the veracity of our proteomic analysis, since 21 out of 37 (57%) of the nascent DNA-bound proteins present on the pulse, were shown to be related to DNA replication (Figure 42). In addition, this analysis also allowed us to define the sensitivity of the approach. In this sense, 21 out of 211 (10%) of the proteins related to DNA replication on the entire GO database were found in our study.

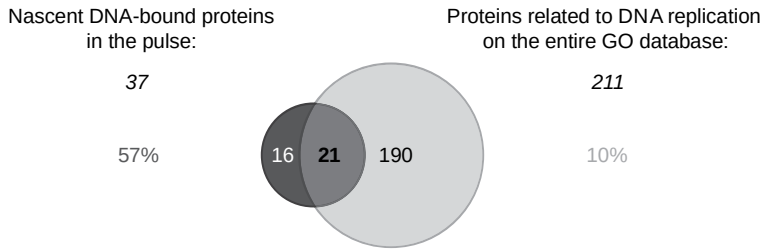

Figure 42. DNA replication-related proteins found in our proteomic analysis.
Venn diagram comparing the proteins classified as nascent DNA-bound proteins on the pulse in our proteomic analysis, with the DNA replication-related proteins found in the entire GO database. Each circle represents a protein group. The total number of proteins in each group is represented (in italic). The number of proteins found in common (in bold) or individually in each group are represented inside the circles. The percentage that a certain protein group represents relative to total proteins is shown.

Notably, from the 29 proteins shown to be enriched at mature chromatin, 9 (31%) were histones. Likewise, further examination (by GO analysis) of the functions related to the proteins found in mature chromatin proved once again the strength of the used approach (Figure 43).

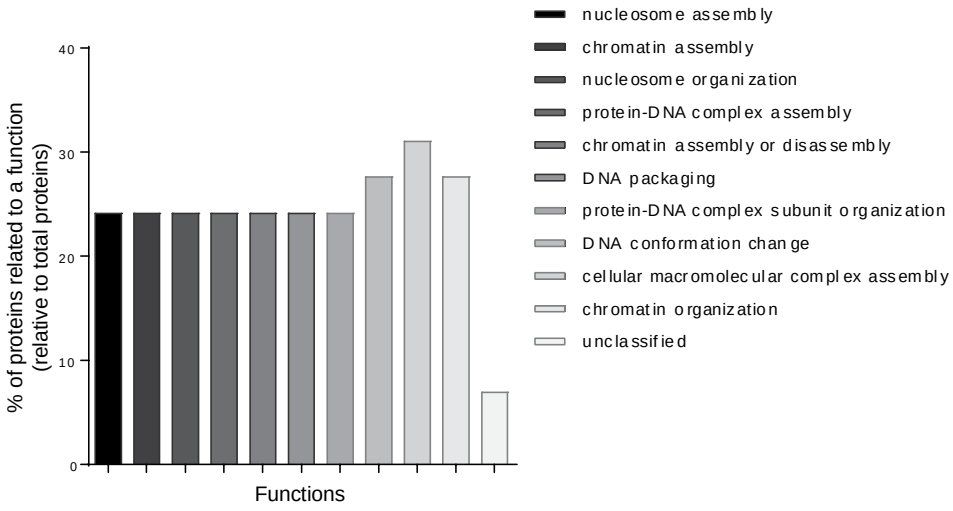

Figure 43. Most of the proteins enriched in the chase condition have mature chromatin-related functions. The proteins found to be enriched in the chase condition in our proteomic analysis were analyzed by GO to determine their best known function. The percentage of proteins related to a certain function relative to total proteins is shown.

An exhaustive comparison of the proteins associated with nascent DNA after a 2-hour but not 14-hour HU treatment, allowed us to select some candidates in order to analyze their implication on fork protection and restart. Nevertheless, due to time limitation, this project will be followed by another Ph.D. student from our group. However, the detailed examination of the HU-induced changes (Appendix 2) highlighted some interesting results that we decided to further analyze on this thesis.

As explained in the introduction, it has been described that stalled replication forks can eventually be remodeled and regressed into chicken foot structures[281,298,299]. Moreover, several recent studies have highlighted that in contrast to what it was thought, fork reversal is a very common event in response to several genotoxic stresses[302,303,310–312], from which replication can be restarted with the help of certain proteins such as RecQ1 or Dna2/WRN[311,312].

Interestingly, our proteomic analysis also pointed to that situation. As explained in the previous chapter, hTERT-RPE cells are able to resume replication from the same forks after a short (2 hour) HU treatment (Figures 23 and 27). Nonetheless, our proteomic results showed that replisome components were dissociated from nascent DNA under this condition (Figure 44). Even the MCM helicase, which is essential for DNA replication and can only be loaded onto chromatin on late mitosis and G1[116], was dissociated from nascent DNA under this condition.

Figure 44. Replisome components of hTERT-RPE cells are dissociated from nascent DNA after a 2-hour HU treatment.
The protein ID of the replisome components found in our iPOND+MS experiment is shown. The NRA value in each condition is represented by certain color intensity as indicated. Proteins in grey are the ones identified only in one of the biological replicates. Black boxes represent lack of data. *(Related to Appendix 2)*

Moreover, our proteomic results also showed that RecQ1, which is involved in the restart from reversed forks[311], was present at replication forks of hTERT-RPE cells after a 2-hour HU treatment (Figure 45). Furthermore, our results from the previous chapter revealed that Rad51, which has been described as an essential protein for fork reversal[312], was also recruited to chromatin after a 2-hour HU treatment (Figures 24 and 25).

Collectively, these results suggest that replication forks of hTERT-RPE cells are regressed into chicken foot structures after a 2-hour HU treatment.

Interestingly, the analysis of fork stability and repair proteins identified in our iPOND+MS experiment showed that some of them, such as FANCD2, FANCI and SMC3, increased their association with nascent DNA in response to HU (Figure 45).

Furthermore, consistent with our previous observations showing that non-transformed human cells, are able to resume replication after short but not long HU treatment, those proteins were present on nascent DNA after a 2-hour HU treatment (Figure 45). Moreover, at least some of them decreased their association with nascent DNA after a 14-hour HU treatment.

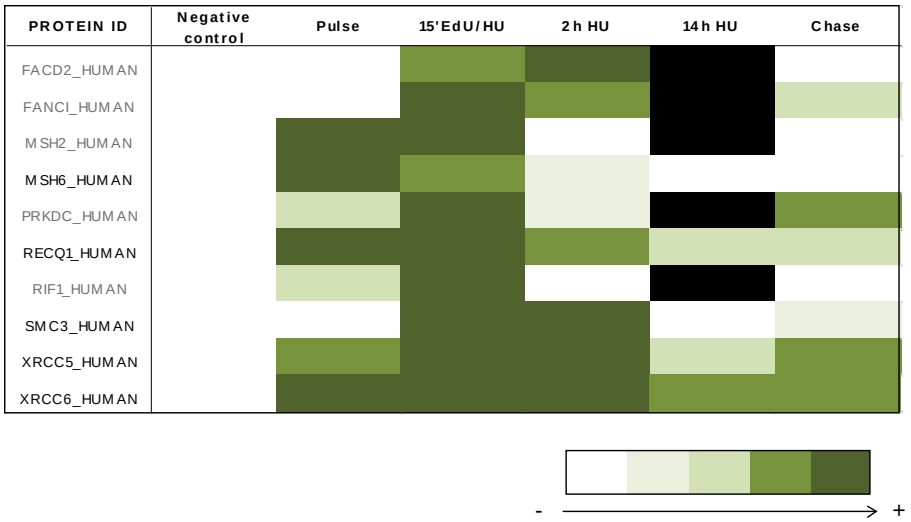

Figure 45. DNA repair proteins are recruited to nascent DNA in response to HU addition.
The protein ID of those proteins identified in our iPOND+MS experiment and classified as DNA repair proteins according to PANTHER database[513] is shown. The NRA value in each condition is represented by certain color intensity as indicated. Proteins in grey are the ones that were identified only in one of the biological replicates. Black boxes represent lack of data. *(Related to Appendix 2)*

As previously shown (Figures 24 and 26), nascent DNA is degraded after a 14-hour HU treatment. Accordingly, only a few proteins were classified as nascent DNA-bound proteins (they present fold enrichments higher than 2 compared to the chase) on the 14h HU condition (Figure 46). In fact, although these proteins were considered as nascent-DNA bound proteins, at least some of them presented a lower relative association with nascent DNA than in the pulse or in the other HU conditions.

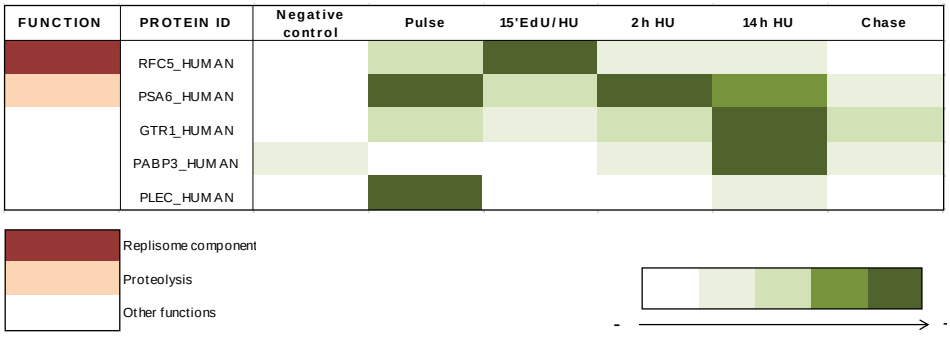

Figure 46. Nascent DNA-bound proteins present on the 14h HU condition.
The protein ID of those proteins from the 14 hour HU condition that showed an enrichment of at least two fold compared to the chase is shown. Their NRA value in each condition is represented by certain color

intensity as indicated. Protein functions, classified according to PANTHER database[513], are represented by different colors as indicated. *(Related to Appendix 2)*

2.2. Replication forks of hTERT-RPE cells are remodeled after a short HU treatment

In agreement with previous works[302,303,310–312], our proteomic results suggested that replication forks of hTERT-RPE cells were being reversed after a short (2 hour) HU treatment. This was underlined by the fact that replisome components were being dissociated from nascent DNA under this condition, despite maintaining the competence to recover. To prove it, we decided to indirectly analyze the formation of these structures in response to HU in hTERT-RPE cells.

2.2.1. Indirect visualization of reversed forks

BrdU immunofluorescence under native conditions has been described to be useful to analyze the accumulation of ssDNA in chromatin[517]. A couple of years ago, this immunofluorescence was used for the first time to indirectly visualize replication intermediates that contain ssDNA, including reversed forks, by reducing the BrdU incorporation time from one day to 10 minutes, to label only the nascent DNA present on replication forks or close by[305].

From the results obtained in the previous chapter, we knew that replication forks of hTERT-RPE cells are not processed into DSBs after a 2-hour HU treatment (Figures 20 and 21). Thus, fork reversal would be the most likely explanation for the presence of single-stranded nascent DNA. The formation of these structures exposes a fragment of ssDNA on the 3' end of the nascent leading strand[312] that can be indirectly visualized by BrdU immunofluorescence[302,305] (Figure 47).

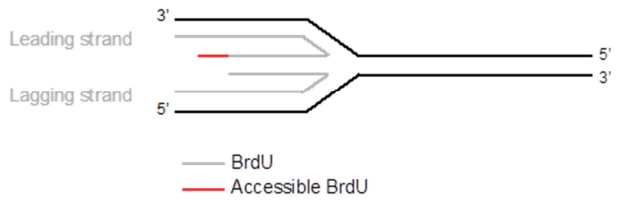

Figure 47. Analysis of fork reversal by BrdU immunofluorescence under native conditions.
Cells are labeled with BrdU for 10min. After that, the presence of single-stranded nascent DNA is detected by BrdU immunofluorescence under native conditions. If forks are reversed as indicated, BrdU antibody can reach the ssDNA present on the 3' end of the leading strand.

BrdU immunofluorescence under native conditions showed that as expected, hTERT-RPE cells presented single-stranded nascent DNA after a 2-hour HU treatment (Figure 48). Moreover, this experiment also showed that replication forks of hTERT-RPE cells treated during 14 hours with HU, which were already processed into DSBs (Figure 20 and 21), accumulated more single-stranded nascent DNA than the ones treated during 2 hours with HU (Figure 48).

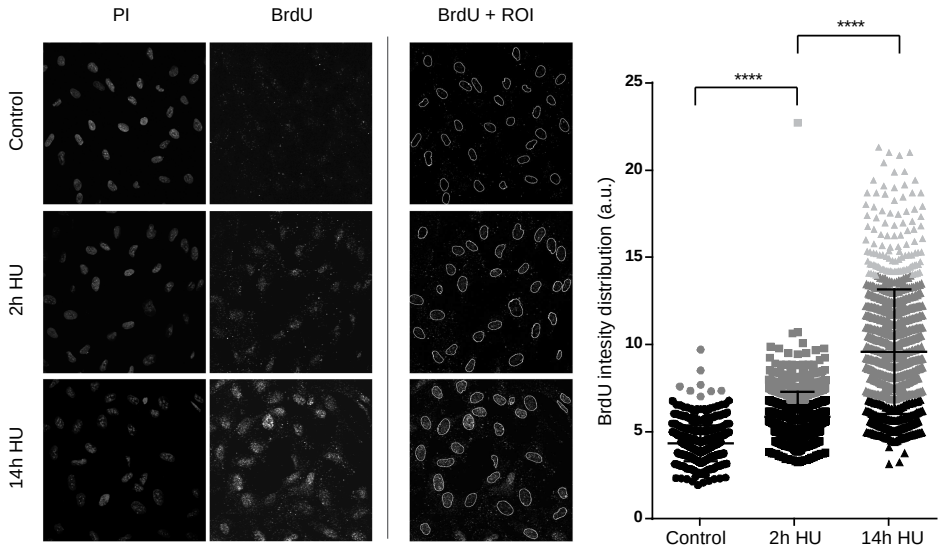

Figure 48. Replication forks of hTERT-RPE cells present single-stranded nascent DNA even after a 2-hour HU treatment.

S-phase synchronized hTERT-RPE cells were treated during the indicated time with HU or left untreated (Control). BrdU was maintained during additional 15min during the HU treatment. After that, cells were harvested and BrdU immunofluorescence was performed under native conditions. DNA was counterstained with propidium iodide (PI). Representative images are shown (left panel). The ROIs used to quantify BrdU intensity are shown. The relative BrdU intensity, in arbitrary units (a.u.), of more than 500 cells per condition from three independent experiments is represented on the scatterplot (right panel). The relative BrdU intensities were enclosed into 3 different groups that are represented with different colors (<7 in black; 7-14 in dark grey; >14 in light grey). Around the 98% of control cells were included in the first group. Error bars indicate the mean and the standard deviation, (unpaired *t test*, n=3).

2.2.2. ATM kinase is activated before replication forks are processed into DSBs

Fork reversal has been described to be able to activate ATM kinase even in the absence of DSB, as it exposes a free DNA end[302]. Accordingly, a 2-hour HU treatment resulted in Chk2 phosphorylation and p53 stabilization in an ATM-dependent manner despite replication forks of hTERT-RPE cells did not present DSBs at this time (Figures 49, 20 and 21). Additionally, although some phosphorylation of RPA32 (analyzed by electrophoretic mobility shift) was already observed after a 2-hour HU treatment, its hyperphosphorylation, which has been describe to occur following DNA breaks in a CtIP-dependent fashion[518], was not observed under these conditions (Figure 49).

Remarkably, both RPA32 hyperphosphorylation and CtIP phosphorylation (analyzed by electrophoretic mobility shift), which are marks of DNA resection[518], were observed after a 14-hour HU treatment (Figure 49). Moreover, in agreement with published data[302], only CtIP phosphorylation was shown to depend on ATM under these conditions.

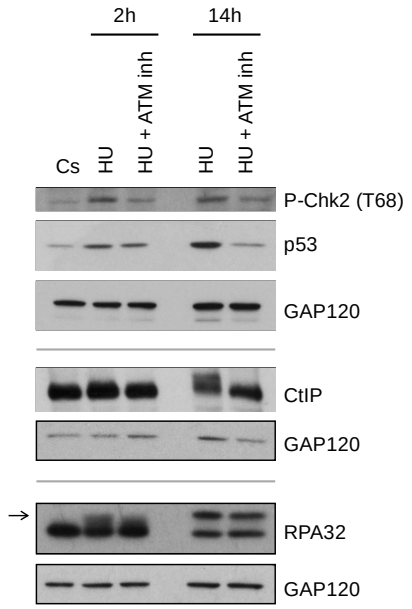

Figure 49. ATM is activated in hTERT-RPE cells before replication forks are processed into DSBs.
hTERT-RPE cells were synchronized in S phase and then treated during the indicated time with HU +/- ATM kinase inhibitor (inh) (KU-55933), or left untreated (Cs). Whole cell lysates were analyzed by WB with the indicated antibodies. GAP120 was used as loading control. The arrow indicates the hyperphosphorylated band of RPA32.

Collectively, all the previous results seem to indicate that replication forks of hTERT-RPE cells are regressed into chicken foot structures after a short HU treatment. Additionally, the increased BrdU staining (Figure 48) and the presence of resection marks (Figure 49), together with the previously observed degradation of nascent DNA after a 14-hour HU treatment, suggests that replication forks of hTERT-RPE cells are not only remodeled but also processed after prolonged HU treatment.

2.3. Replisome components are dissociated from chromatin in hTERT-RPE cells after a long but not short HU treatment

As explained in the introduction, whether fork reversal entails replisome disassembly and if so, how is replication restarted from reversed forks afterwards, are questions that have not been elucidated yet, at least in higher eukaryotes[281,298–300]. Remarkably, since our results suggest that replication forks of hTERT-RPE cells are regressed into chicken foot structures after a short HU treatment, our proteomic analysis may contribute to define the composition of reversed forks, which will let to gain a better understanding of the previous concerns. In this sense, to try to define if replisome components were displaced away from replication forks but still recruited onto chromatin, we decided to validate the proteomic results by iPOND+WB, to study the association of these proteins with chromatin afterwards. Additionally, the combined analysis of the proteins associated with nascent DNA and with chromatin, will contribute to understand how, consistent with our previous data (Figures 23 and 27), replication forks are able to restart after a short but not long HU treatment.

2.3.1. Validation of proteomic results

In order to validate the proteomic results, hTERT-RPE cells were treated as previously (Figure 37) to perform the modified version of iPOND. Nonetheless, in this case, the proteins present on iPOND extracts were analyzed by electrophoresis and WB (iPOND+WB).

This experiment showed that consistent with the proteomic results, replisome components such as PCNA, Fen1 or RFC3, and even the MCM6, were not associated with nascent DNA after a 2-hour HU treatment (Figure 50). Additionally, RPA32, which in contrast to other RPA subunits was shown to increase its association with nascent DNA after a 2-hour HU treatment in the proteomic analysis (Figure 44), was shown to reduce its association with nascent DNA under this condition when analyzed by iPOND+WB (Figure 50).

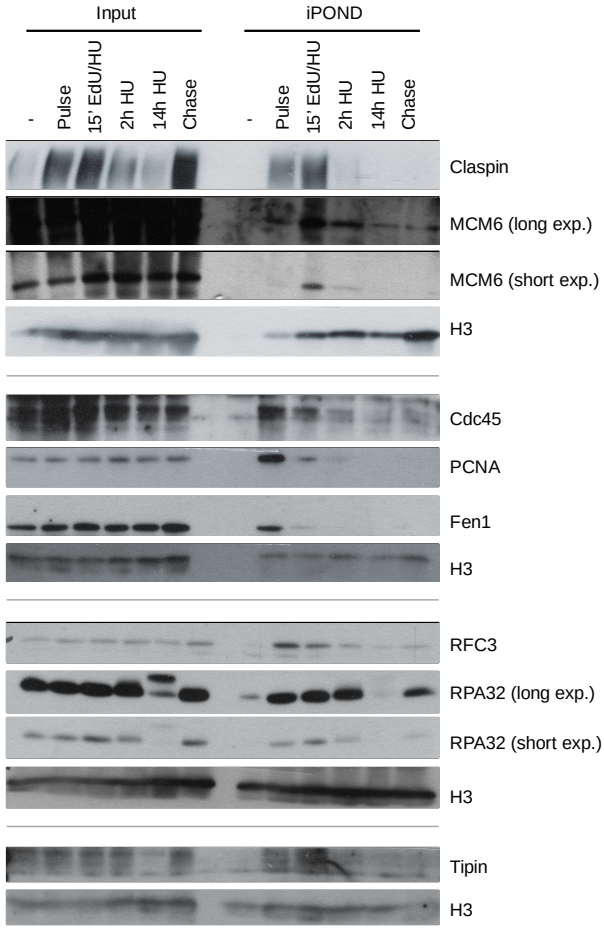

Figure 50. Replisome components of hTERT-RPE cells are dissociated from nascent DNA after a 2-hour HU treatment.

hTERT-RPE cells were synchronized in S phase and then treated, as previously indicated *(Figure 37)*, for iPOND. The proteins present on iPOND extracts were analyzed by WB with the indicated antibodies. Histone 3 (H3) was used as an immunoprecipitation control. Input: nuclear extract. -: negative control. Exp.: exposure.

Remarkably, this experiment also allowed us to observe the dissociation (after a 2-hour HU treatment) of other replisome components (Claspin, Cdc45 and Tipin) that were not identified in the iPOND+MS experiment, further supporting the idea that the replisome was being dissociated from nascent DNA after a 2-hour HU treatment (Figure 50). Moreover, consistent with our previous results, all those proteins were shown to remain dissociated from nascent DNA after a 14-hour HU treatment. Furthermore, RPA32 was clearly hyperphosphorylated under this condition.

Apart from validating the dissociation of replisome components after a 2-hour HU treatment, iPOND+WB analysis also allowed us to confirm that proteins described to be important for fork protection and restart, such as FANCD2[289,395,519] and SMC3[206,399], were associated with nascent DNA under these conditions (Figure 51). Likewise, this experiment also allowed us to confirm that other proteins that had not been identified by MS, but are also thought to be important for fork protection and restart (SMC1[206,399] and Rad51[289,394–396]), were also present on nascent DNA under this condition.

Interestingly, consistent with our previous results showing that replication fork restart was impaired (Figures 23 and 27), and that nascent DNA was being degraded after a 14-hour HU treatment (Figures 24 and 26), all these proteins were shown to decrease their association with nascent DNA under this condition (Figure 51). In addition, in the case of FANCD2, this decreased correlated with a slight reduction on its total nuclear levels (input).

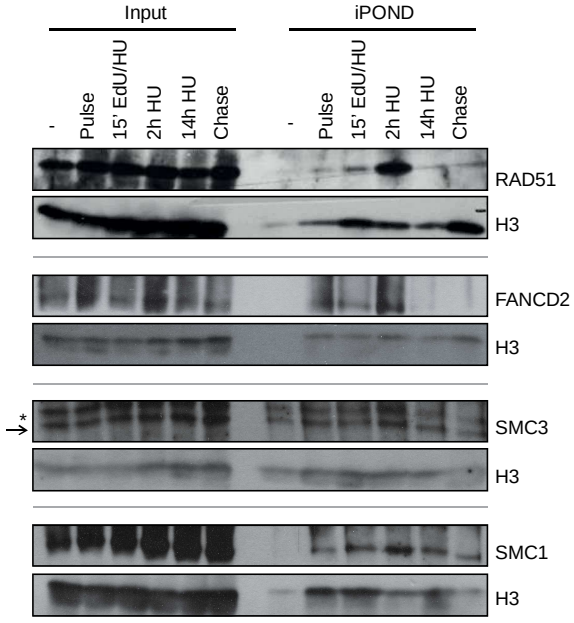

Figure 51. Proteins involved in fork protection and restart are present on nascent DNA after a 2-hour but not 14-hour HU treatment in hTERT-RPE cells.

Same iPOND extracts as in *(Figure 50)* were used to analyze Rad51, FANCD2 and SMC3. New extracts, harvested as in *(Figure 50)*, were used to analyze SMC1. The proteins present on iPOND extracts were analyzed by WB with the indicated antibodies. Histone 3 (H3) was used as an immunoprecipitation control (controls from *(Figure 50)* are displayed again to show which samples were used in each case). Input: nuclear

extract. -: negative control. The asterisk indicates a non-specific band while the arrow indicates the specific band of SMC3.

2.3.2. Chromatin association analysis

In order to discern if the observed dissociation of replisome components from nascent DNA after a 2-hour HU treatment, was due to a real disengagement or if by contrast, was due to a displacement of those proteins away from replication forks, the association of them with chromatin was analyzed. To this end, hTERT-RPE cells were treated during 2 or 14 hours with HU, and then chromatin extracts were prepared and analyzed by electrophoresis and WB.

As shown in Figure 52, the MCM helicases were present on chromatin after a 2-hour HU treatment. Moreover, no dissociation was observed either after a 14-hour HU treatment.

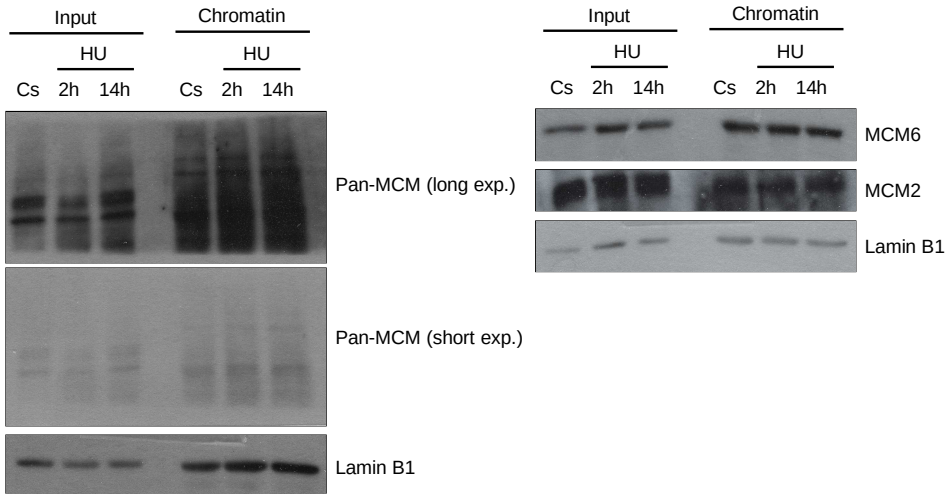

Figure 52. MCM helicases are present on chromatin despite the HU treatment in hTERT-RPE cells.
hTERT-RPE cells were synchronized in S phase and then treated with HU during the indicated time or left untreated (Cs). Chromatin extracts were prepared and the proteins present on them were analyzed by WB with the indicated antibodies. Input: whole cell lysates. Lamin B1 was used as loading control. Exp.: exposure

However, only the ~10% of the licensed origins are fired during a normal replication, which implies that much more MCM2-7 helicases than the ones activated would be associated with DNA during S phase[229]. Thus, it is not surprising to find these proteins loaded onto chromatin even after a 14-hour HU treatment, as the HU may have only an effect in those origins that have been activated, and therefore, the effect may not be noticeable.

Interestingly, the analysis of other replisome components association with chromatin showed that most of them remained loaded onto chromatin after a 2-hour HU treatment (Figure 53), despite not being present on nascent DNA (Figure 50). Even the Cdc45, which is part of the CMG helicase complex (Cdc45-MCM-GINS)[124], was shown to

remain associated with chromatin under this condition (Figure 53). Only the PCNA was shown to decrease its association with chromatin after a 2-hour HU treatment.

Remarkably, most of those replisome components seemed to be released from chromatin after a 14-hour HU treatment, although total protein levels (input) remained constant in most cases (Figure 53). From the analyzed proteins, only the RPA was clearly shown to remain associated with chromatin under this condition. Moreover, consistent with our previous results, RPA32 was shown to be hyperphosphorylated after a 14-hour HU treatment.

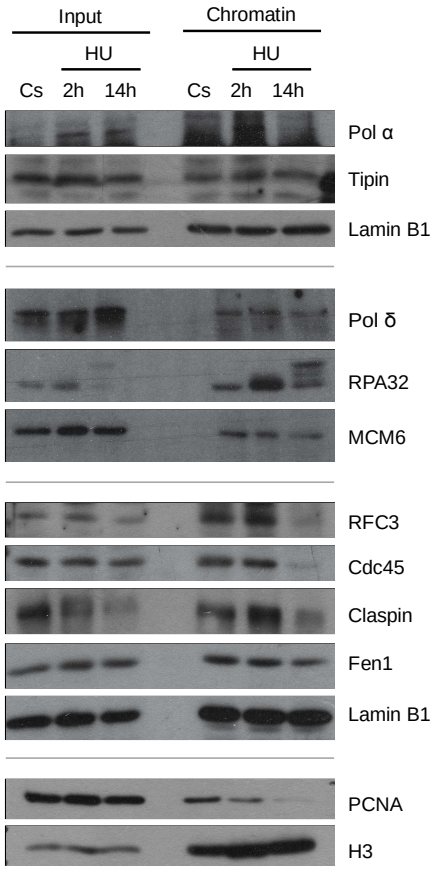

Figure 53. Replisome components of hTERT-RPE cells are dissociated from chromatin after a long but not short HU treatment.
S-phase synchronized hTERT-RPE cells were treated during the indicated time with HU or left untreated (Cs). Chromatin extracts were prepared and analyzed by WB with the indicated antibodies. Input: whole cell lysates. Lamin B1, MCM6 and Histone 3 (H3) were used as loading control.

The analysis of chromatin-bound proteins after HU treatment, also allowed us to determine, that as expected, proteins thought to be important for replication fork restart, such as SMC1 and SMC3[206,399], were present on chromatin after a 2-hour HU

treatment (Figure 54). Moreover, their association with chromatin decreased after a 14-hour HU treatment.

Additionally, consistent with our previous results showing that Rad51 was associated with chromatin in untreated or 2-hour HU-treated cells, but not in 14-hour HU treated cells (Figures 24 and 25), proteins reported to be required for Rad51 recruitment (BRCA2 or FANCD2[520]) recapitulated the same phenotype (Figure 54). Moreover, the association of those proteins with chromatin was not reestablished either after HU removal. Remarkably, consistent with the previously observed decrease in FANCD2 nuclear levels (Figure 51), a reduction on its total levels was observed after a 14-hour HU treatment (Figure 54). To analyze if this decrease was due to degradation, MG132 proteasome inhibitor was added to HU-treated hTERT-RPE cells. Notably, the addition of MG132 disrupts the electrophoretic mobility shift of FANCD2 and other proteins in our hands. Thus, the recovery on FAND2 levels was difficult to analyze. However, the addition of this drug restored BRCA2 and Rad51 association with chromatin.

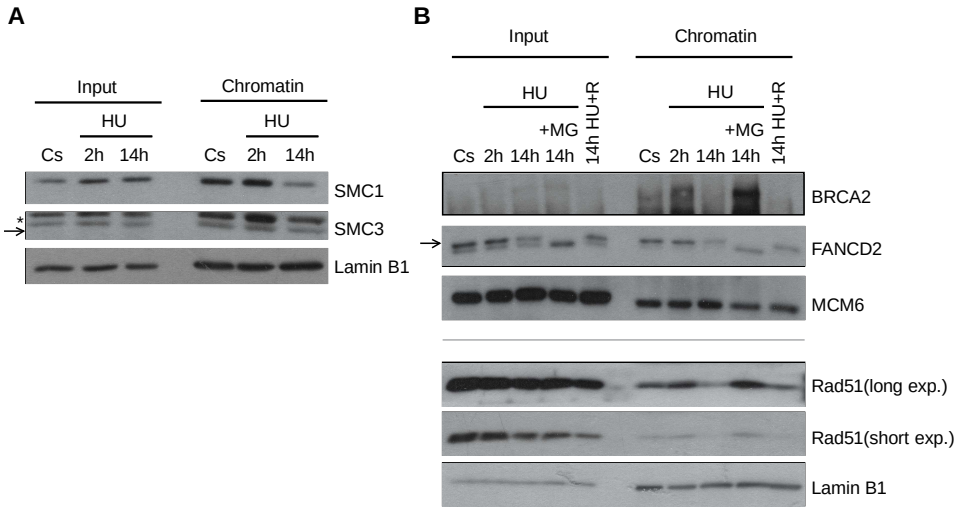

Figure 54. Proteins involved in fork protection and restart are associated with chromatin after a 2-hour but not 14-hour HU treatment in hTERT-RPE cells.
(A) Chromatin samples from *(Figure 53)* were used for SMC1 and SMC3 analysis. The asterisk indicates a non-specific band. The arrow indicates the specific band for SMC3. (B) hTERT-RPE cells were synchronized in S phase and then treated during the indicated time with HU or left untreated (Cs). MG132 (MG) proteasome inhibitor was added during the last 6h of treatment where indicated. Cells were released (R) into fresh medium for 30min where indicated. Chromatin extracts were analyzed with the indicated antibodies. The arrow indicates the phosphorylated band of FANCD2. Input: whole cell lysates. Lamin B1 and MCM6 were used as loading control. Exp.: exposure.

Altogether, the above results suggest that consistent with works done in T4 bacteriophage system[300], metazoan replisome components are displaced away from nascent DNA but are not dissociated from chromatin during fork reversal. Additionally, consistent with our previous results, most of the replisome components are dissociated from chromatin after prolonged HU treatment. Furthermore, proteins reported to be important for replication fork protection and restart have also been shown to be

dissociated from chromatin and nascent DNA under this condition, which all together contributes to explain the previously observed loss of replication recovery competence.

2.4. Replication forks of hTERT-RPE cells are able to restart after a 2-hour HU treatment even in the absence of CDK activity

As explained in the previous chapter, replication forks of hTERT-RPE cells are able to restart after a short but not long HU treatment (Figures 23 and 27). In addition, we have shown that, in contrast to 14-hour HU-treated cells, replisome components are displaced away but not dissociated from chromatin after a short HU treatment. In this sense, it is known from the literature that in contrast to MCM2-7, which is loaded in excess onto chromatin during S phase[229], CMG active helicase complex is only formed at fired origins[124,164,167]. Thus, a previously formed CMG complex would be required to resume replication from the same forks if proteins such as Cdc45, which are part of the CMG complex[124], have been dissociated or displaced away from replication forks as in our case. Collectively, all these results suggest that the same replisome components as the ones used before fork stalling are recycled to resume replication after a short HU treatment.

However, as previously explained, the used DNA fiber approach did not allow us to unequivocally dismiss the possibility that the observed fork restart came from the activation of nearby origins. Thus, to prove that the observed replication restart came from a real fork restart, we decided to perform a DNA fiber experiment using the CDK inhibitor roscovitine[521], to inhibit the CDK2-mediated replisome components phosphorylations, which are essential for origin firing[124,177,178].

For this analysis, asynchronously growing hTERT-RPE cells were labeled with CldU thymidine analog for 30 minutes, and then HU+/- roscovitine was added during 2 hours. As in the previous experiments, CldU was maintained in the media during the first 15 minutes of HU treatment. Finally, cells were incubated with IdU thymidine analog in the presence or absence of roscovitine for 1 hour more.

As shown in Figure 55, consistent with our previous results (Figures 23 and 27), around the 80% of the initially fired replication forks were shown to restart despite the addition of roscovitine (Figure 55). Likewise, the number of stalled forks did not either change due to roscovitine addition. By contrast, the slight increase in the number of new origin firing events, observed after a 2-hour HU treatment, was abrogated by the addition of roscovitine, supporting the idea that origin firing was inhibited under these conditions.

Notably, the length of the IdU tracks (second labeling) was also a bit shorter in the presence of roscovitine, probably due to an impaired activation of nearby origins.

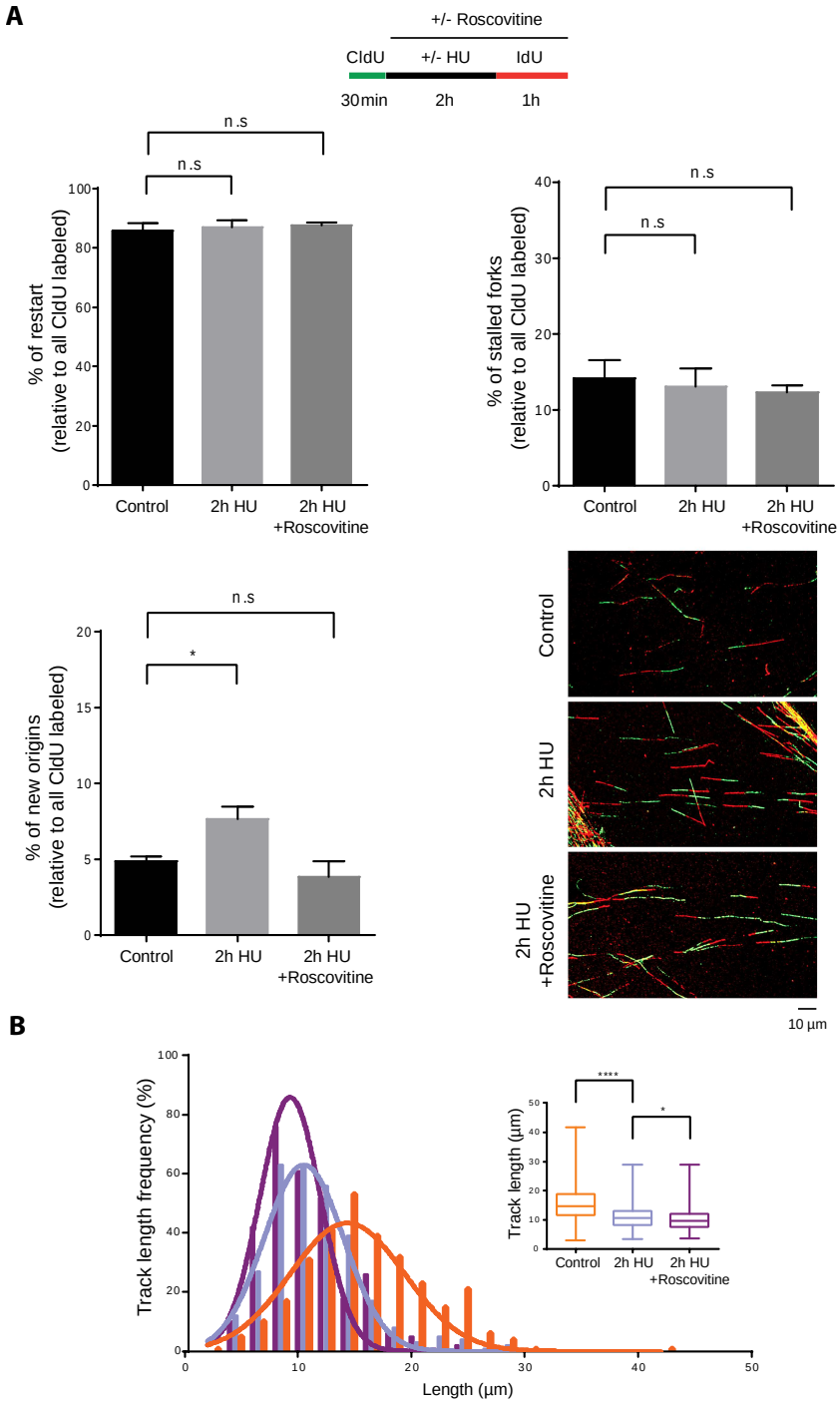

Figure 55. The addition of CDK inhibitor roscovitine does not abrogate fork restart after a 2-hour HU treatment.

(A) Asynchronously growing hTERT-RPE cells were labeled and treated as indicated (upper panel). CldU was present for additional 15min on HU-treated cells. DNA fibers were prepared and stained with BrdU

antibodies. Around 1500 fibers from three independent experiments were counted in each condition. The average percentage of new, stalled and restarted forks, relative to total CldU labeled fibers, is shown. Representative images are shown (bottom-right panel). Error bars represent standard deviation, (paired *t test*, n=3). (B) DNA fibers from *(A)* were used to measure the IdU (second labeling) track length. 300 fibers from three independent experiments were measured. IdU track length distribution and statistical analysis are shown. Box and whiskers show: Min, Max, Median and first quartiles, (unpaired *t test*, n=3).

Collectively, in agreement with previous reports[311,312] and with our previous observations, the above results support the idea that replication can be restarted from reversed forks. Additionally, the fact that replication forks are restarted after a 2-hour HU treatment in the presence of roscovitine, once Cdc45 has been displaced away from replication forks despite being associated with chromatin, suggests that the replisome components used before fork stalling are recycled to reinitiate replication after the stress. In this regard, replisome components dissociation from chromatin, such as the one observed after a 14-hour HU treatment, may contribute to prevent replication fork restart.

2.5. Replication resumption upon short HU treatment does not compromise genome integrity in hTERT-RPE cells

As previously explained, whether fork reversal is pathological or if by contrast, has a protective role under certain conditions, is another concern that still remains to be elucidated[298]. Our previous results suggest that replication forks of hTERT-RPE cells are reversed after a 2-hour HU treatment and that replication is restarted from the same forks afterwards. Thus, we decided to analyze the possible acquisition of genomic instability under these conditions.

As shown in Figure 56, consistent with our previous results, hTERT-RPE cells lost the ability to divide and arrive to G1 after a 14-hour HU treatment. Notably, despite replication forks of those cells presented DSBs under this condition (Figure 29), the number of cells arriving to G1 with DNA damage did not increase (Figure 56). Likewise, the number of cells arriving to G1 with 53BP1 foci did not either increase when cells had been treated during 2 hours with HU. Nevertheless, the percentage of cells that arrive to G1 did not change in this case, consistent with the previously observed maintenance of cell cycle resumption competence after a short HU treatment.

Remarkably, these results support the idea that replication resumption from reversed forks do not necessarily compromise genome integrity, at least if replication forks have not been further processed by nucleases or other proteins that induce fork collapse.

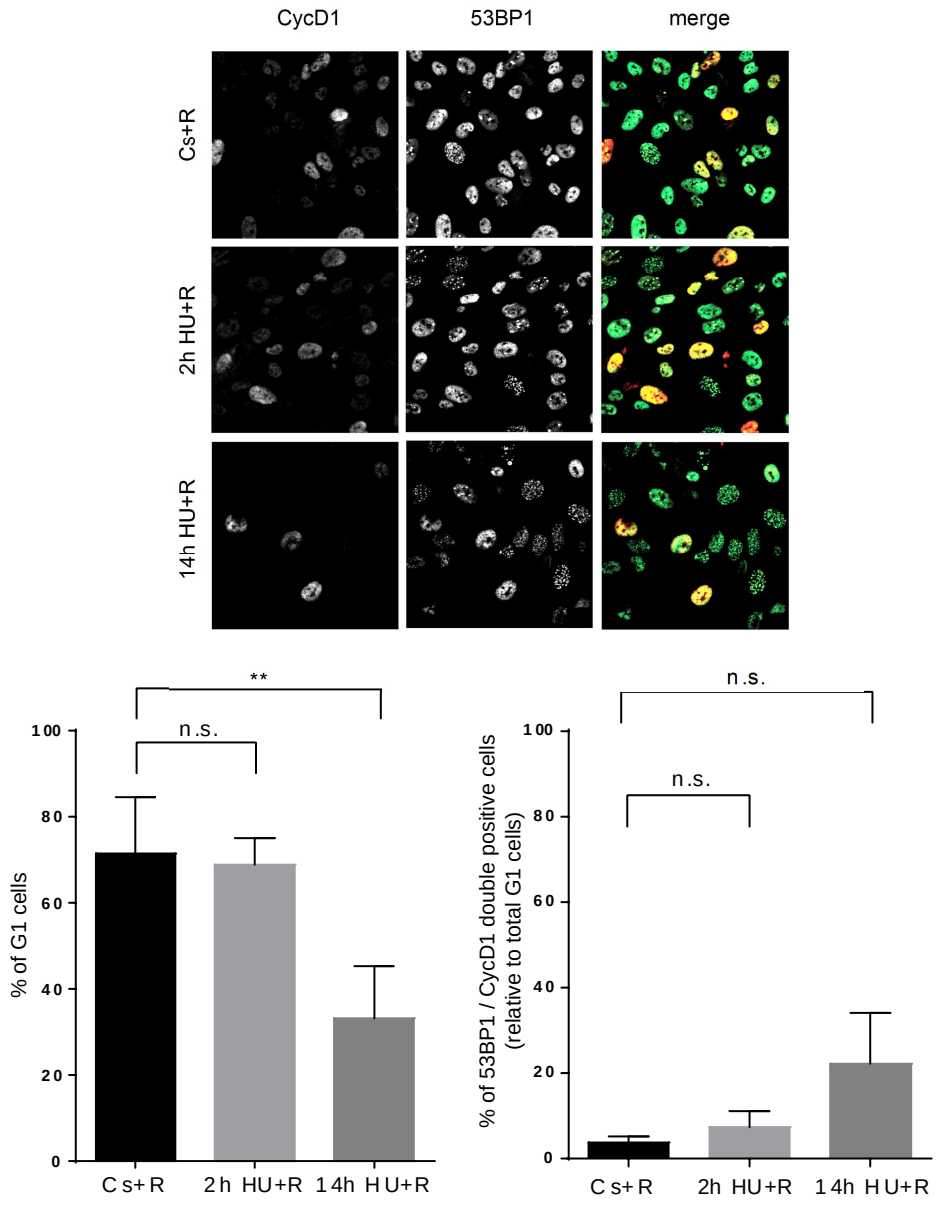

Figure 56. Analysis of the ability to divide of hTERT-RPE cells in the presence of DNA damage.
S-phase synchronized hTERT-RPE cells were treated during the indicated time with HU or left untreated (Cs), and then released (R) for 12h into fresh medium. Representative images are shown (upper panel). The average percentage of G1 cells is shown (bottom-left panel). The average percentage of 53BP1 foci (>6) and Cyclin D1 (CycD1) double positive cells relative to total G1 (Cyclin D1 positive) cells is shown (bottom-right panel). Error bars represent standard deviation, (paired *t test*, n=3).

DISCUSSION

Cell division is essential for all organisms' existence. This process requires an accurate duplication of the genome in order to correctly transmit the genetic and epigenetic information to each daughter cell. In this regard, several mechanisms have evolved to ensure that DNA is replicated completely, accurately and only once per cell cycle, preventing the loss of information and the acquisition of genomic instability, a hallmark of cancer[1,3,478].

Cells are constantly being challenged by endogenous and exogenous forms of damage that can cause RS[2,244,248]. In this sense, the mechanisms involved in monitoring the fidelity of copying the DNA are essential not only in the presence of external agents, but also during unperturbed cell cycle[387–389]. The importance of these mechanisms for cell survival is underlined by the fact that the depletion of some of the proteins involved in these processes, such as ATR or Chk1, results in embryonic lethality[325–327].

In the presence of RS, cells respond by activating several mechanisms to ensure the stabilization and repair of forks, as well as to inhibit cell cycle progression, to avoid cell division in the presence of unreplicated or damaged DNA. In addition, in the cases of persistent damage, these mechanisms prevent cell cycle resumption by driving cells to apoptosis or senescence, to avoid the acquisition of genomic instability[244–248]. Remarkably, oncogene-induced RS results in cellular senescence, which acts as a tumorogenic barrier in premalignant lesions[252,253].

While the DDR has been extensively studied in tumor cells, the pathways involved in the response to RS are less understood, especially in non-transformed human cells. In this regard, the main objective of this thesis was to define and characterize new DNA replication stress response mechanisms that contribute to preserve genome integrity in non-transformed human cells.

Interestingly, our results, together with other works from the literature, have highlighted the complexity and variety of the mechanisms involved in the abrogation of cell cycle resumption after severe replication stress, which may contribute to the safeguarding of genome integrity. In this sense, our result show that in response to a sustained DNA replication inhibition that results in the accumulation of DSBs, the APC/C^{Cdh1} ubiquitin ligase is activated in S phase to prevent origin firing and to inhibit replication resumption in non-transformed human cells (Discussion I). Additionally, we have seen that replication forks of hTERT-RPE cells suffer several changes that may also contribute to the inhibition of cell cycle resumption under these conditions (Discussion II). Notably, although replication forks of hTERT-RPE cells are remodeled already after a short HU treatment (Discussion II), this remodeling does not seem to imply the loss of replication recovery competence and the acquisition of genomic instability, at least unless replication forks are further processed (Discussion II and III).

The fact that replication resumption is compromised once replication forks have been processed into DSBs, underlines the idea that those mechanisms shown to avoid replication resumption after severe replication stress might be implicated in preventing the acquisition of genomic instability (Discussion III). In this sense, replication resumption from or in the presence of broken replication forks has been reported to compromise genome integrity[290,451,456–459]. Interestingly, our results suggest that the

mechanisms involved in replication resumption under these conditions[450,452–455] are inhibited in hTERT-RPE cells, and accordingly, these cells become senescent (Discussion I and II). Remarkably, tumor cells might lack some of those responses since they are able to resume replication under the same conditions[450]. Notably, several works have shown that non-transformed human cells present a more robust DNA replication stress response than tumor cells[324,499,500]. Consistently, our results show that, in agreement with previous reports[153] and with other works done in our laboratory[507], HCT116 cells do not activate APC/C^{Cdh1} in S phase in response to prolonged replication inhibition (Discussion I). Additionally, artificial APC/C^{Cdh1} activation in S phase reduces HU-induced genomic instability in those cells (Discussion III).

Collectively, the results of this thesis show that non-transformed human cells present several DNA replication stress response mechanisms to avoid cell cycle resumption after severe replication stress, which contributes to the safeguarding of genome integrity. Remarkably, our results also suggest that at least some of those mechanisms are compromised in tumor cells.

Discussion I: Implication of APC/C^{Cdh1} in the loss of replication recovery competence upon severe replication stress

Previous results from our group indicated that there was a correlation between the loss of replication recovery competence and the degradation of Cyclin A2 and Cyclin B1 in response to prolonged HU treatment. Thus, we decided to analyze the mechanisms involved in the degradation of these cyclins, in order to define new pathways that might contribute to the loss of replication recovery competence.

1.1. Severe replication stress-induced APC/C^{Cdh1} activation in S phase in non-transformed human cells

The APC/C ubiquitin ligase is one of the regulators of Cyclin A2 and Cyclin B1 during unperturbed cell cycle[29,30]. Additionally, APC/C^{Cdh1} has been reported to become prematurely activated in G2 in response to DNA damage[150–152,443]. Accordingly, our results show that the addition of APC/C inhibitor proTAME or the depletion of Cdh1 induces a recovery on Cyclin A2 and Cyclin B1 proteins levels, indicating that they are degraded by APC/C^{Cdh1} in response to severe replication stress in non-transformed human cells. However, in contrast to previous reports[150–152,443], our results show that this ubiquitin ligase is activated in S phase in response to prolonged HU treatment or after the addition of DNA damage-inducing agents to S-phase synchronized cells, suggesting that this is a general feature in response to several stress agents. In this sense, since previous reports came from works mainly done in tumor cells[150–152,443], which have a less robust DNA replication stress response[324,499,500], we propose that premature APC/C^{Cdh1} activation in S phase is an additional response to severe replication stress of non-transformed human cells that tumor cells may lack. Consistent with this, we have seen that HCT116 colorectal cancer cells do not activate APC/C^{Cdh1} in S phase after prolonged HU treatment, while hTERT-RPE, BJ-5ta and MCF10A non-transformed cells do activate it under this condition. Nevertheless, we cannot rule out the possibility that different agents might induce different responses that depend on the nature of the stress or the cell cycle phase that is affected.

Interestingly, the activation of APC/C^{Cdh1} in S phase is observed once replication forks have been processed into DSBs, suggesting that fork collapse is required for the activation of this ubiquitin ligase in S phase. In this regard, fork stalling, even if it is sustained, might not be sufficient to activate APC/C^{Cdh1} unless replication forks are processed into DSBs. Consistently, thymidine synchronization, which implies a replication blockade of 20 hours, does not activate APC/C^{Cdh1}. In fact, thymidine synchronization results only on a slight advancement on APC/C^{Cdh1} activation timing when compared to serum-starved cells, which is probably due to the fact that more cells are accumulated in S phase by thymidine synchronization than by serum starvation, and thus, the activation of APC/C^{Cdh1} in S phase may be more noticeable in the first case.

The activation of APC/C^{Cdh1} in G2 in response to DNA damage has been described to occur either by ATM-dependent or -independent mechanisms[150,522]. Our results suggest that the activation of APC/C^{Cdh1} in S phase in response to severe replication stress occurs independently of ATM activity. Moreover, in response to prolonged HU treatment, APC/C^{Cdh1} is activated in S phase even after the simultaneous pharmacological inhibition of ATM and ATR, indicating that there is no compensatory effect between these kinases that have an overlapping set of substrates[318,319].

Remarkably, in agreement with previous reports showing that Chk1, the main downstream kinase of ATR[316,327], inhibits APC/C^{Cdh1} in response to RS[381], the inhibition of ATR alone results in advanced APC/C^{Cdh1} activation in S phase in response to prolonged HU treatment. Moreover, the activation of APC/C^{Cdh1} in S phase correlates with a decrease in Chk1 phosphorylation under these conditions. Thus, it is conceivable that a decrease in Chk1 activity collaborates in the initial trigger of APC/C^{Cdh1} activation in S phase. Nevertheless, Chk1 could also positively regulate the activation of APC/C^{Cdh1} by preventing Cdh1 phosphorylation through the inhibition of CDKs[41,42]. In addition, ATR inhibition-promoted advanced APC/C^{Cdh1} activation could also be due to an increase in DSBs. In this sense, ATR/Chk1 are involved in preventing the accumulation of DSBs by inhibit origin firing and Mus81 nuclease-mediated processing among others[391,393]. Thus, since our results suggest that APC/C^{Cdh1} is activated in response to DSBs, we propose that ATR inhibition-promoted accumulation of DSBs is the reason for advanced APC/C^{Cdh1} activation under these conditions.

Additionally, the activation of APC/C^{Cdh1} in response to DNA damage has been reported to depend on p53 and p21[151,152]. Consistent with this, our results show that p53/p21 depletion prevents the activation of APC/C^{Cdh1} in S phase in response to prolonged DNA replication inhibition. Nevertheless, in this case, p21 is not induced during the HU treatment, despite the stabilization of p53. In this sense, as p53 depletion results in reduced p21 levels; and, since p21 is actively degraded during the HU treatment, as observed by the increase in p21 levels after the addition of MG132 proteasome inhibitor, we suggest that the induction of p53 is required to maintain the basal levels of p21 under these conditions. However, p21 is not the sole target of p53[433], and thus, the observed p53 induction upon HU treatment, even at low concentration, might also be important for p21-independent functions.

Interestingly, p21-promoted Emi1 down-regulation has been reported to be the mechanism for p53-/p21-mediated APC/C^{Cdh1} activation in response to DNA damage[151,152]. Consistently, the activation of APC/C^{Cdh1} in S phase in response to prolonged HU treatment correlates with a decrease in Emi1 levels. Moreover, Emi1 depletion in S phase in HCT116 cells, allows the activation of APC/C^{Cdh1} under these conditions. These results suggest that a decrease in Emi1 levels is the responsible for the activation of APC/C^{Cdh1} in S phase in response to severe replication stress.

Notably, p53/p21 depletion results on increased levels of hyperphosphorylated pRb and Emi1, which could explain why APC/C^{Cdh1} is not activated in those cells. However, as previously mentioned, p21 is not induced during the HU treatment and in fact, Emi1 is increased, and more pRb is hyperphosphorylated, already in untreated p53-/p21-

depleted hTERT-RPE cells. Therefore, we consider that p53 and p21 are unlikely the triggers of APC/C^{Cdh1} activation in response to prolonged HU treatment.

Remarkably, the decrease in Emi1 levels in the presence of HU is due to degradation, since the addition of MG132 proteasome inhibitor recovers its levels. Additionally, this degradation of Emi1 occurs independently of p53/p21 depletion. Thus, we propose that Emi1 degradation, rather than p53 or p21, is the trigger of APC/C^{Cdh1} activation in S phase in response to severe replication stress. Nevertheless, p53- or p21-deficient cells may become more resistant to the activation of this ubiquitin ligase due to the presence of higher Emi1 levels.

1.2. Contribution of APC/C^{Cdh1} to the loss of replication recovery competence

The activation of APC/C^{Cdh1} in G2 has been shown to promote a sustained G2 arrest and even senescence upon DNA damage[150–152]. Accordingly, previous results from our group indicated that there was a correlation between the mechanism behind the degradation of Cyclin A2 and Cyclin B1 and the loss of replication recovery competence. In this sense, as previously argued, our results pointed to the activation of APC/C^{Cdh1} in S phase as the mechanism for the degradation of Cyclin A2 and Cyclin B1 after severe replication stress. Interestingly, the fact that APC/C^{Cdh1} remains active after release from HU treatment, when the loss of replication recovery competence is analyzed, strongly suggests that APC/C^{Cdh1} actively contributes to this permanent S-phase arrest. Consistent with this, Cdh1 depletion restores the ability to resume replication after prolonged HU treatment. Moreover, p53/p21 depletion, which compromises the activation of APC/C^{Cdh1} in S phase, also recovers the competence to resume replication upon prolonged DNA replication inhibition. Furthermore, HCT116 cells, which have an impaired activation of APC/C^{Cdh1} in S phase in response to prolonged HU treatment, are able to resume replication and proliferate after this stress. However, the correlation between the lack of APC/C^{Cdh1} activation in S phase and the ability to recover upon prolonged HU treatment in HCT116 could be due to additional mutations that these cancer cells may have acquired to proliferate. Nevertheless, Emi1 depletion in S phase in HCT116 cells compromises the competence to resume replication, at least in a fraction of cells. Remarkably, this indicates that even though HCT116 cells may have acquired additional mutations that favor their proliferation, the sole APC/C^{Cdh1} activation in S phase is sufficient to promote the loss of replication recovery competence in those cells. Collectively, these results strongly support the idea that premature APC/C^{Cdh1} activation in S phase promotes the loss of replication recovery competence after severe replication stress.

However, approximately half of the cells that are commonly arrested in S phase upon prolonged HU treatment remain arrested despite Cdh1 depletion. This indicates that additional APC/C^{Cdh1}-independent mechanisms may also contribute to severe replication stress-promoted S-phase arrest. Notably, those additional mechanisms might not depend on ATM and ATR activity, since the inhibition of those kinases does not prevent prolonged DNA replication inhibition-induced S-phase arrest. Remarkably, the fact that ATM and ATR inhibition does not abrogate prolonged HU treatment-

induced S-phase arrest reinforces once again the idea that the activation of APC/C^{Cdh1} contributes to the loss of replication recovery competence.

According to our previous observations, the activation of APC/C^{Cdh1} in S phase will induce the loss of replication recovery competence once replication forks have been processed into DSBs. Remarkably, replication resumption from or in the presence of broken replication forks has been reported to occur either by origin firing or BIR-mediated mechanisms[450,452–455], which can both compromise genome integrity[290,451,456–459]. Interestingly, our results suggest that these mechanisms are inhibited in hTERT-RPE cells upon severe replication stress.

In this sense, our results show that Cdh1 depletion increases the number of new origin firing events upon prolonged HU treatment. Notably, the used methodology do not allow us to discern if fork restart comes from a real restart or from the firing of nearby origins[159]. This is due to the fact that the maximum length of a replicon is around 120Kb[159], while replication fork speed is around 2-3kb min^{-1} in eukaryotic cells[155]. Thus, since we incubate the cells during 1 hour with the second thymidine analog after the HU treatment, until 180Kb could be labeled during this time. Consequently, origins that are located in the same replicon or even in the adjacent one could be observed as fork restarts under these conditions (Figure 1).

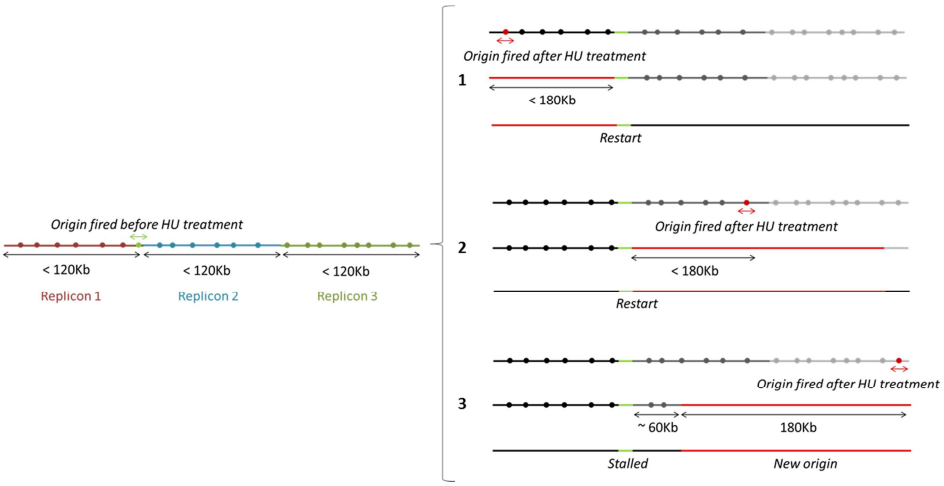

Figure 1. Visualization of origin firing by DNA fiber analysis.
A replication cluster containing three different replicons with several origins on each is represented (left panel). Each replicon has a maximum length of 120Kb. A certain origin (in green) is activated before HU-induced fork stalling. After the treatment, cells are incubated with the second thymidine analog during 1h. Since the eukaryotic replication fork speed is around 2-3Kb min^{-1}, until 180Kb can be labeled during this time. If the origin that is fired after HU treatment (in red) is located in the same or adjacent replicon, it could be observed as a fork restart event (1 and 2, right panel). By contrast, if the origin that is activated after HU treatment is located in a distant replicon, it could be observed as a new origin event (3, right panel).

Interestingly, this suggests that the observed Cdh1 depletion-induced new origin firing events may mainly correspond to the activation of origins located in different replicons, which are far enough so that we can distinguish them. In this sense, ATR/Chk1 has been

implicated in preventing the firing of late origins[118], which are located in different replicons from the early ones[159]. Thus, the observed decrease in Chk1 activity after prolonged HU treatment, when Cdh1 depletion-induced origin firing events are observed, agrees on the fact that the origins that are activated under these conditions may correspond to those located in different replicons. Origin firing requires the sequential action of DDK and CDK2 kinases, which phosphorylate several components to allow the formation of a stable CMG helicase complex[117,119–124]. Thus, the observed APC/C^{Cdh1}-induced Cyclin A2 degradation in S phase in response to severe replication stress, might be sufficient to prevent origin firing under these conditions. Accordingly, the degradation of Cyclin A2 is one of the mechanisms by which APC/C^{Cdh1} prevents origin firing during G1[71–73]. However, it has been reported that Emi1 depletion-induced APC/C^{Cdh1} activation, promotes rereplication in cells in which Cyclin A2 has been degraded[154]. Thus, the degradation of additional substrates must be required for APC/C^{Cdh1}-induced origin firing inhibition in S phase. Consistently, our results show that not only cyclins but also other APC/C^{Cdh1} substrates are degraded after prolonged HU treatment. Notably, Dbf4, the regulatory subunit of DDK, has been described to be an APC/C^{Cdh1} substrate[381]. Therefore, we propose that the degradation of Cyclin A2 may contribute to APC/C^{Cdh1}-induced origin firing inhibition upon prolonged HU treatment, although the degradation of other substrates such as Dbf4 might also be required.

Additionally, our results suggest that BIR-mediated restart is also impaired in hTERT-RPE cells after severe replication stress. This is underlined by the fact that a huge increase in the percentage of stalled forks is observed by DNA fiber in hTERT-RPE cells after a sustained HU treatment that induces DSBs. Moreover, we have seen that Rad51, a protein required to mediate strand invasion during BIR[523,524], is released from chromatin and nascent DNA under these conditions. Notably, Rad51 remains dissociated from chromatin even after HU removal.

Several other evidences also prove that Rad51 is not associated with chromatin after prolonged HU treatment. First, consistent with its already known role in protecting DNA from nucleases degradation[396], nascent DNA is degraded after sustained DNA replication inhibition. Furthermore, proteins involved in the recruitment of Rad51 to damage sites, such as FANCD2 and BRCA2[520], are also released from chromatin under these conditions. Notably, ATR activity, which is important for FANCD2 recruitment[403], also decreases after prolonged HU treatment. Collectively, these results strongly support the idea that Rad51 is released from replication forks upon severe replication stress.

Interestingly, resection marks such as the phosphorylation of CtIP and the hyperphosphorylation of RPA32[518] are also observed after a 14-hour HU treatment. In fact, the high amount of ssDNA generated upon this treatment suggests that an excessive resection is occurring, which has been linked with the inability to recruit Rad51[525]. Nonetheless, the ssDNA generated after a 14-hour HU treatment might also correspond to a normal resection generated in response to severe replication stress[526]. In this sense, extensive resection has been described to be prevented by APC/C^{Cdh1}-mediated degradation of CtIP[525]. Thus, the activation of APC/C^{Cdh1} in S phase in hTERT-RPE cells after prolonged HU treatment should prevent this extensive resection. In any

case, the fact that replication fork restart is compromised after prolonged HU treatment, and that Rad51 is not associated with nascent DNA under these conditions, strongly supports the idea that BIR is impaired in hTERT-RPE cells.

Nevertheless, whether the activation of APC/C^{Cdh1} in S phase upon severe replication stress contributes to the abrogation of BIR-mediated restart is not clear. On the one hand, our results show that the proteins involved in the recruitment of Rad51, and Rad51 itself, are released from chromatin after prolonged HU treatment in a proteasome-dependent manner, since the addition of MG132 recovers their binding to chromatin. In this sense, APC/C^{Cdh1}-mediated those proteins degradation or of other proteins involved in their recruitment could be the responsible for the observed dissociation under these conditions. In fact, in agreement with published data[525], results from our laboratory indicate that CtIP, which has been described to be important for the stabilization of FANCD2 on damage sites[519], is degraded in response to prolonged HU treatment in an APC/C^{Cdh1}-dependent manner (unpublished data). These data agree with the idea of APC/C^{Cdh1} being implicated in preventing BIR-mediated restart after severe replication stress. However, Cdh1 depletion does not recover the loading of Rad51 to chromatin and accordingly, the degradation of nascent DNA is neither prevented under these conditions. Moreover, the percentage of stalled forks does not decrease under these conditions. Thus, APC/C^{Cdh1} does not seem to be implicated in hindering BIR-mediated restart after severe replication stress. Nonetheless, since Cdh1 depletion has been reported to increase CtIP-mediated resection in response to DNA damage, which reduces the formation of Rad51 foci[525], and as our results show that nascent DNA is degraded despite Cdh1 depletion, we cannot exclude the possibility of Rad51 recruitment being compromised due to the absence of appropriate binding site for it in this case. Nevertheless, as previously mentioned, in contrast to Cdh1 depletion, the addition of MG132 proteasome inhibitor is able to recover BRCA2, FANCD2 and Rad51 association with chromatin, which suggests that another ubiquitin ligase is the responsible for those proteins dissociation from chromatin in response to severe replication stress. Therefore, although we cannot rule out a role for APC/C^{Cdh1} in controlling DNA processing and Rad51 dissociation at stalled replication forks, we propose that the main function of APC/C^{Cdh1} to promote the loss of replication recovery competence after severe replication stress is to prevent origin firing under these conditions.

Remarkably, the fact that both origin firing and BIR-mediated restart seem to be inhibited in hTERT-RPE cells upon severe replication stress raises the question whether an individual cell of a certain population lacks both mechanisms or if by contrast, different cells from the same population present only one of those mechanisms inhibited. In this sense, our results show that Cdh1 depletion restores the ability to recover of a fraction of cells, while the other ones remain arrested, after a prolonged HU treatment. An explanation for this would be that those cells that are able to recover under these conditions, present a correct BIR-mediated restart. However, BIR-mediated restart is supposed to repair the DSBs[452,453,455], and by contrast, Cdh1-depleted cells present 53BP1 foci after release from HU treatment, and the ones that resume replication are arrested in G2, suggesting that they still contain DNA damage. Additionally, our results suggest that Cdh1 depletion-promoted new origin firing is

potentially sufficient to completely reestablish DNA synthesis after 14-hour HU treatment. This is shown by the similarities in the number of active forks and in the second thymidine analog incorporation rates, between 2-hour HU-treated and 14-hour HU-treated cells after Cdh1 depletion. Thus, this suggests that the reestablishment of only one of the mechanisms involved in replication resumption after severe replication stress is sufficient to resume replication. Therefore, the inability to resume replication may require both mechanisms to be hindered. Of course, it is also conceivable that the loss of one of the mechanisms has a higher impact than the other for the cells. In any case, since DSBs does not seem to be repaired in those cells that resume replication after Cdh1 depletion, we propose that each individual cell of a population presents both origin firing and BIR-mediated restart hindered, to prevent replication resumption upon severe replication stress. Additionally, we suggest that the inability to recover of Cdh1-depleted cells may rely on the amount of collapsed forks that those cells contain. For instance, a cell with numerous collapsed forks, without licensed origins between converging forks, may rely more on BIR-mediated restart to complete replication after severe replication stress, even after Cdh1 depletion. Moreover, increasing the number of collapsed forks raises the probability of presenting origin-free regions between collapsed converging forks.

Interestingly, our results show that prolonged HU treatment-induced loss of replication recovery competence results in a permanent withdrawal from the cell cycle, in which cells become senescent, as observed by the SA-β-Gal activity and the other senescence markers that they present. Notably, previous reports have described that the activation of APC/C^{Cdh1} in G2 is important to promote senescence after DNA damage[151,522]. Additionally, Emi1 depletion-induced increased APC/C^{Cdh1} activity has also been reported to promote senescence[508]. By contrast, Cdh1 depletion does not reduce the number of senescent cells upon prolonged replication inhibition in hTERT-RPE cells. This suggests that APC/C^{Cdh1} is not the trigger of cellular senescence after sustained replication inhibition. However, Cdh1-depleted cells are arrested in G2 under these conditions, and thus, senescence might be mediated by a G2 checkpoint mechanism in this case. Therefore, we have been unable to analyze the real contribution of premature APC/C^{Cdh1} activation in S phase to cellular senescence. Remarkably, recent reports have shown that the nuclear translocation and retention of Cyclin B1, which precedes the activation of APC/C^{Cdh1}, marks the restriction point for a permanent withdrawal from the cell cycle[475,476]. Notably, this Cyclin B1 retention is mediated by p53 and p21[475,476], and a transient p53 activation has been reported to be sufficient to induce senescence[475]. Consistent with this, in contrast to Cdh1, p53 or p21 depletion strongly reduces the number of senescent cells after prolonged HU treatment, suggesting that p53/p21, rather than APC/C^{Cdh1}, induces senescence upon severe replication stress. Moreover, the fact that APC/C^{Cdh1} remains active even after HU removal, suggests that the activation of APC/C^{Cdh1} in S phase is not sufficient to mark cell to withdrawal from the cell cycle, unless in contrast to p53, a prolonged APC/C^{Cdh1} signaling is required in this case. In this sense, although APC/C^{Cdh1} activation in S phase might not be sufficient to induce senescence, it may be important to maintain the cells arrested in S phase until the mechanism or signal that induces senescence is activated. Therefore, we propose that severe replication stress-induced APC/C^{Cdh1} activation in S

phase reinforces a permanent arrest that can lead to cellular senescence. Moreover, since it has been postulated that unknown senescence pathways might exist[47] and since several lines of evidence indicate that the activation of APC/C^{Cdh1} itself is sufficient to induce senescence[522,527,528], we do not exclude even a direct function of APC/C^{Cdh1} in promoting cellular senescence that we have been unable to observe.

Discussion II: Differences at replication forks of hTERT-RPE cells treated during 2 or 14 hours with HU that determine the loss of replication recovery competence

One of the main goals of our group is to identify new mechanisms involved in the DNA replication stress response of non-transformed human cells. In this sense, since we knew that non-transformed human cells were able to recover after a 2-hour but not 14-hour HU treatment, we decided to compare the proteins associated with replication forks in those conditions, with the aim of defining the changes that promote the loss of replication recovery competence. Additionally, by comparing the proteins present at replication forks of 2-hour but not 14-hour HU-treated cells, we would be able to identify new proteins involved in fork stability and restart.

2.1. iPOND+MS to study the HU-induced changes at replication fork level

iPOND[509] coupled with MS has been described as a powerful tool to characterize the human replisome and replisome-associated proteins[510]. Moreover, a more efficient modified version of iPOND has been developed[511]. Thus, in order to compare the proteins associated with replication forks after short and long HU treatments, we decided to perform an experiment combining the modified version of iPOND[511] with a label-free MS method that in contrast to label-based MS methods allows the comparison of multiple statements. Additionally, we decided to use hTERT-immortalized RPE cells, which are non-transformed human diploid cells that are easily maintained in culture. Moreover, since only the EdU-labeled fraction is immunoprecipitated during iPOND, we decided to synchronize the cells in S phase to increase the immunoprecipitation efficiency, and thus, to obtain more sample from the same amount of initial cells to facilitate the detection of low-abundance proteins.

Regarding the labeling scheme, although according to previous works the most common is to label the cells during 10 minutes with EdU[390,510,511], we decided to perform a labeling of 15 minutes, which has already been validated[514], to raise the number of labeled forks without excessively increasing the length of labeled tracks. Additionally, in agreement with previous reports[392,515], we decided to use a chase time of 2 hours. In addition, since there is some EdU incorporation during the first 15 minutes of HU treatment, we decided to include a condition in which cells were labeled with EdU and then with EdU+HU during 15 minutes. This condition was important to properly analyze the HU-treated samples, since this slight EdU incorporation can increase the number of labeled forks, as well as the length of labeled tracks, and thus, the proteins present on nascent DNA in this case may be different from the ones present on the pulse. Of course, the fact that HU is added to these samples might also change the protein content of nascent DNA under this condition. Therefore, we decided to use both untreated (Pulse) and 15' EdU/HU condition for data analysis.

Additionally, to increase the robustness of the obtained data, based on other published works[392,515], we decided to use three biological replicates for the iPOND+MS experiment. Moreover, the effect of the HU treatment in each biological replicate was

tested before MS analysis, by harvesting samples in parallel for MS and flow cytometry, in order to determine the percentage of cells that were arrested in S phase under these conditions in each case. Likewise, sonication and biotin incorporation were also verified in all cases before MS analysis.

The strength of our iPOND+MS experiment to identify nascent DNA-bound proteins is validated by the fact that the proteins most enriched in the pulse condition compared to the chase are mainly already known replisome components. In this sense, the comparison of the proteins present on nascent DNA after a 2-hour HU treatment but not after a 14-hour HU treatment has allowed us to identify new potential candidates that might be important to maintain the stability of the fork and to promote fork restart upon severe replication stress. However, due to time limitation, the validation and further experiments related to this are going to be followed for someone else.

Nevertheless, taking advantage of the obtained proteomic data, we wanted to analyze the HU-induced changes at replication fork level that might be promoting the loss of replication recovery competence. To this end, the obtained data were processed to facilitate and simplify the analysis. Based on previous reports[390,514], a fold exchange of 2 was considered as the minimum difference to classify the proteins on a certain group. Consistent with this, 37 proteins were classified as nascent DNA-bound proteins on the pulse compare to the chase after data processing. From those, the 81% were already considered as nascent DNA-bound proteins in other similar studies[390,392,510,511,514,515], validating the reliability of the used approach. In this sense, none of the previous studies had been performed in human non-transformed cell lines, and thus, the remaining 19% of the proteins considered as nascent DNA-bound proteins in our analysis might be specific of this cell lines. Nonetheless, at least some of those proteins might also correspond to false positives, since they have been identified only in one of the MS rounds and none else have identified them as nascent DNA-bound proteins. Remarkably, the 57% of the proteins classified as nascent DNA-bound proteins on the pulse in our analysis have already known replication-related functions. Likewise, almost all the proteins considered to be enriched at mature chromatin, present chromatin maturation-related functions, proving altogether the veracity of the used approach. Furthermore, the results obtained by iPOND+WB experiments correlated very well with the classification made by analyzing the data obtained from the iPOND+MS experiment, highlighting once again the robustness of our proteomic data and the accuracy of the used approach for data processing.

Additionally, regarding the sensitivity, the used modified version of iPOND is supposed to be able to immunoprecipitated the 4% of the whole PCNA present at replication forks[511]. In this sense, our proteomic analysis has identified, in the pulse condition, the 10% of the whole proteins found in GO database[516] that present replication-related functions. Hence, we could say that the sensitivity of the used approach has been high in the context of iPOND. Nevertheless, when comparing with other published works[390,392,510,511,514,515], the sensitivity of our iPOND+MS experiment has been a bit low, since we have identified less nascent DNA-bound proteins than in other reports. In this sense, the sensitivity could have been improved by increasing the amount of initial sample to raise the ability to detect low-abundance proteins, or also by including more

replicates as in other studies[510,511,514]. Increasing the amount of replicates would have enhanced the probability of a certain protein to be identified by MS. Consistent with this, due to technical problems we had to perform the MS analysis in two rounds, and unfortunately, some proteins have only been identified in one of them, showing that not all the proteins present on a sample are identified by MS in all cases. In addition, an increase in the number of replicates would have reduced the experimental noise and would have allowed being less stringent when deciding the minimum fold exchange to include a protein on a certain group. Nonetheless, this would have raised the price of the study. Thus, since our main objective was to analyze the general HU-induced changes at replication forks, and as previously argued, three biological replicates are sufficient to obtain robust proteomic data for this purpose, we decided to compromise the sensitivity. Notably, the use of other MS techniques, such as the label-based ones, may also increase the sensitivity of the experiment. However, we wanted to compare several different conditions between them, and hence, label-free methods are more appropriate for this type of studies.

2.2. Changes at replication forks of hTERT-RPE cells that promote the loss of replication recovery competence

As previously mentioned, iPOND+MS is a powerful technique to analyze the HU-induced changes at replication fork level. In this sense, our proteomic analysis has highlighted some interesting issues that, together with other experiments, have allowed us to have a better understanding regarding how non-transformed human cells deal with the DNA replication stress.

2.2.1. Replication fork reversal upon short HU treatment

Our proteomic results, together with the results obtained by iPOND+WB experiments, show that replisome components are dissociated from nascent DNA already after a 2-hour HU treatment. Interestingly, this does not result in the dissociation of those proteins from chromatin at this time, suggesting that replisome components are displaced away rather than dissociated from replication forks after a short HU treatment. Notably, this might be due to replication fork reversal, which does not necessarily imply the dissociation of replisome components[281,298–300].

Several evidences agree on the fact that replication forks of hTERT-RPE cells are regressed into chicken foot structures after a short HU treatment, despite replication forks are not processed into DSBs at this time. In this sense, as previously mentioned, our results show that Rad51, a protein required for fork reversal[312], is recruited to nascent DNA after a short HU treatment. Likewise, RecQ1, a protein involved in the restart from reversed forks[311], is also present on nascent DNA under these conditions. Moreover, as shown by BrdU immunofluorescence under native conditions[302,305], hTERT-RPE cells expose single-strand nascent DNA already after a 2-hour HU treatment. Remarkably, since replication fork do not present DSBs at this time, the presence of reversed forks would be almost the sole explanation for the observed BrdU staining (Figure 2).

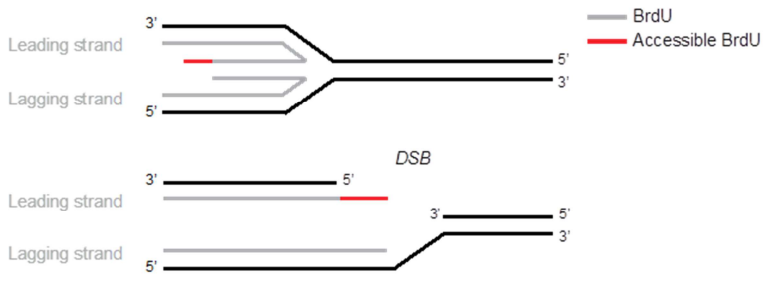

Figure 2. Analysis of single-stranded nascent DNA by BrdU immunofluorescence.
Cells are labeled with BrdU during 10min before analyzing the presence of accessible single-strand nascent DNA fragments. If forks are reversed (upper panel), BrdU antibody can reach the ssDNA present on the 3' end of the leading strand, generated by controlled DNA resection. If forks are processed into DSBs (bottom panel), BrdU antibody can also reach the ssDNA present on nascent DNA after parental strand DNA resection.

Additionally, fork reversal has been reported to promote ATM activation before DSBs are present[302]. Accordingly, our results show that p53 is stabilized and that Chk2 is activated in an ATM-dependent manner in hTERT-RPE cells treated during 2 hours with HU, when DSBs are not still present. Collectively, the above results strongly support the idea that replication forks of hTERT-RPE cells are regressed into chicken foot structures after a short HU treatment.

However, our results showing that RPA, a protein that preferentially binds ssDNA[160,184,185], is not dissociated from chromatin despite being displaced away from nascent DNA after a short HU treatment, make it difficult to figure out how can this protein be associated with chromatin, if replication forks are reversed under these conditions. In this sense, during iPOND, proteins and DNA are crosslinked before immunoprecipitation and thus, the RPA present on parental-unlabeled ssDNA is isolated together with nascent DNA-bound proteins. Thus, since fork reversal entails the annealing of nascent DNA strands together with the reannealing of parental strands[301], the amount of RPA isolated by iPOND should decrease after fork reversal (Figure 3). Accordingly, our results show that the amount of isolated RPA is lower after a 2-hour HU treatment than on the pulse or in 15' EdU/HU condition.

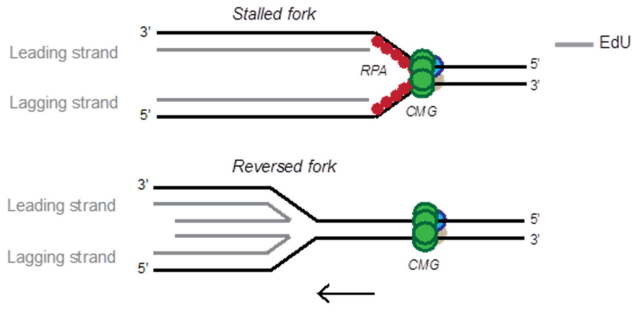

Figure 3. Analysis of replication fork-bound proteins by iPOND.
During iPOND, proteins and DNA are crosslinked before immunoprecipitation. Due to the uncoupling of the replicative polymerases and the helicase, ssDNA, which would be coated by RPA, is accumulated on the

parental strands of stalled replication forks (upper panel). Fragments of around 300Kb are immunoprecipitated by iPOND. Hence, the RPA located at parental ssDNA would be isolated by this technique in this case. By contrast, since fork reversal entails the reannealing of parental strands (bottom panel), the RPA located at this parental strands would be displaced away. Thus, the levels of isolated RPA will decrease in the second case.

In addition, our results also show that Rad51, which can bind the same ssDNA as RPA[464], increases its association with nascent DNA after a short HU treatment. Hence, the substitution of RPA by Rad51 may also explain this decrease in the levels of RPA on nascent DNA. Notably, in contrast to what our results show, this decrease in the levels of RPA isolated by iPOND, should result in a reduced RPA binding to chromatin, unless this displaced RPA is loaded to other chromatin regions under these conditions.

Nonetheless, fork stalling, even if replication forks may not be reversed, cannot explain the absence of RPA on nascent DNA while it is present on total chromatin. Thus, consistent with all the previous evidences, we propose that replication forks of hTERT-RPE cells are reversed after a 2-hour HU treatment.

2.2.2. Mechanisms of replication fork restart after a short HU treatment

During the last years, increasing evidences suggest that replication fork reversal is a very common event in response to several genotoxic stresses[302,303,310–312]. Consistent with this, as previously discussed, our results also pointed to that situation. Interestingly, one of the question that still remains to be elucidated in this regard, is whether fork reversal entails replisome disassembly or not, and if so, how is replication restarted in this case[281,298,299]. In this sense, our results suggest that replisome components are not dissociated from chromatin despite being displaced away from nascent DNA during from reversal. Consistent with this, a recent work have shown that fork reversal can occur without replisome disassembly in T4 bacteriophage system[300].

Remarkably, several recent reports have shown that in contrast to what it was thought, replication can be restarted from reversed forks[300,311,312]. Accordingly, our results show that replication forks of hTERT-RPE cells maintain the ability to restart after a short HU treatment, when replication forks are supposed to be reversed. Interestingly, replication forks of hTERT-RPE cells are able to restart after a 2-hour HU treatment even in the presence of CDK inhibitor roscovitine. Notably, CDK2 activity is required for Cdc45 loading onto MCM2-7 and a stable CMG formation[124,177,178]. In this sense, we have seen that Cdc45 is released from nascent DNA but not chromatin after a short HU treatment. Thus, a previously formed stable CMG complex must be required to restart replication under these conditions, since Cdc45 cannot be loaded in the absence of CDK2 activity. Nonetheless, one should argue that the observed replication restart under these conditions could also be explained by BIR-mediated mechanisms, in which forks progress by D-loop migration. However, BIR is a mechanism to restart replication from broken forks[452–455], and replication forks of hTERT-RPE cells do not present DSBs at this time. Moreover, the replicative CMG helicase is required for BIR and thus, the absence of Cdc45 may also hinder this mechanism[469].

Notably, our results show that fork progression is compromised in the presence of roscovitine, as observed by the shortening on the length of IdU tracks (second labeling)

under this condition. In this sense, since, as previously argued, firing of nearby origins is observed as a fork restart event by the used DNA fiber approach[155,159], this shortening can be explained by the absence of origin firing events due to roscovitine-promoted CDK2 inhibition[124,177,178]. Nevertheless, it has also been postulated that CDK2 activity could be required for replication fork progression[164]. In any case, these observations, together with the decrease in the number of new origin firing events observed after the addition of roscovitine, confirms that roscovitine was properly inhibiting CDK2 in our experimental conditions.

Collectively, the above observations strongly support the idea that previously used replisome components, at least some of them, are recycled to resume replication after a short HU treatment. Remarkably, either direct restart or restart from reversed forks may require the presence of previously formed CMG active helicase complexes on chromatin. Nonetheless, the fact that replisome components are dissociated from nascent DNA indicates that replication forks are being remodeled under this condition. Thus, this result further supports the idea that replication forks of hTERT-RPE cells are restarted from reversed forks after a short HU treatment.

2.2.3. Changes at replication forks that prevent replication fork restart after prolonged HU treatment

Consistent with the observed degradation of nascent DNA after prolonged HU treatment, our proteomic results show that very few protein are found to be enriched at nascent DNA in the 14h HU condition, relative to the chase. Moreover, in agreement with previous works from yeast, showing that replisome components are disassembled from replication forks in the absence of checkpoint kinases[200,291–296], our results show that replisome components are not only displaced away from nascent DNA but also dissociated from chromatin after prolonged HU treatment, when Chk1 activity has already decreased. Notably, replication forks are processed into DSBs under these conditions. Interestingly, as previously discussed, BIR-mediated mechanisms seem to be compromised in hTERT-RPE cells under these conditions. Remarkably, this is also underlined by the observed replisome components dissociation from chromatin, since CMG helicase complex and other replisome components are required for BIR[469].

Strikingly, recent reports have shown that in stark contrast to previous works, most replisome components remain associated with chromatin even after fork collapse[297,390,529]. One of those works shows that in budding yeast, replisome is stably associated with DNA after RS even in the absence of checkpoint kinases[297]. Additionally, using *Xenopus laevis* egg extracts, another work has shown that GINS and Polymerase ξ, but not Cdc45 and MCM2-7, are dissociated from replication forks upon fork collapse[529]. Notably, the authors of this work propose that BIR-mediated mechanisms are required to reload these replisome components, and thus, for replication fork restart. Remarkably, these works have been performed on yeast and *Xenopus* models, while our results have been obtained working with human cells. Hence, the observed differences could be due to the used model in each case. Nonetheless, using human cells, a recent work has shown that replisome components remain associated not only with chromatin, but also with nascent DNA (analyzed by iPOND), after ATR inhibition-

promoted fork collapse[390]. Interestingly, in contrast to our study, this one has been performed with tumor cells. Remarkably, this underlines a possible difference between tumor and non-transformed human cells that may contribute to explain why tumor cells are able to resume replication after severe replication stress, while non-transformed human cells are not. In this sense, consistent with our previous observations suggesting that replisome components are recycled for replication fork restart after a short HU treatment, a release of Cdc45 and other replisome components from chromatin after a 14-hour HU treatment may explain why replication forks of hTERT-RPE cells are unable to restart under these conditions. Moreover, as previously discussed, lack of replisome components' association with chromatin may contribute to hinder BIR-mediated restart in hTERT-RPE cells under these conditions. By contrast, BIR has been described to occur in human U2OS osteosarcoma cells[454]. In this sense, the fact that replisome components are stably associated with chromatin in tumor cells[390] may allow replication to be restarted by BIR in those cells. Furthermore, even if some replisome components such as GINS or Polymerase ξ are dissociated from chromatin after fork collapse in tumor cells, according to the data obtained from *Xenopus laevis* egg extracts[529], BIR-based mechanisms could promote the reloading of the dissociated replisome components in those cells, which will not occur in hTERT-RPE cells under the same conditions. Interestingly, this capability to maintain replisome components stably bound to chromatin[390], contributing to preserve the ability to restart by BIR[469], together with the ability to activate new origins[450], most likely by impaired activation of APC/C^{Cdh1} in S phase, may explain why tumor cells are able to resume replication after severe replication stress while non-transformed human cells are not.

Remarkably, the dissociation of replisome components is not the sole reason that explains the lack of replication fork restart, observed after prolonged HU treatment in hTERT-RPE cells. In this sense, our proteomic results, together with data obtained by iPOND+WB experiments, have shown that proteins described to be important for replication fork restart[206,289,311,394–396,399,519] such as FANCD2, Rad51, SMC1, SMC3 and RecQ1 are present at replication forks of 2-hour HU-treated hTERT-RPE cells, but not at replication forks of 14-hour HU-treated ones. Moreover, our chromatin association analysis shows that FANCD2, Rad51, SMC1, SMC3 and even BRCA2, which is also important for replication fork restart[289,394], are released not only from nascent DNA, but also from chromatin, after prolonged HU treatment. Notably, replication forks have already been processed into DSBs after prolonged HU treatment. Consequently, BIR is the sole option for replication fork restart under these conditions[452–455], which, as previously discussed, is impaired in hTERT-RPE cells. Remarkably, the observed dissociation of the cohesin complex also contributes to explain this lack of BIR, since these proteins are important for sister chromatin cohesion[206,399] and thus, might be required for strand invasion during BIR.

Interestingly, the fact that replication forks of hTERT-RPE cells suffer several different changes that may contribute to explain the lack of fork restart after prolonged HU treatment, raises an interesting question regarding which events occurs before the others. In this sense, lack of BRCA2[394], FANCD2[395] and Rad51[396] will promote Mre11-mediated nascent DNA degradation upon severe replication stress, which in turn, could promote the dissociation of replisome components and other proteins from chromatin

under these conditions. Remarkably, an extensive resection could explain the lack of Rad51 association with chromatin after prolonged HU treatment[525] and consequently, also the observed degradation of nascent DNA under these conditions. Notably, the dissociation of replisome components in turn may also explain this extensive resection, since DNA must be unprotected under these conditions, increasing the risk of nucleases-mediated degradation.

The previous observations suggest that each of the changes observed after prolonged HU treatment could explain the other alterations, showing the difficulty to decipher which is the initial trigger for all of them. In this sense, the total levels of most of the analyzed replisome components remained constant despite their dissociation from chromatin after prolonged HU treatment, indicating that the degradation of replisome components is not the trigger for their dissociation. By contrast, FANCD2 for instance is slightly degraded under these conditions, and in fact, the addition of MG132 proteasome inhibitor recovers the association of BRCA2, FANCD2 and Rad51 with chromatin after a 14-hour HU treatment. Notably, as previously argued, the recovery of those proteins' association with chromatin might prevent the degradation of nascent DNA, which in turn, could avoid the dissociation of replisome components and other proteins. In this regard, the sole degradation of FANCD2 could explain most of the changes induced by prolonged HU treatment at replication fork level. Consistently, it would be interesting to analyze if the addition of MG132 proteasome inhibitor restores the ability to restart upon severe replication stress, to determine if the degradation of this protein is the initial and sole trigger to prevent BIR-based mechanisms under these conditions.

Interestingly, if the degradation of FANCD2 was the sole trigger that prevents fork restart upon severe replication stress, APC/C^{Cdh1} may not be implicated in this process since in contrast to the addition of MG132 Cdh1 depletion does not recover Rad51 levels on chromatin. However, another possibility is that all the observed alterations are due to several different mechanisms that are all activated at the same time. Remarkably, all these alterations are observed ones replication forks have been processed into DSBs, pointing to the acquisition of DNA damage as the trigger. In this sense, as previously discussed, our results suggest that APC/C^{Cdh1} for instance is activated in response to DSBs to prevent origin firing and thus, to avoid replication resumption in the presence of broken forks. Accordingly, we propose that DSBs are also the initial trigger for the different changes observed at replication forks of hTERT-RPE cells, to prevent replication fork restart under this condition. Notably, the fact that both origin firing and replication restart are compromised in non-transformed human cells upon severe replication stress explains why those cells loss the ability to recover under these conditions (Figure 4).

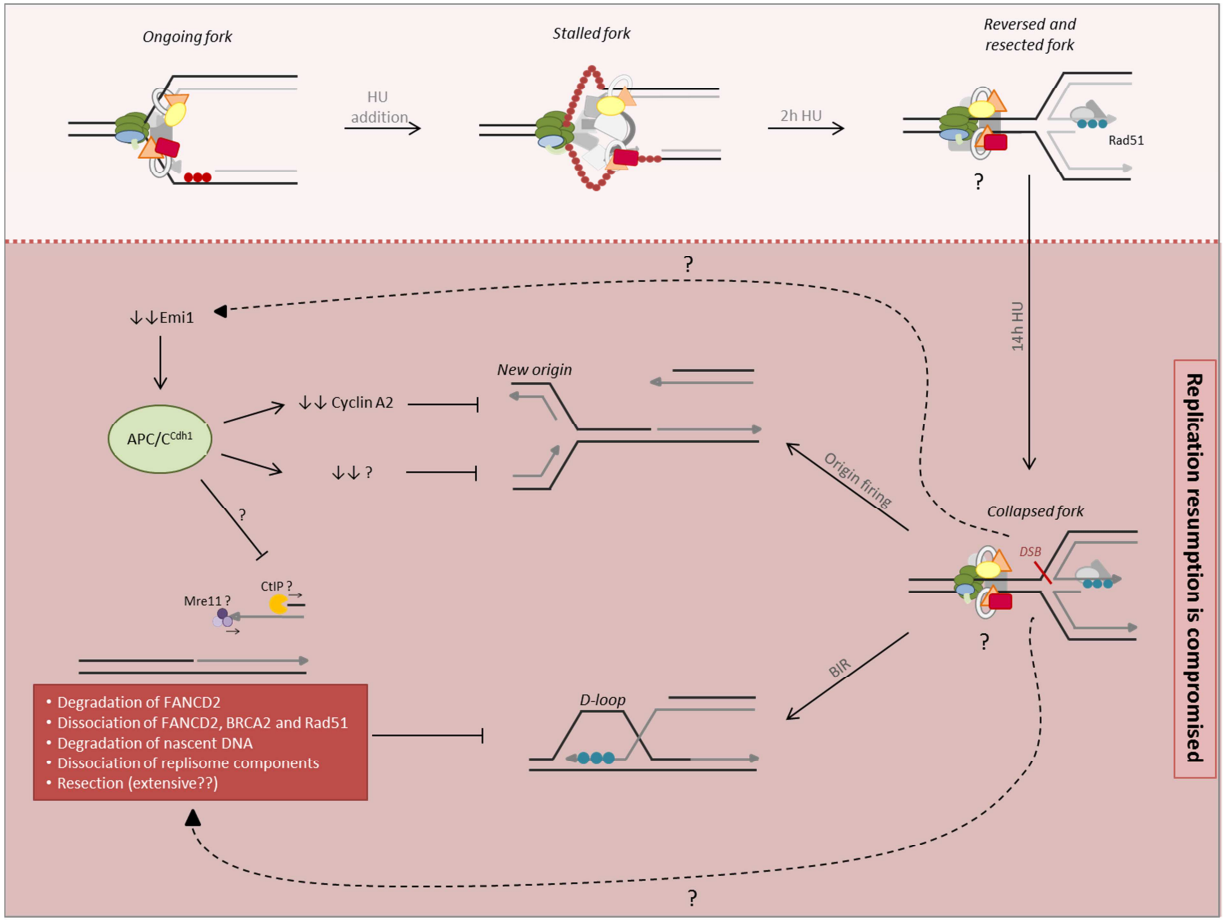

Figure 4. Final model.
In response to fork stalling, replication forks are regressed into chicken foot structures without losing the ability to resume replication once the stress is overcome. At his time, replisome components are displaced away from nascent DNA but they still remain associated with chromatin, perhaps close to the stalled forks. By contrast, if the stalling is persistent, replication forks are prone to collapse and accumulate DSBs. Once this has happened, non-transformed human cells lose the ability to resume replication. This loss of replication recovery competence is accomplished by preventing both new origin firing and BIR-mediated restart. In this sense, the degradation of Emi1 promotes the activation of APC/C^{Cdh1} in S phase. Once activated, this APC/C^{Cdh1} degrades Cyclin A2 and probably also other proteins required for origin firing. Additionally, replication forks suffer several alterations that compromise the ability to resume replication by BIR.

Discussion III: Contribution of the loss of replication recovery competence towards safeguarding genome integrity

The activation of APC/C^{Cdh1} in S phase occurs once replication forks have been processed into DSBs. Moreover, the inhibition of ATR, which may enhance the accumulation of DSBs[391,393], results in advanced activation of APC/C^{Cdh1}. Remarkably, as previously discussed, the activation of this ubiquitin ligase promotes the loss of replication recovery competence in non-transformed human cells under these conditions. Notably, the activation of APC/C^{Cdh1} in S phase correlates with a decrease in Chk1 phosphorylation, suggesting that APC/C^{Cdh1} acts as a long-term response of the DNA replication stress response to prevent replication resumption once DSBs are present. Moreover, our results suggest that replication forks of hTERT-RPE cells suffer numerous changes that also contribute to the loss of replication recovery competence under these conditions. Interestingly, as previously argued, at least some of those mechanisms seem to be abrogated in tumor cells, which are able to resume replication after severe replication stress. Notably, the DSBs generated during S phase can be repaired in G2 phase before cells enter into mitosis, although these DNA repair mechanisms can compromise genome integrity[248,272,450,484]. Thus, we propose that non-transformed human cells avoid replication resumption and are withdrawal from the cell cycle, instead of repairing the breaks and proliferate, to preserve genome integrity.

3.1. Participation of APC/C^{Cdh1}-mediated S-phase arrest in safeguarding genome integrity

As previously explained, Cdh1 depletion restores the ability to resume replication after prolonged HU treatment. Nonetheless, mitotic entry is still compromised under these conditions. Notably, the number of cells containing 53BP1 foci is not reduced after HU removal despite Cdh1 depletion, indicating that DSBs are not repaired although cell are now able to resume replication upon prolonged HU treatment. This suggests that the G2 checkpoint senses those DSBs and acts independently of APC/C^{Cdh1} to prevent mitotic entry in the presence of damaged DNA. Remarkably, p53 or p21 depletion restores not only the ability to resume replication but also to enter into mitosis after severe replication stress, suggesting that as expected[48,49,434], they are also involved in promoting a DNA damage-induced G2 arrest. In this sense, our results show that p21 levels increase after HU removal, supporting the idea that p21 may have an additional function during recovery from severe replication stress. Consistent with this, our results show that in contrast to Cdh1, p53 or p21 depletion strongly reduces the number of senescent cells.

Interestingly, the cells that eventually escape the G2 arrest and arrive to mitosis, present Y-H2AX foci, highlighting the importance of preventing cell cycle resumption after severe replication stress to safeguard genome integrity. In this sense, p21-depleted cells, which are able to resume replication and enter into mitosis after prolonged HU treatment, arrive to G1 with DNA damage, as indicated by the presence of 53BP1 foci containing G1 cells. Moreover, cells presenting micronuclei are also found under these conditions. Notably, since Cdh1-depleted cells are arrested in G2 under

these conditions, it is difficult to analyze the contribution of APC/C^{Cdh1} activation in S phase towards safeguarding genome integrity. In this sense, as previously argued, Cdh1 depletion-induced new origin firing may correspond mainly to the activation of origins located in different replicons. Remarkably, this may alter the replication timing program which can result in epigenetic changes that may contribute to the acquisition of epigenome instability[155–157,159,271,272]. Additionally, our results suggest that DSBs are not repaired after replication resumption in Cdh1-depleted cells. Moreover, the cells that escape the G2 arrest, can arrive to mitosis with DSBs. Thus, we propose that premature APC/C^{Cdh1} activation in S phase is important to prevent genomic instability by adding a barrier prior to the G2 arrest.

Notably, Cdh1 depletion induces DNA damage due to a premature S-phase entry[145–147], which can result in numerical and structural chromosomal aberrations[148]. Therefore, all the experiments in which Cdh1 was depleted were done by synchronizing the cells in S phase (by thymidine addition) before siRNA transfection, to prevent the damage induced by Cdh1 knockdown by itself.

Remarkably, the fact that Cdh1 depletion results in the acquisition of genomic instability[72,73,144], suggests that APC/C^{Cdh1} may act as a tumor suppressor. Consistent with this, APC/C has been shown to be mutated in several tumor cells[153]. Accordingly, data from our laboratory also indicates that tumors cell lines are predominantly deficient in the activation of APC/C^{Cdh1} in S phase in response to prolonged HU treatment[507]. In this sense, our results show that HCT116 cells, which do not activate APC/C^{Cdh1} in S phase in response to severe replication stress, are able to divide in the presence of DNA damage. Interestingly, we have seen that Emi1 depletion-promoted artificial APC/C^{Cdh1} activation in S phase in HCT116 tumor cells decreases the number of cells that are able to divide in the presence of DNA damage, as well as the number of cells presenting micronuclei after prolonged HU treatment. Thus, these results further support the idea that the activation of APC/C^{Cdh1} in S phase prevents the acquisition of genomic instability after severe replication stress.

Notably, Emi1-induced aberrant APC/C^{Cdh1} activation has been shown to promote rereplication[154,508], which results in the acquisition of DNA damage and chromosomal breakages[154,279,508]. Therefore, to prevent rereplication, we decided to deplete Emi1 in S-phase arrested cells, first by thymidine and by HU afterwards. Despite that, the presence of cells presenting a DNA content above 4n, suggest that, in agreement with previous reports[154,508], Emi1-depleted cells that maintain the ability to resume replication after prolonged HU treatment can in fact rereplicate.

Collectively, the above observations strongly support the idea that lack of APC/C^{Cdh1} activation in S phase promotes the acquisition of genomic instability in response to severe replication stress.

3.2. Other mechanisms involved in safeguarding genome integrity

As previously discussed, our results suggest that replication forks of hTERT-RPE cells are regressed into chicken foot structures after a 2-hour HU treatment, when replication forks are not still processed into DSBs. In this sense, during the last years increasing evidences agree on a possible function of fork reversal in the maintenance of genome

integrity[298]. Notably, our results agree with this idea, since replication restart after a short HU treatment that is thought to promote fork reversal does not result in the acquisition of genomic instability in hTERT-RPE cells.

By contrast, several works have also reported that reversed forks are processed by nucleases and/or break repair mechanisms, inducing toxic intermediates[280,292,305–308] and in fact, the DNA replication stress response and other mechanisms have been describe to prevent this remodeling[305,307,309]. In this sense, our results show that replication forks are processed into DSBs after prolonged HU treatment. Moreover, apart from the presence of DSBs, replication forks of hTERT-RPE cells suffer several other modifications under these conditions. Notably, our results suggest that restoring the ability to resume replication under these conditions contributes to the acquisition of genomic instability.

Based on the above evidences, we suggest that fork reversal by itself is not pathological for the cell, until under certain circumstances, replication forks are further processed. In this sense, the inhibition of Chk1 kinase for instance, which according to our results occurs after prolonged HU treatment, will allow Mus81-mediated processing[393] of reversed forks, resulting in the formation of DSBs that can lead to the acquisition of genomic instability.

Additionally, as previously mentioned, the ssDNA present at replication forks must be protected to prevent its nucleases-mediated degradation[394–396]. In this sense, the uncoupling of the replicative polymerases and the helicase for instance can generate long fragments of ssDNA[319,342]. Thus, it is also conceivable that under this or similar circumstances, fork reversal is also involved in reducing the amount of exposed ssDNA by generating four-branched structures. Nonetheless, our results suggest that some ssDNA is already exposed at reversed forks after a short HU treatment. Notably, this ssDNA may correspond to the one present on the 3' end of the leading strand (Figure 2), which is generated by controlled Dna2-/WRN-mediated processing[312] and which according to our results, may correspond to small DNA fragments that are protected by Rad51. Remarkably, the removal of Rad51 will lead to Mre11-mediated extensive ssDNA degradation[396] at reversed forks, resulting in the generation of toxic intermediates. However, once again, this might only occur under certain circumstances and fork reversal will not promote genomic instability until this further processing.

Finally, the fact that the alterations at replication forks of hTERT-RPE cells that compromise fork restart, occur once replication forks have been processed into DSBs, suggests, once again, that this alterations arise to prevent replication resumption from or in the presence of broken replication forks, which can compromise genome integrity[290,451,456–459]. Accordingly, as previously discussed, some of these changes may not occur in tumor cells[390], which maintain the competence to restart[454]. Moreover, as previously argued, these alterations compromise BIR-mediated restart, which has been described to be highly mutagenic[456–459], and in fact, BIR-based mechanisms can explain the complexity of the chromosomal changes that occur on cancer cells[252,253,485–487]. Therefore, we propose that, as in the case of APC/C^{Cdh1}-mediated origin firing inhibition, the impairment of BIR-mediated restart upon severe replication stress is a

mechanism of non-transformed human cells that contributes to the safeguarding of genome integrity.

CONCLUSIONS

Based on the initially defined objectives and the exposed results, the conclusions of this thesis are:

I. Conclusions from the study of the mechanisms involved in the loss of replication recovery competence in non-transformed human cells.

1.1) The loss of replication recovery competence upon prolonged HU treatment correlates with the appearance of senescence markers in hTERT-RPE cells.

1.2) APC/C^{Cdh1} is prematurely activated in S phase in non-transformed human cells, in response to a severe replication stress that induces DSBs.

1.3) The activation of APC/C^{Cdh1} in S phase correlates with a decrease in Emi1 levels, is not prevented by the inhibition of ATM/ATR, but is abrogated in p53- or p21-depleted cells.

1.4) The activation of APC/C^{Cdh1} in S phase contributes to the loss of replication recovery competence.

1.5) New origin firing inhibition is the main function of APC/C^{Cdh1} in S phase to promote the loss of replication recovery competence.

1.6) Fork restart is impaired in hTERT-RPE cells after a sustained HU treatment that induces DSBs.

II. Conclusions from the analysis of the differences, at replication fork level, between short and long HU treatments that determine the loss of replication recovery competence in hTERT-RPE cells.

2.1) iPOND+MS is a powerful tool to analyze the HU-induced changes at replication fork level.

2.2) Replication forks of hTERT-RPE cells are remodeled after a 2-hour HU treatment that results in the displacement of replisome components without their dissociation from chromatin.

2.3) Replication forks of hTERT-RPE cells maintain the competence to restart, even in the absence of CDK activity, after a 2-hour HU treatment that promotes the displacement of the replisome away from nascent DNA.

2.4) Replisome components are released from chromatin after a 14-hour HU treatment that compromises the competence to recover of hTERT-RPE cells.

2.5) The dissociation, from nascent DNA and chromatin, of the proteins involved in fork protection and restart after a 14-hour HU treatment that promotes DSBs, correlates with the degradation of nascent DNA.

III. Conclusions from the analysis of the contribution of severe replication stress-induced S-phase arrest towards safeguarding genome integrity.

3.1) Replication resumption is abrogated in non-transformed human cells once replication forks have been processed into DSBs.

3.2) Lack of APC/C^{Cdh1} activation-promoted S-phase arrest, increases genome instability after prolonged replication inhibition.

3.3) Replication resumption after a short HU treatment that results in fork remodeling, does not compromise genome integrity unless replication forks are further processed.

MATERIALS AND METHODS

1. Cell culture and treatments

1.1. Cell lines and culture conditions

Cell line	Medium	Origin	Immortalization method
hTERT-RPE, human retinal pigment epithelial cells	DMEM: F12 (1:1), 6% FBS (fetal-bovine serum)	ATCC	hTERT
BJ-5ta, human foreskin fibroblasts	DMEM:M199 (4:1), 10% FBS	ECACC	hTERT
MCF10A, human mammary epithelial cells	DMEM: F12 (1:1), 5% HS (horse serum)	ATCC	-
HCT116, human colorectal cancer cells	DMEM: F12 (1:1), 6% FBS	Dr. Capellà, ICO	-
**All culture media were supplemented with: essential amino acids (1%), L-glutamine (2mM), pyruvic acid (1mM) and antibiotics (penicillin/streptomycin; 50units/mL and 50µg/mL respectively)* **MCF10A cells were additionally supplemented with EGF (epidermal growth factor) (20ng/mL), hydrocortisone (0.5µg/mL) and insulin (10µg/mL)*			

1.2. Synchronization methods

Cell synchronization is used to obtain a population enriched in a certain cell cycle phase. There are several protocols that can be used to synchronize the cells. Two different methods have been used in this thesis:

- *Synchronization by serum starvation*

  Serum starvation promotes a reversible quiescent state at G0/G1 as a result of the removal of growth factors, which can be easily abrogated by the addition of serum to the media. Every cell line presents a different cell division rate, and thus, the method used to accumulate those cells in a certain cell cycle phase is different in each case.

  - *Synchronization of hTERT-RPE cells by serum starvation:* Cells were cultured very confluent for 48 hours to inhibit cell proliferation by contact inhibition. After that, cells were diluted 1:4, and cultured in serum-free medium for 36-48 hours. Cells were finally forced to re-enter the cell cycle by the addition of serum, to obtain an S-phase enriched population after 16 hours. Around the 40-50% of the cells are accumulated in S phase by this method.

- *Single thymidine synchronization*

  The addition of thymidine to the media induces a reversible S-phase arrest due to the presence of excessive nucleosides, which can be easily reverted by removing the thymidine from the media, to allow the cell to re-enter into S phase. This synchronization method is more efficient than the previous one, resulting in the accumulation of the 80% of the population in S phase. However, it should be taken

into account that this drug may promote replication stress, as it promotes fork stalling, and thus, in some cases other methods might be preferentially used.

This synchronization method can be used to synchronize any cell line in S phase in the same way. Therefore, if not specified otherwise, cells were always synchronized by this method. To this end, cells were incubated with thymidine for 20-24 hours, and then released into fresh medium for 2 hours more. In the case of siRNA-transfected cells, if not specified otherwise, siRNA transfection was performed 12 hours before the addition of thymidine.

1.3. Drugs

Name	Reference	Working concentration	Function
Hydroxyurea	H8627-Sigma	10mM, if not specified otherwise	Ribonucleotide reductase inhibitor
Etoposide	E1383-Sigma	50µM, if not specified otherwise	DNA topoisomerase II inhibitor
Camptothecin	C9911-Sigma	0.5µM	DNA topoisomerase I inhibitor
Thymidine	T1895-Sigma	1.5mM, hTERT-RPE 2.5mM, other cell lines, if not specified otherwise	Deoxynucleoside
Nocodazole	M-1404-Sigma	250ng/mL, tumor cell lines 500ng/mL, non-transformed cell lines	Inhibitor of microtubule polymerization
KU-55933	S1092-Selleckhem	20µM	ATM kinase inhibitor
VE 821	1893-Axon Medchem	10µM	ATR kinase inhibitor
MG132	S2619-SelleckBio	20µM	Proteasome inhibitor
proTAME	I-440-BostonBiochem	50µM	APC/C ubiquitin ligase inhibitor
BrdU	B5002-Sigma	10µM, asynchronously growing cells 20µM, synchronized cells	Thymidine analog
CldU	C6891-Sigma	25µM, if not specified otherwise	Thymidine analog
IdU	I7125-Sigma	250µM	Thymidine analog
EdU	A10044-Invitrogen	50µM	Thymidine analog
Roscovitine	R7772-Sigma	25µM	CDK inhibitor

1.4. siRNA transfection

Transient siRNA transfections were performed using HiPerfect Transfection Reagent (Qiagen) or Lipofectamine® RNAiMAX (Invitrogen), according to manufactures

guidelines. HiPerfect-mediated transfections were performed using cells in suspension. The number of cells used in each case was calculated according to manufactures guidelines. siRNAs were mixed with the transfection reagent on a specific culture medium (Opti-MEM; Gibco) in both cases. Filter tips and gloves were used in all cases.

To eliminate possible off-side effects, oligo sets containing 4 different sequences (ON-TARGETplus SMARTpools; Dharmacon) were used in all cases. The siRNA concentration that results in an efficient decrease in target protein levels was analyzed for each of them before experiments were conducted. At the end, 50nM was the final concentration used for all of them.

The following siRNA oligos were used in each case:

Target protein	Reference	Sequences
Cdh1	L-015377-00-0005	5'-CCACAGGAUUAACGAGAAU-3' 5'-GGAACACGCUGACAGGACA-3' 5'-GCAACGAUGUGUCUCCCU A-3' 5'-GAAGAAGGGUCUGUUCACG-3'
p21	L-003471-00-0005	5'-CGACUGUGAUGCGCUAAUG-3' 5'-CCUAAUCCGCCCACAGGAA-3' 5'-CGUCAGAACCCAUGCGGCA-3' 5'-AGACCAGCAUGACAGAUUU-3'
p53	L-003329-00-0005	5'-GAAAUUUGCGUGUGGAGUA-3' 5'-GUGCAGCUGUGGGUUGAUU-3' 5'-GCAGUCAGAUCCUAGCGUC-3' 5'-GGAGAAUAUUU CACCCUUC-3'
Emi1	L-012434-00-0005	5'-CAACAGACACUUAAUAGUA-3' 5'-CGAAGUGUCUCUGUAAUUA-3' 5'-UGUAUUGGGUCACCGAUUG-3' 5'-GAAUUUCGGUGACAGUCUA-3'
Non-target (NT)	D-001810-10-20	5'-UGGUUUACAUGUCGACUAA-3' 5'-UGGUUUACAUGUUGUGUGA-3' 5'-UGGUUUACAUGUUUUCUGA-3' 5'-UGGUUUACAUGUUUUCCUA-3'

2. Cell proliferation and survival assays

2.1. Cell proliferation assay

Cell proliferation assay is based on crystal violet-mediated protein and DNA staining, which can be used to estimate the amount of cells present on a plate. This method is useful to analyze cell proliferation during several days.

For this assay, cells were cultured in 12-well plates at low confluence and then treated as indicated. Plates were harvested before and just after the treatment (0h) and at the indicated time after release. To this end, cells were extensively rinsed with PBS (phosphate buffered saline) and then fixed with 4% PFA- (paraformaldehyde) PBS for 15 minutes at RT (room temperature), stained with 0.25% crystal violet-containing

ultrapure water for 5 minutes and finally washed several times with deionized water. The absorbance of crystal violet (λ595) was measured and used to determine the cell confluency in each condition.

2.2. Colony formation assay

Colony formation assay is also based on crystal violet-mediated protein and DNA staining. However, in this case, crystal violet is used to improve the visualization of colonies. This assay is used to study cell viability long time after the treatment.

For colony formation assays, cells were cultured in 12-well plates and treated as indicated. After 12 hours of release, cells were plated diluted (250 cells in each well) in 6-well plates. 8 days later, cells were fixed and stained with 1% crystal violet-containing 70% ethanol for 10 minutes at RT, and the number of colonies was counted.

3. SA-β-Gal (senescence-associated β-galactosidase) activity assay

The analysis of SA-β-Gal activity can be used to quantify the number of senescent cells on a plate[530]. For this analysis, cells were plated on 24-well plates, treated as indicated, washed several times with PBS and then fixed with 2% PFA-/0.2% glutaraldehyde-PBS for 3 minutes at RT. After fixation, cells were washed several times with PBS and then incubated with X-gal- (B4252, Sigma) containing staining solution for 15 hours at 37ºC in the dark. Finally, staining solution was removed, cells were washed a couple of times with PBS and then incubated with methanol absolute (300µL in each well) until its evaporation (inside the hood).

- *Staining solution (pH 6)*

- *40mM citric acid/ Na phosphate buffer*
- *5mM $K_4[Fe(CN)_6]\cdot 3H2O$*
- *5mM $K_3[Fe/(CN)_6]$*
- *150mM NaCL*
- *2mM $MgCl_2$*
- *1mg/mL X-gal*

4. Electrophoresis and WB (Western blot)

4.1. Preparation of samples

Three different types of samples: whole cell lysates, chromatin-enriched fractions and iPOND extracts have been used for electrophoresis and WB analysis in this thesis. The preparation of each of them was performed as follows:

- *Whole cell lysates*

  Cells were washed with PBS and then lysed by the addition of SDS- (sodium dodecyl sulfate) containing lysis buffer. Cells were finally collected with the help of a scrapper and stored at -20ºC.

Since SDS is an anionic detergent that denaturalizes all the proteins, the addition of inhibitors is not required in this case. Nonetheless, SDS precipitates at low temperature. Thus, samples must be collected at RT in this case.

- *Chromatin-enriched fractions*

Chromatin extraction was performed following a modified version of the protocol described on Mendez & Stillman[531]:

- First, cells were harvested in ice-cold PBS with the help of a scraper, and then centrifuged at 660g for 5 minutes at 4ºC. (Pellets can be stored at -80ºC during several weeks).
- Next, cells were lysed by the addition of buffer A (8 times the volume of the pellet), supplemented with freshly added protease and phosphatase inhibitors, and Triton X-100. The optimal concentration of Triton X-100 and the incubation time must be set up for each cell line. In the case of hTERT-RPE cells, lysis was performed in 0.1% Triton X-100-containing buffer A during 10 minutes on ice. After that, cells were centrifuged at 600g for 5 minutes at 4ºC.
- Supernatants (S1 fractions), corresponding to the cytoplasmic fraction of cells, were collected in new tubes and stored at -20ºC.
- Pellets (nuclei) were washed with buffer A (8 times the volume of the pellet) supplemented with inhibitors but without Triton X-100, and then centrifuged at 600g for 5 minutes at 4ºC.
- Supernatants were discarded, and pellets were incubated during 10 minutes on ice with buffer B (8 times the volume of the pellet) supplemented with freshly added protease and phosphatase inhibitors. After incubation, nuclei were centrifuged at 1700g for 5 minutes at 4ºC.
- Supernatants (S2 fractions), corresponding to the nuclear soluble fractions, were collected in new tubes and stored at -20ºC.
- Pellets, corresponding to chromatin-associated and nuclear matrix-bound proteins, were washed with buffer B supplemented with inhibitors until they became transparent. Supernatants were discarded each time by centrifugation at 600g for 5 minutes at 4ºC.
- Finally, pellets were resuspended in lysis buffer (3 times the volume of the pellet) and stored at -20ºC.

** Samples must be kept on ice all the time.*

- *iPOND extracts*

Nascent DNA-bound proteins were isolated by a modified version of iPOND[511] as explained in section (5). The protein concentration of each extract is not measured in this case. Instead, the same volume of each iPOND extract is loaded during the

electrophoresis. Samples are boiled during 20 minutes at 95ºC before the electrophoresis and WB.

- *Lysis Buffer (pH 6.8)*

- *67mM tris*
- *2% SDS*

- *Buffer A*

- *10mM hepes, pH 7.4*
- *10mM KCl*
- *1.5mM $MgCl_2$*
- *0.34 M sucrose*
- *10% glycerol*
- *1mM DTT*
- *Protease inhibitors: 10µg/mL leupeptine; 1µg/mL aprotinine; 1mM PMSF*
- *Phosphatase inhibitors: 1mM NaF; 0.1mM Na_3VO_4*

- *Buffer B*

- *3mM EDTA*
- *0.2mM EGTA*
- *1mM DTT*
- *Protease inhibitors: 10µg/mL leupeptine; 1µg/mL aprotinine; 1mM PMSF*
- *Phosphatase inhibitors: 1mM NaF; 0.1mM Na_3VO_4*

4.2. Protein quantification

Protein quantification was performed using Lowry[532] or BCA methods (according to manufactures (ThermoFisher scientific) guidelines), which are compatible with SDS-containing samples. Due to SDS-promoted DNA denaturalization, samples are very viscous, and thus, they must be boiled at 95ºC during 15 minutes before quantification to degrade the DNA.

** These boiled samples can be stored at -20ºC during months.*

4.3. Electrophoresis and WB

Electrophoresis coupled with WB is a semi-quantitative method used to detect and quantify the relative abundance of proteins of interest on a certain sample. The first step consists in separating the proteins by SDS-PAGE electrophoresis. The SDS present on the samples, the gel and the buffers denatures the proteins and adds negative charges to them so they can migrate towards a positive pole, while they are separated according to their molecular weight. Separated proteins are then transferred to nitrocellulose membranes, where they are detected by incubation with primary and secondary antibodies. The primary antibodies are associated with the proteins of interest. These primary antibodies are then recognized by secondary antibodies conjugated to HRP (horseradish peroxidase) enzyme on their constant region (Fc).

Finally, these secondary antibodies are detected by the addition of peroxidase substrate ECL (enhanced chemiluminescent substrate), which reacts with the HRP enzyme present on the secondary antibody, giving a chemiluminescent substrate.

** The electrophoresis and WB experiments were performed at least three times in each case.*

- *SDS-PAGE electrophoresis*

Samples were prepared to load between 25-50µg of protein in each well. The volumes of the different samples were normalized between them by adding lysis buffer. Finally, loading buffer (Laemmli buffer[533]) was added at 1x final concentration, samples were boiled for 5 minutes at 95ºC, and run in polyacrylamide gels at 100V using standard protocols.

- *Transference of proteins to nitrocellulose membranes*

After separation, proteins were transferred to nitrocellulose membranes by incubating the gel with nitrocellulose membranes for 1 hour and 30 minutes at 70V, using standard protocols. For proteins with a molecular weight higher that 120KDa, the transference was performed using a 2x transference buffer during 2 hours at 70V, which contains twice the SDS and electrolyte concentration.

- *Blocking of membranes*

Membranes must be blocked to avoid the antibodies to be non-specifically attached to the membranes. Blocking of membranes was performed using 3% milk- (for total proteins) or 3% BSA- (bovine-serum albumin; for phosphoproteins) containing TBS-T. Nitrocellulose membranes were incubated with those buffers for 1 hour at RT.

- *Incubation with primary and secondary antibodies*

Blocked membranes were incubated overnight at 4ºC with primary antibodies against the proteins of interest, diluted in 3% BSA-containing blocking solution. After that, membranes were washed several times with TBS-T and then incubated during 1 hour at RT with secondary antibodies against the primary antibodies, diluted in 5% milk-containing TBS-T (1/3000 for whole cell lysates and 1/2000 for chromatin-enriched fractions and iPOND extracts; 1/10000 and 1/5000 respectively in the case of the anti-goat secondary antibody).

- *Developing*

After incubation with secondary antibodies, membranes were washed twice with TBS-T and once with TBS. Finally, they were developed by adding an ECL solution (EZ-ECL, Biological Industries) that reacts with the HRP enzyme present on the secondary antibody, giving a chemiluminescent reaction.

- *Antibodies*

Antibody	Reference	Dilution
Actin	sc-8432	1/2000
Aurora A	#3092	1/500
BRCA2	ab123491	1/2000
Cdc45 (G-12)	sc-55569	1/200
Cdh1	Homemade (by R. Freire)	1/1000
CDK4 (H-303)	sc-709	1/500
Claspin	Homemade (by R. Freire)	1/5000
CtIP	A300488a	1/1000
Cyclin A2 (H-432)	sc-751	1/500
Cyclin B1 (GNS1)	sc-245	1/200
Emi1	37-6600	1/100
FANCD2	ab2187	1/5000
Fen1	BD-611294	1/1000
GAP120	sc-63	1/200
H3	ab1791	1/2000
H4	05-858	1/1000
Lamin B1 (M-20)	sc-6217	1/500
MCM2 (H-126)	sc-10771	1/200
MCM6 (C-20)	sc-9843	1/200
p21 (Ab-1)	OP64	1/1000
p53	MS-186	1/1000
Pan-MCM	A303-477A	1/1000
P-Chk1 (S296)	#2349	1/1000
P-Chk2 (T68)	NB100-92502	1/1000
PCNA	ab18197	1/1000
Plk1 (F-8)	sc-17783	1/50
Pol α	sc-5921	1/200
Pol δ	ab10362	1/1000
pRb (IF-8)	sc-102	1/500
Rad51 (H-92)	sc-8349	1/200
RPA32	#2208	1/1000
RFC3	ab154899	1/1000
SMC1	A300-055A	1/1000
SMC3	A300-060A	1/1000
Tipin	Homemade (by R. Freire)	1/2000

- *Electrophoresis buffer*

- *14,41g/L glicine*
- *3.03g/L tris*
- *1g/L SDS*

- *Transference buffer*

- *14.41g/L glicine*
- *3.016g/L tris*

- *0.2g/L SDS*
- *20% ethanol*

- *2x transference buffer*

- *28.82g/L glicine*
- *6.032g/L tris*
- *0.4g/L SDS*
- *20% ethanol*

- *TBS*

- *20mM tris HCl, pH 7.5*
- *150mM NaCl*

- *TBS-T*

- *20mM tris HCl, pH 7.5*
- *150mM NaCl*
- *0.05% Tween -20*

5. iPOND: isolation of proteins on nascent DNA

iPOND[509] is a powerful technique to analyze the replisome components as well as the changes at replication forks after certain treatments or conditions. The proteins obtained by iPOND can be visualized by electrophoresis and WB (iPOND+WB); or by contrast, they can be identified/quantified by MS (iPOND+MS). In both cases, the modified version of iPOND[511] was performed in the same way with the only difference that for MS analysis 3 p150 plates per condition were used, while only 1 p100 was used for WB. The biotinylation and sonication of the samples was always validated before performing the modified version iPOND.

5.1. Preparation of cell extracts

Cells were cultured and treated as indicated, and then crosslinked with 1% PFA for 10 minutes at RT. After crosslinking, PFA was quenched with 0.125mM glycine (pH 7) for 5 minutes at RT. After that, cells were harvested in ice-cold PBS, supplemented with protease inhibitor cocktail (PIC, Roche), with the help of a scraper. Cell pellets were obtained by centrifugation at 1000g for 10 minutes at 4ºC and finally stored at -80ºC.

**Pellets can be stored at -80ºC during a couple of weeks.*

- *Processing: biotinylation and sonication of samples*

- Cell pellets were lysed by incubation with lysis buffer (ChIP Express kit, Active Motif) during 30 minutes on ice.
- Lysates were passed 10 times through a 21-gauge needle, and then nuclei were pelleted by centrifugation at 2400g for 10 minutes at 4ºC.

- Pellets were rinsed with PBS supplemented with PIC and centrifuged again at 2400g for 10 minutes at 4ºC.
- In order to conjugate biotin to the EdU present on the samples, click reaction was performed. To this end, cell pellets were incubated during 30 minutes at RT with click reaction solution. After click reaction, nuclei were pelleted by centrifugation, rinsed again as previously with PBS supplemented with PIC, and then pelleted again by centrifugation at 2400g for 10 minutes at 4ºC.
- Finally, pellets were resuspended in shearing buffer (ChIP Express kit, Active motif), sonicated (Bioruptor, Diagenode) for 15 minutes at high intensity (30-s/30-s on/off pulses), and centrifuged at 15.000g for 20 minutes at 4ºC. After that, supernatants were collected and stored at -20ºC.

** Samples must be kept on ice if not specified otherwise.*

- *Click reaction solution*

- *100mM tris HCl, pH 8*
- *2mM $CuSO_4$*
- *0,2mM biotin azide*
- *100mM ascorbic acid*

** Reagents must be added to ultrapure water in this certain order.*

5.2. DNA purification and validation of sonication

For DNA purification, 30µL (5%) of processed cell extracts were mixed and incubated overnight at 65ºC with 170µL of ultrapure water, 10µL of NaCl (5M) and 1µL of RNAse (10µg/µL) to reverse the crosslinks. After that, 2µL of Proteinase K (10µg/µL) were added, and samples were incubated at 55ºC during more than 4 hours. Next, 250µL of ultrapure water were added to each sample, and finally phenol: chloroform extraction[534] was used to separate proteins from DNA.

The obtained DNA was quantified using a nanodrop (ThermoFisher scientific). After that, 0.5µg of DNA were loaded and separated in a SYBR® Safe-containing (Sigma; according to manufactures guidance) 1.5% agarose gel. Finally, DNA fragments were visualized using a Gel Doc® EZ System (Bio-Rad).

5.3. Dot-blot

The biotinylation of the samples was analyzed by dot-blot. To this end, 1µL of processed cell extract was spotted onto a nylon membrane (Hybond-N+, Amersham) in triplicate. After that, membranes were air-dried at RT for 15 minutes, and then DNA was crosslinked to the membrane by UV light (4000µJx100). After crosslinking, membranes were rehydrated with TBS-T, blocked with 5mg/mL salmon sperm DNA-(Sigma) containing TBS-T for 1 hour at RT, and washed several times with TBS-T before incubation with primary antibody. A primary antibody against Avidin, which was already conjugated to HRP enzyme, was used in this case. Membranes were incubated

during 15 minutes at RT with the primary antibody (1/1000), washed several times with TBS-T and finally developed using ECL.

** A serially diluted 5'-biotinylated oligonucleotide served as standard (5'-CTCATAGCT CACGCTGTAGGTATCTCAGTTCGG-3').*

5.4. iPOND

The modified version of iPOND was performed as follows:

Streptavidin-conjugated Dynabeads M-280 (Invitrogen) were washed three times with 1x ChIP buffer and then blocked during 1 hour at RT with 10 mg/mL salmon sperm DNA- (Sigma-Aldrich) containing PBS. Processed cell extracts were then incubated with previously blocked Dynabeads (1:10) for 30 minutes at RT. Finally, beads were washed twice with low salt buffer and twice with high salt buffer, and then resuspended in Laemmli buffer[533] either by MS or WB analysis.

** Samples must be kept on ice before the addition of Laemmli buffer if not specified otherwise.*

- *1x ChIP buffer*

- *1% Triton X-100*
- *2mM EDTA, pH 8*
- *150mM NaCl*
- *20mM tris HCl, pH 8*
- *20mM beta-glycerol phosphate*
- *2mM Na_3VO_4*

- *Low salt buffer*

- *1% Triton X-100*
- *2mM EDTA, pH 8*
- *150mM NaCl*
- *20mM tris HCl, pH 8*

- *High salt buffer*

- *1% Triton X-100*
- *2mM EDTA, pH 8*
- *500mM NaCl*
- *20mM tris HCl, pH 8*

6. High-resolution MS

Due to technical problems, the MS analysis had to be performed in two rounds. The steps explained below were performed individually for each MS round. Additionally, the 14h HU sample of the first biological replicate was analyzed in the second MS round, together with the samples of the second and third replicates. Thus, the calculations to obtain the nRA values of the proteins present on the 14h HU condition

of the first biological replicate were performed per duplicate with the values of the second and third replicates in each case. As a result, for each protein, two different nRA values were obtained in the 14h HU condition of the first replicate. Therefore, in order to normalize this condition with the other ones, we calculated the average of both nRA values in this case.

6.1. Protein separation and silver staining

The proteins present on iPOND extracts were slightly separated in a 10% polyacrylamide gel by SDS-PAGE electrophoresis (as previously explained) and then silver-stained.

The staining was performed using a MS compatible method as follows:

- Gels were rinsed with ultrapure water.
- After that, gels were fixed by incubation with H2O: methanol: acetic acid (50:40:10) solution for 45 minutes at RT.
- After fixation, gels were washed several times with ultrapure water during more than 1.5 hours at RT.
- Gels were then incubated with 0.02% (w/v) sodium thiosulfate for 3 minutes at RT.
- Two washes of 1 minute each with ultrapure water were performed.
- After that, gels were stained with 0.1% (w/v) silver nitrate solution for 30 minutes at 4ºC in the dark.
- Two washes of 1 minute each with ultrapure water were performed.
- Finally, gels were developed with 0.04% PFA-containing 2% (w/v) sodium carbonate at 4ºC. Developing solution was changed with a new one when it turned yellow. Gels were incubated with developer until proteins bands were visible. Once protein bands were visible, developer was removed and reaction was stopped by the addition of 5% acetic acid.

** All the reagents were freshly prepared with sterilized ultrapure water. Clean trays were used and gels were always manipulated using gloves to avoid keratin contamination. All washes and incubations were performed in a shaker.*

For the identification/quantification of nascent DNA-bound proteins, silver-stained gel lanes (each of them corresponding to a certain condition (Figure 1)) were sent to the proteomic service of the *Karolinska Institutet* to analyze them by high-resolution MS. This analysis allowed us not only to identify but also to compare the relative protein abundance values between samples, using a label-free quantification method.

The in-gel digestion, MS analysis (liquid chromatography tandem MS), database search and protein identification /quantification were performed by the proteomic service of the *Karolinska Institutet*.

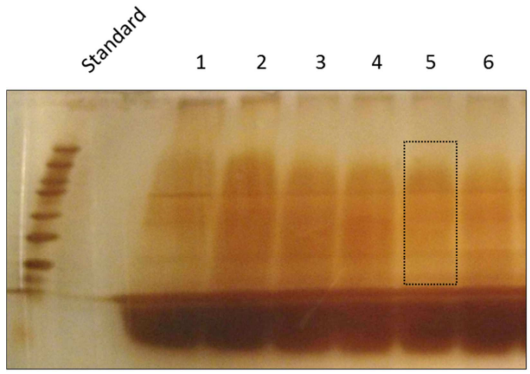

Figure 1. Protein visualization by silver staining.
A representative image of a silver-stained polyacrylamide gel is shown. The proteins present on iPOND extracts were separated in a 10% polyacrylamide gel, and then stained with silver. Each lane, representing a certain condition, was isolated as indicated (with a black box) and sent to the proteomic service for further analysis.

6.2. In-gel digestion of silver-stained gel bands

Each gel lane was divided into several pieces, which were de-stained in 50mM ammonium bicarbonate and 50% acetonitrile. Liquid was removed and the gel pieces were directly subjected to a tryptic digestion protocol carried out by a liquid handling robot (MultiProbe II, Perkin Elmer). This included the reduction of proteins for 30 minutes in 10mM DTT at 56 °C and their alkylation in 15mM iodacetamide for 30 minutes at RT in the dark. Gel pieces were dehydrated in 100% acetonitrile, trypsin was added to a final concentration of 13ng/µl, and the pieces were digested for 5 hours at 37°C. Extracted peptides from each lane were pooled into one sample.

6.3. Liquid chromatography tandem MS

- *First MS round*

Tryptic peptides were cleaned with C18 StageTips (Thermo Fisher Scientific Inc) and the resulting peptide mixture was injected into an Easy-nLC system (Thermo Scientific, Bremen, Germany) in-line coupled to a hybrid LTQ Orbitrap Velos ETD mass spectrometer (Thermo Scientific, San Jose, USA). The chromatographic separation of the peptides was achieved using a 10 cm fused Silica Tip column (New Objective, Inc.) self-packed with 3-µm C18-AQ ReproSil-Pur (Dr. Maisch GmbH) using a linear gradient from 3−48% acetonitrile in 1 hour and 29 minutes, at flow rate of 300 nl/min.

The MS acquisition method was comprised of one survey full scan ranging from m/z 300 to m/z 2000 acquired in the FT-Orbitrap with a resolution of R= 60,000 at m/z 200 followed by up to five data-dependent CID fragmentation scans in profile mode from the most intense precursor ions with a charge state ≥ 2.

- *Second MS round*

Tryptic peptides were cleaned with C18 StageTips (Thermo Fisher Scientific Inc) and the resulting peptide mixture was injected into a nano-Ultimate system (Thermo Scientific, Bremen, Germany) in-line coupled to a Fusion Orbitrap mass spectrometer (Thermo Scientific, San Jose, USA). The chromatographic separation of the peptides was achieved using a 15cm long prepacked Thermo Scientific EASY-Spray column (3um, 75 um ID) at 55°C with the following gradient: 4−30% acetonitrile in 1 hour 54 minutes, 30−96% ACN for 5 minutes and 96% ACN for 8 minutes all at a flow rate of 300nl/min.

The MS acquisition method was comprised of one survey full scan ranging from m/z 300 to m/z 1750 acquired with a resolution of R= 60,000 at m/z 200 and a target value of $2x10^5$, followed by data-dependent higher-energy collisional dissociation fragmentation scans in Top Speed data mode for precursor ions with a charge state ≥ 2. Sequencing was done with a target value of $5x10^4$ ions determined with predictive automatic gain control, for which the isolation of precursors was performed with a window of 2 m/z. Scans were acquired with a resolution of R=15000 and normalized collision energy was set to 35.

6.4. Database search and protein identification/quantification

Fragmentation spectra were extracted using Raw2MGF (in-house developed software), and the resulting mascot generic files were searched against a SwissProt protein database (reversed protein sequences had been added to database for decoy search) using the Mascot 2.3.0 (Matrix Science Ltd.). Mascot was set up to search a concatenated SwissProt protein database with enzyme specificity set as C-terminal to arginine and lysine, allowing cleavage before proline and a maximum of and two missed cleavage sites. The allowed peptide mass deviation was set to 10ppm and 0.6 or 0.02Da (first and second round respectively) for the fragment ions. Carbamidomethylation of cysteine was specified as a fixed modification, whereas oxidation of methionine and deamidation of asparagine and glutamine were defined as variable modifications.

Quantitative information was extracted using the software package Quanti[535]. This software performs extracted ion current quantification for label free quantitation and normalization. Only peptides identified with a Mascot score higher than 28 or 37 (first and second round respectively) were selected. Such a threshold was set to fulfill condition of no more than 1% FDR over the total peptide population. Only proteins quantified with such peptides were considered for quantitation.

7. Flow cytometry

Flow cytometry is used to analyze different cell features such as DNA content, as well as to determine the number mitotic cells. For this analysis, cells were harvested by trypsinization, and centrifuged at 660g for 5 minutes at 4ºC in all cases. After that, cell pellets were washed with ice-cold PBS and centrifuged again as before. Finally, pellets

were resuspended in ice-cold PBS, diluted 1:10 in ethanol (70%) and stored at -20ºC at least during 2 hours to fix them.

** Samples can be stored during several months at -20ºC.*

7.1. DNA content analysis

DNA content was analyzed by staining the DNA with PI (propidium iodide) in the presence of RNAse. The PI is intercalated into DNA and RNA, proportionally to the amount of them. Therefore, since RNA is degraded by the addition of RNAse, the incorporated PI will be proportional to the amount of DNA.

For this analysis, after fixation, cells were washed with 0.05% Tween-20- containing PBS (PBS-T), centrifuged at 660g for 5 minutes at 4ºC and resuspended in 1% PI-containing PBS, supplemented with 1mg/mL RNAse. Cells were incubated with this buffer for 30 minutes at 37ºC to ensure that RNA was degraded.

7.2. BrdU/MPM2 and PI analysis

A combined analysis of BrdU, MPM2 and DNA content was used to analyze the number of cells arrested in S phase, as well as the number of mitotic cells.

For this analysis, cells were incubated with BrdU-containing medium before treating them as indicated. Cells were then fixed as previously explained. After fixation, cells were washed with PBS-T, and then centrifuged at 660g for 5 minutes at 4ºC. After that, DNA was denatured by incubation with 0.1% Triton X-100-containing 2M HCl-PBS solution for 15 minutes at RT. HCl was then neutralized by washing twice with borate buffer (borate solution was removed each time by centrifugation at 660g for 5 minutes at 4ºC). After neutralization, cell pellets were rinsed with PBS-T, blocked by incubation with 3% BSA-containing PBS-T for 1 hour at RT, and then incubated with primary antibodies (anti-BrdU (Abcam, ab6326; 1/250) and anti-MPM2 (Millipore, #05-368; 1/250) diluted in blocking solution) for 1 hour at RT. Finally, cell pellets were washed with PBS-T, incubated with secondary antibodies (anti-rat488 (Invitrogen; 1/400) and anti-mouse647 (Invitrogen; 1/500) diluted in PBT-T) for 45 minutes at RT, washed again with PBT-T and finally resuspended in 1% PI-containing PBS, supplemented with 1mg/mL RNAse. Cells were incubated with this solution during 30 minutes at 37ºC before flow cytometric analysis.

- *Borate buffer (pH 8.5)*

- *0.1M $Na_2B_4O_7$*10H_2O*

** Ajust the pH by adding 0.1M boric acid solution.*

8. Immunofluorescence

As flow cytometry, immunofluorescence is a useful technique to analyze several cell features. These techniques consist in labeling the proteins of interest with primary

antibodies, to visualize them afterwards by their detection with secondary antibodies conjugated to fluorescent molecules.

For flow cytometric analysis, cells are maintained in suspension. By contrast, cells are attached to coverslips for immunofluorescence techniques. To improve microscope imaging, coverslips are mounted onto slides with mowiol after the immunofluorescence.

Images were obtained using Leica TCS-SL or TCS-SP5 confocal microscopes and then analyzed using Fiji (Image J) software in all cases.

8.1. CldU/IdU immunofluorescence

For CldU and IdU immunofluorescence, previously labeled and treated cells were fixed during 10 minutes with 70% ethanol at RT. Cells were then rinsed with PBS and incubated with 0.2% Triton X-100 containing 2M HCl-PBS solution for 30 minutes at RT. HCl was neutralized by washing three times with borate buffer. Cells were then washed twice with PBS and blocked with 1% BSA- containing PBS for 15 minutes. Finally, cells were incubated with primary anti-BrdU (Abcam, ab6326; 1/250 for CldU labeling and Becton Dickinson, 347580; 1/50 for IdU labeling) antibodies for 1 hour at 37ºC, and with secondary, anti-rat (Alexa488 conjugated; 1/500) and anti-mouse (Alexa647 conjugated; 1/500) antibodies, for 45 minutes at 37ºC, all of them diluted in blocking buffer. DNA was counterstained with DAPI before mounting.

8.2. 53BP1/YH2AX, 53BP1/CycD1 and 53BP1immunofluorescence

Previously treated cells were rinsed with PBS and fixed with 2% PFA-PBS for 20 minutes at RT. After extensive washing, cells were permeabilized with 0.2% Triton X-100-containing PBS for 10 minutes at RT, and washed with PBS for 5 minutes. Cells were then blocked with 3% FBS-containing 0.1% Triton X-100-PBS for 1 hour at RT, and then incubated with the indicated antibodies, diluted in blocking solution, for 45 minutes at 37ºC. The following primary antibodies were used: anti-γ-H2AX (Millipore, #05-636; 1/3000), anti-53BP1 (Abcam, ab36823; 1/500), anti-Cyclin D1 (DCS-6, sc-20044; 1/100). After extensive washing in blocking solution, cells were incubated with Alexa488-, Alexa555-, or Alexa647-conjugated secondary antibodies (Invitrogen, 1/500 diluted in blocking solution) for 20 minutes at 37ºC. Finally, cells were counterstained either with 1% PI-containing 0.1 mg/mL RNAse A- (Fermentas) PBS solution or with DAPI (Sigma-Aldrich). Cells were maintained at 37ºC during 15 minutes in the case of PI staining.

For EdU staining, previously labeled and treated cells were fixed with 4% PFA-PBS for 30 minutes at RT, and then click reaction was performed (as previously described) with 1 µM Alexa488-azide (Invitrogen).

8.3. ssDNA analysis by BrdU immunofluorescence under native conditions

For ssDNA detection, previously labeled and treated cells were rinsed with PBS, permeabilized with 0.5% Triton X-100-PBS for 10 minutes at 4ºC, and then fixed with 3%PFA/2%sucrose-PBS solution for 10 minutes at RT. After several washing with PBS, cells were blocked by incubation during 1 hour at RT with 3% BSA-containing PBS-T.

Cells were then incubated with the anti-BrdU (Becton Dickinson; 1/50) antibody, diluted in blocking solution, for 1 hour at 37ºC, washed with blocking solution for 15 minutes at RT, and then incubated with the secondary antibody (anti-mouse 488; 1/500) for 20 minutes at 37ºC. Finally, cells were washed again with blocking solution for 15 minutes at RT, and DNA was counterstained with 0.1mg/mL RNAse-containing 1% PI solution (15 minutes at 37ºC).

9. DNA fiber analysis

DNA fiber assay is a powerful technic to analyze replication dynamics[506]. DNA fibers are labeled with different thymidine analogs, which are visualized by staining them with anti-BrdU antibodies that present different specificities for each of them. The incubation of cells with defined and different analogs, before and after the HU treatment, allowed us to determine the number of restarted (stained with both colors), stalled (stained only with the first color) and new origin firing (stained with the second color) events in each case.

DNA fiber was performed as follows:

- First, hTERT-RPE cells were pulse labeled with CldU/IdU and treated as indicated. Labeled cells were washed with PBS, centrifuged at 660g for 5 minutes at 4ºC, harvested by trypsinization and resuspended in ice-cold PBS at 5 x 10^5 cells/mL concentration.
- After that, DNA spreading was performed. To this end, 2µL of cells were spotted onto glass slides and lysed with 7µL of spreading buffer. Slides were tilted (15º to horizontal), allowing a stream of DNA to run slowly down the slide, air-dried for 1 hour at RT, and then fixed with methanol/acetic acid (3:1) solution for 10 minutes (inside the hood). (Slides can be stored at 4ºC overnight after fixation).
- For CldU and IdU immunostaining, slides were first washed twice during 5 minutes with ultrapure water.
- Then, slides were incubated with 2.5M HCl solution during 1 hour and 15 minutes (inside the hood). After this time, HCl was removed from slides by washing twice with PBS, and then twice (during 5 minutes each) with blocking solution.
- Once washed, slides were blocked by incubation during 1 hour with 1% BSA- and 0.1% Tween-20-containing PBS solution at RT, and then incubated with anti-BrdU primary antibodies (Abcam, ab6326; 1/1000 for CldU labeling and Becton Dickinson, 347580; 1/200 for IdU labeling) diluted in blocking solution for 1 hour and 30 minutes at 37ºC.
- After that, slides were washed three times with PBS, fixed with 4%PFA-containing PBS for 10 minutes at RT, washed again three times with PBS and then twice (during 5 minutes each) with blocking solution.
- Finally, slides were incubated with secondary antibodies (Alexa488-conjugated anti-rat and Alexa555-conjugated anti-mouse; 1/500) diluted in blocking solution for 1 hour and 30 minutes at 37ºC, washed five times with PBS and mounted with mowiol.

- *Spreading buffer*

- *0.5% SDS*
- *200mM tris HCl, pH 7.4*
- *50mM EDTA*

** All material and reagents used for DNA fiber spreading and staining were previously sterilized.*

10. DNA break analysis by PFGE (pulse-field gel electrophoresis)

PFGE can be used to detect the presence of DSBs on genomic DNA[505]. In the absence of breaks, chromosomes are unable to enter inside the agarose gel due to their size. By contrast, once broken, DNA fragments can enter and migrate thought the gel.

For DNA break analysis, cells were washed with PBS, centrifuged at 660g for 5 minutes at 4ºC, trypsinized and then resuspended in incubation buffer at 8.33 x 10^6 cells/mL concentration. 120µL of diluted cells were mixed 1:1 with 1% low-melting point agarose (Sigma), to obtain two agarose inserts each of them containing 0.5 x 10^6 cells. After that, cells in plugs were lysed for 48 hours at 50ºC, washed three times with TE buffer and run in 1% agarose gel (chromosomal grade; Bio-Rad) in a CHEF DR III PFGE apparatus (Bio-Rad; 120 angle; 60–240 s switch time; 4 V/cm) at 14ºC for 20 hours. Finally, gels were stained with SYBR® Safe (Sigma) and analyzed by LAS-4000 system (Fujifilm).

- *Incubation buffer*

- *0.25mM EDTA*
- *20mM NaCl*
- *10mM tris HCl, pH 7.5*

- *Lysis buffer*

- *0.25mM EDTA*
- *20mM NaCl*
- *10mM tris HCl, pH 7.5*
- *1% N-laurylsarcosyl*
- *1 mg/ml proteinase K*

- *TE buffer*

- *10mM tris HCl, pH 7.5*
- *1mM EDTA*

11. Statistical analysis

Statistical analysis was always performed using Graphpad Prism 6 software. Paired or unpaired *t test* analyses were performed as indicated. Values marked with asterisks are significantly different: *p < 0.05, **p < 0.01, ***p < 0.001, ****p < 0.0001). n.s. was used to indicate absence of statistical significance.

APPENDIX

Appendix 1. Raw data.

The protein ID and the relative abundance values, in each condition and replicate, of the proteins identified in our iPOND+MS experiment are shown. Data from each MS round are separated with a grey line. In light grey, proteins that were identified as reversed. Proteins that were not identified in one of the MS rounds are represented as empty boxes. Conditions have been previously described *(Figure 37)*.

	n=1					n=1 (14 h HU); n=2; n=3											
						n=2						n=3					n=1
PROTEIN ID	**Negative control**	**Pulse**	**15' EdU/HU**	**2h HU**	**Chase**	**Negative control**	**Pulse**	**15' EdU/HU**	**2h HU**	**14h HU**	**Chase**	**Pulse**	**15' EdU/HU**	**2h HU**	**14h HU**	**Chase**	**14h HU**
1433B_HUMAN	1,324	1,146	0,761	0,684	1,268												
1433E_HUMAN	1,554	0,325	0,707	1,731	1,936												
1433F_HUMAN	0,764	0,626	3,325	0,828	0,779												
1433G_HUMAN	1,100	0,792	1,255	0,843	1,204	0,000	0,784	1,843	1,540	0,792	0,305	1,675	0,762	1,264	0,870	0,897	1,273
1433S_HUMAN	0,206	5,140	0,000	0,000	0,000												
1433T_HUMAN	0,770	0,726	1,283	1,611	1,034												
1433Z_HUMAN	1,085	0,898	0,874	1,084	1,081	0,000	0,885	0,699	0,975	0,292	1,454	0,865	0,283	1,385	1,584	2,341	2,927
2AAB_HUMAN	0,965	0,894	1,129	0,859	1,245												
2ABD_HUMAN	1,057	1,323	0,537	1,318	0,969												
5HT6R_HUMAN						0,173	0,989	1,294	1,009	1,351	1,712	1,798	1,894	1,286	0,999	1,044	0,350
5NTC_HUMAN	1,074	0,000	0,598	2,200	0,708												
5NTD_HUMAN	1,120	0,561	1,557	0,900	1,108												
6PGD_HUMAN	0,901	0,716	1,115	1,198	1,145	1,823	1,009	0,305	0,917	1,652	1,643	2,217	0,748	0,561	1,167	0,415	1,327
AATM_HUMAN	1,241	0,908	0,483	1,655	1,192												
ABC3B_HUMAN	0,814	0,355	1,449	0,947	2,459												
ABCA7_HUMAN	0,867	1,586	0,798	1,200	0,794												
ABCB6_HUMAN	1,431	0,916	1,594	0,174	2,632												
ABCE1_HUMAN	1,138	1,499	0,861	0,747	0,964												
ACACA_HUMAN	0,828	1,067	0,709	1,485	1,045												
ACADM_HUMAN	2,548	0,406	0,227	1,969	1,946												
ACL6B_HUMAN						0,000	0,364	2,152	3,791	0,644	0,000	0,163	3,728	1,429	1,063	0,776	0,567
ACLY_HUMAN	0,997	0,879	1,879	0,942	1,052	1,852	0,080	0,682	2,290	2,534	0,803	4,123	1,196	0,900	1,922	0,599	0,495
ACON_HUMAN	3,937	0,000	0,189	2,211	0,643												
ACTBL_HUMAN	1,028	0,000	3,120	0,464	0,660												
ACTG_HUMAN	1,115	0,812	0,780	1,469	0,948	1,847	0,743	0,764	0,699	1,089	0,664	1,170	0,960	0,920	0,955	1,198	1,455
ACTN1_HUMAN	1,850	0,858	0,945	0,878	0,792	0,000	1,257	0,204	0,262	1,206	1,244	0,897	1,133	0,894	1,446	1,578	2,448

ACTN4_HUMAN	1,176	0,798	1,001	1,331	0,799	8,105	1,178	1,114	0,689	1,053	0,141	0,333	0,745	0,432	0,903	2,119	1,970
ACTZ_HUMAN	1,382	0,686	1,388	1,552	1,381												
ADK_HUMAN	1,593	0,331	0,485	1,808	2,069												
ADNP_HUMAN						0,000	0,000	1,190	0,957	0,000	0,705	0,000	1,230	0,942	1,095	0,981	0,000
ADT2_HUMAN	1,631	0,406	0,392	2,388	1,677												
ADT3_HUMAN						0,909	0,733	0,951	1,891	1,717	1,133	1,087	0,254	1,648	0,563	1,094	1,215
AHNK_HUMAN	1,747	0,775	1,256	0,663	0,912	0,608	4,371	0,431	0,904	0,271	0,729	0,106	2,909	1,840	1,710	2,320	2,062
ALBU_HUMAN	1,391	0,912	1,220	0,802	0,789	4,854	0,277	0,261	0,559	0,520	10,628	1,247	1,027	1,053	0,785	0,561	0,613
ALDOA_HUMAN	1,006	0,596	0,835	1,297	1,365	1,454	1,051	0,876	0,860	0,750	1,013	1,491	1,108	0,935	0,577	0,648	1,454
AN32E_HUMAN	0,056	1,845	3,014	1,127	3,034	0,000	2,872	5,892	4,404	0,288	1,721	4,265	0,160	3,736	0,109	1,417	0,066
ANLN_HUMAN	0,118	1,992	2,897	0,959	1,500	0,000	2,929	2,249	2,461	0,197	0,920	1,417	1,223	2,964	0,681	1,088	0,110
ANM1_HUMAN	0,573	1,132	1,290	0,973	1,283	0,000	1,193	0,294	0,646	0,000	6,136	2,646	0,695	10,91	0,262	0,593	0,000
ANXA1_HUMAN	1,146	0,875	1,007	0,784	1,266	2,384	2,337	1,563	2,531	0,245	1,276	1,725	0,429	1,338	0,245	1,542	0,593
ANXA2_HUMAN	1,470	0,656	0,721	1,236	1,099	2,662	1,076	0,941	0,939	0,644	0,800	1,128	0,780	0,950	0,720	1,148	1,108
ANXA5_HUMAN	1,109	0,936	0,971	1,000	1,075	0,259	4,517	2,023	5,373	1,004	1,023	2,205	0,081	1,145	1,474	2,866	0,312
ANXA6_HUMAN						0,000	0,320	2,206	0,573	0,786	0,209	0,000	0,810	1,471	1,933	0,770	1,437
APEX1_HUMAN	1,737	0,837	1,400	1,058	2,066	0,343	0,430	0,502	0,995	0,691	1,180	0,424	1,603	3,260	0,986	1,876	2,429
API5_HUMAN	0,511	1,278	1,529	0,909	1,009												
ARF4_HUMAN	0,971	1,247	1,021	0,665	1,490												
ARF5_HUMAN						2,266	0,271	0,741	0,905	0,623	2,434	0,890	0,513	1,996	0,405	0,197	11,928
ARMC6_HUMAN	0,000	0,000	0,000	0,096	8,268												
ARP3_HUMAN	1,286	0,992	0,969	1,287	0,725												
ARPC2_HUMAN	1,834	1,732	0,538	2,992	2,689												
ARPC4_HUMAN	1,182	1,749	0,516	0,976	0,973	0,310	0,494	1,859	0,817	2,444	1,826	1,035	0,571	0,955	0,729	2,748	2,463
ARPC5_HUMAN	1,048	3,395	0,397	0,204	3,386												
ASAP2_HUMAN	1,957	0,437	1,544	3,094	0,251	0,707	4,809	3,432	3,451	2,860	0,285	3,877	2,633	0,242	0,208	0,371	0,193
AT1A1_HUMAN	2,201	0,433	0,973	2,212	0,632												
ATD3A_HUMAN	1,592	0,779	0,766	1,582	1,092												
ATPA_HUMAN	1,141	0,953	0,815	1,499	0,763	1,124	1,741	0,827	1,013	1,625	0,594	1,139	2,152	1,409	0,928	0,163	1,512
ATPB_HUMAN	1,424	0,869	0,628	1,497	0,884	0,697	2,234	1,225	2,081	2,133	0,304	2,416	1,506	1,483	0,976	0,162	0,712
ATPO_HUMAN	1,227	1,430	0,427	1,137	1,254												
BAZ1B_HUMAN	0,000	2,378	2,371	0,583	0,305												
BRD4_HUMAN	0,000	0,000	0,000	1,000	0,000												

BUB3_HUMAN	0,397	0,277	2,527	1,419	2,508												
BZW1_HUMAN	1,839	0,675	0,742	1,206	1,064												
C1TC_HUMAN	0,916	0,930	1,232	1,366	0,852												
CAF1A_HUMAN	2,308	4,183	1,285	0,143	1,943												
CAF1B_HUMAN	0,000	1,934	0,000	0,508	0,000												
CALD1_HUMAN						14,540	1,567	3,464	0,669	1,564	0,676	0,391	0,263	0,526	0,389	4,304	0,541
CAMP2_HUMAN						0,000	0,000	0,272	0,895	0,604	0,955	17,512	2,087	1,326	0,000	0,210	0,000
CAN2_HUMAN	1,318	0,883	1,092	0,667	1,102												
CAND1_HUMAN	0,596	1,066	1,605	1,012	0,873	2,859	1,485	1,670	2,613	0,960	0,560	0,505	1,363	0,635	1,063	0,705	0,490
CAP1_HUMAN	1,645	0,877	0,801	0,932	0,966	1,442	2,894	0,157	0,469	1,498	0,505	0,833	1,669	2,382	0,180	2,977	2,618
CAPR1_HUMAN	5,219	0,256	2,283	1,327	0,300												
CAPZB_HUMAN	0,537	1,866	0,349	1,910	2,367												
CATD_HUMAN						0,641	0,189	4,283	2,313	0,524	0,678	0,519	0,171	3,982	1,571	0,294	8,297
CAZA2_HUMAN	1,133	0,991	0,837	0,879	1,240												
CBX3_HUMAN						0,074	0,927	1,408	2,166	0,654	0,036	2,269	3,402	3,559	2,576	2,159	1,869
CBX5_HUMAN						0,000	0,454	1,131	1,277	0,791	1,299	1,997	0,901	1,310	0,913	1,360	0,560
CCD93_HUMAN	1,131	0,814	0,853	1,137	1,138												
CCDC8_HUMAN	0,801	0,746	1,335	0,945	1,229												
CDC37_HUMAN	0,404	1,007	1,283	1,342	1,425												
CDC5L_HUMAN						0,000	2,638	0,992	0,533	1,037	0,881	1,013	1,014	1,207	1,489	0,642	0,000
CDK1_HUMAN	0,609	1,141	1,304	1,092	0,995												
CDSN_HUMAN	1,882	2,299	0,199	1,122	0,986												
CE290_HUMAN	2,467	1,871	0,754	0,257	1,247												
CERU_HUMAN	0,000	0,000	0,314	3,213	0,000												
CH60_HUMAN	1,240	1,132	0,692	1,391	0,775	0,771	2,274	0,796	1,187	0,547	0,848	1,465	2,364	1,484	0,623	0,453	0,786
CHCH3_HUMAN						1,637	0,000	0,000	0,000	0,000	0,000	0,000	0,329	3,344	0,354	0,000	1,594
CISY_HUMAN						1,278	0,232	0,793	1,694	0,772	0,512	6,776	2,984	2,085	0,851	0,344	0,455
CKAP4_HUMAN	1,259	1,051	0,762	0,929	0,966												
CLH1_HUMAN	1,331	0,765	0,962	1,027	0,946	0,381	1,612	1,016	0,554	1,526	0,525	0,597	1,321	1,230	1,904	0,990	2,277
CLIC1_HUMAN	0,739	0,866	1,055	1,460	1,350												
CLIC4_HUMAN	0,735	0,276	0,305	4,426	4,047												
CNN2_HUMAN	1,290	0,764	0,921	1,013	1,106	0,282	1,182	1,612	0,445	1,762	1,377	0,408	1,507	1,144	1,112	1,091	2,298
CNTP4_HUMAN						0,217	1,452	0,983	1,159	0,629	1,512	1,276	1,191	1,446	1,050	1,838	0,531

CO4B_HUMAN	1,780	2,822	0,903	0,286	0,782	3,643	0,301	1,043	0,730	1,017	1,351	1,441	1,768	1,314	0,596	0,579	0,705
COF1_HUMAN	0,875	0,977	1,215	0,684	1,485												
COPA_HUMAN						402,854	0,522	0,229	0,000	0,492	0,252	0,000	0,715	0,000	0,591	0,346	1,397
COPB2_HUMAN						0,337	0,671	0,954	0,792	2,722	1,182	0,487	1,460	0,323	1,486	1,981	2,422
COPG1_HUMAN	1,335	0,841	0,880	1,488	0,907	2,248	0,755	0,314	0,879	1,366	1,320	0,557	1,830	0,474	0,757	1,145	1,310
COR1C_HUMAN	1,189	1,069	0,979	0,870	0,928												
CP2CJ_HUMAN						0,416	1,107	4,398	4,434	0,930	3,114	0,605	0,643	2,229	0,229	0,541	0,376
CPNE1_HUMAN	1,246	1,237	0,943	0,637	1,113	29,164	0,998	1,997	3,160	0,820	1,195	0,470	0,449	0,668	0,513	1,556	0,451
CPNE3_HUMAN	0,547	1,129	2,148	1,170	0,646												
CPNE9_HUMAN						0,981	4,325	1,567	1,571	1,475	2,492	1,567	0,626	0,347	0,677	0,304	0,756
CPSF6_HUMAN	0,826	0,879	1,183	0,745	1,856	0,000	0,931	0,331	1,760	1,401	1,931	0,654	1,314	0,949	0,904	1,922	0,269
CSN4_HUMAN	0,895	0,741	1,166	0,817	1,598												
CSPG2_HUMAN	0,000	0,232	0,486	11,72	0,723												
CTBP1_HUMAN	0,218	2,737	0,952	1,725	1,208	0,348	0,345	11,025	3,032	17,461	0,431	0,308	0,157	0,631	0,199	29,289	0,081
CTBP2_HUMAN	0,000	0,692	0,000	2,572	0,571	0,000	2,028	1,475	0,442	0,000	0,000	0,980	0,800	0,000	2,657	0,395	0,000
CTNA1_HUMAN	1,565	3,006	0,871	0,754	1,850												
CUL4B_HUMAN	0,460	1,678	2,284	0,564	1,064												
CUX1_HUMAN	0,420	0,000	0,000	2,768	0,000												
CYBP_HUMAN	0,392	0,546	1,468	1,455	2,258	1,595	1,155	1,853	0,843	0,280	0,535	1,227	1,132	0,308	1,122	4,774	0,725
DAZP1_HUMAN	0,260	1,012	0,783	1,864	2,599												
DDX1_HUMAN	1,247	1,480	0,996	0,718	0,890	0,000	4,351	0,655	1,357	1,800	0,531	0,288	0,414	2,603	1,690	0,378	1,269
DDX17_HUMAN	0,256	0,751	2,969	1,631	1,574	1,631	0,778	0,980	1,811	0,904	1,621	0,768	0,403	1,312	1,368	1,159	0,256
DDX21_HUMAN	0,530	1,017	1,799	0,939	2,588	3,673	3,754	0,254	0,751	0,560	1,923	0,125	0,197	1,065	2,797	12,414	0,509
DDX23_HUMAN						1,401	0,126	0,075	0,753	5,468	0,187	0,086	5,935	1,507	2,190	7,826	5,093
DDX3X_HUMAN	1,203	1,148	0,897	0,959	0,845												
DDX5_HUMAN	0,438	1,038	1,706	0,915	1,387	1,279	1,864	1,162	2,630	0,745	3,268	0,359	0,698	1,061	1,133	0,788	0,242
DEK_HUMAN	0,172	0,582	2,097	1,477	3,048	0,064	1,368	2,819	2,935	1,431	0,802	2,508	1,729	2,410	2,177	2,487	0,037
DESP_HUMAN	1,284	2,213	0,692	0,715	0,743	1,943	4,110	1,199	0,317	3,552	1,160	0,287	0,921	0,912	0,827	0,752	0,509
DHB4_HUMAN	0,864	0,512	1,263	2,002	0,907												
DHE4_HUMAN	0,753	0,895	0,517	3,166	1,228												
DHSA_HUMAN	0,923	1,282	0,912	1,197	0,762												
DHX15_HUMAN	0,410	1,334	1,919	0,824	1,629												
DHX9_HUMAN	0,411	1,240	1,696	0,792	1,403	0,219	1,324	1,067	4,076	1,617	0,744	0,772	0,555	1,066	0,236	1,683	0,844

DLDH_HUMAN						0,000	0,000	0,415	0,381	3,094	0,435	0,806	1,904	1,014	1,279	3,445	0,773
DNJC9_HUMAN						0,000	3,460	2,655	2,522	0,427	0,403	5,176	0,135	2,370	1,835	0,886	0,080
DNLI1_HUMAN	0,000	5,775	2,259	0,541	0,145												
DNM1L_HUMAN	1,514	0,717	0,691	1,338	1,027												
DNMT1_HUMAN	0,916	4,540	1,944	0,247	0,432	1,405	12,32	0,527	0,476	0,271	2,474	16,668	0,891	0,403	0,316	0,195	0,944
DPOA2_HUMAN	0,533	2,173	3,753	0,762	0,287												
DPOD1_HUMAN	0,000	1,864	2,852	0,559	0,364	0,000	4,427	9,094	1,226	0,080	0,299	8,245	2,286	2,042	0,136	0,088	0,000
DPOD3_HUMAN	0,000	2,640	1,396	0,262	0,000												
DPOE1_HUMAN	0,219	2,340	5,744	0,155	0,000												
DPYL2_HUMAN	1,035	1,871	0,936	0,842	0,620	1,225	1,228	0,898	1,088	1,081	1,395	0,956	0,456	0,885	1,309	0,918	0,895
DPYL5_HUMAN						0,618	0,351	1,068	0,740	0,918	0,923	1,700	2,168	0,932	1,091	1,429	1,080
DRG1_HUMAN	3,659	0,417	0,470	1,502	0,926												
DSC1_HUMAN	1,459	1,853	0,613	0,988	0,611												
DSG1_HUMAN	1,528	1,830	0,534	0,889	0,753	12,809	1,510	0,650	0,880	0,930	0,485	1,364	0,687	0,789	0,876	0,403	1,158
DX39B_HUMAN	0,441	1,151	1,516	1,050	1,359	0,000	3,879	0,701	2,892	0,661	2,093	1,230	0,915	1,053	0,445	0,696	0,468
DYH5_HUMAN	1,158	0,347	1,245	1,688	1,242	0,748	2,991	1,060	0,970	0,926	0,792	1,205	0,869	0,900	0,538	1,078	1,041
DYHC1_HUMAN	1,657	0,798	0,711	1,057	1,131	0,000	2,206	0,795	0,521	1,406	2,719	0,286	1,656	0,592	0,518	1,480	1,590
DYR_HUMAN	0,000	0,535	1,601	0,478	2,323	0,000	1,542	1,099	8,947	0,783	0,000	0,849	1,293	0,300	0,852	0,562	0,616
E2AK2_HUMAN	0,871	0,708	1,253	1,121	1,142												
ECHA_HUMAN	1,541	1,474	0,441	1,578	0,650												
ECHM_HUMAN	0,828	0,935	0,750	1,360	1,315												
EF1A3_HUMAN	1,509	0,884	0,800	1,033	0,939	1,616	1,069	0,882	0,684	0,799	1,049	1,005	0,942	1,002	0,653	0,691	2,016
EF1D_HUMAN	3,656	1,528	0,500	0,994	0,993	0,848	1,314	1,433	0,994	0,942	0,599	0,999	0,443	1,628	0,835	1,585	1,140
EF1G_HUMAN	1,375	0,912	1,123	0,805	0,963	0,573	0,992	0,597	0,639	0,790	0,495	1,064	0,826	1,571	1,258	0,911	7,074
EF2_HUMAN	1,279	1,047	0,973	0,924	0,817	0,940	1,238	0,967	0,765	1,010	1,163	0,783	1,160	0,949	0,866	0,981	1,329
EFTU_HUMAN	1,294	0,597	0,658	1,702	1,280	4,509	1,040	0,631	0,794	0,555	0,231	2,607	1,914	0,732	0,426	0,390	1,105
EIF3A_HUMAN	1,217	1,009	1,072	0,830	0,938												
EIF3F_HUMAN	1,674	1,430	0,650	0,609	1,035												
EIF3L_HUMAN	1,405	1,178	0,828	1,374	0,593												
ELAV1_HUMAN	0,478	1,257	1,761	0,874	2,334	0,246	1,380	1,779	2,160	0,932	1,091	1,355	0,785	1,355	1,659	1,428	0,377
ENOA_HUMAN	0,781	1,155	0,757	1,185	1,194	1,204	1,279	1,049	1,186	0,829	0,812	1,070	0,807	0,514	1,229	0,708	1,810
ENOB_HUMAN	0,867	0,987	0,757	1,239	1,262												
ENPL_HUMAN	1,346	0,250	0,898	2,287	1,546	1,243	3,692	1,157	0,411	3,021	0,132	0,609	0,302	0,248	3,338	0,722	2,542

EPIPL_HUMAN	0,811	4,419	0,000	0,000	0,298												
ESTD_HUMAN						0,000	0,857	0,919	1,124	1,171	0,000	1,469	0,000	0,576	0,724	1,425	0,000
ESYT1_HUMAN	1,463	1,148	0,629	0,847	1,140	1,178	9,015	0,414	0,418	1,158	8,602	0,334	0,664	0,493	0,760	1,030	1,162
EWS_HUMAN	0,198	1,496	0,720	1,910	2,431												
EZRI_HUMAN	1,254	0,546	1,286	1,084	1,046	0,626	1,407	1,379	0,921	1,081	0,334	1,224	0,461	1,293	3,509	1,151	0,601
FA84B_HUMAN						0,207	2,073	0,219	0,973	2,275	4,417	2,751	0,248	2,012	2,410	2,168	0,160
FACD2_HUMAN	0,000	0,237	3,202	4,006	0,306												
FANCI_HUMAN	0,000	0,179	2,474	1,908	1,114												
FAS_HUMAN	1,291	0,874	1,089	0,809	1,017	17,956	1,489	1,441	0,559	1,132	0,763	0,524	1,191	0,885	0,379	0,725	0,915
FBF1_HUMAN	0,766	0,871	1,118	1,140	1,245	0,115	0,332	1,789	2,098	2,133	1,571	1,916	0,099	3,391	2,724	3,863	0,302
FBRL_HUMAN						0,000	1,710	0,805	0,587	0,581	0,000	0,574	0,532	0,787	1,096	19,145	0,536
FEN1_HUMAN	0,191	2,762	2,582	0,735	1,037	0,000	1,655	1,600	1,346	0,516	1,136	3,189	1,728	2,022	0,889	0,534	0,084
FILA2_HUMAN	2,699	0,902	0,416	1,453	0,686												
FINC_HUMAN						0,000	12,81	1,226	0,162	0,460	0,776	0,000	0,427	0,539	0,262	6,985	2,606
FLNA_HUMAN	1,197	0,909	1,060	0,968	0,884	0,868	1,496	0,766	0,636	0,933	0,865	0,697	1,187	1,059	0,975	1,237	1,932
FLNB_HUMAN						0,285	2,462	0,996	1,179	1,374	0,195	0,200	1,058	1,535	1,370	2,009	3,118
FLNC_HUMAN	1,585	0,726	1,067	0,904	0,959	0,405	2,079	1,067	0,945	1,465	0,455	0,402	1,008	1,023	1,403	1,551	1,900
FSCN1_HUMAN	0,772	0,781	0,816	1,359	1,456	1,886	1,149	0,716	1,654	5,542	0,274	0,554	1,177	1,023	0,667	0,901	0,640
FUBP1_HUMAN	0,924	0,755	1,338	1,139	1,390	0,239	0,130	2,778	2,854	2,360	0,333	2,503	0,346	0,223	3,139	3,263	2,302
FUBP2_HUMAN	0,700	0,862	1,483	0,791	1,386	0,234	1,668	1,629	1,185	1,265	3,842	0,203	0,427	1,239	2,858	2,324	0,398
FUS_HUMAN	0,579	1,101	2,037	1,051	1,154												
FXR1_HUMAN	2,381	0,478	1,118	0,904	0,838												
G3P_HUMAN	0,951	0,809	0,756	1,157	1,595	1,189	0,250	1,469	1,398	1,152	2,714	1,214	0,968	0,955	0,772	0,985	0,729
G3PT_HUMAN	2,032	1,120	0,768	0,628	0,900												
G6PI_HUMAN	2,030	0,604	0,715	2,968	0,380												
GBLP_HUMAN	1,508	0,873	0,838	1,053	0,912	0,104	1,066	1,359	1,530	1,293	1,649	1,121	1,031	1,677	1,272	2,098	0,344
GDF11_HUMAN	2,209	0,227	2,069	0,318	2,303												
GDIB_HUMAN	1,638	0,931	0,688	1,134	0,874												
GFAP_HUMAN	1,763	0,236	8,588	0,502	0,553												
GLSK_HUMAN						0,000	0,703	0,467	0,394	0,955	0,610	1,521	1,288	7,979	1,877	0,554	0,765
GLYM_HUMAN	1,259	0,853	0,677	1,564	0,867	1,270	1,039	2,044	0,732	1,411	0,337	3,963	1,103	1,474	0,469	0,363	0,369
GNA13_HUMAN	1,829	0,504	1,059	1,071	0,989												
GOGA2_HUMAN	2,448	0,287	2,867	0,424	1,149												

GRP75_HUMAN	1,505	0,898	0,567	1,339	0,948	3,256	0,879	0,665	0,997	0,856	0,263	1,223	1,635	0,882	1,486	0,589	1,590
GRP78_HUMAN	1,125	0,923	0,653	1,604	1,038	0,880	1,117	0,794	0,859	1,599	1,540	1,322	0,225	0,788	3,722	0,445	1,887
GRWD1_HUMAN	0,691	5,388	1,300	0,620	0,455												
GSDMA_HUMAN	0,622	0,462	0,956	2,563	1,412	3,902	1,648	1,075	0,958	0,660	1,444	0,511	1,411	0,672	0,762	0,268	0,000
GSTP1_HUMAN	0,750	1,061	1,214	0,812	1,256												
GTF2I_HUMAN	0,361	1,726	2,474	0,853	0,821	1,927	0,945	1,070	1,988	0,216	1,723	1,050	0,771	0,414	0,787	0,395	7,841
GTR1_HUMAN	0,311	1,646	0,955	1,821	1,111	0,222	1,167	0,956	1,522	6,853	1,158	0,426	0,597	0,635	3,398	1,115	1,924
GUAA_HUMAN	0,294	1,799	1,498	0,998	1,329	0,000	1,489	1,600	3,016	1,510	1,517	1,646	1,748	1,349	0,971	0,287	0,115
H12_HUMAN						0,098	0,397	1,127	1,402	0,681	5,752	0,767	1,082	1,402	1,451	2,532	0,667
H14_HUMAN	0,327	0,528	1,111	1,212	4,022												
H15_HUMAN	0,172	0,624	1,356	1,427	4,849	0,021	0,535	1,390	1,687	1,084	2,644	0,963	1,178	1,841	3,015	2,904	0,611
H1X_HUMAN						3,631	0,042	1,233	3,059	0,197	17,059	0,443	0,690	1,490	2,399	7,113	0,094
H2A2C_HUMAN	0,055	1,271	3,657	1,739	3,319	0,035	0,506	5,514	1,763	1,495	0,007	2,735	2,531	2,366	2,702	2,729	2,609
H2A3_HUMAN	0,000	0,488	0,370	1,599	3,334												
H2AX_HUMAN	0,266	0,871	0,945	1,725	2,541	0,053	0,120	2,223	1,273	1,134	1,986	1,958	1,576	1,149	2,324	1,961	1,982
H2AY_HUMAN	0,155	0,726	1,463	2,084	4,501	0,029	0,215	2,427	2,719	3,787	7,461	0,300	0,199	1,081	7,645	1,209	1,666
H2AZ_HUMAN	0,434	0,380	2,869	2,913	5,759	1,563	0,216	14,656	8,857	1,548	0,495	0,100	0,354	6,910	0,691	0,580	0,153
H2B2E_HUMAN						0,875	0,279	1,330	0,969	0,857	0,050	1,699	1,224	1,277	1,596	1,697	1,401
H2BFS_HUMAN	0,189	0,775	1,767	1,038	3,757	0,080	0,313	1,387	0,961	0,949	1,323	1,515	1,798	1,488	1,773	2,216	2,065
H31_HUMAN	0,291	1,192	0,360	3,006	2,858												
H32_HUMAN	0,321	0,933	2,895	0,668	2,375	1,028	0,433	1,292	0,973	0,788	0,883	1,476	1,038	0,949	1,307	1,248	1,176
H33_HUMAN	0,558	0,871	2,367	0,989	1,296												
H4_HUMAN	0,242	1,101	1,535	0,975	2,622	0,222	0,170	1,325	1,186	1,190	1,234	1,341	1,904	0,922	1,890	1,666	1,550
HAT1_HUMAN	1,080	0,674	1,250	0,750	1,494												
HBA_HUMAN	1,327	0,744	0,915	1,273	1,057												
HCD2_HUMAN	1,368	0,810	0,932	2,898	0,873												
HCDH_HUMAN	1,597	0,507	0,587	1,630	1,024												
HMGA1_HUMAN	0,072	1,026	2,688	0,882	5,725	0,000	0,008	2,063	1,605	0,705	0,786	2,414	1,830	1,802	2,069	2,128	2,037
HMGB1_HUMAN	0,118	1,145	1,832	2,379	1,844	0,000	0,075	1,622	3,196	1,625	0,190	1,792	0,713	0,689	1,097	1,994	4,236
HMGB2_HUMAN						0,000	0,352	0,588	1,433	0,840	0,000	1,883	1,825	0,473	1,377	1,667	1,095
HMGN1_HUMAN						0,000	0,000	0,000	0,508	0,245	2,070	0,144	1,659	1,990	2,003	2,971	1,280
HNRDL_HUMAN	0,346	0,797	2,156	0,556	3,165	0,164	1,380	1,960	2,204	1,218	0,012	1,926	1,719	1,711	1,493	2,048	1,992
HNRH1_HUMAN	0,270	0,816	2,247	1,517	1,605												

HNRH2_HUMAN						0,091	0,918	1,155	1,377	1,630	0,858	1,396	1,528	1,683	1,885	0,772	1,049
HNRH3_HUMAN	0,863	0,801	1,015	0,894	1,617												
HNRL1_HUMAN	0,000	0,566	1,411	1,714	1,074												
HNRL2_HUMAN						0,000	2,121	0,808	0,496	0,266	1,999	8,274	0,826	0,601	0,859	0,696	0,000
HNRPC_HUMAN	0,622	0,732	1,424	0,940	1,703	0,184	0,878	1,252	1,302	0,855	2,128	1,527	1,273	1,411	1,291	1,122	0,668
HNRPD_HUMAN	0,499	1,103	1,444	0,820	1,487	0,195	1,990	1,245	0,777	0,834	596,003	0,003	2,579	0,796	0,678	0,783	2,914
HNRPF_HUMAN	0,559	0,948	1,612	0,799	1,669												
HNRPK_HUMAN	0,553	0,972	1,404	1,051	1,282	0,136	0,761	1,363	1,388	1,240	1,660	1,306	1,072	1,166	1,296	1,474	0,647
HNRPL_HUMAN	0,311	0,940	1,731	1,513	1,435	0,169	1,724	2,910	1,601	0,948	1,441	1,524	1,647	2,249	1,235	1,468	0,159
HNRPM_HUMAN	0,417	0,869	1,705	1,178	1,405	0,324	0,514	1,522	2,328	1,463	2,076	1,128	0,774	1,199	1,848	1,599	0,196
HNRPQ_HUMAN	1,224	0,937	0,979	0,949	0,942												
HNRPR_HUMAN	0,213	0,552	3,213	1,384	2,277	61,345	0,813	10,018	0,611	0,247	16,227	0,048	0,159	0,117	1,043	0,861	0,363
HNRPU_HUMAN	0,518	0,936	1,450	1,003	1,392	0,126	0,696	1,750	1,641	1,094	3,589	0,503	1,615	1,202	1,631	1,440	0,378
HORN_HUMAN	0,919	0,978	1,049	0,893	1,171	0,128	0,000	1,466	0,830	1,908	2,038	0,617	2,453	0,907	1,178	0,896	0,989
HP1B3_HUMAN	0,762	0,413	0,808	2,977	1,851	0,460	0,132	0,895	2,401	3,826	3,121	0,149	0,480	1,395	8,995	3,471	0,076
HPT_HUMAN	1,467	1,160	0,664	0,624	1,381												
HS90A_HUMAN	0,874	1,040	0,987	1,171	0,989	0,205	1,400	2,018	2,305	2,327	0,409	1,412	0,524	0,465	2,035	0,797	1,496
HS90B_HUMAN	0,962	1,044	1,077	0,935	1,030	2,523	1,095	1,000	0,924	0,889	0,984	0,971	0,896	0,857	0,847	0,724	1,172
HSDL2_HUMAN	1,140	0,000	0,664	1,436	0,879												
HSP7C_HUMAN	0,704	1,198	1,162	1,168	0,863	1,130	0,955	0,945	1,057	0,855	1,175	1,057	0,974	0,927	1,065	0,793	1,247
HSPB1_HUMAN	1,034	1,272	1,132	0,733	0,991	0,074	1,318	1,182	1,178	1,319	2,853	1,106	1,373	1,402	0,488	1,211	1,544
HUTH_HUMAN	1,352	1,435	0,203	2,377	1,016												
IF2A_HUMAN						0,000	0,462	0,000	0,000	0,000	5,445	0,000	0,000	1,004	0,397	0,000	0,000
IF2B2_HUMAN	0,646	1,152	1,617	1,274	0,648												
IF2G_HUMAN	1,401	1,224	0,686	2,214	1,423												
IF4A1_HUMAN	1,572	0,787	0,984	0,946	0,852	1,058	2,991	0,414	1,918	1,265	1,324	0,951	0,630	0,964	0,622	0,533	1,124
IF4A3_HUMAN	0,545	0,621	0,891	1,744	1,869	0,021	0,428	0,774	1,420	1,542	19,897	1,567	1,072	1,113	2,593	0,964	0,381
IF4B_HUMAN	0,595	0,000	2,702	1,630	0,474												
IF4G1_HUMAN	1,132	2,196	1,820	2,575	1,478												
IF4H_HUMAN	0,808	0,438	0,870	1,827	2,320	0,551	1,587	5,790	6,600	2,348	0,120	2,574	0,000	0,108	0,616	2,734	0,308
IF5_HUMAN	2,245	0,330	0,856	1,687	0,907												
IF5A1_HUMAN	0,833	1,025	1,461	0,688	1,142												
IF5AL_HUMAN						0,157	3,989	0,697	0,780	0,578	1,237	1,530	0,821	0,642	0,491	0,955	1,778

IF6_HUMAN	0,716	1,156	0,626	2,571	0,688												
IGHG1_HUMAN						245,376	0,302	0,500	89,32	0,260	0,573	0,276	0,312	0,427	0,569	0,144	0,187
IKIP_HUMAN	0,767	0,000	0,000	1,645	0,829												
ILF2_HUMAN	0,651	0,890	1,378	0,619	1,991	0,000	0,663	1,102	1,161	1,822	1,355	0,377	0,638	0,535	1,817	2,243	1,145
ILF3_HUMAN	0,679	0,818	1,354	0,919	1,465	0,144	2,159	2,712	1,624	1,674	0,266	1,166	1,935	2,306	3,067	3,128	0,086
IMA2_HUMAN	0,359	1,065	1,008	4,120	0,629												
IMA7_HUMAN	0,885	1,131	1,737	0,815	0,740												
IMB1_HUMAN	1,311	1,140	0,988	0,848	1,003												
IMDH2_HUMAN	4,062	0,885	0,499	0,480	1,112	6,009	3,086	0,779	0,692	1,054	1,719	1,414	1,363	0,354	0,197	0,819	0,490
INF2_HUMAN	3,056	0,355	1,023	1,155	0,810												
IPO5_HUMAN	1,568	3,397	0,979	0,744	0,685												
IPO7_HUMAN	0,680	0,714	0,747	1,812	1,826												
IPO9_HUMAN	0,642	0,567	1,821	1,538	1,144												
IQGA1_HUMAN	1,045	0,710	1,029	1,137	1,156	0,399	3,530	1,971	0,477	1,806	0,971	0,490	2,388	1,069	0,887	1,111	0,941
ITB1_HUMAN	1,291	1,561	0,318	1,139	1,270	0,254	2,767	1,939	1,075	0,427	0,851	0,623	1,454	1,116	1,369	2,674	1,183
K121P_HUMAN	0,000	0,000	29,327	0,000	0,032												
K1C10_HUMAN	1,258	1,968	0,590	1,102	0,625	4,301	1,266	0,759	0,984	1,346	0,901	1,019	1,074	0,572	0,808	0,363	0,819
K1C12_HUMAN	2,279	0,441	2,287	0,382	1,159												
K1C13_HUMAN	1,647	0,946	1,617	0,736	0,550	0,341	13,39	5,210	9,172	0,582	0,863	0,354	0,000	0,000	0,024	0,000	0,000
K1C14_HUMAN	1,406	1,448	0,491	0,899	1,029	4,421	1,079	0,426	1,353	1,885	0,088	1,841	1,297	1,151	1,259	0,461	1,146
K1C16_HUMAN	1,076	2,334	0,498	0,751	1,014	3,831	0,619	0,736	0,806	1,251	0,559	1,134	0,941	0,970	1,190	0,436	1,233
K1C17_HUMAN	1,467	0,707	0,385	2,335	1,069	13,115	0,471	0,718	0,658	0,748	0,880	1,641	1,117	0,773	0,985	0,419	0,781
K1C18_HUMAN	1,075	0,464	1,527	2,267	0,899	0,133	1,683	0,569	0,895	1,280	0,621	1,333	0,967	1,161	1,330	1,237	1,994
K1C24_HUMAN	7,438	0,137	4,034	0,429	1,038												
K1C9_HUMAN	1,414	1,313	0,935	0,865	0,681	3,617	0,902	1,076	0,975	1,388	1,090	0,951	1,115	0,690	0,693	0,456	0,710
K1H1_HUMAN	4,096	0,262	14,814	3,165	0,269	0,000	0,122	0,082	0,318	2,168	64,017	0,990	2,374	0,905	1,296	0,327	0,000
K22E_HUMAN	1,194	1,485	0,664	1,165	0,734	4,324	0,917	1,053	0,812	1,273	0,898	0,839	1,295	0,740	0,904	0,374	0,941
K2C1_HUMAN	1,325	1,555	0,732	1,034	0,642	4,125	1,013	1,074	1,112	1,454	0,800	0,951	1,008	0,577	0,959	0,359	0,867
K2C1B_HUMAN	1,582	1,145	0,579	1,626	0,599	2,255	1,271	0,838	0,554	12,744	118,012	0,530	0,444	0,308	0,464	0,095	0,126
K2C3_HUMAN	1,575	2,148	0,416	0,831	1,069	0,000	1,856	0,000	0,159	0,337	0,605	0,000	0,000	0,000	4,244	1,626	0,991
K2C4_HUMAN	1,451	1,042	0,720	0,999	1,093	5,068	2,457	1,255	2,477	0,922	0,281	0,000	0,000	0,244	0,000	0,287	0,000
K2C5_HUMAN	1,403	1,912	0,637	0,873	0,652	6,500	1,045	0,713	0,914	1,195	1,225	0,894	1,079	0,685	0,732	0,362	0,897
K2C6A_HUMAN	1,431	2,230	0,448	2,141	0,530	9,171	1,023	0,814	1,291	0,842	0,813	1,223	0,847	0,625	0,885	0,365	0,568

K2C6B_HUMAN	1,738	2,169	0,207	1,538	0,866												
K2C73_HUMAN	1,004	0,000	0,000	1,013	1,039												
K2C74_HUMAN	0,000	0,000	0,000	0,739	1,354												
K2C78_HUMAN	1,611	1,869	0,489	1,133	0,631	3,624	3,750	0,826	2,056	3,198	0,239	0,833	2,419	0,289	1,444	0,261	0,185
K2C8_HUMAN	0,945	0,937	1,037	0,944	1,153	0,657	2,346	0,349	0,307	0,928	0,732	0,796	1,628	1,063	1,150	1,482	2,834
K2C80_HUMAN	1,779	1,871	0,511	1,603	0,676												
KCY_HUMAN	0,838	1,566	0,992	0,538	1,413												
KHDR2_HUMAN						0,802	0,474	0,129	1,801	1,431	1,988	1,373	1,160	2,260	1,000	1,661	0,606
KI21B_HUMAN						0,000	0,512	1,419	0,770	0,000	0,000	0,000	0,000	1,833	0,000	1,002	0,000
KI67_HUMAN						0,000	1,017	0,245	0,287	2,088	1,736	0,000	0,525	1,285	1,553	7,692	0,441
KIF4A_HUMAN	1,575	1,851	1,106	0,449	0,933												
KINH_HUMAN						0,000	3,305	1,018	0,820	1,191	0,000	0,416	0,348	1,372	1,138	1,106	1,295
KMT2D_HUMAN						0,464	1,933	1,684	1,986	1,644	2,225	2,781	0,305	0,114	1,594	0,982	0,669
KPYM_HUMAN	1,131	0,881	0,889	1,110	1,019	3,042	0,858	0,983	1,121	0,831	0,934	1,241	0,860	0,682	0,919	0,708	1,045
KR111_HUMAN	0,166	0,662	9,324	0,000	0,000	7,096	36,30	0,150	0,331	0,000	0,293	22,749	0,000	0,000	0,013	0,000	0,000
KRA31_HUMAN	0,496	0,000	0,000	2,063	0,000												
KRA33_HUMAN	0,956	0,214	0,000	6,196	0,000												
KRT34_HUMAN	2,328	2,443	1,218	0,581	0,588												
KRT35_HUMAN	0,251	0,162	24,456	0,481	0,000	0,000	0,042	0,000	0,105	4,883	9,933	0,075	4,599	4,110	5,903	5,186	0,109
KRT36_HUMAN	0,062	0,418	37,201	0,065	0,000	3,737	0,101	0,000	7,976	2,834	0,933	148,928	0,146	0,103	0,077	0,000	0,477
KRT81_HUMAN	0,863	0,000	0,000	1,159	0,000												
KRT82_HUMAN	0,582	0,425	307,778	0,180	0,276												
KRT83_HUMAN	1,162	0,124	8,341	0,889	0,000	0,794	0,073	0,999	17,85	5,594	2,868	203,32	0,253	0,282	0,144	0,243	0,145
KRT84_HUMAN	6,802	0,824	0,724	0,205	1,540	0,882	50,57	0,173	0,198	0,089	13,825	0,321	6,566	0,165	0,351	0,339	9,929
KRT85_HUMAN	4,449	0,446	0,934	3,437	0,177												
KRT86_HUMAN	5,512	1,330	0,078	4,590	0,381												
KT33A_HUMAN	0,000	0,000	0,382	2,801	0,000	2,368	0,221	0,048	7,182	0,351	1,176	224,57	1,103	0,362	0,223	1,104	0,885
KT33B_HUMAN	3,672	0,000	0,000	1,655	0,362												
LA_HUMAN	0,230	1,243	1,893	1,184	2,624												
LAC3_HUMAN						0,912	0,000	0,000	13,43	0,000	0,000	0,000	0,000	0,102	0,000	0,000	0,000
LAP2A_HUMAN						0,000	0,768	0,296	4,858	0,000	7,606	0,155	0,442	2,078	3,543	0,800	0,209
LAP2B_HUMAN	0,669	0,239	1,776	1,098	3,267	0,000	0,469	0,622	1,086	1,170	1,678	0,896	0,331	0,624	2,374	1,456	0,866
LDH6B_HUMAN	0,541	1,676	1,216	0,554	1,546												

LDHA_HUMAN	1,063	1,067	0,886	0,782	1,217	3,477	0,937	0,941	0,947	0,603	0,603	1,303	0,910	1,213	0,765	0,784	1,210
LDHB_HUMAN	1,351	0,668	0,749	1,336	1,142	3,638	1,168	2,740	1,981	0,508	0,036	1,227	0,614	2,539	1,132	1,552	0,877
LEG7_HUMAN	0,666	38,89	0,131	0,193	0,402												
LIPB2_HUMAN	2,352	0,078	2,425	1,409	1,553												
LMNA_HUMAN	0,375	0,743	1,349	1,156	2,478	0,094	0,728	0,980	1,271	1,381	2,191	0,877	1,031	1,104	2,354	1,547	1,048
LMNB1_HUMAN	0,228	0,686	0,777	1,961	4,611	0,107	0,743	0,749	2,027	2,251	3,383	0,335	0,708	0,896	4,048	2,260	0,953
LMNB2_HUMAN	5,720	0,359	5,940	0,031	5,918	0,336	0,357	0,675	1,441	2,459	1,714	0,216	0,760	1,042	5,086	1,999	0,556
LONM_HUMAN	0,708	0,000	0,000	3,148	0,266												
LPPRC_HUMAN	1,228	0,641	0,815	1,592	0,976												
LRC59_HUMAN	1,498	0,345	1,012	2,119	0,941												
LST2_HUMAN						0,000	5,960	0,502	0,877	0,431	0,787	0,000	0,000	0,604	0,726	1,690	0,000
MAD3_HUMAN	0,718	1,023	1,224	0,813	1,370												
MAP1B_HUMAN						0,000	3,532	0,698	0,358	1,367	0,338	0,751	0,000	0,817	0,402	1,591	1,216
MAP4_HUMAN	1,231	1,038	0,830	1,472	0,760												
MATR3_HUMAN	0,677	0,960	1,227	0,839	1,492	0,000	0,696	0,884	0,948	0,811	1,057	1,346	1,186	1,039	1,068	1,290	0,860
MBB1A_HUMAN	0,000	1,446	1,062	0,890	0,912												
MCCA_HUMAN	0,984	0,898	0,834	1,493	0,907	0,694	0,506	0,738	1,813	0,674	1,146	0,563	0,942	1,647	1,897	0,747	2,208
MCCB_HUMAN	0,832	0,966	1,023	1,511	0,845												
MCM2_HUMAN	0,231	2,490	3,131	0,935	1,128	9,695	1,518	7,362	1,939	0,189	0,724	1,610	0,769	0,811	0,178	0,531	0,465
MCM3_HUMAN	0,296	1,858	2,550	0,674	1,118	0,000	8,366	10,442	6,297	0,181	0,945	0,568	1,206	1,399	0,377	0,269	0,151
MCM4_HUMAN	0,653	2,447	2,926	0,592	0,567	5,016	1,277	13,241	0,987	0,406	0,470	0,794	0,363	0,483	0,475	0,000	0,000
MCM5_HUMAN	0,000	1,796	2,111	0,547	0,475	21,721	1,149	6,540	1,958	0,417	2,542	0,669	1,938	3,283	0,300	0,297	0,121
MCM6_HUMAN	0,225	1,351	2,393	1,004	1,282	0,000	5,016	1,128	4,415	0,389	2,359	1,814	1,102	0,522	0,149	0,304	0,000
MCM7_HUMAN	0,191	2,548	3,141	0,887	0,915	0,000	0,000	1,756	0,495	0,963	0,185	2,184	0,831	1,267	1,915	1,484	0,000
MDHM_HUMAN	1,181	0,845	0,562	1,523	1,284	1,935	0,276	0,777	0,800	0,415	0,649	0,707	1,497	10,83	0,220	0,186	23,170
MIF_HUMAN	1,259	1,149	1,160	0,615	0,970												
ML12B_HUMAN	1,252	1,107	1,164	0,525	1,159												
MMS19_HUMAN	1,540	0,405	1,219	2,728	0,515												
MMS22_HUMAN	0,000	0,901	5,910	1,125	0,155												
MOES_HUMAN	1,057	1,036	0,929	1,022	0,889	0,325	1,491	0,844	0,856	1,289	0,910	1,427	1,068	0,888	1,819	1,514	0,738
MORC1_HUMAN	4,738	0,375	0,097	9,436	0,618												
MPCP_HUMAN						0,000	0,985	0,000	0,977	0,746	1,445	0,000	0,000	0,000	0,973	1,051	0,933
MPPA_HUMAN	2,863	0,454	0,281	1,915	1,884												

MSH2_HUMAN	0,178	4,361	4,641	0,865	0,339	45,922	5,831	1,457	0,139	1,787	16,220	0,096	2,857	0,094	0,096	0,050	13,476
MSH6_HUMAN	0,163	6,533	7,553	0,398	0,313	0,000	3,837	3,926	1,812	0,130	0,764	17,531	2,102	1,559	0,170	0,161	0,141
MT2_HUMAN	0,454	0,974	1,563	0,918	1,630												
MYH10_HUMAN						0,356	3,143	0,957	0,227	1,022	1,131	0,413	0,276	0,706	1,465	4,865	2,889
MYH9_HUMAN	1,348	0,810	1,121	0,835	0,963	0,646	1,354	0,684	0,602	0,848	0,652	0,769	1,103	1,073	1,148	1,934	2,496
MYL6_HUMAN	1,328	1,118	1,122	0,497	1,216	1,863	0,793	1,535	0,907	0,740	0,179	1,564	0,972	0,848	0,941	1,267	1,976
MYO1C_HUMAN	3,818	0,310	1,567	0,736	0,783												
MYOF_HUMAN	0,982	0,845	1,295	0,821	1,048	0,755	3,512	0,762	0,364	1,863	0,363	0,189	1,274	1,609	0,517	1,580	4,001
NAA16_HUMAN						0,000	0,312	0,315	4,840	0,493	2,514	1,389	2,242	1,122	2,653	1,591	0,125
NACA_HUMAN	1,663	0,241	1,036	1,783	1,446												
NAR4_HUMAN	1,379	0,952	1,323	0,584	0,930	27,536	5,141	9,552	0,145	0,051	11,745	0,276	2,245	1,530	0,053	0,000	0,131
NASP_HUMAN						0,000	2,085	1,303	7,405	0,210	3,528	0,733	1,379	0,219	1,898	0,157	0,000
NC2A_HUMAN	0,000	0,604	1,194	0,711	1,847												
NDC1_HUMAN						0,000	0,320	1,641	0,782	0,843	0,551	1,987	0,929	0,773	1,116	0,596	1,734
NDKB_HUMAN						1,813	1,071	2,126	1,107	1,067	0,205	1,697	1,007	1,268	0,650	0,791	2,086
NDUA9_HUMAN	0,470	0,360	0,000	2,393	2,631												
NDUAA_HUMAN	1,591	0,359	0,884	1,356	1,332												
NFIC_HUMAN	0,959	0,000	0,000	0,000	1,080												
NFIX_HUMAN						0,000	0,457	0,870	5,532	0,493	9,428	1,086	0,518	0,587	0,505	0,588	0,000
NOLC1_HUMAN	0,294	0,789	2,214	0,849	2,251												
NONO_HUMAN	0,525	1,143	1,620	1,085	1,053	0,000	0,868	0,459	2,632	1,381	1,753	1,622	0,459	0,824	1,597	1,813	0,173
NOP56_HUMAN	0,738	0,873	1,993	1,241	0,613												
NP1L1_HUMAN	1,342	0,447	1,747	0,934	1,005												
NPM_HUMAN	0,473	0,728	1,649	0,757	2,579	0,428	1,020	0,936	1,999	0,993	0,836	2,284	0,782	0,987	1,384	3,800	0,181
NQO1_HUMAN						0,000	0,245	0,532	0,270	1,941	0,376	1,047	1,486	5,540	0,678	5,680	1,076
NSUN2_HUMAN						0,000	0,606	0,863	0,757	0,749	19,691	0,898	0,000	0,000	0,599	0,374	0,000
NTKL_HUMAN	4,773	67,30	0,071	0,126	0,344												
NUCL_HUMAN	0,521	0,994	1,416	0,948	1,411	0,128	1,614	1,353	1,465	0,913	3,561	0,933	1,049	1,427	1,289	2,406	0,164
NUMA1_HUMAN						5,895	0,894	0,557	1,387	0,473	2,616	1,080	0,834	1,106	1,256	0,791	0,224
OAT_HUMAN	1,294	0,513	0,651	2,392	1,134	0,000	0,771	0,567	0,526	0,707	0,000	2,972	1,529	0,853	0,699	0,000	2,149
ODO2_HUMAN	0,839	0,962	1,177	1,621	0,970												
ODP2_HUMAN	3,335	0,838	0,541	1,710	0,363												
ODPA_HUMAN	0,000	0,000	0,000	1,000	0,000												

OLA1_HUMAN	1,236	1,055	0,790	0,915	0,969												
OST48_HUMAN	1,433	0,724	0,719	0,962	1,402	0,332	0,746	0,900	1,892	3,192	0,143	2,777	0,745	1,283	2,238	1,434	0,775
P5CR1_HUMAN	2,148	0,498	0,194	2,926	1,747												
P5CS_HUMAN	1,444	0,814	0,747	1,677	0,679	0,216	1,283	0,438	0,244	2,361	0,228	0,961	4,018	2,918	3,068	0,569	1,084
P63_HUMAN						3,142	0,996	1,337	0,984	2,159	0,001	3,678	3,514	2,551	1,116	1,636	2,817
P66B_HUMAN						0,000	0,896	1,078	0,915	1,819	16,166	1,436	0,860	0,531	0,208	0,804	0,434
PA2G4_HUMAN	1,115	0,922	0,727	0,915	1,377												
PABP1_HUMAN	1,466	0,981	0,859	1,012	0,822												
PABP3_HUMAN						0,957	0,825	0,583	1,030	3,535	0,481	0,627	0,538	0,667	4,125	1,435	0,835
PAIRB_HUMAN	1,647	0,946	1,596	0,695	1,180	0,168	0,000	1,779	1,474	2,221	0,993	2,576	1,236	0,770	1,464	1,708	0,161
PAPS1_HUMAN	0,095	1,746	2,619	1,732	1,247												
PAPS2_HUMAN	0,211	1,756	1,488	1,291	1,435												
PARP1_HUMAN	0,082	1,612	2,893	1,369	2,329	0,000	0,541	2,666	1,604	0,588	5,355	1,988	0,290	1,206	0,802	1,652	0,126
PCBP1_HUMAN	1,314	0,703	1,592	0,982	1,422	0,830	1,008	1,577	1,260	0,764	2,770	0,803	0,724	0,866	0,782	0,749	0,843
PCBP2_HUMAN	1,006	0,929	1,262	0,733	1,191												
PCCA_HUMAN	0,891	1,352	0,541	2,304	0,732	2,132	0,351	0,774	0,474	0,790	0,506	3,086	1,437	1,263	1,039	0,882	1,847
PCCB_HUMAN	0,941	1,320	0,685	1,459	0,823	1,250	0,773	0,689	0,655	1,073	0,377	2,741	0,937	1,886	1,689	0,694	0,656
PCNA_HUMAN	0,153	4,155	3,500	1,127	0,363	0,070	4,351	4,735	3,487	0,210	0,666	18,856	3,790	2,967	0,463	0,249	0,052
PDC6I_HUMAN	1,026	0,967	0,735	1,506	1,158												
PDCD4_HUMAN						0,000	1,597	0,000	0,000	0,000	0,970	0,931	1,064	1,027	0,486	0,000	0,773
PDE12_HUMAN	0,312	0,000	0,919	2,452	1,221												
PDIA1_HUMAN						0,000	1,311	0,411	1,756	0,000	1,192	0,000	0,000	0,000	1,283	0,791	0,871
PDIA3_HUMAN	2,558	0,239	0,907	1,548	1,196												
PDLI1_HUMAN						0,370	6,103	0,270	0,313	6,247	2,034	0,374	0,216	0,302	0,700	9,452	1,556
PDLI5_HUMAN	0,000	1,671	1,160	1,075	0,000					0,512							
PDLI7_HUMAN						0,000	2,153	0,789	0,617	0,921	0,959	0,688	1,526	1,150	0,833	2,500	0,573
PDS5B_HUMAN	0,000	0,806	1,927	0,771	0,815												
PGK1_HUMAN	0,745	0,954	0,837	1,017	2,070												
PHB_HUMAN	1,357	0,716	0,954	1,003	1,095	1,584	0,714	1,462	3,414	1,547	13,723	4,851	0,202	0,186	0,366	0,937	0,473
PHB2_HUMAN	1,402	0,691	0,830	1,107	1,093	0,488	1,073	0,905	0,981	0,535	0,655	1,949	0,412	2,109	2,056	2,971	0,678
PLAK_HUMAN	1,497	3,066	0,567	0,838	0,552												
PLEC_HUMAN						1,143	6,604	0,496	0,914	2,106	0,659	0,357	0,720	1,265	0,391	1,199	1,206
PML_HUMAN						0,000	0,631	1,402	0,723	1,313	3,125	0,440	0,904	0,644	2,470	1,410	0,718

PNMA2_HUMAN	2,512	0,709	0,620	1,623	0,557												
PP1G_HUMAN	0,915	0,864	0,936	0,729	1,851												
PP1R7_HUMAN	1,456	0,228	0,912	1,414	2,393												
PPIA_HUMAN	0,855	1,069	1,237	0,686	1,264	1,655	0,863	1,041	0,847	0,654	1,029	1,575	1,255	1,101	0,722	0,676	1,208
PPIB_HUMAN						0,661	1,226	1,242	0,580	0,705	1,189	0,656	1,055	0,825	0,451	1,523	4,458
PPM1G_HUMAN						0,000	0,000	2,361	1,697	0,403	2,949	2,039	0,281	0,361	1,326	0,914	0,000
PPR18_HUMAN						0,000	1,548	0,612	0,557	0,477	1,882	0,614	1,912	1,060	0,751	1,499	1,429
PPR35_HUMAN	0,196	0,151	5,923	2,230	3,372												
PRDX1_HUMAN	1,074	1,083	1,055	0,751	1,103	4,807	0,669	0,788	0,878	0,545	4,802	0,874	0,686	0,587	0,492	0,560	1,414
PRDX2_HUMAN	0,970	0,873	0,975	1,243	1,230												
PRDX3_HUMAN	0,736	0,761	1,272	2,223	1,109	3,385	1,991	0,743	0,741	1,042	0,188	1,461	1,274	1,831	0,691	0,904	3,131
PRI2_HUMAN	0,091	7,797	9,402	1,011	0,177	0,000	0,000	1,671	0,532	0,000	0,000	1,697	0,847	0,749	0,000	0,000	0,000
PRKDC_HUMAN	0,286	1,303	2,539	0,729	1,537	1,625	1,548	1,484	1,428	0,944	1,062	0,929	1,294	1,780	1,254	0,891	0,219
PROF1_HUMAN	0,886	1,583	1,064	0,689	0,950	2,053	0,474	1,093	0,833	0,946	1,155	1,587	0,985	0,359	0,554	1,474	0,973
PRP8_HUMAN	0,349	0,680	3,779	1,421	1,471												
PRS6B_HUMAN	1,090	2,559	1,182	0,980	0,732												
PRS8_HUMAN	0,589	1,399	0,942	2,064	0,553												
PSA1_HUMAN						0,573	1,087	2,933	2,293	0,932	0,551	3,556	0,528	1,023	1,271	1,188	0,156
PSA2_HUMAN	0,514	0,774	0,825	1,675	1,828												
PSA4_HUMAN	4,489	0,746	1,086	0,195	1,435	0,663	2,233	0,566	2,669	1,624	0,433	0,314	0,365	3,395	0,795	1,626	0,532
PSA6_HUMAN	1,028	1,189	0,829	2,653	0,888	0,134	1,737	2,044	2,282	1,896	0,039	2,648	0,635	1,313	1,144	1,451	2,080
PSA7_HUMAN	0,846	0,847	1,098	2,145	1,520												
PSB3_HUMAN	0,744	1,284	0,820	0,907	1,486												
PSB5_HUMAN	0,463	0,845	1,382	1,839	1,454												
PSB6_HUMAN	0,965	1,199	0,676	1,008	1,310	0,153	2,771	3,729	3,585	0,828	2,410	0,978	0,162	0,720	1,907	0,185	2,124
PSD12_HUMAN	0,838	1,347	0,956	0,937	1,048												
PSDE_HUMAN	0,703	0,000	0,574	1,152	2,268	0,000	1,410	1,769	1,497	1,620	0,427	0,509	0,145	2,377	1,059	0,674	0,928
PSIP1_HUMAN	0,000	0,134	1,307	1,528	3,897	0,000	0,000	0,992	0,867	0,819	2,224	0,949	1,251	1,418	1,639	1,278	0,164
PSMD1_HUMAN	1,464	0,331	0,949	1,809	1,165												
PSMD2_HUMAN	3,178	0,759	0,785	1,486	1,339	0,711	1,958	0,720	0,683	1,704	2,073	0,569	0,786	1,661	2,483	1,161	0,259
PSMD4_HUMAN	2,063	0,382	0,326	1,945	1,911												
PTBP1_HUMAN	0,545	1,313	1,435	0,836	1,171	0,046	1,179	2,019	1,405	1,526	1,112	1,967	0,967	1,890	1,542	1,442	0,352
PTBP2_HUMAN	0,598	1,150	1,564	1,009	0,919	0,076	1,198	1,793	1,758	1,210	0,301	1,899	1,506	1,883	1,724	1,206	0,639

PTHD1_HUMAN	7,396	0,000	0,637	0,243	0,820												
PUR6_HUMAN	1,157	1,773	1,338	0,845	3,141	2,496	1,000	1,865	1,563	1,659	8,308	0,828	0,482	0,232	1,406	0,182	0,401
PYC_HUMAN	0,925	0,322	0,984	1,854	2,939												
PYGB_HUMAN	2,312	0,653	1,518	0,543	0,806												
QCR1_HUMAN	1,438	0,000	0,205	1,660	1,938	8,345	0,565	0,272	0,377	0,558	0,250	2,033	1,430	3,201	0,971	0,650	11,256
QCR2_HUMAN	1,123	1,886	0,200	2,296	1,106												
RAB10_HUMAN	1,564	0,299	1,199	1,206	1,542												
RAB3B_HUMAN	0,368	0,352	2,213	1,302	2,893												
RAB5C_HUMAN	1,444	0,878	0,995	0,994	0,801												
RALY_HUMAN						0,000	0,814	4,417	6,282	0,891	2,957	0,241	0,325	0,451	0,544	0,832	0,000
RALYL_HUMAN	0,200	0,363	3,051	1,430	3,120												
RAN_HUMAN	0,258	1,347	1,486	1,135	1,805	1,639	0,090	7,960	0,565	8,221	0,396	1,916	0,787	0,000	0,000	1,825	0,267
RBBP7_HUMAN	21,543	0,201	0,615	0,847	0,462												
RBM14_HUMAN	0,558	0,844	1,733	0,600	1,906	0,000	0,643	0,884	1,230	1,324	0,200	0,538	1,579	2,173	2,396	2,054	0,711
RBMX_HUMAN	0,285	0,623	1,736	1,370	2,334												
RCC1_HUMAN						0,000	1,593	0,248	3,131	0,856	4,134	0,701	0,283	1,398	1,412	1,173	1,190
RCC2_HUMAN						0,000	0,200	4,042	1,525	1,868	4,484	0,549	0,419	0,599	3,316	0,662	0,138
RECQ1_HUMAN	0,159	1,837	2,468	0,815	1,721	0,000	1,610	1,593	2,165	1,041	0,442	0,956	0,502	1,587	1,882	0,698	0,250
CD33_HUMAN						0,225	0,065	0,680	2,810	1,736	70,431	2,052	1,638	1,998	2,133	1,402	0,031
CP250_HUMAN						11,715	0,025	2,057	0,281	5,554	115,423	0,052	9,316	0,604	0,014	0,290	24,014
F184A_HUMAN						0,739	4,086	1,867	1,269	0,292	0,744	0,163	0,271	1,510	2,169	2,494	1,830
GFOD2_HUMAN						0,217	2,562	3,872	3,605	1,477	1,596	1,671	1,011	0,261	2,859	0,976	0,048
HOME3_HUMAN						0,067	0,663	1,679	1,368	0,915	3,155	0,807	1,408	1,373	1,178	1,181	1,037
MOD5_HUMAN						0,666	0,304	3,448	0,180	3,012	2,156	0,456	1,169	1,471	0,717	3,272	0,656
NLRC3_HUMAN						0,290	0,000	0,613	1,319	0,888	0,692	4,240	1,304	1,857	1,648	0,976	0,544
PCM1_HUMAN						1,330	0,092	0,554	1,857	0,634	1,812	2,006	1,727	1,417	0,696	4,113	0,487
PCY2_HUMAN						1,136	0,383	1,120	0,716	1,336	1,272	0,109	2,489	2,394	1,162	1,573	1,639
RGS13_HUMAN						2,604	1,236	0,816	0,752	0,911	0,839	1,059	1,051	0,847	0,709	0,891	1,239
RNF8_HUMAN						0,000	1,189	0,822	2,104	1,014	2,686	0,386	0,448	0,456	0,976	1,736	1,475
TITIN_HUMAN						0,000	17,62	1,249	0,589	0,492	0,584	0,000	0,000	0,494	0,537	1,277	0,758
UBP19_HUMAN						0,078	1,463	2,030	0,446	1,321	0,510	0,402	1,707	2,601	1,567	1,937	2,280
VP37A_HUMAN						1,302	1,378	0,955	0,889	0,834	0,919	1,070	1,026	0,981	0,982	0,691	1,186
WNK1_HUMAN						63,303	0,280	25,905	0,236	0,113	0,253	7,002	0,271	0,180	0,128	0,131	59,150

ZW10_HUMAN						0,000	0,392	0,000	3,697	0,747	0,000	0,866	0,808	1,613	0,305	3,516	0,926
RFA1_HUMAN	0,000	1,660	2,772	1,334	0,372	28,086	0,336	0,683	2,611	0,743	0,262	1,978	0,755	2,112	1,363	0,182	0,261
RFA2_HUMAN	0,194	1,386	2,925	3,399	1,637	0,000	1,855	1,540	3,339	0,895	0,310	1,148	1,218	4,061	1,597	0,628	0,072
RFC1_HUMAN	0,000	4,751	4,976	0,332	0,144												
RFC2_HUMAN	0,079	8,081	6,037	1,307	0,260	1,070	6,839	0,819	0,385	0,131	1,066	22,784	1,005	8,082	0,194	0,150	0,126
RFC3_HUMAN	0,000	1,972	3,307	0,581	0,276	0,000	0,828	5,606	4,874	0,238	1,272	11,679	0,000	0,000	0,080	0,147	0,000
RFC4_HUMAN	0,332	4,022	3,436	0,590	0,385	0,000	3,846	7,846	5,284	0,060	0,560	14,495	1,981	3,194	0,113	0,150	0,227
RFC5_HUMAN	0,072	4,980	4,173	1,052	0,614	0,000	0,341	3,612	0,890	0,709	0,000	1,302	2,660	0,981	0,766	0,380	0,981
RIF1_HUMAN	0,074	4,923	9,480	0,495	0,818												
RINI_HUMAN	0,714	1,181	1,127	0,936	1,211	0,100	3,225	2,190	3,745	1,580	3,420	0,156	1,167	0,204	0,587	0,981	0,699
RIR2_HUMAN						2,438	6,062	3,355	0,217	1,403	0,365	1,279	1,376	2,496	0,091	1,273	0,118
RL10_HUMAN	1,031	0,762	1,280	0,996	1,007	0,000	0,000	0,000	0,468	1,082	0,000	0,398	0,000	1,575	0,487	6,322	0,000
RL10A_HUMAN	1,098	0,884	1,113	0,978	1,047												
RL11_HUMAN	0,986	1,075	1,088	0,794	1,154	0,221	0,459	0,607	0,496	0,610	278,381	0,685	0,738	0,612	0,578	0,542	1,598
RL12_HUMAN	1,351	1,191	0,854	0,655	1,066	0,863	0,804	1,411	0,828	1,083	0,083	1,470	1,988	1,402	1,043	1,325	2,985
RL13_HUMAN	0,795	0,944	1,012	1,060	1,286	0,312	0,168	0,705	0,725	1,026	0,607	1,325	1,297	1,090	1,190	1,318	5,424
RL13A_HUMAN	0,926	0,985	0,840	1,197	1,334	0,000	0,182	2,612	1,017	1,001	0,133	2,406	1,148	3,542	0,817	1,096	1,918
RL14_HUMAN	0,849	0,984	0,996	0,982	1,289	0,171	0,278	1,140	1,313	0,899	3,846	0,601	0,466	1,480	1,511	1,465	5,868
RL15_HUMAN	0,789	1,002	1,257	0,818	1,277	0,151	0,247	1,728	0,596	1,894	0,696	0,938	1,804	1,179	1,365	2,385	2,965
RL17_HUMAN	0,847	0,945	0,958	1,238	1,093	0,054	0,459	1,255	0,454	2,355	0,715	0,920	1,083	1,495	1,374	2,011	8,443
RL18_HUMAN	0,660	0,910	1,180	1,254	1,198	0,612	0,276	1,382	0,979	1,332	1,134	1,378	1,025	1,081	1,178	1,373	1,629
RL18A_HUMAN	0,757	0,746	1,107	1,332	1,210	0,520	0,296	2,048	0,561	0,958	1,081	1,195	0,616	1,469	1,198	1,619	2,887
RL19_HUMAN	0,662	1,075	1,073	1,080	1,182												
RL1D1_HUMAN	0,660	0,000	0,920	1,272	1,290	0,000	2,162	0,376	1,228	1,341	1,459	0,287	0,476	0,734	2,160	2,727	0,515
RL21_HUMAN	2,137	0,114	5,012	0,436	1,440												
RL22_HUMAN	1,078	1,528	1,072	0,595	1,004												
RL23_HUMAN	0,791	0,605	1,234	1,142	1,272												
RL23A_HUMAN	1,043	0,995	1,007	0,870	1,068												
RL24_HUMAN	0,956	1,104	0,895	1,065	0,979	0,000	0,000	0,353	0,298	4,827	0,085	12,338	0,529	2,319	4,053	5,157	0,121
RL26_HUMAN	1,035	0,995	1,116	0,757	1,217	0,226	1,424	3,604	0,461	0,585	0,507	0,839	3,189	2,445	0,385	0,876	2,699
RL27_HUMAN	1,141	1,301	1,030	0,507	1,266	1,133	0,500	1,310	0,642	1,011	0,046	2,399	2,610	1,959	1,228	1,337	5,557
RL27A_HUMAN	0,858	1,451	0,832	0,878	1,076	2,193	0,402	0,792	0,452	0,664	5,140	1,148	1,066	0,651	0,693	0,661	2,324
RL28_HUMAN	0,755	0,772	1,499	0,945	1,209	0,191	0,103	2,060	1,697	1,321	0,000	1,937	0,000	0,000	2,248	2,464	0,000

RL29_HUMAN	0,953	1,060	0,848	1,212	1,029	0,262	0,377	0,237	0,475	3,941	4,700	0,096	0,105	4,451	4,652	3,812	6,478
RL3_HUMAN	0,903	0,633	1,159	1,295	1,137	0,130	0,737	1,228	0,991	1,039	1,615	1,248	1,250	1,393	1,305	1,275	1,260
RL30_HUMAN	0,999	1,233	1,280	0,596	1,063												
RL31_HUMAN	1,158	0,707	1,357	0,789	1,319												
RL32_HUMAN	0,225	2,293	0,981	2,600	2,538												
RL35_HUMAN	0,528	1,263	1,407	0,877	1,350	2,337	0,406	0,898	0,505	0,844	0,647	1,809	1,501	1,023	0,887	0,948	1,646
RL35A_HUMAN	0,686	0,932	1,983	0,651	1,283												
RL36_HUMAN	0,713	1,147	0,865	2,794	0,761	0,205	0,284	1,223	1,103	2,507	0,159	2,664	1,037	1,517	1,559	3,761	1,164
RL37A_HUMAN	1,024	1,522	1,097	0,661	0,880	0,000	0,000	0,365	0,681	0,311	0,229	4,814	5,249	0,600	1,822	2,472	1,010
RL4_HUMAN	0,819	0,819	1,090	1,285	1,073	0,072	0,793	0,560	0,593	1,305	1,395	0,967	1,678	2,238	1,436	2,121	1,719
RL5_HUMAN	1,046	1,019	0,844	0,978	1,196	1,276	2,466	2,929	2,988	0,925	1,973	0,406	0,947	1,222	0,242	0,386	0,432
RL6_HUMAN	0,895	1,114	1,154	0,692	1,271	1,778	4,979	0,195	0,482	0,738	1,569	0,620	3,727	0,716	1,784	1,227	0,393
RL7_HUMAN	0,931	0,816	1,261	0,925	1,187												
RL7A_HUMAN	0,982	0,763	1,081	1,146	1,034	0,543	0,182	0,604	0,291	0,280	0,726	2,688	2,084	2,987	2,135	2,736	3,488
RL8_HUMAN	0,952	0,724	0,901	1,400	1,168	0,776	0,848	0,899	0,728	0,629	1,251	0,649	2,155	2,293	1,035	0,912	1,511
RL9_HUMAN	1,204	0,510	1,157	1,107	1,207												
RLA0_HUMAN	1,434	0,701	0,919	1,042	1,054	0,759	1,455	0,865	0,805	0,683	0,089	0,782	0,814	2,794	0,825	2,742	4,419
RMXL3_HUMAN						0,028	0,918	1,786	3,580	2,162	5,697	0,141	1,848	1,172	1,906	0,605	0,568
RN166_HUMAN	0,000	4,089	0,780	0,266	0,000												
RO60_HUMAN						0,000	1,669	1,398	0,805	0,952	0,000	0,741	0,739	1,517	0,334	1,025	2,566
ROA0_HUMAN						0,000	0,000	3,099	0,890	0,528	0,456	4,523	0,702	0,811	0,882	1,265	0,564
ROA1_HUMAN	0,758	0,650	1,128	1,146	1,481	0,545	0,559	0,926	1,530	1,170	0,840	1,786	1,044	1,120	1,321	1,591	0,816
ROA2_HUMAN	0,621	0,814	1,370	0,884	1,650	0,136	0,398	1,022	1,112	0,913	1,526	1,906	1,538	1,355	1,406	1,564	1,385
ROA3_HUMAN	0,211	2,181	0,411	1,716	2,976												
ROAA_HUMAN	0,285	0,261	3,573	2,286	2,955	0,150	1,537	3,341	3,634	1,832	2,108	0,812	0,320	4,160	0,387	0,497	0,259
RPA34_HUMAN	1,099	1,000	1,027	0,973	1,000												
RPC4_HUMAN	2,705	4,329	0,933	0,121	0,760												
RPN1_HUMAN	0,884	1,108	1,069	0,920	1,002	0,112	2,262	1,695	0,563	3,616	0,172	0,280	0,987	1,450	4,168	2,438	1,505
RPN2_HUMAN	1,710	1,080	0,000	2,376	0,273												
RRBP1_HUMAN	1,474	0,669	1,259	1,432	0,582	0,100	2,290	3,281	0,600	0,000	0,000	1,052	0,000	0,000	3,034	1,078	0,327
RS10_HUMAN	1,694	0,918	0,879	2,775	0,739												
RS11_HUMAN	1,087	4,685	0,692	5,298	0,814	0,150	0,300	0,951	0,492	0,709	0,907	2,266	1,568	1,733	1,464	2,065	4,022
RS12_HUMAN						0,465	0,096	3,170	1,611	2,292	0,388	3,002	2,042	2,422	0,098	2,520	1,570

RS13_HUMAN	0,980	1,157	1,060	0,693	1,234	0,299	0,546	1,231	0,665	1,224	0,300	1,256	1,737	1,192	0,777	1,413	5,469
RS14_HUMAN	1,071	1,230	1,035	0,636	1,142	0,000	0,019	0,000	0,068	0,171	1,840	3,630	3,324	3,661	3,482	3,504	5,398
RS15_HUMAN	1,155	1,685	0,799	0,733	1,037	0,403	0,165	0,602	0,074	0,768	1,224	2,305	2,872	0,693	1,168	4,293	2,875
RS15A_HUMAN	0,944	0,988	1,399	0,843	0,915												
RS16_HUMAN	1,061	1,116	1,206	0,640	1,112	2,178	0,180	0,799	0,257	1,567	1,487	1,138	2,111	1,277	1,257	1,787	1,201
RS17_HUMAN	0,977	2,169	1,183	0,645	1,180												
RS18_HUMAN	1,251	1,110	0,881	0,663	1,072	0,887	2,261	3,986	2,567	1,427	0,105	1,425	0,369	0,436	2,619	1,199	0,528
RS19_HUMAN	1,304	1,618	0,952	0,878	0,579	0,409	0,480	1,639	0,794	1,354	0,782	1,561	0,719	1,047	1,137	1,122	1,866
RS2_HUMAN	0,880	0,693	1,135	1,383	1,085	0,431	0,861	1,266	0,999	1,169	1,051	1,195	1,143	1,525	1,216	1,498	0,567
RS20_HUMAN	0,837	1,055	1,490	0,815	0,937												
RS23_HUMAN	0,844	1,043	1,337	0,652	1,249	0,456	0,840	1,832	0,870	1,918	0,055	0,592	1,557	1,792	1,232	2,398	1,234
RS24_HUMAN	0,819	1,162	0,856	1,191	1,072	0,264	0,517	1,220	1,596	2,189	0,274	1,297	1,631	0,230	0,993	3,167	2,181
RS25_HUMAN	1,151	1,140	1,016	0,619	1,218	2,414	2,197	0,410	0,090	0,282	2,368	2,799	3,236	0,995	0,720	2,152	0,490
RS26_HUMAN	1,097	1,207	0,879	0,748	1,130												
RS3_HUMAN	1,296	0,888	1,029	0,893	0,945	0,810	0,854	1,076	0,961	0,960	1,289	1,193	0,902	1,266	1,253	1,268	0,744
RS3A_HUMAN	1,267	0,765	0,967	1,156	0,944	2,614	0,657	0,346	1,345	0,770	1,914	0,470	0,321	1,595	2,976	2,564	0,787
RS4X_HUMAN	1,011	0,921	0,916	1,068	1,054												
RS4Y2_HUMAN						0,238	0,556	1,090	0,605	1,052	0,825	1,542	1,710	1,273	1,020	1,631	2,729
RS5_HUMAN	0,834	1,160	0,965	1,054	0,998	2,598	0,411	0,604	1,300	0,062	0,243	3,537	6,294	1,454	1,417	1,487	1,937
RS6_HUMAN	0,903	0,987	1,126	0,976	1,065	0,170	0,616	1,227	0,380	1,228	1,137	1,253	0,794	1,439	1,328	1,741	1,400
RS7_HUMAN	1,140	0,729	0,854	1,177	1,334	0,449	1,792	1,612	3,030	1,625	2,352	0,510	0,601	0,123	0,591	0,761	4,459
RS8_HUMAN	1,124	0,894	0,899	1,076	1,089	0,129	1,099	1,773	1,638	2,118	0,010	2,168	1,987	1,918	1,750	2,489	2,363
RS9_HUMAN	0,764	0,885	1,360	0,757	1,389	0,160	1,232	2,640	1,830	0,810	0,381	0,472	0,645	1,455	0,342	2,478	2,918
RSF1_HUMAN						159,325	0,026	376,281	0,103	288,84	0,053	534,82	0,036	0,022	0,387	0,015	0,131
RSMN_HUMAN	0,975	0,518	1,316	0,891	1,704	0,141	1,568	1,991	2,461	1,460	0,107	1,840	1,719	2,172	1,498	1,467	1,499
RSSA_HUMAN	1,515	0,815	0,864	0,851	1,033	3,464	0,709	0,973	0,668	0,723	1,637	1,095	1,284	0,940	0,582	0,547	0,965
RT05_HUMAN						5,512	2,575	0,229	0,825	0,000	0,936	0,940	0,552	5,422	1,140	0,092	0,378
RTCB_HUMAN	0,407	1,458	1,573	1,408	0,530												
RTL1_HUMAN						0,078	1,176	1,564	1,930	1,152	1,070	0,290	0,626	1,599	2,361	2,245	1,833
RU17_HUMAN						0,000	0,314	1,741	1,935	0,000	0,405	0,000	0,000	0,000	2,051	0,000	0,000
RUVB1_HUMAN						0,449	2,888	0,449	1,738	2,986	0,669	1,095	0,928	5,715	1,765	0,627	0,280
RUVB2_HUMAN	0,000	1,300	1,161	1,057	0,647	0,117	2,824	1,816	2,614	1,754	2,475	0,518	0,702	1,508	0,309	1,187	0,617
S10A6_HUMAN	0,630	1,807	1,047	0,600	1,435												

S10A8_HUMAN	0,444	8,260	0,400	1,657	0,617												
S10A9_HUMAN						0,000	0,000	0,000	1,661	0,000	0,000	0,725	0,000	0,000	0,000	0,770	0,000
S4A11_HUMAN						5,212	1,281	1,257	1,173	1,464	0,489	0,843	0,885	0,569	0,886	0,246	1,531
S61A1_HUMAN						1,120	1,033	1,106	0,465	0,806	3,261	0,307	1,011	1,098	1,406	0,831	1,918
S61A2_HUMAN	1,127	0,675	0,621	2,834	0,704												
SAE1_HUMAN	0,231	0,248	1,867	3,232	2,570												
SAFB1_HUMAN						0,000	0,961	2,190	1,841	0,585	2,035	0,905	0,155	1,119	3,530	1,793	0,257
SAHH_HUMAN	1,012	1,226	1,035	0,796	0,982	0,141	1,738	2,358	1,844	2,557	0,800	2,663	1,455	1,922	1,050	0,906	0,050
SARNP_HUMAN	0,876	0,815	0,487	1,320	2,133												
SBSN_HUMAN	0,481	0,000	1,278	2,509	0,541												
SCOT1_HUMAN	1,350	1,042	0,697	1,506	0,692												
SEC13_HUMAN						1,771	1,296	0,476	0,583	0,452	0,765	0,872	0,457	2,717	0,810	2,157	1,104
SEMG1_HUMAN						2,611	0,000	0,866	0,447	0,935	0,000	0,000	0,000	0,000	0,657	0,801	2,078
SERA_HUMAN	1,266	0,783	1,152	1,034	0,915												
SERPH_HUMAN	0,000	0,000	1,472	0,935	0,739	1,195	0,845	0,236	2,036	1,491	1,033	0,654	0,985	0,598	0,798	1,479	1,494
SF01_HUMAN						0,000	0,308	1,477	2,074	0,000	0,000	0,000	0,000	0,000	1,118	0,000	0,000
SF3B1_HUMAN	1,983	1,097	2,803	0,669	1,454												
SF3B2_HUMAN	0,503	4,671	1,795	0,200	0,999	0,000	3,634	2,082	3,625	0,560	4,353	0,126	0,409	1,368	1,768	1,073	0,130
SF3B3_HUMAN	0,999	1,176	1,879	0,683	1,329	0,000	2,433	2,721	2,862	1,353	0,301	0,455	0,426	2,725	1,613	2,438	0,147
SFPQ_HUMAN	0,713	0,973	1,391	0,995	1,113	0,144	4,496	5,200	3,935	0,100	2,068	0,198	0,191	2,670	4,972	1,019	1,090
SHRM3_HUMAN	2,386	0,954	0,746	1,424	1,018												
SHRM4_HUMAN	6,240	0,088	7,715	0,151	1,850												
SK2L2_HUMAN	0,400	1,316	1,866	1,900	0,783	0,000	0,821	1,823	1,353	0,599	0,000	0,544	0,465	0,702	0,766	2,162	2,168
SMC1A_HUMAN	0,607	0,598	2,686	1,280	1,925	0,101	0,993	1,789	2,128	0,727	3,419	4,406	1,005	2,417	0,389	1,702	0,148
SMC2_HUMAN						0,869	1,521	2,881	0,728	1,231	3,923	1,040	0,557	1,634	0,313	0,839	0,778
SMC3_HUMAN	0,000	0,350	3,735	0,710	1,327	0,000	0,605	4,859	3,064	0,257	0,711	0,201	0,554	11,172	0,272	1,718	0,000
SMC4_HUMAN	0,000	0,000	1,568	0,000	0,630												
SMCA5_HUMAN	0,000	1,658	2,340	0,270	0,947												
SMD1_HUMAN	1,213	1,068	0,963	0,706	1,029												
SMD3_HUMAN	0,797	1,402	1,536	0,451	1,309	0,196	0,995	2,462	1,341	1,112	0,005	2,287	1,767	1,511	1,163	1,371	1,392
SMTN_HUMAN	0,278	1,465	0,760	1,680	1,922	0,000	1,354	3,134	3,041	3,009	0,045	0,202	0,403	2,792	4,285	2,234	0,273
SND1_HUMAN	1,416	0,875	0,779	1,201	0,877												
SNUT2_HUMAN						0,245	1,913	1,040	2,185	1,395	0,328	1,296	1,283	1,235	0,837	1,489	0,154

SP16H_HUMAN	0,103	2,581	3,381	1,158	0,775	0,000	2,749	2,737	1,812	0,253	0,210	2,193	3,149	0,930	0,776	0,612	0,389
SPB12_HUMAN	2,616	2,106	0,399	1,155	0,681												
SPB4_HUMAN	4,642	21,47	0,000	0,299	0,051												
SPIN1_HUMAN						0,000	0,332	0,719	0,999	1,587	6,673	1,355	2,147	2,970	0,610	0,549	0,462
SPTB2_HUMAN						0,697	13,35	1,822	0,273	0,311	0,492	0,769	0,309	2,942	0,957	2,012	0,833
SPTN1_HUMAN	4,220	0,513	0,333	0,887	1,567	0,445	1,091	0,670	0,565	0,661	27,775	0,416	0,530	0,616	0,896	1,121	1,500
SRP14_HUMAN	0,431	1,728	1,536	0,533	1,656	0,000	0,250	0,820	1,108	0,155	1,021	3,923	0,866	5,249	1,158	2,047	0,614
SRRT_HUMAN						0,000	0,763	4,009	1,110	0,423	9,893	0,614	0,652	0,801	0,477	0,969	0,437
SRS10_HUMAN	0,148	0,274	2,965	2,045	4,058												
SRSF1_HUMAN	0,392	0,459	1,863	1,113	2,696												
SRSF3_HUMAN	0,530	1,027	1,563	0,706	1,677												
SRSF6_HUMAN						0,231	0,080	2,353	4,222	1,367	1,158	1,562	0,313	1,697	1,751	3,915	0,316
SRSF8_HUMAN	0,247	1,034	1,854	0,965	2,268	0,385	0,963	3,609	3,024	1,331	3,618	2,180	0,412	0,924	0,085	2,330	0,254
SSRP1_HUMAN	0,059	2,364	2,988	2,264	1,878	0,443	1,882	2,106	1,712	0,763	0,248	2,800	2,229	1,426	1,082	0,553	0,154
STAG2_HUMAN	0,000	0,622	1,881	1,137	0,803												
STMN1_HUMAN						1,256	1,802	2,559	0,686	1,116	0,065	1,465	1,344	1,889	0,677	1,091	0,432
SUMO4_HUMAN	0,252	5,452	2,789	0,557	1,477	0,000	0,818	1,324	0,919	0,729	1,030	1,805	1,712	1,186	1,080	0,805	0,463
SYEP_HUMAN						0,000	0,956	1,318	0,235	0,563	0,559	0,653	2,921	3,556	0,436	1,550	2,071
SYK_HUMAN	1,668	1,090	0,630	1,058	0,805												
TADBP_HUMAN	0,000	0,000	0,606	1,203	1,395												
TAGL2_HUMAN	1,173	1,224	0,513	1,180	1,183	0,453	1,613	1,117	3,190	0,571	0,849	1,238	0,172	0,652	1,346	2,831	1,436
TALDO_HUMAN	0,000	0,000	0,458	0,762	2,867												
TBA1A_HUMAN	1,414	0,849	0,924	1,067	0,832												
TBA1B_HUMAN						0,132	1,664	1,271	1,449	2,054	8,179	2,070	2,024	0,268	1,051	2,010	0,211
TBA1C_HUMAN						0,079	4,205	3,783	3,564	6,483	0,287	0,504	4,233	0,182	1,047	3,940	0,288
TBA4A_HUMAN	1,018	1,879	0,833	0,790	0,784												
TBA4B_HUMAN	1,644	1,189	1,035	0,758	0,630												
TBB3_HUMAN	2,441	0,792	0,579	3,303	0,724												
TBB4B_HUMAN						0,780	4,622	1,113	2,272	1,613	2,425	0,122	0,875	1,074	1,017	0,325	0,931
TBB5_HUMAN	1,714	1,050	0,980	0,712	0,785	3,503	1,288	0,874	0,865	0,869	0,505	1,181	1,239	0,779	0,811	0,854	1,286
TBB6_HUMAN	1,215	1,045	0,936	1,105	0,752												
TBC8B_HUMAN						0,000	3,248	0,457	2,282	0,503	0,000	1,447	0,293	6,015	0,329	3,084	0,221
TCPA_HUMAN	0,968	1,175	1,190	0,814	0,870	0,945	3,450	1,756	1,329	1,944	0,120	1,167	1,167	0,789	0,825	1,292	0,458

TCPB_HUMAN	1,249	1,064	1,105	0,915	0,734	0,106	5,142	4,103	3,179	3,019	0,146	1,405	0,819	0,383	1,201	1,846	0,144
TCPD_HUMAN	0,685	1,039	1,474	1,255	0,763	0,470	2,226	3,023	2,600	1,704	0,417	1,084	0,501	0,476	0,994	1,341	0,218
TCPE_HUMAN	2,069	1,738	0,885	1,358	0,759	820,085	0,064	113,928	0,229	0,261	3,071	1,043	0,250	0,248	0,424	0,236	0,214
TCPG_HUMAN	1,107	1,167	1,131	0,951	0,738	0,453	2,656	1,509	1,374	1,020	0,712	0,845	1,036	1,228	1,160	0,575	0,555
TCPH_HUMAN	0,788	1,368	0,961	1,131	0,878												
TCPQ_HUMAN	1,004	1,038	1,252	1,079	0,697	0,130	2,149	2,159	1,388	1,494	0,397	1,435	1,368	1,534	0,888	1,424	1,016
TCPZ_HUMAN	1,123	0,879	1,090	1,031	0,924	1,748	1,598	1,485	1,071	0,776	1,703	0,461	1,474	1,752	0,382	0,686	0,459
TERA_HUMAN	0,963	1,425	1,091	0,660	0,938	0,000	0,347	0,406	0,839	0,988	15,921	1,992	0,705	3,985	1,223	0,267	0,148
TGM2_HUMAN	1,161	0,909	1,038	0,916	0,964												
TGM3_HUMAN	2,050	2,351	0,363	0,594	0,934	5,149	0,746	0,425	0,551	2,671	2,658	0,805	1,024	0,846	0,872	0,262	0,552
THIL_HUMAN	1,331	0,634	0,474	2,559	1,384	0,951	0,909	1,511	0,703	0,501	0,392	1,046	7,429	2,605	0,559	0,661	0,999
THIO_HUMAN	1,859	2,560	1,092	0,421	0,508	4,218	1,046	1,381	0,546	0,916	1,164	0,934	1,805	1,277	0,373	0,568	0,582
THOC4_HUMAN	1,973	0,791	1,290	1,381	1,406												
TIF1B_HUMAN	0,338	1,634	2,185	0,892	1,144	0,153	1,570	2,399	2,026	0,307	1,073	1,993	1,676	1,301	1,383	0,894	0,225
TITIN_HUMAN	7,348	18,33	22,004	2,490	1,693	7,348	18,33	22,004	2,490	1,693	0,163	0,093	0,495	0,469	0,233	0,164	0,423
TKT_HUMAN	0,374	1,426	1,340	1,045	1,347	0,217	1,774	2,262	3,375	1,160	2,061	0,503	0,648	1,180	2,432	0,484	0,348
TLN1_HUMAN	1,099	0,898	1,142	1,241	0,840	0,791	3,199	0,567	0,607	1,486	0,851	0,530	0,874	1,208	0,784	1,235	1,538
TLR7_HUMAN						0,110	0,935	2,050	2,275	1,554	3,332	0,887	1,039	1,189	0,918	1,173	0,444
TNPO1_HUMAN						0,883	2,460	2,739	1,653	2,967	0,220	0,171	0,714	0,638	1,871	2,595	0,559
TOM34_HUMAN	1,235	0,776	0,672	1,317	1,273												
TOM70_HUMAN	1,807	7,101	0,515	0,357	0,425												
TOP1_HUMAN	0,000	0,714	1,590	0,595	1,469	0,000	0,000	0,158	1,734	1,409	2,857	0,498	0,878	0,346	1,893	3,257	0,000
TOP2A_HUMAN	0,211	1,628	2,942	0,828	1,232	0,216	1,107	2,852	1,661	1,036	1,013	1,760	1,820	1,744	1,329	1,322	0,069
TPIS_HUMAN	0,486	0,423	0,595	3,374	2,804	0,183	0,724	1,426	1,933	0,661	1,079	0,993	1,649	1,835	0,837	0,588	2,676
TPM4_HUMAN						0,450	3,253	1,142	1,340	0,717	0,647	0,813	0,517	1,172	0,922	1,605	1,137
TPR_HUMAN						0,000	0,805	0,591	1,361	1,099	3,098	0,446	0,626	0,973	0,814	0,661	0,000
TPX2_HUMAN	0,254	1,355	2,172	0,729	1,882												
TR150_HUMAN						0,000	0,659	0,301	0,800	11,432	0,818	0,513	0,188	0,645	1,451	38,477	0,211
TRAF7_HUMAN						0,000	0,429	1,355	1,696	5,335	0,853	0,442	0,431	1,341	1,383	1,027	0,261
TRAP1_HUMAN	1,126	1,471	0,911	0,803	0,818	2,067	0,840	0,834	0,681	0,635	5,780	0,942	0,907	0,946	0,709	0,586	1,091
TRI16_HUMAN						0,896	0,664	0,742	1,070	1,146	2,417	0,698	0,820	0,969	2,006	0,956	0,831
TRXR1_HUMAN	0,632	1,211	0,356	1,683	2,406												
TRY1_HUMAN	2,078	0,950	0,682	0,873	0,868												

TTLL5_HUMAN	2,062	1,932	1,590	0,111	1,502												
TUT4_HUMAN	0,196	0,885	1,887	1,059	2,883												
TXTP_HUMAN	0,927	0,712	1,107	5,447	3,898												
U2AF1_HUMAN						0,000	1,639	1,702	1,620	0,803	1,627	1,550	1,225	1,429	0,124	1,523	0,367
U2AF2_HUMAN	0,368	1,074	1,555	1,096	2,248												
U520_HUMAN						0,000	0,925	1,574	1,690	2,381	0,395	1,121	1,805	0,166	2,839	1,475	0,329
U5S1_HUMAN						0,000	0,695	0,970	1,039	1,972	0,000	0,000	0,890	1,963	0,581	1,005	0,000
UBA1_HUMAN	0,766	1,283	1,093	0,771	1,172	0,176	5,745	2,642	3,036	0,688	1,214	1,133	0,273	0,858	1,237	0,778	0,446
UBC_HUMAN	0,298	1,652	1,736	1,744	3,125	1,042	0,554	1,074	1,342	0,902	2,152	0,825	0,917	1,027	1,026	1,070	0,842
UBP2L_HUMAN						0,000	1,217	0,000	0,000	0,000	0,000	0,000	1,068	1,011	0,196	0,000	0,000
UCHL1_HUMAN	1,174	1,453	0,975	0,668	0,991												
UGDH_HUMAN	0,424	2,009	1,074	0,914	1,250	0,099	2,139	2,754	3,351	1,026	0,670	1,831	0,816	2,229	2,962	0,362	0,352
VDAC1_HUMAN	0,953	0,898	1,182	0,984	1,090	1,796	1,107	0,979	1,345	0,233	0,494	0,982	0,878	2,769	2,522	2,244	0,808
VDAC2_HUMAN	1,146	0,615	0,822	1,412	1,259	2,421	0,748	0,607	0,766	0,767	0,722	1,352	0,665	1,342	1,238	1,410	1,151
VDAC3_HUMAN	0,969	0,480	1,603	1,051	1,455	0,250	0,941	0,529	6,143	0,417	0,101	1,001	0,209	3,810	8,660	6,800	1,640
VIME_HUMAN	1,054	0,893	1,161	1,042	0,910	1,623	1,457	0,662	0,787	0,910	0,990	0,861	0,915	0,905	0,772	0,972	1,512
VINC_HUMAN	1,372	1,120	0,948	0,868	0,825	0,497	1,855	1,216	0,804	1,000	0,949	0,492	0,877	1,100	0,894	1,163	2,291
VPS35_HUMAN	1,758	0,828	0,655	1,216	1,004												
WDHD1_HUMAN	0,495	0,856	5,391	0,428	0,000												
WDR1_HUMAN	0,601	1,235	0,847	1,802	1,104	0,000	12,21	2,023	1,667	0,445	3,306	0,467	0,413	0,295	0,530	0,569	1,099
XPO1_HUMAN	0,652	0,466	1,951	0,867	1,942												
XPO2_HUMAN	0,498	1,255	1,626	0,981	1,177	1,044	0,167	1,226	1,011	1,327	3,153	0,973	1,418	1,016	1,076	1,377	0,268
XRCC5_HUMAN	0,158	1,390	2,395	1,428	1,527	0,077	1,303	2,214	1,836	1,309	1,658	1,492	1,195	1,406	1,479	1,066	0,335
XRCC6_HUMAN	0,130	1,237	2,556	1,381	1,741	0,152	0,943	1,165	1,162	1,128	1,557	1,735	1,260	1,385	1,307	1,137	0,762
XRN2_HUMAN						0,000	1,150	1,197	0,588	1,384	1,271	0,573	0,205	1,919	0,894	3,057	0,000
YBOX3_HUMAN						5,572	0,288	0,983	0,967	1,622	0,293	3,629	1,301	0,365	1,188	0,986	1,007
YES_HUMAN	0,513	1,134	1,967	0,648	1,268												
ZA2G_HUMAN	0,776	0,714	1,072	1,507	1,090												
ZAGL1_HUMAN						20,886	4,113	0,371	0,787	0,539	0,297	1,156	0,790	0,771	0,917	0,369	0,393
ZNF34_HUMAN						0,099	0,320	3,600	4,118	3,691	0,240	2,095	0,000	0,058	5,581	2,441	0,000

Appendix 2. Functions and NRA values of the proteins identified in our iPOND+MS experiment.
The protein ID, function (represented by different colors as indicated) and NRA values of the proteins identified in our iPOND+MS experiment are shown. The NRA values are clustered into five different groups (from lowest to highest), each of them represented with certain color intensity to create a heatmap in order to make the results more visual. Proteins in grey represent the ones that were identified only in the first MS round. Conditions have been previously described *(Figure 37)*.

Protein classification (by function)

- Replisome components
- Fork stability and DNA repair
- Histones and histone variants
- Proteolysis
- Other functions

NRA values classification

- 0.8 -1
- 0.6-0.8
- 0.4-0.6
- 0.2-0.4
- 0-0.2

FUNCTION	PROTEIN ID	Negative control	Pulse	15'EdU/HU	2h HU	14h HU	Chase
	DNLI1_HUMAN	0,000	1,000	0,391	0,094		0,025
	DPOA2_HUMAN	0,142	0,579	1,000	0,203		0,076
	DPOD1_HUMAN	0,000	0,940	1,000	0,205	0,008	0,057
	DPOD3_HUMAN	0,000	1,000	0,529	0,099		0,000
	DPOE1_HUMAN	0,038	0,407	1,000	0,027		0,000
	FEN1_HUMAN	0,023	1,000	0,814	0,571	0,210	0,410
	MCM2_HUMAN	0,074	0,795	1,000	0,299		0,360
	MCM3_HUMAN	0,041	0,676	1,000	0,652	0,116	0,241
	MCM5_HUMAN	0,000	0,851	1,000	0,259		0,225
	MCM6_HUMAN	0,037	1,000	0,714	0,529	0,053	0,391
	MCM7_HUMAN	0,026	0,761	1,000	0,481	0,475	0,359
	PCNA_HUMAN	0,019	1,000	0,700	0,388	0,025	0,080
	PRI2_HUMAN	0,004	0,732	1,000	0,347	0,000	0,006
	RFA1_HUMAN	0,000	0,599	1,000	0,481		0,134
	RFA2_HUMAN	0,019	0,415	0,541	1,000	0,227	0,243
	RFC1_HUMAN	0,000	0,955	1,000	0,067		0,029
	RFC2_HUMAN	0,071	1,000	0,304	0,191	0,013	0,065
	RFC3_HUMAN	0,000	0,872	1,000	0,400	0,016	0,108
	RFC4_HUMAN	0,033	1,000	0,799	0,347	0,013	0,059
	RFC5_HUMAN	0,005	0,558	1,000	0,291	0,268	0,089
	FACD2_HUMAN	0,000	0,059	0,799	1,000		0,076
	FANCI_HUMAN	0,000	0,072	1,000	0,772		0,450
	MSH2_HUMAN	0,038	0,940	1,000	0,186		0,073
	MSH6_HUMAN	0,008	1,000	0,746	0,201	0,022	0,082
	PRKDC_HUMAN	0,113	0,513	1,000	0,287		0,605
	RECQ1_HUMAN	0,030	0,918	0,922	0,789	0,581	0,460

	RIF1_HUMAN	0,008	0,519	1,000	0,052		0,086
	SMC3_HUMAN	0,000	0,115	1,000	0,888	0,026	0,218
	XRCC5_HUMAN	0,054	0,774	1,000	0,846	0,590	0,700
	XRCC6_HUMAN	0,096	0,844	1,000	0,823	0,647	0,779
	H12_HUMAN	0,028	0,186	0,312	0,399	0,346	1,000
	H14_HUMAN	0,081	0,131	0,276	0,301		1,000
	H15_HUMAN	0,017	0,219	0,404	0,521	0,549	1,000
	H1X_HUMAN	0,362	0,032	0,085	0,194	0,174	1,000
	H2AY_HUMAN	0,019	0,106	0,313	0,449	0,801	1,000
	H2BFS_HUMAN	0,049	0,378	0,773	0,555	0,830	1,000
	H31_HUMAN	0,097	0,396	0,120	1,000		0,951
	H33_HUMAN	0,236	0,368	1,000	0,418		0,548
	H4_HUMAN	0,134	0,446	0,921	0,624	0,997	1,000
	PRS6B_HUMAN	0,426	1,000	0,462	0,383		0,286
	PSA2_HUMAN	0,281	0,423	0,451	0,916		1,000
	PSA6_HUMAN	0,199	0,885	0,580	0,940	0,795	0,319
	PSA7_HUMAN	0,395	0,395	0,512	1,000		0,709
	PSB3_HUMAN	0,501	0,864	0,552	0,610		1,000
	PSB5_HUMAN	0,252	0,459	0,751	1,000		0,790
	1433T_HUMAN	0,478	0,450	0,796	1,000		0,642
	CAND1_HUMAN	0,371	0,664	1,000	0,630		0,544
	CLIC1_HUMAN	0,506	0,593	0,722	1,000		0,924
	CPNE3_HUMAN	0,255	0,526	1,000	0,545		0,301
	DDX17_HUMAN	0,086	0,253	1,000	0,549		0,530
	DHE4_HUMAN	0,238	0,283	0,163	1,000		0,388
	DHX15_HUMAN	0,214	0,695	1,000	0,429		0,849
	DNMT1_HUMAN	0,133	1,000	0,175	0,039	0,036	0,103
	FUS_HUMAN	0,284	0,540	1,000	0,516		0,566
	GRP78_HUMAN	0,541	0,592	0,350	0,635	1,000	0,628
	GRWD1_HUMAN	0,128	1,000	0,241	0,115		0,084
	GTF2I_HUMAN	0,146	0,698	1,000	0,345		0,332
	GTR1_HUMAN	0,111	0,495	0,346	0,581	1,000	0,457
	GUAA_HUMAN	0,067	1,000	0,970	0,776	0,369	0,469
	HCD2_HUMAN	0,472	0,279	0,322	1,000		0,301
	IF4G1_HUMAN	0,440	0,853	0,707	1,000		0,574
	ILF2_HUMAN	0,119	0,357	0,576	0,432	0,867	1,000
	ILF3_HUMAN	0,221	0,679	1,000	0,772	0,542	0,699
	IPO5_HUMAN	0,462	1,000	0,288	0,219		0,202
	IPO9_HUMAN	0,352	0,311	1,000	0,845		0,628

	LA_HUMAN	0,088	0,474	0,721	0,451		1,000
	LAP2B_HUMAN	0,078	0,279	0,403	0,477	0,818	1,000
	LEG7_HUMAN	0,017	1,000	0,003	0,005		0,010
	LMNA_HUMAN	0,088	0,378	0,538	0,570	0,787	1,000
	LMNB1_HUMAN	0,042	0,176	0,221	0,487	0,752	1,000
	LMNB2_HUMAN	0,101	0,094	0,212	0,395	1,000	0,545
	MCCA_HUMAN	0,491	0,410	0,510	1,000	0,827	0,544
	NPM_HUMAN	0,211	0,576	0,543	0,642	0,385	1,000
	NUCL_HUMAN	0,153	0,515	0,606	0,559	0,283	1,000
	PABP3_HUMAN	0,251	0,193	0,148	0,227	1,000	0,242
	PCBP1_HUMAN	0,300	0,364	0,569	0,455	0,276	1,000
	PGK1_HUMAN	0,360	0,461	0,405	0,492		1,000
	PLAK_HUMAN	0,488	1,000	0,185	0,273		0,180
	PLEC_HUMAN	0,173	1,000	0,075	0,138	0,319	0,100
	PP1G_HUMAN	0,494	0,467	0,506	0,394		1,000
	PRP8_HUMAN	0,092	0,180	1,000	0,376		0,389
	PSIP1_HUMAN	0,000	0,221	0,556	0,593	0,523	1,000
	PTBP2_HUMAN	0,167	0,861	1,000	0,937	0,643	0,464
	PYC_HUMAN	0,315	0,109	0,335	0,631		1,000
	RBMX_HUMAN	0,122	0,267	0,744	0,587		1,000
	RINI_HUMAN	0,255	0,715	0,913	0,707	0,479	1,000
	S10A8_HUMAN	0,054	1,000	0,048	0,201		0,075
	S61A1_HUMAN	0,343	0,317	0,339	0,143	0,247	1,000
	SP16H_HUMAN	0,010	0,821	1,000	0,433	0,157	0,167
	SRSF8_HUMAN	0,127	0,552	0,664	0,552	0,165	1,000
	SSRP1_HUMAN	0,139	0,960	1,000	0,722	0,271	0,315
	SUMO4_HUMAN	0,018	1,000	0,940	0,484	0,484	0,498
	TCPD_HUMAN	0,409	0,948	1,000	0,727	0,474	0,552
	TIF1B_HUMAN	0,104	0,846	1,000	0,671	0,309	0,473
	TOP1_HUMAN	0,000	0,206	0,453	0,372	0,367	1,000
	TOP2A_HUMAN	0,089	0,636	1,000	0,607	0,375	0,500
	TPIS_HUMAN	0,113	0,347	0,604	1,000	0,599	0,570
	TRXR1_HUMAN	0,263	0,503	0,148	0,699		1,000
	TXTP_HUMAN	0,170	0,131	0,203	1,000		0,716
	U2AF2_HUMAN	0,164	0,478	0,692	0,488		1,000
	UGDH_HUMAN	0,122	1,000	0,723	0,736	0,473	0,315

Appendix 3. Comparative analysis of the nascent DNA-bound proteins found in the pulse condition on different iPOND+MS studies.
The protein ID and function (represented by different colors as indicated on Appendix 2), of the proteins considered as nascent DNA-bound proteins in the pulse condition in our proteomic analysis are shown. The results from our proteomic analysis were compared with data from other published works. Boxes in light grey represent the proteins that were considered nascent DNA-bound proteins in the pulse condition on published works.

Nascent DNA-bound proteins in the pulse							
Current proteomic study		*Lopez-contreras, A et al. 2013*[510]	*Lossaint, G et al. 2013*[392]	*Sirbu, B et al. 2013*[514]	*Constance, A et al. 2014*[515]	*Aranda, S et al. 2014*[511]	*Dungrawala, H et al. 2015*[390]
FUNCTION	**PROTEIN ID**						
	DNLI1_HUMAN						
	DPOA2_HUMAN						
	DPOD1_HUMAN						
	DPOD3_HUMAN						
	DPOE1_HUMAN						
	FEN1_HUMAN						
	MCM2_HUMAN						
	MCM3_HUMAN						
	MCM5_HUMAN						
	MCM6_HUMAN						
	MCM7_HUMAN						
	PCNA_HUMAN						
	PRI2_HUMAN						
	RFA1_HUMAN						
	RFC1_HUMAN						
	RFC2_HUMAN						
	RFC3_HUMAN						

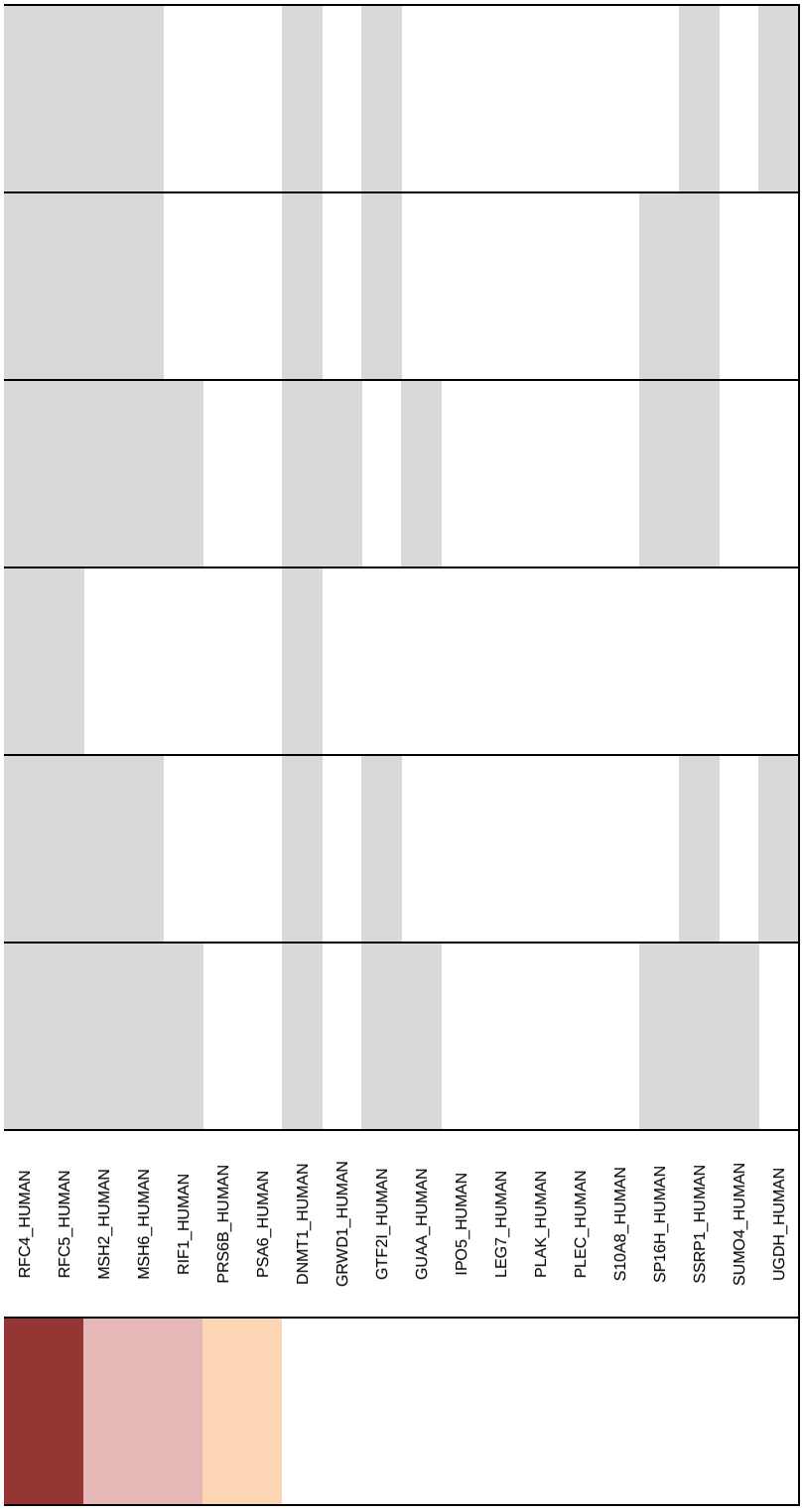
RFC4_HUMAN
RFC5_HUMAN
MSH2_HUMAN
MSH6_HUMAN
RIF1_HUMAN
PRS6B_HUMAN
PSA6_HUMAN
DNMT1_HUMAN
GRWD1_HUMAN
GTF2I_HUMAN
GUAA_HUMAN
IPO5_HUMAN
LEG7_HUMAN
PLAK_HUMAN
PLEC_HUMAN
S10A8_HUMAN
SP16H_HUMAN
SSRP1_HUMAN
SUMO4_HUMAN
UGDH_HUMAN

BIBLIOGRAPHY

1. Morgan, D. O. The Cell Cycle: principles of Control. *Book.* (2007).
2. Branzei, D. & Foiani, M. Maintaining genome stability at the replication fork. *Nat. Rev. Mol. Cell Biol.* **11,** 208–19 (2010).
3. Kastan, M. B. & Bartek, J. Cell-cycle checkpoints and cancer. *Nature* **432,** 316–23 (2004).
4. Satyanarayana, A. & Kaldis, P. Mammalian cell-cycle regulation: several Cdks, numerous cyclins and diverse compensatory mechanisms. *Oncogene* **28,** 2925–39 (2009).
5. Malumbres, M. & Barbacid, M. Cell cycle, CDKs and cancer: a changing paradigm. *Nat. Rev. Cancer* **9,** 153–66 (2009).
6. Lim S, K. P. Cdks, cyclins and CKIs: roles beyond cell cycle regulation. *Development* **140,** 3079-93 (2013).
7. Vermeulen,K.,Van Bockstaele,D.R.,Berneman, Z. N., Vermeulen, K., Van Bockstaele, D. R. & Berneman, Z. N. The cell cycle:a review of regulation,deregulation and therapeutic targets in cancer. *Cell Prolif.* **36,** 131–49 (2003).
8. Santamaría D1, Barrière C, Cerqueira A, Hunt S, Tardy C, Newton K, Cáceres JF, Dubus P, Malumbres M, B. M. Cdk1 is sufficient to drive the mammalian cell cycle. *Nature* **448,** 811–5 (2007).
9. Berthet, C., Aleem, E., Coppola, V., Tessarollo, L. & Kaldis, P. Cdk2 knockout mice are viable. *Curr. Biol.* **13,** 1775–85 (2003).
10. Ortega, S. *et al.* Cyclin-dependent kinase 2 is essential for meiosis but not for mitotic cell division in mice. *Nat. Genet.* **35,** 25–31 (2003).
11. Murphy, M. *et al.* Delayed early embryonic lethality following disruption of the murine cyclin A2 gene. *Nat. Genet.* **15,** 83–6 (1997).
12. Brandeis, M. *et al.* Cyclin B2-null mice develop normally and are fertile whereas cyclin B1-null mice die in utero. *Proc. Natl. Acad. Sci. U. S. A.* **95,** 4344–9 (1998).
13. Geng, Y. *et al.* Cyclin E ablation in the mouse. *Cell* **114,** 431–43 (2003).
14. Kozar, K. *et al.* Mouse development and cell proliferation in the absence of D-cyclins. *Cell* **118,** 477–91 (2004).
15. Udvardy, A. The role of controlled proteolysis in cell-cycle regulation. *Eur. J. Biochem.* **240,** 307–13 (1996).
16. JM, Obayaa AJ, S. Regulation of cyclin-Cdk activity in mammalian cells. *Cell Mol Life Sci.* **59,** 126–42 (2002).
17. Dimova, D. K. & Dyson, N. J. The E2F transcriptional network: old acquaintances with new faces. *Oncogene* **24,** 2810–26 (2005).
18. Iglesias-Ara, a *et al.* Accelerated DNA replication in E2F1- and E2F2-deficient macrophages leads to induction of the DNA damage response and p21(CIP1)-dependent senescence. *Oncogene* **29,** 5579–5590 (2010).
19. Wong, J. V, Dong, P., Nevins, J. R., Mathey-Prevot, B. & You, L. Network calisthenics: control of E2F dynamics in cell cycle entry. *Cell Cycle* **10,** 3086–94 (2011).
20. Chen, H.-Z., Tsai, S.-Y. & Leone, G. Emerging roles of E2Fs in cancer: an exit from cell cycle control. *Nat. Rev. Cancer* **9,** 785–97 (2009).
21. Cam, H. & Dynlacht, B. D. Emerging roles for E2F: beyond the G1/S transition and DNA replication. *Cancer Cell* **3,** 311–6 (2003).
22. Lindqvist, A., Rodríguez-Bravo, V. & Medema, R. H. The decision to enter mitosis: feedback and redundancy in the mitotic entry network. *J. Cell Biol.* **185,** 193–202 (2009).
23. Nakayama, K. I. & Nakayama, K. Ubiquitin ligases: cell-cycle control and cancer. *Nat. Rev. Cancer* **6,** 369–81 (2006).
24. Singer, J. D., Gurian-West, M., Clurman, B. & Roberts, J. M. Cullin-3 targets cyclin E for ubiquitination and controls S phase in mammalian cells. *Genes Dev.* **13,** 2375–87 (1999).
25. Germain, D., Russell, A., Thompson, A. & Hendley, J. Ubiquitination of free cyclin D1 is independent of phosphorylation on threonine 286. *J. Biol. Chem.* **275,** 12074–9 (2000).
26. Wang, Y. *et al.* Deletion of the Cul1 gene in mice causes arrest in early embryogenesis and accumulation of cyclin E. *Curr. Biol.* **9,** 1191–4 (1999).
27. Dealy, M. J. *et al.* Loss of Cul1 results in early embryonic lethality and dysregulation of cyclin E. *Nat. Genet.* **23,** 245–8 (1999).

28. Yu, Z. K., Gervais, J. L. & Zhang, H. Human CUL-1 associates with the SKP1/SKP2 complex and regulates p21(CIP1/WAF1) and cyclin D proteins. *Proc. Natl. Acad. Sci. U. S. A.* **95,** 11324–9 (1998).
29. Klotzbücher, A., Stewart, E., Harrison, D. & Hunt, T. The 'destruction box' of cyclin A allows B-type cyclins to be ubiquitinated, but not efficiently destroyed. *EMBO J.* **15,** 3053–64 (1996).
30. Sudakin, V. *et al.* The cyclosome, a large complex containing cyclin-selective ubiquitin ligase activity, targets cyclins for destruction at the end of mitosis. *Mol. Biol. Cell* **6,** 185–97 (1995).
31. Krek, W. & Nigg, E. A. Cell cycle regulation of vertebrate p34cdc2 activity: identification of Thr161 as an essential in vivo phosphorylation site. *New Biol.* **4,** 323–9 (1992).
32. Solomon, M. J., Lee, T. & Kirschner, M. W. Role of phosphorylation in p34cdc2 activation: identification of an activating kinase. *Mol. Biol. Cell* **3,** 13–27 (1992).
33. Gu, Y., Rosenblatt, J. & Morgan, D. O. Cell cycle regulation of CDK2 activity by phosphorylation of Thr160 and Tyr15. *EMBO J.* **11,** 3995–4005 (1992).
34. Lolli, G. & Johnson, L. N. CAK-Cyclin-dependent Activating Kinase: a key kinase in cell cycle control and a target for drugs? *Cell Cycle* **4,** 572–7 (2005).
35. Poon, R. Y. C. & Hunter, T. Dephosphorylation of Cdk2 Thr160 by the Cyclin-Dependent Kinase-Interacting Phosphatase KAP in the Absence of Cyclin. *Science* **270,** 90–93 (1995).
36. Krek, W. & Nigg, E. A. Differential phosphorylation of vertebrate p34cdc2 kinase at the G1/S and G2/M transitions of the cell cycle: identification of major phosphorylation sites. *EMBO J.* **10,** 305–16 (1991).
37. Norbury, C., Blow, J. & Nurse, P. Regulatory phosphorylation of the p34cdc2 protein kinase in vertebrates. *EMBO J.* **10,** 3321–9 (1991).
38. Booher, R. N., Holman, P. S. & Fattaey, A. Human Myt1 is a cell cycle-regulated kinase that inhibits Cdc2 but not Cdk2 activity. *J. Biol. Chem.* **272,** 22300–6 (1997).
39. McGowan, C. H. & Russell, P. Human Wee1 kinase inhibits cell division by phosphorylating p34cdc2 exclusively on Tyr15. *EMBO J.* **12,** 75–85 (1993).
40. Heald, R., McLoughlin, M. & McKeon, F. Human wee1 maintains mitotic timing by protecting the nucleus from cytoplasmically activated Cdc2 kinase. *Cell* **74,** 463–74 (1993).
41. Boutros, R., Dozier, C. & Ducommun, B. The when and wheres of CDC25 phosphatases. *Curr. Opin. Cell Biol.* **18,** 185–91 (2006).
42. Perry, J. A. & Kornbluth, S. Cdc25 and Wee1: analogous opposites? *Cell Div.* **2,** (2007). doi: 10.1186/1747-1028-2-12.
43. Sherr, C. J. & Roberts, J. M. CDK inhibitors: positive and negative regulators of G1-phase progression. *Genes Dev.* **13,** 1501–1512 (1999).
44. Besson, A., Dowdy, S. F. & Roberts, J. M. CDK Inhibitors: Cell Cycle Regulators and Beyond. *Dev. Cell* **14,** 159–169 (2008).
45. Abbas, T. & Dutta, A. p21 in cancer: intricate networks and multiple activities. *Nat. Rev. Cancer* **9,** 400–14 (2009).
46. Warfel, N. A. & El-Deiry, W. S. p21WAF1 and tumourigenesis. *Curr. Opin. Oncol.* **25,** 52–58 (2013).
47. Campisi, J. & d'Adda di Fagagna, F. Cellular senescence: when bad things happen to good cells. *Nat. Rev. Mol. Cell Biol.* **8,** 729–740 (2007).
48. el-Deiry, W. S. *et al.* WAF1, a potential mediator of p53 tumor suppression. *Cell* **75,** 817–25 (1993).
49. Gartel, A. L. & Tyner, A. L. Transcriptional regulation of the p21((WAF1/CIP1)) gene. *Exp. Cell Res.* **246,** 280–9 (1999).
50. Delavaine, L. & La Thangue, N. B. Control of E2F activity by p21Waf1/Cip1. *Oncogene* **18,** 5381–92 (1999).
51. Harper, J. W. & Elledge, S. J. The role of Cdk7 in CAK function, a retro-retrospective. *Genes Dev.* **12,** 285–289 (1998).
52. Teixeira, L. K. & Reed, S. I. Ubiquitin ligases and cell cycle control. *Annu. Rev. Biochem.* **82,** 387–414 (2013).
53. Bassermann, F., Eichner, R. & Pagano, M. The ubiquitin proteasome system - implications for cell cycle control and the targeted treatment of cancer. *Biochim. Biophys. Acta* **1843,** 150–62 (2014).
54. Jin, J. *et al.* Systematic analysis and nomenclature of mammalian F-box proteins. *Genes Dev.* **18,** 2573–80 (2004).

55. Bornstein, G. *et al.* Role of the SCFSkp2 ubiquitin ligase in the degradation of p21Cip1 in S phase. *J. Biol. Chem.* **278,** 25752–7 (2003).
56. Tsvetkov, L. M., Yeh, K. H., Lee, S. J., Sun, H. & Zhang, H. p27(Kip1) ubiquitination and degradation is regulated by the SCF(Skp2) complex through phosphorylated Thr187 in p27. *Curr. Biol.* **9,** 661–4 (1999).
57. Carrano, A. C., Eytan, E., Hershko, A. & Pagano, M. SKP2 is required for ubiquitin-mediated degradation of the CDK inhibitor p27. *Nat. Cell Biol.* **1,** 193–9 (1999).
58. Sutterlüty, H. *et al.* p45SKP2 promotes p27Kip1 degradation and induces S phase in quiescent cells. *Nat. Cell Biol.* **1,** 207–14 (1999).
59. Tedesco, D., Lukas, J. & Reed, S. I. The pRb-related protein p130 is regulated by phosphorylation-dependent proteolysis via the protein-ubiquitin ligase SCF(Skp2). *Genes Dev.* **16,** 2946–57 (2002).
60. Moberg, K. H., Bell, D. W., Wahrer, D. C., Haber, D. A. & Hariharan, I. K. Archipelago regulates Cyclin E levels in Drosophila and is mutated in human cancer cell lines. *Nature* **413,** 311–6 (2001).
61. Strohmaier, H. *et al.* Human F-box protein hCdc4 targets cyclin E for proteolysis and is mutated in a breast cancer cell line. *Nature* **413,** 316–322 (2001).
62. Koepp, D. M. *et al.* Phosphorylation-dependent ubiquitination of cyclin E by the SCFFbw7 ubiquitin ligase. *Science* **294,** 173–7 (2001).
63. Nakayama, K. I. & Nakayama, K. Regulation of the cell cycle by SCF-type ubiquitin ligases. *Semin. Cell Dev. Biol.* **16,** 323–33 (2005).
64. Watanabe, N. *et al.* M-phase kinases induce phospho-dependent ubiquitination of somatic Wee1 by SCFbeta-TrCP. *Proc. Natl. Acad. Sci. U. S. A.* **101,** 4419–24 (2004).
65. Busino, L. *et al.* Degradation of Cdc25A by beta-TrCP during S phase and in response to DNA damage. *Nature* **426,** 87–91 (2003).
66. Guardavaccaro, D. *et al.* Control of meiotic and mitotic progression by the F box protein beta-Trcp1 in vivo. *Dev. Cell* **4,** 799–812 (2003).
67. Margottin-Goguet, F. *et al.* Prophase destruction of Emi1 by the SCF(betaTrCP/Slimb) ubiquitin ligase activates the anaphase promoting complex to allow progression beyond prometaphase. *Dev. Cell* **4,** 813–26 (2003).
68. Barford, D. *Structure, function and mechanism of the anaphase promoting complex (APC/C). Quarterly reviews of biophysics* **44,** 153-190(2011).
69. Pines, J. Mitosis: A matter of getting rid of the right protein at the right time. *Trends Cell Biol.* **16,** 55–63 (2006).
70. Eguren, M., Manchado, E. & Malumbres, M. Non-mitotic functions of the Anaphase-Promoting Complex. *Semin. Cell Dev. Biol.* **22,** 572–578 (2011).
71. van Leuken, R., Clijsters, L. & Wolthuis, R. To cell cycle, swing the APC/C. *Biochim. Biophys. Acta - Rev. Cancer* **1786,** 49–59 (2008).
72. Qiao, X., Zhang, L., Gamper, A. M., Fujita, T. & Wan, Y. APC/C-Cdh1: from cell cycle to cellular differentiation and genomic integrity. *Cell Cycle* **9,** 3904–12 (2010).
73. Manchado, E., Eguren, M. & Malumbres, M. The anaphase-promoting complex/cyclosome (APC/C): cell-cycle-dependent and -independent functions. *Biochem. Soc. Trans.* **38,** 65–71 (2010).
74. Li, M. & Zhang, P. The function of APC/CCdh1 in cell cycle and beyond. *Cell Div.* **4,** (2009). doi: 10.1186/1747-1028-4-2.
75. Di Fiore, B. & Pines, J. Defining the role of Emi1 in the DNA replication-segregation cycle. *Chromosoma* **117,** 333–338 (2008).
76. Pesin, J. A. & Orr-Weaver, T. L. Regulation of APC/C activators in mitosis and meiosis. *Annu. Rev. Cell Dev. Biol.* **24,** 475–99 (2008).
77. Peters, J.-M. The anaphase promoting complex/cyclosome: a machine designed to destroy. *Nat. Rev. Mol. Cell Biol.* **7,** 644–56 (2006).
78. Rape, M. & Kirschner, M. W. Autonomous regulation of the anaphase-promoting complex couples mitosis to S-phase entry. *Nature* **432,** 588–95 (2004).
79. Listovsky, T. *et al.* Mammalian Cdh1/Fzr mediates its own degradation. *EMBO J.* **23,** 1619–26 (2004).
80. Benmaamar, R. & Pagano, M. Involvement of the SCF complex in the control of Cdh1 degradation in S-phase. *Cell Cycle* **4,** 1230–2 (2005).

81. Zachariae, W. Control of Cyclin Ubiquitination by CDK-Regulated Binding of Hct1 to the Anaphase Promoting Complex. *Science (80-.).* **282,** 1721–1724 (1998).
82. Jaspersen, S. L., Charles, J. F. & Morgan, D. O. Inhibitory phosphorylation of the APC regulator Hct1 is controlled by the kinase Cdc28 and the phosphatase Cdc14. *Curr. Biol.* **9,** 227–36 (1999).
83. Lukas, C. *et al.* Accumulation of cyclin B1 requires E2F and cyclin-A-dependent rearrangement of the anaphase-promoting complex. *Nature* **401,** 815–8 (1999).
84. Blanco, M. A., Sánchez-Díaz, A., de Prada, J. M. & Moreno, S. APC(ste9/srw1) promotes degradation of mitotic cyclins in G(1) and is inhibited by cdc2 phosphorylation. *EMBO J.* **19,** 3945–55 (2000).
85. Kramer, E. R., Scheuringer, N., Podtelejnikov, A. V, Mann, M. & Peters, J. M. Mitotic regulation of the APC activator proteins CDC20 and CDH1. *Mol. Biol. Cell* **11,** 1555–69 (2000).
86. Yamaguchi, S., Okayama, H. & Nurse, P. Fission yeast Fizzy-related protein srw1p is a G(1)-specific promoter of mitotic cyclin B degradation. *EMBO J.* **19,** 3968–77 (2000).
87. Huang, J. N., Park, I., Ellingson, E., Littlepage, L. E. & Pellman, D. Activity of the APC(Cdh1) form of the anaphase-promoting complex persists until S phase and prevents the premature expression of Cdc20p. *J. Cell Biol.* **154,** 85–94 (2001).
88. Sørensen, C. S. *et al.* A conserved cyclin-binding domain determines functional interplay between anaphase-promoting complex-Cdh1 and cyclin A-Cdk2 during cell cycle progression. *Mol. Cell. Biol.* **21,** 3692–703 (2001).
89. Keck, J. M. *et al.* Cyclin E overexpression impairs progression through mitosis by inhibiting APC(Cdh1). *J. Cell Biol.* **178,** 371–85 (2007).
90. Miller, J. J. *et al.* Emi1 stably binds and inhibits the anaphase-promoting complex/cyclosome as a pseudosubstrate inhibitor. *Genes Dev.* **20,** 2410–20 (2006).
91. Reimann, J. D. R. Emi1 regulates the anaphase-promoting complex by a different mechanism than Mad2 proteins. *Genes Dev.* **15,** 3278–3285 (2001).
92. Reimann, J. D. *et al.* Emi1 is a mitotic regulator that interacts with Cdc20 and inhibits the anaphase promoting complex. *Cell* **105,** 645–55 (2001).
93. Hsu, J. Y., Reimann, J. D. R., Sørensen, C. S., Lukas, J. & Jackson, P. K. E2F-dependent accumulation of hEmi1 regulates S phase entry by inhibiting APC(Cdh1). *Nat. Cell Biol.* **4,** 358–66 (2002).
94. Hansen, D. V, Loktev, A. V, Ban, K. H. & Jackson, P. K. Plk1 regulates activation of the anaphase promoting complex by phosphorylating and triggering SCFbetaTrCP-dependent destruction of the APC Inhibitor Emi1. *Mol. Biol. Cell* **15,** 5623–34 (2004).
95. Moshe, Y., Boulaire, J., Pagano, M. & Hershko, A. Role of Polo-like kinase in the degradation of early mitotic inhibitor 1, a regulator of the anaphase promoting complex/cyclosome. *Proc. Natl. Acad. Sci. U. S. A.* **101,** 7937–42 (2004).
96. Eldridge, A. G. *et al.* The evi5 oncogene regulates cyclin accumulation by stabilizing the anaphase-promoting complex inhibitor emi1. *Cell* **124,** 367–80 (2006).
97. Moshe, Y., Bar-On, O., Ganoth, D. & Hershko, A. Regulation of the Action of Early Mitotic Inhibitor 1 on the Anaphase-promoting Complex/Cyclosome by Cyclin-dependent Kinases. *J. Biol. Chem.* **286,** 16647–16657 (2011).
98. Peters, J.-M. The anaphase-promoting complex: proteolysis in mitosis and beyond. *Mol. Cell* **9,** 931–43 (2002).
99. Di Fiore, B. & Pines, J. Emi1 is needed to couple DNA replication with mitosis but does not regulate activation of the mitotic APC/C. *J. Cell Biol.* **177,** 425–37 (2007).
100. Geley, S. *et al.* Anaphase-promoting complex/cyclosome-dependent proteolysis of human cyclin A starts at the beginning of mitosis and is not subject to the spindle assembly checkpoint. *J. Cell Biol.* **153,** 137–48 (2001).
101. Hames, R. S., Wattam, S. L., Yamano, H., Bacchieri, R. & Fry, A. M. APC/C-mediated destruction of the centrosomal kinase Nek2A occurs in early mitosis and depends upon a cyclin A-type D-box. *EMBO J.* **20,** 7117–27 (2001).
102. Amador, V., Ge, S., Santamaría, P. G., Guardavaccaro, D. & Pagano, M. APC/C(Cdc20) controls the ubiquitin-mediated degradation of p21 in prometaphase. *Mol. Cell* **27,** 462–73 (2007).
103. Dawson, I. A., Roth, S. & Artavanis-Tsakonas, S. The Drosophila cell cycle gene fizzy is required for normal degradation of cyclins A and B during mitosis and has homology to the CDC20 gene of

Saccharomyces cerevisiae. *J. Cell Biol.* **129,** 725–37 (1995).

104. D'Amours, D. & Amon, A. At the interface between signaling and executing anaphase--Cdc14 and the FEAR network. *Genes Dev.* **18,** 2581–95 (2004).
105. Sullivan, M. & Morgan, D. O. Finishing mitosis, one step at a time. *Nat. Rev. Mol. Cell Biol.* **8,** 894–903 (2007).
106. Pfleger, C. M. & Kirschner, M. W. The KEN box: an APC recognition signal distinct from the D box targeted by Cdh1. *Genes Dev.* **14,** 655–65 (2000).
107. Prinz, S., Hwang, E. S., Visintin, R. & Amon, A. The regulation of Cdc20 proteolysis reveals a role for APC components Cdc23 and Cdc27 during S phase and early mitosis. *Curr. Biol.* **8,** 750–60 (1998).
108. Zur, A. & Brandeis, M. Securin degradation is mediated by fzy and fzr, and is required for complete chromatid separation but not for cytokinesis. *EMBO J.* **20,** 792–801 (2001).
109. Zou, H. Identification of a Vertebrate Sister-Chromatid Separation Inhibitor Involved in Transformation and Tumorigenesis. *Science (80-.).* **285,** 418–422 (1999).
110. Lindon, C. & Pines, J. Ordered proteolysis in anaphase inactivates Plk1 to contribute to proper mitotic exit in human cells. *J. Cell Biol.* **164,** 233–41 (2004).
111. Castro, A. *et al.* APC/Fizzy-Related targets Aurora-A kinase for proteolysis. *EMBO Rep.* **3,** 457–62 (2002).
112. Castro, A. *et al.* The D-Box-activating domain (DAD) is a new proteolysis signal that stimulates the silent D-Box sequence of Aurora-A. *EMBO Rep.* **3,** 1209–14 (2002).
113. Stewart, S. & Fang, G. Anaphase-promoting complex/cyclosome controls the stability of TPX2 during mitotic exit. *Mol. Cell. Biol.* **25,** 10516–27 (2005).
114. Sigrist, S. J. & Lehner, C. F. Drosophila fizzy-related Down-Regulates Mitotic Cyclins and Is Required for Cell Proliferation Arrest and Entry into Endocycles. *Cell* **90,** 671–681 (1997).
115. Arias, E. E. & Walter, J. C. Strength in numbers: preventing rereplication via multiple mechanisms in eukaryotic cells. *Genes Dev.* **21,** 497–518 (2007).
116. Blow, J. J. & Dutta, A. Preventing re-replication of chromosomal DNA. *Nat. Rev. Mol. Cell Biol.* **6,** 476–86 (2005).
117. Gillespie, P. J., Li, A. & Blow, J. J. Reconstitution of licensed replication origins on Xenopus sperm nuclei using purified proteins. *BMC Biochem.* **2,** (2001). doi: 10.1186/1471-2091-2-15.
118. Alver, R. C., Chadha, G. S. & Blow, J. J. The contribution of dormant origins to genome stability: from cell biology to human genetics. *DNA Repair (Amst).* **19,** 182–9 (2014).
119. Evrin, C. *et al.* A double-hexameric MCM2-7 complex is loaded onto origin DNA during licensing of eukaryotic DNA replication. *Proc. Natl. Acad. Sci. U. S. A.* **106,** 20240–5 (2009).
120. Fernández-Cid, A. *et al.* An ORC/Cdc6/MCM2-7 complex is formed in a multistep reaction to serve as a platform for MCM double-hexamer assembly. *Mol. Cell* **50,** 577–88 (2013).
121. Frigola, J., Remus, D., Mehanna, A. & Diffley, J. F. X. ATPase-dependent quality control of DNA replication origin licensing. *Nature* **495,** 339–43 (2013).
122. Gambus, A., Khoudoli, G. A., Jones, R. C. & Blow, J. J. MCM2-7 form double hexamers at licensed origins in Xenopus egg extract. *J. Biol. Chem.* **286,** 11855–64 (2011).
123. Remus, D. *et al.* Concerted loading of Mcm2-7 double hexamers around DNA during DNA replication origin licensing. *Cell* **139,** 719–30 (2009).
124. Ilves, I., Petojevic, T., Pesavento, J. J. & Botchan, M. R. Activation of the MCM2-7 helicase by association with Cdc45 and GINS proteins. *Mol. Cell* **37,** 247–58 (2010).
125. Blow, J. J., Ge, X. Q. & Jackson, D. A. How dormant origins promote complete genome replication. *Trends Biochem. Sci.* **36,** 405–14 (2011).
126. Donzelli, M. *et al.* Dual mode of degradation of Cdc25 A phosphatase. *EMBO J.* **21,** 4875–84 (2002).
127. Ayad, N. G. *et al.* Tome-1, a trigger of mitotic entry, is degraded during G1 via the APC. *Cell* **113,** 101–13 (2003).
128. Wei, W. *et al.* Degradation of the SCF component Skp2 in cell-cycle phase G1 by the anaphase-promoting complex. *Nature* **428,** 194–8 (2004).
129. Bashir, T., Dorrello, N. V., Amador, V., Guardavaccaro, D. & Pagano, M. Control of the SCF(Skp2-Cks1) ubiquitin ligase by the APC/C(Cdh1) ubiquitin ligase. *Nature* **428,** 190–3 (2004).
130. McGarry, T. J. & Kirschner, M. W. Geminin, an inhibitor of DNA replication, is degraded during mitosis.

Cell **93,** 1043–53 (1998).

131. Zielke, N., Querings, S., Rottig, C., Lehner, C. & Sprenger, F. The anaphase-promoting complex/cyclosome (APC/C) is required for rereplication control in endoreplication cycles. *Genes Dev.* **22,** 1690–703 (2008).
132. Wohlschlegel, J. A. *et al.* Inhibition of eukaryotic DNA replication by geminin binding to Cdt1. *Science* **290,** 2309–12 (2000).
133. Tada, S., Li, A., Maiorano, D., Méchali, M. & Blow, J. J. Repression of origin assembly in metaphase depends on inhibition of RLF-B/Cdt1 by geminin. *Nat. Cell Biol.* **3,** 107–13 (2001).
134. Drury, L. S., Perkins, G. & Diffley, J. F. The Cdc4/34/53 pathway targets Cdc6p for proteolysis in budding yeast. *EMBO J.* **16,** 5966–76 (1997).
135. Sánchez, M., Calzada, A. & Bueno, A. The Cdc6 protein is ubiquitinated in vivo for proteolysis in Saccharomyces cerevisiae. *J. Biol. Chem.* **274,** 9092–7 (1999).
136. Drury, L. S., Perkins, G. & Diffley, J. F. The cyclin-dependent kinase Cdc28p regulates distinct modes of Cdc6p proteolysis during the budding yeast cell cycle. *Curr. Biol.* **10,** 231–40 (2000).
137. Elsasser, S., Chi, Y., Yang, P. & Campbell, J. L. Phosphorylation controls timing of Cdc6p destruction: A biochemical analysis. *Mol. Biol. Cell* **10,** 3263–77 (1999).
138. Petersen, B. O., Lukas, J., Sørensen, C. S., Bartek, J. & Helin, K. Phosphorylation of mammalian CDC6 by cyclin A/CDK2 regulates its subcellular localization. *EMBO J.* **18,** 396–410 (1999).
139. Jiang, W., Wells, N. J. & Hunter, T. Multistep regulation of DNA replication by Cdk phosphorylation of HsCdc6. *Proc. Natl. Acad. Sci. U. S. A.* **96,** 6193–8 (1999).
140. Petersen, B. O. *et al.* Cell cycle- and cell growth-regulated proteolysis of mammalian CDC6 is dependent on APC-CDH1. *Genes Dev.* **14,** 2330–43 (2000).
141. Mailand, N. & Diffley, J. F. X. CDKs promote DNA replication origin licensing in human cells by protecting Cdc6 from APC/C-dependent proteolysis. *Cell* **122,** 915–26 (2005).
142. Ke, P.-Y. & Chang, Z.-F. Mitotic degradation of human thymidine kinase 1 is dependent on the anaphase-promoting complex/cyclosome-CDH1-mediated pathway. *Mol. Cell. Biol.* **24,** 514–26 (2004).
143. Ke, P.-Y., Kuo, Y.-Y., Hu, C.-M. & Chang, Z.-F. Control of dTTP pool size by anaphase promoting complex/cyclosome is essential for the maintenance of genetic stability. *Genes Dev.* **19,** 1920–33 (2005).
144. Skaar, J. R. & Pagano, M. Control of cell growth by the SCF and APC/C ubiquitin ligases. *Curr. Opin. Cell Biol.* **21,** 816–24 (2009).
145. Yuan, X., Srividhya, J., De Luca, T., Lee, J.-H. E. & Pomerening, J. R. Uncovering the role of APC-Cdh1 in generating the dynamics of S-phase onset. *Mol. Biol. Cell* **25,** 441–56 (2014).
146. Sigl, R. *et al.* Loss of the mammalian APC/C activator FZR1 shortens G1 and lengthens S phase but has little effect on exit from mitosis. *J. Cell Sci.* **122,** 4208–17 (2009).
147. Engelbert, D., Schnerch, D., Baumgarten, A. & Wäsch, R. The ubiquitin ligase APC(Cdh1) is required to maintain genome integrity in primary human cells. *Oncogene* **27,** 907–17 (2008).
148. García-Higuera, I. *et al.* Genomic stability and tumour suppression by the APC/C cofactor Cdh1. *Nat. Cell Biol.* **10,** 802–11 (2008).
149. Greil, C. *et al.* The role of APC/C(Cdh1) in replication stress and origin of genomic instability. *Oncogene* (2015). doi:10.1038/onc.2015.367.
150. Bassermann, F. *et al.* The Cdc14B-Cdh1-Plk1 axis controls the G2 DNA-damage-response checkpoint. *Cell* **134,** 256–67 (2008).
151. Wiebusch, L. & Hagemeier, C. p53- and p21-dependent premature APC/C-Cdh1 activation in G2 is part of the long-term response to genotoxic stress. *Oncogene* **29,** 3477–89 (2010).
152. Lee, J., Kim, J. A., Barbier, V., Fotedar, A. & Fotedar, R. DNA damage triggers p21WAF1-dependent Emi1 down-regulation that maintains G2 arrest. *Mol. Biol. Cell* **20,** 1891–902 (2009).
153. Wang, Q. *et al.* Alterations of anaphase-promoting complex genes in human colon cancer cells. *Oncogene* **22,** 1486–90 (2003).
154. Machida, Y. J. & Dutta, A. The APC/C inhibitor, Emi1, is essential for prevention of rereplication. *Genes Dev.* **21,** 184–94 (2007).
155. Alabert, C. & Groth, A. Chromatin replication and epigenome maintenance. *Nat. Rev. Mol. Cell Biol.* **13,** 153–67 (2012).

156. MacAlpine, D. M. & Almouzni, G. Chromatin and DNA replication. *Cold Spring Harb. Perspect. Biol.* **5,** a010207 (2013).
157. Cea, V., Cipolla, L. & Sabbioneda, S. Replication of Structured DNA and its implication in epigenetic stability. *Front. Genet.* **6,** (2015). doi: 10.3389/fgene.2015.00209.
158. Renard-Guillet, C., Kanoh, Y., Shirahige, K. & Masai, H. Temporal and spatial regulation of eukaryotic DNA replication: from regulated initiation to genome-scale timing program. *Semin. Cell Dev. Biol.* **30,** 110–20 (2014).
159. Fragkos, M., Ganier, O., Coulombe, P. & Méchali, M. DNA replication origin activation in space and time. *Nat. Rev. Mol. Cell Biol.* **16,** 360–74 (2015).
160. MackNeil, S (ed.). The Eukaryotic Replisome: a Guide to Protein Structure and Function. *Book.* (2012).
161. Jones, R. M. & Petermann, E. Replication fork dynamics and the DNA damage response. *Biochem. J.* **443,** 13–26 (2012).
162. Lei, M. *et al.* Mcm2 is a target of regulation by Cdc7-Dbf4 during the initiation of DNA synthesis. *Genes Dev.* **11,** 3365–74 (1997).
163. Krude, T., Jackman, M., Pines, J. & Laskey, R. A. Cyclin/Cdk-Dependent Initiation of DNA Replication in a Human Cell-Free System. *Cell* **88,** 109–119 (1997).
164. Labib, K. How do Cdc7 and cyclin-dependent kinases trigger the initiation of chromosome replication in eukaryotic cells? *Genes Dev.* **24,** 1208–19 (2010).
165. Araki, H. Initiation of chromosomal DNA replication in eukaryotic cells; contribution of yeast genetics to the elucidation. *Genes Genet. Syst.* **86,** 141–149 (2011).
166. Weinreich, M. & Stillman, B. Cdc7p-Dbf4p kinase binds to chromatin during S phase and is regulated by both the APC and the RAD53 checkpoint pathway. *EMBO J.* **18,** 5334–46 (1999).
167. Araki, H. Cyclin-dependent kinase-dependent initiation of chromosomal DNA replication. *Curr. Opin. Cell Biol.* **22,** 766–71 (2010).
168. Tak, Y.-S., Tanaka, Y., Endo, S., Kamimura, Y. & Araki, H. A CDK-catalysed regulatory phosphorylation for formation of the DNA replication complex Sld2-Dpb11. *EMBO J.* **25,** 1987–96 (2006).
169. Masumoto, H., Muramatsu, S., Kamimura, Y. & Araki, H. S-Cdk-dependent phosphorylation of Sld2 essential for chromosomal DNA replication in budding yeast. *Nature* **415,** 651–5 (2002).
170. Tanaka, S. *et al.* CDK-dependent phosphorylation of Sld2 and Sld3 initiates DNA replication in budding yeast. *Nature* **445,** 328–32 (2007).
171. Zegerman, P. & Diffley, J. F. X. Phosphorylation of Sld2 and Sld3 by cyclin-dependent kinases promotes DNA replication in budding yeast. *Nature* **445,** 281–5 (2007).
172. Kamimura, Y., Tak, Y. S., Sugino, A. & Araki, H. Sld3, which interacts with Cdc45 (Sld4), functions for chromosomal DNA replication in Saccharomyces cerevisiae. *EMBO J.* **20,** 2097–107 (2001).
173. Kanemaki, M. & Labib, K. Distinct roles for Sld3 and GINS during establishment and progression of eukaryotic DNA replication forks. *EMBO J.* **25,** 1753–63 (2006).
174. Muramatsu, S., Hirai, K., Tak, Y.-S., Kamimura, Y. & Araki, H. CDK-dependent complex formation between replication proteins Dpb11, Sld2, Pol (epsilon}, and GINS in budding yeast. *Genes Dev.* **24,** 602–12 (2010).
175. Im, J.-S. *et al.* Assembly of the Cdc45-Mcm2-7-GINS complex in human cells requires the Ctf4/And-1, RecQL4, and Mcm10 proteins. *Proc. Natl. Acad. Sci. U. S. A.* **106,** 15628–32 (2009).
176. Schmidt, U. *et al.* Characterization of the interaction between the human DNA topoisomerase IIbeta-binding protein 1 (TopBP1) and the cell division cycle 45 (Cdc45) protein. *Biochem. J.* **409,** 169–77 (2008).
177. Kumagai, A., Shevchenko, A., Shevchenko, A. & Dunphy, W. G. Direct regulation of Treslin by cyclin-dependent kinase is essential for the onset of DNA replication. *J. Cell Biol.* **193,** 995–1007 (2011).
178. Kumagai, A., Shevchenko, A., Shevchenko, A. & Dunphy, W. G. Treslin collaborates with TopBP1 in triggering the initiation of DNA replication. *Cell* **140,** 349–59 (2010).
179. Matsuno, K., Kumano, M., Kubota, Y., Hashimoto, Y. & Takisawa, H. The N-terminal noncatalytic region of Xenopus RecQ4 is required for chromatin binding of DNA polymerase alpha in the initiation of DNA replication. *Mol. Cell. Biol.* **26,** 4843–52 (2006).
180. Sangrithi, M. N. *et al.* Initiation of DNA replication requires the RECQL4 protein mutated in Rothmund-Thomson syndrome. *Cell* **121,** 887–98 (2005).

181. Balestrini, A., Cosentino, C., Errico, A., Garner, E. & Costanzo, V. GEMC1 is a TopBP1-interacting protein required for chromosomal DNA replication. *Nat. Cell Biol.* **12,** 484–91 (2010).

182. Chowdhury, A. *et al.* The DNA unwinding element binding protein DUE-B interacts with Cdc45 in preinitiation complex formation. *Mol. Cell. Biol.* **30,** 1495–507 (2010).

183. Thu, Y. M. & Bielinsky, A.-K. MCM10: one tool for all-Integrity, maintenance and damage control. *Semin. Cell Dev. Biol.* **30,** 121–30 (2014).

184. Wold, M. S. & Kelly, T. Purification and characterization of replication protein A, a cellular protein required for in vitro replication of simian virus 40 DNA. *Proc. Natl. Acad. Sci. U. S. A.* **85,** 2523–7 (1988).

185. Alani, E., Thresher, R., Griffith, J. D. & Kolodner, R. D. Characterization of DNA-binding and strand-exchange stimulation properties of y-RPA, a yeast single-strand-DNA-binding protein. *J. Mol. Biol.* **227,** 54–71 (1992).

186. Chen, S. H., Chan, N.-L. & Hsieh, T. New mechanistic and functional insights into DNA topoisomerases. *Annu. Rev. Biochem.* **82,** 139–70 (2013).

187. LEHMAN, I. R., BESSMAN, M. J., SIMMS, E. S. & KORNBERG, A. Enzymatic synthesis of deoxyribonucleic acid. I. Preparation of substrates and partial purification of an enzyme from Escherichia coli. *J. Biol. Chem.* **233,** 163–70 (1958).

188. Pursell, Z. F., Isoz, I., Lundstrom, E.-B., Johansson, E. & Kunkel, T. A. Yeast DNA Polymerase Participates in Leading-Strand DNA Replication. *Science (80-.).* **317,** 127–130 (2007).

189. Nick McElhinny, S. A., Gordenin, D. A., Stith, C. M., Burgers, P. M. J. & Kunkel, T. A. Division of labor at the eukaryotic replication fork. *Mol. Cell* **30,** 137–44 (2008).

190. Stillman, B. DNA polymerases at the replication fork in eukaryotes. *Spring* **30,** 259–260 (2008).

191. Kunkel, T. A. & Burgers, P. M. Dividing the workload at a eukaryotic replication fork. *Trends Cell Biol.* **18,** 521–7 (2008).

192. Sugimoto, K., Okazaki, T. & Okazaki, R. Mechanism of DNA chain growth, II. Accumulation of newly synthesized short chains in E. coli infected with ligase-defective T4 phages. *Proc. Natl. Acad. Sci. U. S. A.* **60,** 1356–62 (1968).

193. Nethanel, T., Zlotkin, T. & Kaufmann, G. Assembly of simian virus 40 Okazaki pieces from DNA primers is reversibly arrested by ATP depletion. *J. Virol.* **66,** 6634–40 (1992).

194. Fisher, P. A., Wang, T. S. & Korn, D. Enzymological characterization of DNA polymerase alpha. Basic catalytic properties processivity, and gap utilization of the homogeneous enzyme from human KB cells. *J. Biol. Chem.* **254,** 6128–37 (1979).

195. Tsurimoto, T. & Stillman, B. Replication factors required for SV40 DNA replication in vitro. II. Switching of DNA polymerase alpha and delta during initiation of leading and lagging strand synthesis. *J. Biol. Chem.* **266,** 1961–8 (1991).

196. Prelich, G. *et al.* Functional identity of proliferating cell nuclear antigen and a DNA polymerase-delta auxiliary protein. *Nature* **326,** 517–20

197. Majka, J. & Burgers, P. M. J. The PCNA-RFC families of DNA clamps and clamp loaders. *Prog. Nucleic Acid Res. Mol. Biol.* **78,** 227–60 (2004).

198. Waga, S., Bauer, G. & Stillman, B. Reconstitution of complete SV40 DNA replication with purified replication factors. *J. Biol. Chem.* **269,** 10923–34 (1994).

199. Errico, A. & Costanzo, V. Mechanisms of replication fork protection: a safeguard for genome stability. *Crit. Rev. Biochem. Mol. Biol.* **47,** 222–235 (2012).

200. Cobb, J. A. *et al.* Replisome instability, fork collapse, and gross chromosomal rearrangements arise synergistically from Mec1 kinase and RecQ helicase mutations. *Genes Dev.* **19,** 3055–69 (2005).

201. Sogo, J. M., Lopes, M. & Foiani, M. Fork reversal and ssDNA accumulation at stalled replication forks owing to checkpoint defects. *Science* **297,** 599–602 (2002).

202. Cortez, D., Glick, G. & Elledge, S. J. Minichromosome maintenance proteins are direct targets of the ATM and ATR checkpoint kinases. *Proc. Natl. Acad. Sci. U. S. A.* **101,** 10078–83 (2004).

203. Tsao, C.-C., Geisen, C. & Abraham, R. T. Interaction between human MCM7 and Rad17 proteins is required for replication checkpoint signaling. *EMBO J.* **23,** 4660–9 (2004).

204. Gambus, A. *et al.* GINS maintains association of Cdc45 with MCM in replisome progression complexes at eukaryotic DNA replication forks. *Nat. Cell Biol.* **8,** 358–66 (2006).

205. Gambus, A. *et al.* A key role for Ctf4 in coupling the MCM2-7 helicase to DNA polymerase α within the

eukaryotic replisome. *EMBO J.* **28,** 2992–3004 (2009).

206. Remeseiro, S. & Losada, A. Cohesin, a chromatin engagement ring. *Curr. Opin. Cell Biol.* **25,** 63–71 (2013).
207. Bailey, R., Priego Moreno, S. & Gambus, A. Termination of DNA replication forks: 'Breaking up is hard to do'. *Nucleus* **1034,** 1–10 (2015).
208. Dewar, J. M., Budzowska, M. & Walter, J. C. The mechanism of DNA replication termination in vertebrates. *Nature* **525,** 345–50 (2015).
209. Sundin, O. & Varshavsky, A. Terminal stages of SV40 DNA replication proceed via multiply intertwined catenated dimers. *Cell* **21,** 103–14 (1980).
210. Ishimi, Y., Sugasawa, K., Hanaoka, F., Eki, T. & Hurwitz, J. Topoisomerase II plays an essential role as a swivelase in the late stage of SV40 chromosome replication in vitro. *J. Biol. Chem.* **267,** 462–6 (1992).
211. Moreno, S. P., Bailey, R., Campion, N., Herron, S. & Gambus, A. Polyubiquitylation drives replisome disassembly at the termination of DNA replication. *Science* **346,** 477–81 (2014).
212. Maric, M., Maculins, T., De Piccoli, G. & Labib, K. Cdc48 and a ubiquitin ligase drive disassembly of the CMG helicase at the end of DNA replication. *Science* **346,** (2014). doi: 10.1126/science.1253596.
213. Maculins, T., Nkosi, P. J., Nishikawa, H. & Labib, K. Tethering of SCF(Dia2) to the Replisome Promotes Efficient Ubiquitylation and Disassembly of the CMG Helicase. *Curr. Biol.* **25,** 2254–9 (2015).
214. Luger, K., Dechassa, M. L. & Tremethick, D. J. New insights into nucleosome and chromatin structure: an ordered state or a disordered affair? *Nat. Rev. Mol. Cell Biol.* **13,** 436–447 (2012).
215. Marzluff, W. F., Wagner, E. J. & Duronio, R. J. Metabolism and regulation of canonical histone mRNAs: life without a poly(A) tail. *Nat. Rev. Genet.* **9,** 843–54 (2008).
216. Shibahara, K. & Stillman, B. Replication-dependent marking of DNA by PCNA facilitates CAF-1-coupled inheritance of chromatin. *Cell* **96,** 575–85 (1999).
217. Moggs, J. G. *et al.* A CAF-1-PCNA-mediated chromatin assembly pathway triggered by sensing DNA damage. *Mol. Cell. Biol.* **20,** 1206–18 (2000).
218. Gérard, A. *et al.* The replication kinase Cdc7-Dbf4 promotes the interaction of the p150 subunit of chromatin assembly factor 1 with proliferating cell nuclear antigen. *EMBO Rep.* **7,** 817–23 (2006).
219. Tyler, J. K. *et al.* The RCAF complex mediates chromatin assembly during DNA replication and repair. *Nature* **402,** 555–60 (1999).
220. Mello, J. A. *et al.* Human Asf1 and CAF-1 interact and synergize in a repair-coupled nucleosome assembly pathway. *EMBO Rep.* **3,** 329–34 (2002).
221. Groth, A. *et al.* Regulation of replication fork progression through histone supply and demand. *Science* **318,** 1928–31 (2007).
222. Tyler, J. K. *et al.* Interaction between the Drosophila CAF-1 and ASF1 chromatin assembly factors. *Mol. Cell. Biol.* **21,** 6574–84 (2001).
223. Zlatanova, J., Seebart, C. & Tomschik, M. Nap1: taking a closer look at a juggler protein of extraordinary skills. *FASEB J.* **21,** 1294–310 (2007).
224. Formosa, T. The role of FACT in making and breaking nucleosomes. *Biochim. Biophys. Acta* **1819,** 247–55 (2012).
225. Kimura, H. & Cook, P. R. Kinetics of core histones in living human cells: little exchange of H3 and H4 and some rapid exchange of H2B. *J. Cell Biol.* **153,** 1341–53 (2001).
226. Francis, N. J., Follmer, N. E., Simon, M. D., Aghia, G. & Butler, J. D. Polycomb proteins remain bound to chromatin and DNA during DNA replication in vitro. *Cell* **137,** 110–22 (2009).
227. Alabert, C. *et al.* Two distinct modes for propagation of histone PTMs across the cell cycle. *Genes Dev.* **29,** 585–90 (2015).
228. Besnard, E. *et al.* Unraveling cell type-specific and reprogrammable human replication origin signatures associated with G-quadruplex consensus motifs. *Nat. Struct. Mol. Biol.* **19,** 837–44 (2012).
229. McIntosh, D. & Blow, J. J. Dormant origins, the licensing checkpoint, and the response to replicative stresses. *Cold Spring Harb. Perspect. Biol.* **4,** a012955 (2012).
230. Woodward, A. M. *et al.* Excess Mcm2-7 license dormant origins of replication that can be used under conditions of replicative stress. *J. Cell Biol.* **173,** 673–83 (2006).
231. Ibarra, A., Schwob, E. & Méndez, J. Excess MCM proteins protect human cells from replicative stress by

licensing backup origins of replication. *Proc. Natl. Acad. Sci. U. S. A.* **105,** 8956–61 (2008).

232. Ge, X. Q., Jackson, D. A. & Blow, J. J. Dormant origins licensed by excess Mcm2-7 are required for human cells to survive replicative stress. *Genes Dev.* **21,** 3331–41 (2007).
233. Cayrou, C. *et al.* Genome-scale analysis of metazoan replication origins reveals their organization in specific but flexible sites defined by conserved features. *Genome Res.* **21,** 1438–49 (2011).
234. Yamazaki, S. *et al.* Rif1 regulates the replication timing domains on the human genome. *EMBO J.* **31,** 3667–77 (2012).
235. Hayano, M. *et al.* Rif1 is a global regulator of timing of replication origin firing in fission yeast. *Genes Dev.* **26,** 137–50 (2012).
236. Cornacchia, D. *et al.* Mouse Rif1 is a key regulator of the replication-timing programme in mammalian cells. *EMBO J.* **31,** 3678–90 (2012).
237. Yamazaki, S., Hayano, M. & Masai, H. Replication timing regulation of eukaryotic replicons: Rif1 as a global regulator of replication timing. *Trends Genet.* **29,** 449–60 (2013).
238. Sheehan, M. A., Mills, A. D., Sleeman, A. M., Laskey, R. A. & Blow, J. J. Steps in the assembly of replication-competent nuclei in a cell-free system from Xenopus eggs. *J. Cell Biol.* **106,** 1–12 (1988).
239. Moir, R. D., Spann, T. P., Herrmann, H. & Goldman, R. D. Disruption of nuclear lamin organization blocks the elongation phase of DNA replication. *J. Cell Biol.* **149,** 1179–92 (2000).
240. Guelen, L. *et al.* Domain organization of human chromosomes revealed by mapping of nuclear lamina interactions. *Nature* **453,** 948–51 (2008).
241. Hansen, R. S. *et al.* Sequencing newly replicated DNA reveals widespread plasticity in human replication timing. *Proc. Natl. Acad. Sci. U. S. A.* **107,** 139–44 (2010).
242. Meister, P., Taddei, A., Ponti, A., Baldacci, G. & Gasser, S. M. Replication foci dynamics: replication patterns are modulated by S-phase checkpoint kinases in fission yeast. *EMBO J.* **26,** 1315–26 (2007).
243. Chagin, V. O., Stear, J. H. & Cardoso, M. C. Organization of DNA replication. *Cold Spring Harb. Perspect. Biol.* **2,** a000737 (2010).
244. Zeman, M. K. & Cimprich, K. A. Causes and consequences of replication stress. *Nat. Cell Biol.* **16,** 2–9 (2014).
245. Lecona, E. & Fernández-Capetillo, O. Replication stress and cancer: It takes two to tango. *Exp. Cell Res.* **329,** 26–34 (2014).
246. Gaillard, H., García-Muse, T. & Aguilera, A. Replication stress and cancer. *Nat. Rev. Cancer* **15,** 276–289 (2015).
247. Branzei, D. & Foiani, M. The checkpoint response to replication stress. *DNA Repair (Amst).* **8,** 1038–1046 (2009).
248. Magdalou, I., Lopez, B. S., Pasero, P. & Lambert, S. A. E. The causes of replication stress and their consequences on genome stability and cell fate. *Semin. Cell Dev. Biol.* **30,** 154–64 (2014).
249. Yekezare, M., Gómez-González, B. & Diffley, J. F. X. Controlling DNA replication origins in response to DNA damage - inhibit globally, activate locally. *J. Cell Sci.* **126,** 1297–306 (2013).
250. Elford, H. L. Effect of hydroxyurea on ribonucleotide reductase. *Biochem. Biophys. Res. Commun.* **33,** 129–35 (1968).
251. Eklund, H., Uhlin, U., Färnegårdh, M., Logan, D. T. D. T. & Nordlund, P. Structure and function of the radical enzyme ribonucleotide reductase. *Prog. Biophys. Mol. Biol.* **77,** 177–268 (2001).
252. Di Micco, R. *et al.* Oncogene-induced senescence is a DNA damage response triggered by DNA hyper-replication. *Nature* **444,** 638–42 (2006).
253. Bartkova, J. *et al.* Oncogene-induced senescence is part of the tumorigenesis barrier imposed by DNA damage checkpoints. *Nature* **444,** 633–7 (2006).
254. Bester, A. C. *et al.* Nucleotide Deficiency Promotes Genomic Instability in Early Stages of Cancer Development. *Cell* **145,** 435–446 (2011).
255. Clemente-Ruiz, M. & Prado, F. Chromatin assembly controls replication fork stability. *EMBO Rep.* **10,** 790–6 (2009).
256. Clemente-Ruiz, M., González-Prieto, R. & Prado, F. Histone H3K56 acetylation, CAF1, and Rtt106 coordinate nucleosome assembly and stability of advancing replication forks. *PLoS Genet.* **7,** e1002376 (2011).

257. Mejlvang, J. *et al.* New histone supply regulates replication fork speed and PCNA unloading. *J. Cell Biol.* **204,** 29–43 (2014).
258. Rizzo, A. *et al.* Stabilization of quadruplex DNA perturbs telomere replication leading to the activation of an ATR-dependent ATM signaling pathway. *Nucleic Acids Res.* **37,** 5353–64 (2009).
259. Gottipati, P., Cassel, T. N., Savolainen, L. & Helleday, T. Transcription-associated recombination is dependent on replication in Mammalian cells. *Mol. Cell. Biol.* **28,** 154–64 (2008).
260. Jones, R. M. *et al.* Increased replication initiation and conflicts with transcription underlie Cyclin E-induced replication stress. *Oncogene* **32,** 3744–53 (2013).
261. Bermejo, R., Lai, M. S. & Foiani, M. Preventing replication stress to maintain genome stability: resolving conflicts between replication and transcription. *Mol. Cell* **45,** 710–8 (2012).
262. Tuduri, S. *et al.* Topoisomerase I suppresses genomic instability by preventing interference between replication and transcription. *Nat. Cell Biol.* **11,** 1315–24 (2009).
263. Bermejo, R. *et al.* Genome-organizing factors Top2 and Hmo1 prevent chromosome fragility at sites of S phase transcription. *Cell* **138,** 870–84 (2009).
264. Domínguez-Sánchez, M. S., Barroso, S., Gómez-González, B., Luna, R. & Aguilera, A. Genome instability and transcription elongation impairment in human cells depleted of THO/TREX. *PLoS Genet.* **7,** e1002386 (2011).
265. Thomas, M., White, R. L. & Davis, R. W. Hybridization of RNA to double-stranded DNA: formation of R-loops. *Proc. Natl. Acad. Sci. U. S. A.* **73,** 2294–8 (1976).
266. Stirling, P. C. *et al.* R-loop-mediated genome instability in mRNA cleavage and polyadenylation mutants. *Genes Dev.* **26,** 163–75 (2012).
267. Mischo, H. E. *et al.* Yeast Sen1 helicase protects the genome from transcription-associated instability. *Mol. Cell* **41,** 21–32 (2011).
268. Alzu, A. *et al.* Senataxin associates with replication forks to protect fork integrity across RNA-polymerase-II-transcribed genes. *Cell* **151,** 835–46 (2012).
269. Kawabata, T. *et al.* Stalled fork rescue via dormant replication origins in unchallenged S phase promotes proper chromosome segregation and tumor suppression. *Mol. Cell* **41,** 543–53 (2011).
270. Ekholm-Reed, S. *et al.* Deregulation of cyclin E in human cells interferes with prereplication complex assembly. *J. Cell Biol.* **165,** 789–800 (2004).
271. Méchali, M., Yoshida, K., Coulombe, P. & Pasero, P. Genetic and epigenetic determinants of DNA replication origins, position and activation. *Curr. Opin. Genet. Dev.* **23,** 124–31 (2013).
272. Zaratiegui, M. *et al.* RNAi promotes heterochromatic silencing through replication-coupled release of RNA Pol II. *Nature* **479,** 135–8 (2011).
273. Li, A. & Blow, J. J. Cdt1 downregulation by proteolysis and geminin inhibition prevents DNA re-replication in Xenopus. *EMBO J.* **24,** 395–404 (2005).
274. Liontos, M. *et al.* Deregulated overexpression of hCdt1 and hCdc6 promotes malignant behavior. *Cancer Res.* **67,** 10899–909 (2007).
275. Melixetian, M. *et al.* Loss of Geminin induces rereplication in the presence of functional p53. *J. Cell Biol.* **165,** 473–82 (2004).
276. Bartkova, J. *et al.* DNA damage response as a candidate anti-cancer barrier in early human tumorigenesis. *Nature* **434,** 864–70 (2005).
277. Tardat, M. *et al.* The histone H4 Lys 20 methyltransferase PR-Set7 regulates replication origins in mammalian cells. *Nat. Cell Biol.* **12,** 1086–93 (2010).
278. Black, J. C. *et al.* KDM4A lysine demethylase induces site-specific copy gain and rereplication of regions amplified in tumors. *Cell* **154,** 541–55 (2013).
279. Neelsen, K. J. *et al.* Deregulated origin licensing leads to chromosomal breaks by rereplication of a gapped DNA template. *Genes Dev.* **27,** 2537–42 (2013).
280. Yeeles, J. T. P., Poli, J., Marians, K. J. & Pasero, P. Rescuing stalled or damaged replication forks. *Cold Spring Harb. Perspect. Biol.* **5,** a012815 (2013).
281. Berti, M. & Vindigni, A. Replication stress: getting back on track. *Nat. Struct. Mol. Biol.* **23,** 103–109 (2016).
282. Vaziri, C. & Masai, H. Integrating DNA replication with trans-lesion synthesis via Cdc7. *Cell Cycle* **9,** 4818–

23 (2010).

283. Heller, R. C. & Marians, K. J. Replication fork reactivation downstream of a blocked nascent leading strand. *Nature* **439,** 557–62 (2006).
284. Yeeles, J. T. P. & Marians, K. J. The Escherichia coli replisome is inherently DNA damage tolerant. *Science* **334,** 235–8 (2011).
285. Elvers, I., Johansson, F., Groth, P., Erixon, K. & Helleday, T. UV stalled replication forks restart by re-priming in human fibroblasts. *Nucleic Acids Res.* **39,** 7049–57 (2011).
286. García-Gómez, S. *et al.* PrimPol, an Archaic Primase/Polymerase Operating in Human Cells. *Mol. Cell* **52,** 541–553 (2013).
287. Bianchi, J. *et al.* PrimPol bypasses UV photoproducts during eukaryotic chromosomal DNA replication. *Mol. Cell* **52,** 566–73 (2013).
288. Mourón, S. *et al.* Repriming of DNA synthesis at stalled replication forks by human PrimPol. *Nat. Struct. Mol. Biol.* **20,** 1383–9 (2013).
289. Petermann, E. & Helleday, T. Pathways of mammalian replication fork restart. *Nat. Rev. Mol. Cell Biol.* **11,** 683–7 (2010).
290. Cortez, D. Preventing Replication Fork Collapse to Maintain Genome Integrity. *DNA Repair (Amst).* **32,** 149–57 (2015).
291. Cobb, J. A., Bjergbaek, L., Shimada, K., Frei, C. & Gasser, S. M. DNA polymerase stabilization at stalled replication forks requires Mec1 and the RecQ helicase Sgs1. *EMBO J.* **22,** 4325–36 (2003).
292. Cotta-Ramusino, C. *et al.* Exo1 processes stalled replication forks and counteracts fork reversal in checkpoint-defective cells. *Mol. Cell* **17,** 153–9 (2005).
293. Katou, Y. *et al.* S-phase checkpoint proteins Tof1 and Mrc1 form a stable replication-pausing complex. *Nature* **424,** 1078–83 (2003).
294. Lucca, C. *et al.* Checkpoint-mediated control of replisome-fork association and signalling in response to replication pausing. *Oncogene* **23,** 1206–13 (2004).
295. Naylor, M. L., Li, J., Osborn, A. J. & Elledge, S. J. Mrc1 phosphorylation in response to DNA replication stress is required for Mec1 accumulation at the stalled fork. *Proc. Natl. Acad. Sci. U. S. A.* **106,** 12765–70 (2009).
296. Raveendranathan, M. *et al.* Genome-wide replication profiles of S-phase checkpoint mutants reveal fragile sites in yeast. *EMBO J.* **25,** 3627–39 (2006).
297. De Piccoli, G. *et al.* Replisome stability at defective DNA replication forks is independent of S phase checkpoint kinases. *Mol. Cell* **45,** 696–704 (2012).
298. Neelsen, K. J. & Lopes, M. Replication fork reversal in eukaryotes: from dead end to dynamic response. *Nat. Rev. Mol. Cell Biol.* **16,** 207–220 (2015).
299. Atkinson, J. & McGlynn, P. Replication fork reversal and the maintenance of genome stability. *Nucleic Acids Res.* **37,** 3475–92 (2009).
300. Manosas, M., Perumal, S. K., Croquette, V. & Benkovic, S. J. Direct observation of stalled fork restart via fork regression in the T4 replication system. *Science* **338,** 1217–20 (2012).
301. Higgins, N. P., Kato, K. & Strauss, B. A model for replication repair in mammalian cells. *J. Mol. Biol.* **101,** 417–425 (1976).
302. Fugger, K. *et al.* FBH1 Catalyzes Regression of Stalled Replication Forks. *Cell Rep.* **10,** 1749–1757 (2015).
303. Zellweger, R. *et al.* Rad51-mediated replication fork reversal is a global response to genotoxic treatments in human cells. *J. Cell Biol.* **208,** 563–79 (2015).
304. Lopes, M. *et al.* The DNA replication checkpoint response stabilizes stalled replication forks. *Nature* **412,** 557–61 (2001).
305. Couch, F. B. *et al.* ATR phosphorylates SMARCAL1 to prevent replication fork collapse. *Genes Dev.* **27,** 1610–23 (2013).
306. Doe, C. L., Ahn, J. S., Dixon, J. & Whitby, M. C. Mus81-Eme1 and Rqh1 involvement in processing stalled and collapsed replication forks. *J. Biol. Chem.* **277,** 32753–9 (2002).
307. Hu, J. *et al.* The intra-S phase checkpoint targets Dna2 to prevent stalled replication forks from reversing. *Cell* **149,** 1221–32 (2012).
308. Sun, W. *et al.* The FANCM ortholog Fml1 promotes recombination at stalled replication forks and limits

crossing over during DNA double-strand break repair. *Mol. Cell* **32,** 118–28 (2008).

309. Xue, X. *et al.* Restriction of Replication Fork Regression Activities by a Conserved SMC Complex. *Mol. Cell* **56,** 436–445 (2014).
310. Ray Chaudhuri, A. *et al.* Topoisomerase I poisoning results in PARP-mediated replication fork reversal. *Nat. Struct. Mol. Biol.* **19,** 417–23 (2012).
311. Berti, M. *et al.* Human RECQ1 promotes restart of replication forks reversed by DNA topoisomerase I inhibition. *Nat. Struct. Mol. Biol.* **20,** 347–54 (2013).
312. Thangavel, S. *et al.* DNA2 drives processing and restart of reversed replication forks in human cells. *J. Cell Biol.* **208,** 545–62 (2015).
313. Neelsen, K. J., Zanini, I. M. Y., Herrador, R. & Lopes, M. Oncogenes induce genotoxic stress by mitotic processing of unusual replication intermediates. *J. Cell Biol.* **200,** 699–708 (2013).
314. Ray Chaudhuri, A., Ahuja, A. K., Herrador, R. & Lopes, M. Poly(ADP-ribosyl) glycohydrolase prevents the accumulation of unusual replication structures during unperturbed S phase. *Mol. Cell. Biol.* **35,** 856–65 (2015).
315. Follonier, C., Oehler, J., Herrador, R. & Lopes, M. Friedreich's ataxia-associated GAA repeats induce replication-fork reversal and unusual molecular junctions. *Nat. Struct. Mol. Biol.* **20,** 486–94 (2013).
316. Nyberg, K. A., Michelson, R. J., Putnam, C. W. & Weinert, T. A. Toward maintaining the genome: DNA damage and replication checkpoints. *Annu. Rev. Genet.* **36,** 617–656 (2002).
317. Abraham, R. T. Cell cycle checkpoint signaling through the ATM and ATR kinases. *Genes Dev.* **15,** 2177–2196 (2001).
318. López-Contreras, A. J. & Fernandez-Capetillo, O. The ATR barrier to replication-born DNA damage. *DNA Repair (Amst).* **9,** 1249–1255 (2010).
319. Cimprich, K. A. & Cortez, D. ATR: An Essential Regulator of Genome Integrity. *Mol. Cell. Biol.* **9,** 616–627 (2008).
320. Reinhardt, H. C. & Yaffe, M. B. Kinases that control the cell cycle in response to DNA damage: Chk1, Chk2, and MK2. *Curr. Opin. Cell Biol.* **21,** 245–55 (2009).
321. Gutierrez, G. J. *et al.* JNK-mediated phosphorylation of Cdc25C regulates cell cycle entry and G(2)/M DNA damage checkpoint. *J. Biol. Chem.* **285,** 14217–28 (2010).
322. Gutierrez, G. J., Tsuji, T., Chen, M., Jiang, W. & Ronai, Z. A. Interplay between Cdh1 and JNK activity during the cell cycle. *Nat. Cell Biol.* **12,** 686–95 (2010).
323. Uchida, S. *et al.* Stress-activated mitogen-activated protein kinases c-Jun NH2-terminal kinase and p38 target Cdc25B for degradation. *Cancer Res.* **69,** 6438–44 (2009).
324. Llopis, A. *et al.* The stress-activated protein kinases p38α/β and JNK1/2 cooperate with Chk1 to inhibit mitotic entry upon DNA replication arrest. *Cell Cycle* **11,** 3627–3637 (2012).
325. de Klein, A. *et al.* Targeted disruption of the cell-cycle checkpoint gene ATR leads to early embryonic lethality in mice. *Curr. Biol.* **10,** 479–82 (2000).
326. Brown, E. J. & Baltimore, D. ATR disruption leads to chromosomal fragmentation and early embryonic lethality. *Genes Dev.* **14,** 397–402 (2000).
327. Liu, Q. *et al.* Chk1 is an essential kinase that is regulated by Atr and required for the G2/M DNA damage checkpoint. *Genes & Dev.* **14,** 1448–1459 (2000).
328. Xu, Y. *et al.* Targeted disruption of ATM leads to growth retardation, chromosomal fragmentation during meiosis, immune defects, and thymic lymphoma. *Genes Dev.* **10,** 2411–22 (1996).
329. Barlow, C. *et al.* Atm-deficient mice: a paradigm of ataxia telangiectasia. *Cell* **86,** 159–71 (1996).
330. Elson, A. *et al.* Pleiotropic defects in ataxia-telangiectasia protein-deficient mice. *Proc. Natl. Acad. Sci. U. S. A.* **93,** 13084–9 (1996).
331. Daniel, J. A. *et al.* Loss of ATM kinase activity leads to embryonic lethality in mice. *J. Cell Biol.* **198,** 295–304 (2012).
332. Nam, E. A. A. & Cortez, D. ATR signalling: more than meeting at the fork. *Biochem. J.* **436,** 527–36 (2011).
333. Stiff, T. *et al.* ATM and DNA-PK function redundantly to phosphorylate H2AX after exposure to ionizing radiation. *Cancer Res.* **64,** 2390–6 (2004).
334. Ward, I. M. & Chen, J. Histone H2AX Is Phosphorylated in an ATR-dependent Manner in Response to Replicational Stress. *J. Biol. Chem.* **276,** 47759–47762 (2001).

335. Rogakou, E. P., Pilch, D. R., Orr, A. H., Ivanova, V. S. & Bonner, W. M. DNA Double-stranded Breaks Induce Histone H2AX Phosphorylation on Serine 139. *J. Biol. Chem.* **273,** 5858–5868 (1998).

336. de Feraudy, S., Revet, I., Bezrookove, V., Feeney, L. & Cleaver, J. E. A minority of foci or pan-nuclear apoptotic staining of gammaH2AX in the S phase after UV damage contain DNA double-strand breaks. *Proc. Natl. Acad. Sci. U. S. A.* **107,** 6870–5 (2010).

337. Maréchal, A. & Zou, L. RPA-coated single-stranded DNA as a platform for post-translational modifications in the DNA damage response. *Cell Res.* **25,** 9–23 (2015).

338. Din, S., Brill, S. J., Fairman, M. P. & Stillman, B. Cell-cycle-regulated phosphorylation of DNA replication factor A from human and yeast cells. *Genes Dev.* **4,** 968–77 (1990).

339. Dutta, A. & Stillman, B. cdc2 family kinases phosphorylate a human cell DNA replication factor, RPA, and activate DNA replication. *EMBO J.* **11,** 2189–99 (1992).

340. Fang, F. & Newport, J. W. Distinct roles of cdk2 and cdc2 in RP-A phosphorylation during the cell cycle. *J. Cell Sci.* **106,** 983–94 (1993).

341. Pan, Z. Q., Amin, A. A., Gibbs, E., Niu, H. & Hurwitz, J. Phosphorylation of the p34 subunit of human single-stranded-DNA-binding protein in cyclin A-activated G1 extracts is catalyzed by cdk-cyclin A complex and DNA-dependent protein kinase. *Proc. Natl. Acad. Sci. U. S. A.* **91,** 8343–7 (1994).

342. Hustedt, N., Gasser, S. M. & Shimada, K. Replication checkpoint: Tuning and coordination of replication forks in S phase. *Genes (Basel).* **4,** 388–434 (2013).

343. Jossen, R. & Bermejo, R. The DNA damage checkpoint response to replication stress: A Game of Forks. *Front. Genet.* **4,** 1–14 (2013).

344. Cortez, D., Guntuku, S., Qin, J. & Elledge, S. J. ATR and ATRIP: partners in checkpoint signaling. *Science* **294,** 1713–6 (2001).

345. Itakura, E. *et al.* ATR-dependent phosphorylation of ATRIP in response to genotoxic stress. *Biochem. Biophys. Res. Commun.* **323,** 1197–202 (2004).

346. Zhang, H. *et al.* ATRIP Deacetylation by SIRT2 Drives ATR Checkpoint Activation by Promoting Binding to RPA-ssDNA. *Cell Rep.* **14,** 1435–47 (2016).

347. St Onge, R. P., Besley, B. D. A., Pelley, J. L. & Davey, S. A role for the phosphorylation of hRad9 in checkpoint signaling. *J. Biol. Chem.* **278,** 26620–8 (2003).

348. Takeishi, Y. *et al.* Casein kinase 2-dependent phosphorylation of human Rad9 mediates the interaction between human Rad9-Hus1-Rad1 complex and TopBP1. *Genes Cells* **15,** 761–71 (2010).

349. Lee, J., Kumagai, A. & Dunphy, W. G. The Rad9-Hus1-Rad1 checkpoint clamp regulates interaction of TopBP1 with ATR. *J. Biol. Chem.* **282,** 28036–44 (2007).

350. Delacroix, S., Wagner, J. M., Kobayashi, M., Yamamoto, K. -i. & Karnitz, L. M. The Rad9-Hus1-Rad1 (9-1-1) clamp activates checkpoint signaling via TopBP1. *Genes Dev.* **21,** 1472–1477 (2007).

351. Furuya, K., Poitelea, M., Guo, L., Caspari, T. & Carr, A. M. Chk1 activation requires Rad9 S/TQ-site phosphorylation to promote association with C-terminal BRCT domains of Rad4TOPBP1. *Genes Dev.* **18,** 1154–64 (2004).

352. Parrilla-Castellar, E. R., Arlander, S. J. H. & Karnitz, L. Dial 9-1-1 for DNA damage: the Rad9-Hus1-Rad1 (9-1-1) clamp complex. *DNA Repair (Amst).* **3,** 1009–14 (2004).

353. Lindsey-Boltz, L. A., Bermudez, V. P., Hurwitz, J. & Sancar, A. Purification and characterization of human DNA damage checkpoint Rad complexes. *Proc. Natl. Acad. Sci. U. S. A.* **98,** 11236–41 (2001).

354. Bermudez, V. P. *et al.* Loading of the human 9-1-1 checkpoint complex onto DNA by the checkpoint clamp loader hRad17-replication factor C complex in vitro. *Proc. Natl. Acad. Sci. U. S. A.* **100,** 1633–8 (2003).

355. Kumagai, A., Lee, J., Yoo, H. Y. & Dunphy, W. G. TopBP1 activates the ATR-ATRIP complex. *Cell* **124,** 943–55 (2006).

356. Mordes, D. A., Glick, G. G., Zhao, R. & Cortez, D. TopBP1 activates ATR through ATRIP and a PIKK regulatory domain. *Genes Dev.* **22,** 1478–89 (2008).

357. Wardlaw, C. P., Carr, A. M. & Oliver, A. W. TopBP1: A BRCT-scaffold protein functioning in multiple cellular pathways. *DNA Repair (Amst).* **22,** 1–10 (2014).

358. Liu, S. *et al.* ATR autophosphorylation as a molecular switch for checkpoint activation. *Mol. Cell* **43,** 192–202 (2011).

359. Nam, E. A. *et al.* Thr-1989 phosphorylation is a marker of active ataxia telangiectasia-mutated and Rad3-

related (ATR) kinase. *J. Biol. Chem.* **286,** 28707–14 (2011).

360. Yoo, H. Y., Kumagai, A., Shevchenko, A., Shevchenko, A. & Dunphy, W. G. Ataxia-telangiectasia mutated (ATM)-dependent activation of ATR occurs through phosphorylation of TopBP1 by ATM. *J. Biol. Chem.* **282,** 17501–6 (2007).
361. Cotta-Ramusino, C. *et al.* A DNA damage response screen identifies RHINO, a 9-1-1 and TopBP1 interacting protein required for ATR signaling. *Science* **332,** 1313–7 (2011).
362. Collis, S. J. *et al.* FANCM and FAAP24 function in ATR-mediated checkpoint signaling independently of the Fanconi anemia core complex. *Mol. Cell* **32,** 313–24 (2008).
363. Kumar, S. & Burgers, P. M. Lagging strand maturation factor Dna2 is a component of the replication checkpoint initiation machinery. *Genes Dev.* **27,** 313–21 (2013).
364. MacDougall, C. A., Byun, T. S., Van, C., Yee, M. & Cimprich, K. A. The structural determinants of checkpoint activation. *Genes Dev.* **21,** 898–903 (2007).
365. Smits, V. A. J., Reaper, P. M. & Jackson, S. P. Rapid PIKK-dependent release of Chk1 from chromatin promotes the DNA-damage checkpoint response. *Curr. Biol.* **16,** 150–9 (2006).
366. Zhao, H. & Piwnica-Worms, H. ATR-mediated checkpoint pathways regulate phosphorylation and activation of human Chk1. *Mol. Cell. Biol.* **21,** 4129–39 (2001).
367. Kasahara, K. *et al.* 14-3-3gamma mediates Cdc25A proteolysis to block premature mitotic entry after DNA damage. *EMBO J.* **29,** 2802–12 (2010).
368. Kumagai, A. & Dunphy, W. G. Claspin, a novel protein required for the activation of Chk1 during a DNA replication checkpoint response in Xenopus egg extracts. *Mol. Cell* **6,** 839–49 (2000).
369. Kumagai, A. & Dunphy, W. G. Repeated phosphopeptide motifs in Claspin mediate the regulated binding of Chk1. *Nat. Cell Biol.* **5,** 161–5 (2003).
370. Clarke, C. A. L. & Clarke, P. R. DNA-dependent phosphorylation of Chk1 and Claspin in a human cell-free system. *Biochem. J.* **388,** 705–12 (2005).
371. Meng, Z., Capalbo, L., Glover, D. M. & Dunphy, W. G. Role for casein kinase 1 in the phosphorylation of Claspin on critical residues necessary for the activation of Chk1. *Mol. Biol. Cell* **22,** 2834–47 (2011).
372. Unsal-Kaçmaz, K. *et al.* The human Tim/Tipin complex coordinates an Intra-S checkpoint response to UV that slows replication fork displacement. *Mol. Cell. Biol.* **27,** 3131–42 (2007).
373. Errico, A., Costanzo, V. & Hunt, T. Tipin is required for stalled replication forks to resume DNA replication after removal of aphidicolin in Xenopus egg extracts. *Proc. Natl. Acad. Sci. U. S. A.* **104,** 14929–34 (2007).
374. Melixetian, M., Klein, D. K., Sørensen, C. S. & Helin, K. NEK11 regulates CDC25A degradation and the IR-induced G2/M checkpoint. *Nat. Cell Biol.* **11,** 1247–53 (2009).
375. Chen, Y.-H. *et al.* ATR-mediated phosphorylation of FANCI regulates dormant origin firing in response to replication stress. *Mol. Cell* **58,** 323–38 (2015).
376. Guo, C. *et al.* Interaction of Chk1 with Treslin Negatively Regulates the Initiation of Chromosomal DNA Replication. *Mol. Cell* **57,** 1–14 (2014).
377. Lee, A. Y.-L. *et al.* Dbf4 is direct downstream target of ataxia telangiectasia mutated (ATM) and ataxia telangiectasia and Rad3-related (ATR) protein to regulate intra-S-phase checkpoint. *J. Biol. Chem.* **287,** 2531–43 (2012).
378. Yamada, M., Masai, H. & Bartek, J. Regulation and roles of Cdc7 kinase under replication stress. *Cell Cycle* **13,** 1859–66 (2014).
379. Kim, J. M. *et al.* Cdc7 kinase mediates Claspin phosphorylation in DNA replication checkpoint. *Oncogene* **27,** 3475–82 (2008).
380. Rainey, M. D., Harhen, B., Wang, G.-N., Murphy, P. V & Santocanale, C. Cdc7-dependent and -independent phosphorylation of Claspin in the induction of the DNA replication checkpoint. *Cell Cycle* **12,** 1560–8 (2013).
381. Yamada, M. *et al.* ATR-Chk1-APC/CCdh1-dependent stabilization of Cdc7-ASK (Dbf4) kinase is required for DNA lesion bypass under replication stress. *Genes Dev.* **27,** 2459–72 (2013).
382. Poh, W. T., Chadha, G. S., Gillespie, P. J., Kaldis, P. & Blow, J. J. Xenopus Cdc7 executes its essential function early in S phase and is counteracted by checkpoint-regulated protein phosphatase 1. *Open Biol.* **4,** (2014). doi: 10.1098/rsob.130138.
383. Hiraga, S.-I. *et al.* Rif1 controls DNA replication by directing Protein Phosphatase 1 to reverse Cdc7-mediated phosphorylation of the MCM complex. *Genes Dev.* **28,** 372–83 (2014).

384. Davé, A., Cooley, C., Garg, M. & Bianchi, A. Protein phosphatase 1 recruitment by Rif1 regulates DNA replication origin firing by counteracting DDK activity. *Cell Rep.* **7,** 53–61 (2014).
385. Ge, X. Q. & Blow, J. J. Chk1 inhibits replication factory activation but allows dormant origin firing in existing factories. *J. Cell Biol.* **191,** 1285–97 (2010).
386. Trenz, K., Errico, A. & Costanzo, V. Plx1 is required for chromosomal DNA replication under stressful conditions. *EMBO J.* **27,** 876–85 (2008).
387. Shechter, D., Costanzo, V. & Gautier, J. ATR and ATM regulate the timing of DNA replication origin firing. *Nat. Cell Biol.* **6,** 648–55 (2004).
388. Petermann, E., Woodcock, M. & Helleday, T. Chk1 promotes replication fork progression by controlling replication initiation. *Proc. Natl. Acad. Sci. U. S. A.* **107,** 16090–5 (2010).
389. Petermann, E., Helleday, T. & Caldecott, K. W. Claspin promotes normal replication fork rates in human cells. *Mol. Biol. Cell* **19,** 2373–8 (2008).
390. Dungrawala, H. *et al.* The Replication Checkpoint Prevents Two Types of Fork Collapse without Regulating Replisome Stability. *Mol. Cell* **59,** 998–1010 (2015).
391. Toledo, L. I. *et al.* ATR prohibits replication catastrophe by preventing global exhaustion of RPA. *Cell* **155,** 1088–103 (2013).
392. Lossaint, G. *et al.* FANCD2 binds MCM proteins and controls replisome function upon activation of s phase checkpoint signaling. *Mol. Cell* **51,** 678–90 (2013).
393. Forment, J. V, Blasius, M., Guerini, I. & Jackson, S. P. Structure-specific DNA endonuclease Mus81/Eme1 generates DNA damage caused by Chk1 inactivation. *PLoS One* **6,** e23517 (2011).
394. Schlacher, K. *et al.* Double-strand break repair-independent role for BRCA2 in blocking stalled replication fork degradation by MRE11. *Cell* **145,** 529–42 (2011).
395. Schlacher, K., Wu, H. & Jasin, M. A Distinct Replication Fork Protection Pathway Connects Fanconi Anemia Tumor Suppressors to RAD51-BRCA1/2. *Cancer Cell* **22,** 106–116 (2012).
396. Hashimoto, Y., Ray Chaudhuri, A., Lopes, M. & Costanzo, V. Rad51 protects nascent DNA from Mre11-dependent degradation and promotes continuous DNA synthesis. *Nat. Struct. Mol. Biol.* **17,** 1305–11 (2010).
397. Su, F. *et al.* Nonenzymatic role for WRN in preserving nascent DNA strands after replication stress. *Cell Rep.* **9,** 1387–401 (2014).
398. Costanzo, V. Brca2, Rad51 and Mre11: performing balancing acts on replication forks. *DNA Repair (Amst).* **10,** 1060–5 (2011).
399. Wu, N. & Yu, H. The Smc complexes in DNA damage response. *Cell Biosci.* **2,** (2012). doi: 10.1186/2045-3701-2-5.
400. Tittel-Elmer, M. *et al.* Cohesin association to replication sites depends on rad50 and promotes fork restart. *Mol. Cell* **48,** 98–108 (2012).
401. Wang, H., Wang, H., Powell, S. N., Iliakis, G. & Wang, Y. ATR affecting cell radiosensitivity is dependent on homologous recombination repair but independent of nonhomologous end joining. *Cancer Res.* **64,** 7139–43 (2004).
402. Tibbetts, R. S. *et al.* Functional interactions between BRCA1 and the checkpoint kinase ATR during genotoxic stress. *Genes Dev.* **14,** 2989–3002 (2000).
403. Ho, G. P. H., Margossian, S., Taniguchi, T. & D'Andrea, A. D. Phosphorylation of FANCD2 on two novel sites is required for mitomycin C resistance. *Mol. Cell. Biol.* **26,** 7005–15 (2006).
404. Huang, M. *et al.* Chk1 and Chk2 are differentially involved in homologous recombination repair and cell cycle arrest in response to DNA double-strand breaks induced by camptothecins. *Mol. Cancer Ther.* **7,** 1440–9 (2008).
405. Sørensen, C. S. *et al.* The cell-cycle checkpoint kinase Chk1 is required for mammalian homologous recombination repair. *Nat. Cell Biol.* **7,** 195–201 (2005).
406. Bahassi, E. M. *et al.* The checkpoint kinases Chk1 and Chk2 regulate the functional associations between hBRCA2 and Rad51 in response to DNA damage. *Oncogene* **27,** 3977–85 (2008).
407. Alabert, C., Bianco, J. N. & Pasero, P. Differential regulation of homologous recombination at DNA breaks and replication forks by the Mrc1 branch of the S-phase checkpoint. *EMBO J.* **28,** 1131–41 (2009).
408. Barlow, J. H. & Rothstein, R. Rad52 recruitment is DNA replication independent and regulated by Cdc28 and the Mec1 kinase. *EMBO J.* **28,** 1121–30 (2009).

409. Meister, P. *et al.* Temporal separation of replication and recombination requires the intra-S checkpoint. *J. Cell Biol.* **168,** 537–44 (2005).
410. Sirbu, B. M. *et al.* ATR-p53 restricts homologous recombination in response to replicative stress but does not limit DNA interstrand crosslink repair in lung cancer cells. *PLoS One* **6,** e23053 (2011).
411. Tercero, J. A., Longhese, M. P. & Diffley, J. F. X. A central role for DNA replication forks in checkpoint activation and response. *Mol. Cell* **11,** 1323–36 (2003).
412. Jackson, S. P. & Bartek, J. The DNA-damage response in human biology and disease. *Nature* **461,** 1071–8 (2009).
413. Lavin, M. F. ATM and the Mre11 complex combine to recognize and signal DNA double-strand breaks. *Oncogene* **26,** 7749–58 (2007).
414. Stracker, T. H. & Petrini, J. H. J. The MRE11 complex: starting from the ends. *Nat. Rev. Mol. Cell Biol.* **12,** 90–103 (2011).
415. Paull, T. T. Mechanisms of ATM Activation. *Annu. Rev. Biochem.* **84,** 711–38 (2015).
416. Uziel, T. *et al.* Requirement of the MRN complex for ATM activation by DNA damage. *EMBO J.* **22,** 5612–21 (2003).
417. Falck, J., Coates, J. & Jackson, S. P. Conserved modes of recruitment of ATM, ATR and DNA-PKcs to sites of DNA damage. *Nature* **434,** 605–11 (2005).
418. Lee, J.-H. & Paull, T. T. ATM activation by DNA double-strand breaks through the Mre11-Rad50-Nbs1 complex. *Science* **308,** 551–4 (2005).
419. Bakkenist, C. J. & Kastan, M. B. DNA damage activates ATM through intermolecular autophosphorylation and dimer dissociation. *Nature* **421,** 499–506 (2003).
420. Sun, Y., Jiang, X., Chen, S., Fernandes, N. & Price, B. D. A role for the Tip60 histone acetyltransferase in the acetylation and activation of ATM. *Proc. Natl. Acad. Sci. U. S. A.* **102,** 13182–7 (2005).
421. Sun, Y., Xu, Y., Roy, K. & Price, B. D. DNA damage-induced acetylation of lysine 3016 of ATM activates ATM kinase activity. *Mol. Cell. Biol.* **27,** 8502–9 (2007).
422. Matsuoka, S. *et al.* Ataxia telangiectasia-mutated phosphorylates Chk2 in vivo and in vitro. *Proc. Natl. Acad. Sci. U. S. A.* **97,** 10389–94 (2000).
423. Lukas, C. *et al.* Mdc1 couples DNA double-strand break recognition by Nbs1 with its H2AX-dependent chromatin retention. *EMBO J.* **23,** 2674–83 (2004).
424. Wang, Q. *et al.* Rad17 recruits the MRE11-RAD50-NBS1 complex to regulate the cellular response to DNA double-strand breaks. *EMBO J.* **33,** 862–77 (2014).
425. Lou, Z. *et al.* MDC1 maintains genomic stability by participating in the amplification of ATM-dependent DNA damage signals. *Mol. Cell* **21,** 187–200 (2006).
426. Peng, A., Lewellyn, A. L. & Maller, J. L. Undamaged DNA transmits and enhances DNA damage checkpoint signals in early embryos. *Mol. Cell. Biol.* **27,** 6852–62 (2007).
427. Lukas, J., Lukas, C. & Bartek, J. More than just a focus: The chromatin response to DNA damage and its role in genome integrity maintenance. *Nat. Cell Biol.* **13,** 1161–9 (2011).
428. Huen, M. S. Y. *et al.* RNF8 transduces the DNA-damage signal via histone ubiquitylation and checkpoint protein assembly. *Cell* **131,** 901–14 (2007).
429. Mailand, N. *et al.* RNF8 ubiquitylates histones at DNA double-strand breaks and promotes assembly of repair proteins. *Cell* **131,** 887–900 (2007).
430. Doil, C. *et al.* RNF168 binds and amplifies ubiquitin conjugates on damaged chromosomes to allow accumulation of repair proteins. *Cell* **136,** 435–46 (2009).
431. Stewart, G. S. *et al.* The RIDDLE syndrome protein mediates a ubiquitin-dependent signaling cascade at sites of DNA damage. *Cell* **136,** 420–34 (2009).
432. Daley, J. M. & Sung, P. 53BP1, BRCA1, and the choice between recombination and end joining at DNA double-strand breaks. *Mol. Cell. Biol.* **34,** 1380–8 (2014).
433. Reinhardt, H. C. & Schumacher, B. The p53 network: Cellular and systemic DNA damage responses in aging and cancer. *Trends Genet.* **28,** 128–136 (2012).
434. Taylor, W. R. & Stark, G. R. Regulation of the G2/M transition by p53. *Oncogene* **20,** 1803–15 (2001).
435. Canman, C. E. *et al.* Activation of the ATM kinase by ionizing radiation and phosphorylation of p53. *Science* **281,** 1677–9 (1998).

436. Dumaz, N. & Meek, D. W. Serine15 phosphorylation stimulates p53 transactivation but does not directly influence interaction with HDM2. *EMBO J.* **18,** 7002–10 (1999).

437. Chehab, N. H., Malikzay, A., Appel, M. & Halazonetis, T. D. Chk2/hCds1 functions as a DNA damage checkpoint in G(1) by stabilizing p53. *Genes Dev.* **14,** 278–88 (2000).

438. Haupt, Y., Maya, R., Kazaz, A. & Oren, M. Mdm2 promotes the rapid degradation of p53. *Nature* **387,** 296–9 (1997).

439. Hirao, A. *et al.* DNA damage-induced activation of p53 by the checkpoint kinase Chk2. *Science* **287,** 1824–7 (2000).

440. Shieh, S. Y., Ahn, J., Tamai, K., Taya, Y. & Prives, C. The human homologs of checkpoint kinases Chk1 and Cds1 (Chk2) phosphorylate p53 at multiple DNA damage-inducible sites. *Genes Dev.* **14,** 289–300 (2000).

441. Khosravi, R. *et al.* Rapid ATM-dependent phosphorylation of MDM2 precedes p53 accumulation in response to DNA damage. *Proc. Natl. Acad. Sci.* **96,** 14973–14977 (1999).

442. Luo, Y., Hurwitz, J. & Massagué, J. Cell-cycle inhibition by independent CDK and PCNA binding domains in p21Cip1. *Nature* **375,** 159–61 (1995).

443. Sudo, T. *et al.* Activation of Cdh1-dependent APC is required for G1 cell cycle arrest and DNA damage-induced G2 checkpoint in vertebrate cells. *EMBO J.* **20,** 6499–508 (2001).

444. Moldovan, G.-L., Pfander, B. & Jentsch, S. PCNA, the Maestro of the Replication Fork. *Cell* **129,** 665–679 (2007).

445. Soria, G., Podhajcer, O., Prives, C. & Gottifredi, V. P21Cip1/WAF1 downregulation is required for efficient PCNA ubiquitination after UV irradiation. *Oncogene* **25,** 2829–38 (2006).

446. Soria, G., Speroni, J., Podhajcer, O. L., Prives, C. & Gottifredi, V. p21 differentially regulates DNA replication and DNA-repair-associated processes after UV irradiation. *J. Cell Sci.* **121,** 3271–82 (2008).

447. Tibbetts, R. S. *et al.* A role for ATR in the DNA damage-induced phosphorylation of p53. *Genes Dev.* **13,** 152–7 (1999).

448. Toledo, L. I., Murga, M., Gutierrez-Martinez, P., Soria, R. & Fernandez-Capetillo, O. ATR signaling can drive cells into senescence in the absence of DNA breaks. *Genes Dev.* **22,** 297–302 (2008).

449. Hiratani, I. & Gilbert, D. M. Replication timing as an epigenetic mark. *Epigenetics* **4,** 93–7 (2009).

450. Petermann, E., Orta, M. L. L., Issaeva, N., Schultz, N. & Helleday, T. Hydroxyurea-stalled replication forks become progressively inactivated and require two different RAD51-mediated pathways for restart and repair. *Mol. Cell* **37,** 492–502 (2010).

451. Abbas, T., Keaton, M. A. & Dutta, A. Genomic instability in cancer. *Cold Spring Harb. Perspect. Biol.* **5,** a012914 (2013).

452. Anand, R. P., Lovett, S. T. & Haber, J. E. Break-induced DNA replication. *Cold Spring Harb. Perspect. Biol.* **5,** a010397 (2013).

453. Malkova, A. & Ira, G. Break-induced replication: functions and molecular mechanism. *Curr. Opin. Genet. Dev.* **23,** 271–9 (2013).

454. Costantino, L. *et al.* Break-induced replication repair of damaged forks induces genomic duplications in human cells. *Science* **343,** 88–91 (2014).

455. Llorente, B., Smith, C. E. & Symington, L. S. Break-induced replication: What is it and what is it for? *Cell Cycle* **7,** 859–864 (2008).

456. Smith, C. E., Llorente, B. & Symington, L. S. Template switching during break-induced replication. *Nature* **447,** 102–5 (2007).

457. Anand, R. P. *et al.* Chromosome rearrangements via template switching between diverged repeated sequences. *Genes Dev.* **28,** 2394–406 (2014).

458. Deem, A. *et al.* Break-induced replication is highly inaccurate. *PLoS Biol.* **9,** e1000594 (2011).

459. Sakofsky, C. J., Ayyar, S. & Malkova, A. Break-induced replication and genome stability. *Biomolecules* **2,** 483–504 (2012).

460. Karanam, K., Kafri, R., Loewer, A. & Lahav, G. Quantitative live cell imaging reveals a gradual shift between DNA repair mechanisms and a maximal use of HR in mid S phase. *Mol. Cell* **47,** 320–9 (2012).

461. Bunting, S. F. *et al.* 53BP1 Inhibits Homologous Recombination in Brca1-Deficient Cells by Blocking Resection of DNA Breaks. *Cell* **141,** 243–254 (2010).

462. Bothmer, A. *et al.* 53BP1 regulates DNA resection and the choice between classical and alternative end

joining during class switch recombination. *J. Exp. Med.* **207,** 855–65 (2010).

463. Mehta, A. & Haber, J. E. Sources of DNA double-strand breaks and models of recombinational DNA repair. *Cold Spring Harb. Perspect. Biol.* **6,** a016428 (2014).
464. Prakash, R., Zhang, Y., Feng, W. & Jasin, M. Homologous recombination and human health: The roles of BRCA1, BRCA2, and associated proteins. *Cold Spring Harb. Perspect. Biol.* **7,** 1–37 (2015).
465. Hanada, K. *et al.* The structure-specific endonuclease Mus81 contributes to replication restart by generating double-strand DNA breaks. *Nat. Struct. Mol. Biol.* **14,** 1096–104 (2007).
466. Donnianni, R. A. & Symington, L. S. Break-induced replication occurs by conservative DNA synthesis. *Proc. Natl. Acad. Sci. U. S. A.* **110,** 13475–80 (2013).
467. Saini, N. *et al.* Migrating bubble during break-induced replication drives conservative DNA synthesis. *Nature* **502,** 389–92 (2013).
468. Wilson, M. A. *et al.* Pif1 helicase and Polδ promote recombination-coupled DNA synthesis via bubble migration. *Nature* **502,** 393–6 (2013).
469. Lydeard, J. R. *et al.* Break-induced replication requires all essential DNA replication factors except those specific for pre-RC assembly. *Genes Dev.* **24,** 1133–44 (2010).
470. Clarke, A. R. *et al.* Thymocyte apoptosis induced by p53-dependent and independent pathways. *Nature* **362,** 849–52 (1993).
471. Di Leonardo, A., Linke, S. P., Clarkin, K. & Wahl, G. M. DNA damage triggers a prolonged p53-dependent G1 arrest and long-term induction of Cip1 in normal human fibroblasts. *Genes Dev.* **8,** 2540–51 (1994).
472. Sancar, A. *et al.* Molecular mechanisms of mammalian DNA repair and the DNA damage checkpoints. *Annu. Rev. Biochem.* **73,** 39–85 (2004).
473. Muñoz-Espín, D. & Serrano, M. Cellular senescence: from physiology to pathology. *Nat. Rev. Mol. Cell Biol.* **15,** 482–96 (2014).
474. Kosar, M. *et al.* Senescence-associated heterochromatin foci are dispensable for cellular senescence, occur in a cell type- and insult-dependent manner and follow expression of p16(ink4a). *Cell Cycle* **10,** 457–68 (2011).
475. Krenning, L., Feringa, F. M., Shaltiel, I. A., van den Berg, J. & Medema, R. H. Transient Activation of p53 in G2 Phase Is Sufficient to Induce Senescence. *Mol. Cell* **55,** 59–72 (2014).
476. Müllers, E., Silva Cascales, H., Jaiswal, H., Saurin, A. T. & Lindqvist, A. Nuclear translocation of Cyclin B1 marks the restriction point for terminal cell cycle exit in G2 phase. *Cell Cycle* **13,** 2733–43 (2014).
477. Charrier-Savournin, F. B. *et al.* p21-Mediated nuclear retention of cyclin B1-Cdk1 in response to genotoxic stress. *Mol. Biol. Cell* **15,** 3965–76 (2004).
478. Macheret, M. & Halazonetis, T. D. DNA replication stress as a hallmark of cancer. *Annu. Rev. Pathol.* **10,** 425–48 (2015).
479. Medical, T., Unit, C. & Road, H. *Chromosomal Instability in Cancer*. (2015). doi:10.1007/978-3-319-20291-4.
480. Hanahan, D. & Weinberg, R. A. Hallmarks of cancer: the next generation. *Cell* **144,** 646–74 (2011).
481. Gad, H. *et al.* MTH1 inhibition eradicates cancer by preventing sanitation of the dNTP pool. *Nature* **508,** 215–21 (2014).
482. Franchitto, A. & Pichierri, P. Understanding the molecular basis of common fragile sites instability: role of the proteins involved in the recovery of stalled replication forks. *Cell Cycle* **10,** 4039–46 (2011).
483. Shima, N. *et al.* A viable allele of Mcm4 causes chromosome instability and mammary adenocarcinomas in mice. *Nat. Genet.* **39,** 93–8 (2007).
484. Iraqui, I. *et al.* Recovery of arrested replication forks by homologous recombination is error-prone. *PLoS Genet.* **8,** e1002976 (2012).
485. Burrell, R. A. *et al.* Replication stress links structural and numerical cancer chromosomal instability. *Nature* **494,** 492–496 (2013).
486. Dereli-Öz, A., Versini, G. & Halazonetis, T. D. Studies of genomic copy number changes in human cancers reveal signatures of DNA replication stress. *Mol. Oncol.* **5,** 308–14 (2011).
487. Hastings, P. J., Ira, G. & Lupski, J. R. A microhomology-mediated break-induced replication model for the origin of human copy number variation. *PLoS Genet.* **5,** e1000327 (2009).
488. Collado, M. *et al.* Tumour biology: senescence in premalignant tumours. *Nature* **436,** (2005). doi:

10.1038/436642a.

489. Michaloglou, C. *et al.* BRAFE600-associated senescence-like cell cycle arrest of human naevi. *Nature* **436,** 720–724 (2005).
490. Gorgoulis, V. G. *et al.* Activation of the DNA damage checkpoint and genomic instability in human precancerous lesions. *Nature* **434,** 907–13 (2005).
491. Mallette, F. A., Gaumont-Leclerc, M.-F. & Ferbeyre, G. The DNA damage signaling pathway is a critical mediator of oncogene-induced senescence. *Genes Dev.* **21,** 43–8 (2007).
492. López-Contreras, A. J., Gutierrez-Martinez, P., Specks, J., Rodrigo-Perez, S. & Fernandez-Capetillo, O. An extra allele of Chk1 limits oncogene-induced replicative stress and promotes transformation. *J. Exp. Med.* **209,** 455–61 (2012).
493. Aird, K. M. *et al.* Suppression of nucleotide metabolism underlies the establishment and maintenance of oncogene-induced senescence. *Cell Rep.* **3,** 1252–65 (2013).
494. Mannava, S. *et al.* Depletion of deoxyribonucleotide pools is an endogenous source of DNA damage in cells undergoing oncogene-induced senescence. *Am. J. Pathol.* **182,** 142–51 (2013).
495. Mannava, S. *et al.* Ribonucleotide reductase and thymidylate synthase or exogenous deoxyribonucleosides reduce DNA damage and senescence caused by C-MYC depletion. *Aging (Albany. NY).* **4,** 917–922 (2012).
496. Aye, Y., Li, M., Long, M. J. C. & Weiss, R. S. Ribonucleotide reductase and cancer: biological mechanisms and targeted therapies. *Oncogene* **34,** 2011–21 (2015).
497. Kuznetsova, A. Y. *et al.* Chromosomal instability, tolerance of mitotic errors and multidrug resistance are promoted by tetraploidization in human cells. *Cell Cycle* **14,** 2810–20 (2015).
498. Bakhoum, S. F. *et al.* The mitotic origin of chromosomal instability. *CURBIO* **24,** R148–R149 (2014).
499. Florensa, R., Bachs, O. & Agell, N. ATM/ATR-independent inhibition of cyclin B accumulation in response to hydroxyurea in nontransformed cell lines is altered in tumour cell lines. *Oncogene* **22,** 8283–92 (2003).
500. Rodriguez-Bravo, V., Guaita-Esteruelas, S., Salvador, N., Bachs, O. & Agell, N. Different S/M Checkpoint Responses of Tumor and Non Tumor Cell Lines to DNA Replication Inhibition. *Cancer Res.* **67,** 11648–11656 (2007).
501. Jiang, X. R. *et al.* Telomerase expression in human somatic cells does not induce changes associated with a transformed phenotype. *Nat. Genet.* **21,** 111–4 (1999).
502. Dimri, G. P. *et al.* A biomarker that identifies senescent human cells in culture and in aging skin in vivo. *Proc. Natl. Acad. Sci. U. S. A.* **92,** 9363–7 (1995).
503. Zeng, X. *et al.* Pharmacologic inhibition of the anaphase-promoting complex induces a spindle checkpoint-dependent mitotic arrest in the absence of spindle damage. *Cancer Cell* **18,** 382–95 (2010).
504. Huyen, Y. *et al.* Methylated lysine 79 of histone H3 targets 53BP1 to DNA double-strand breaks. *Nature* **432,** 406–11 (2004).
505. Bryant, H. E. DNA double-strand break damage and repair assessed by pulsed-field gel electrophoresis. *Methods Mol. Biol.* **920,** 315–21 (2012).
506. Schwab, R. A. V & Niedzwiedz, W. Visualization of DNA replication in the vertebrate model system DT40 using the DNA fiber technique. *J. Vis. Exp.* e3255 (2011).
507. Ercilla, A. *et al.* New origin firing is inhibited by APC/CCdh1 activation in S-phase after severe replication stress. *Nucleic Acids Res.* (2016). doi:10.1093/nar/gkw132.
508. Verschuren, E. W., Ban, K. H., Masek, M. A., Lehman, N. L. & Jackson, P. K. Loss of Emi1-dependent anaphase-promoting complex/cyclosome inhibition deregulates E2F target expression and elicits DNA damage-induced senescence. *Mol. Cell. Biol.* **27,** 7955–65 (2007).
509. Sirbu, B. M. *et al.* Analysis of protein dynamics at active, stalled, and collapsed replication forks. *Genes Dev.* **25,** 1320–7 (2011).
510. Lopez-Contreras, A. J. *et al.* A proteomic characterization of factors enriched at nascent DNA molecules. *Cell Rep.* **3,** 1105–16 (2013).
511. Aranda, S., Rutishauser, D. & Ernfors, P. Identification of a large protein network involved in epigenetic transmission in replicating DNA of embryonic stem cells. *Nucleic Acids Res.* **42,** 6972–86 (2014).
512. Kliszczak, A. E., Rainey, M. D., Harhen, B., Boisvert, F. M. & Santocanale, C. DNA mediated chromatin pull-down for the study of chromatin replication. *Sci. Rep.* **1,** (2011). doi: 10.1038/srep00095.

513. Mi, H., Muruganujan, A., Casagrande, J. T. & Thomas, P. D. Large-scale gene function analysis with the PANTHER classification system. *Nat. Protoc.* **8,** 1551–66 (2013).
514. Sirbu, B. M. *et al.* Identification of proteins at active, stalled, and collapsed replication forks using isolation of proteins on nascent DNA (iPOND) coupled with mass spectrometry. *J. Biol. Chem.* **288,** 31458–67 (2013).
515. Alabert, C. *et al.* Nascent chromatin capture proteomics determines chromatin dynamics during DNA replication and identifies unknown fork components. *Nat. Cell Biol.* **16,** 281–293 (2014).
516. Ashburner, M. *et al.* Gene ontology: tool for the unification of biology. The Gene Ontology Consortium. *Nat. Genet.* **25,** 25–9 (2000).
517. Raderschall, E., Golub, E. I. & Haaf, T. Nuclear foci of mammalian recombination proteins are located at single-stranded DNA regions formed after DNA damage. *Proc. Natl. Acad. Sci.* **96,** 1921–1926 (1999).
518. Sartori, A. A. *et al.* Human CtIP promotes DNA end resection. *Nature* **450,** 509–14 (2007).
519. Yeo, J. E., Lee, E. H., Hendrickson, E. A. & Sobeck, A. CtIP mediates replication fork recovery in a FANCD2-regulated manner. *Hum. Mol. Genet.* **23,** 3695–705 (2014).
520. Moldovan, G.-L. & D'Andrea, A. D. How the fanconi anemia pathway guards the genome. *Annu. Rev. Genet.* **43,** 223–49 (2009).
521. Meijer, L. *et al.* Biochemical and cellular effects of roscovitine, a potent and selective inhibitor of the cyclin-dependent kinases cdc2, cdk2 and cdk5. *Eur. J. Biochem.* **243,** 527–36 (1997).
522. Takahashi, A. *et al.* DNA damage signaling triggers degradation of histone methyltransferases through APC/C(Cdh1) in senescent cells. *Mol. Cell* **45,** 123–31 (2012).
523. Davis, A. P. & Symington, L. S. RAD51-dependent break-induced replication in yeast. *Mol. Cell. Biol.* **24,** 2344–51 (2004).
524. Malkova, A., Naylor, M. L., Yamaguchi, M., Ira, G. & Haber, J. E. RAD51-dependent break-induced replication differs in kinetics and checkpoint responses from RAD51-mediated gene conversion. *Mol. Cell. Biol.* **25,** 933–44 (2005).
525. Lafranchi, L. *et al.* APC/C(Cdh1) controls CtIP stability during the cell cycle and in response to DNA damage. *EMBO J.* **33,** 2860–79 (2014).
526. Chung, W.-H., Zhu, Z., Papusha, A., Malkova, A. & Ira, G. Defective resection at DNA double-strand breaks leads to de novo telomere formation and enhances gene targeting. *PLoS Genet.* **6,** e1000948 (2010).
527. Shankar, S. R. *et al.* G9a, a multipotent regulator of gene expression. *Epigenetics* **8,** 16–22 (2013).
528. Fujita, T., Liu, W., Doihara, H. & Wan, Y. Regulation of Skp2-p27 axis by the Cdh1/anaphase-promoting complex pathway in colorectal tumorigenesis. *Am. J. Pathol.* **173,** 217–28 (2008).
529. Hashimoto, Y., Puddu, F. & Costanzo, V. RAD51- and MRE11-dependent reassembly of uncoupled CMG helicase complex at collapsed replication forks. *Nat. Struct. Mol. Biol.* **19,** 17–24 (2012).
530. Debacq-Chainiaux, F., Erusalimsky, J. D., Campisi, J. & Toussaint, O. Protocols to detect senescence-associated beta-galactosidase (SA-betagal) activity, a biomarker of senescent cells in culture and in vivo. *Nat. Protoc.* **4,** 1798–806 (2009).
531. Méndez, J. & Stillman, B. Chromatin association of human origin recognition complex, cdc6, and minichromosome maintenance proteins during the cell cycle: assembly of prereplication complexes in late mitosis. *Mol. Cell. Biol.* **20,** 8602–12 (2000).
532. Lowry, O. H. O. H. *et al.* Article : Protein Measurement With the Folin Phenol Reagent. *J. Biol. Chem.* **193,** 265–275 (1951).
533. LAEMMLI, U. K. Cleavage of Structural Proteins during the Assembly of the Head of Bacteriophage T4. *Nature* **227,** 680–685 (1970).
534. Sambrook, J. & Russell, D. W. Purification of nucleic acids by extraction with phenol:chloroform. *CSH Protoc.* **2006,** pdb.prot4455– (2006).
535. Lyutvinskiy, Y., Yang, H., Rutishauser, D. & Zubarev, R. A. In silico instrumental response correction improves precision of label-free proteomics and accuracy of proteomics-based predictive models. *Mol. Cell. Proteomics* **12,** 2324–31 (2013).